論文 / 著書情報
Article / Book Information

題目(和文)	量子場の理論における非摂動的側面について
Title(English)	Some nonperturbative aspects of quantum field theories
著者(和文)	伊藤健児
Author(English)	
出典(和文)	学位:博士(理学), 学位授与機関:東京工業大学, 報告番号:甲第4607号, 授与年月日:2001年3月26日, 学位の種別:課程博士, 審査員:坂井 典佑
Citation(English)	Degree:Doctor (Science), Conferring organization: Tokyo Institute of Technology, Report number:甲第4607号, Conferred date:2001/3/26, Degree Type:Course doctor, Examiner:
学位種別(和文)	博士論文
Type(English)	Doctoral Thesis

Ph. D. thesis

Some Nonperturbative Aspects of Quantum Field Theories

Kenji Ito[1]

Department of Physics, Tokyo Institute of Technology
Oh-okayama, Meguro, Tokyo 152-8551, Japan

March 2001

[1]e-mail: kito@th.phys.titech.ac.jp

Abstract

At present, fundamental interactions other than gravity are believed to be described by a gauge theory, the so–called standard model, which consists of Quantum Chromodynamics (QCD) and the Weinberg–Salam model. So far it seems that there is no explicit contradiction between the standard model and many kinds of experiments. However, the low energy dynamics of QCD, such as color confinement and dynamical chiral symmetry breaking, cannot be derived from first principles. It is because the gauge coupling becomes so strong that perturbation theory is unreliable at low energy.

In this thesis, using powerful tools, large N expansion and supersymmetry, we obtained exact solutions of two models having common properties with QCD, and clarified nonperturbative effects of the models.

One of the models is two dimensional gauged four–Fermi model, which combines and extends the 't Hooft model and the Gross–Neveu model. Considering the model in the large N limit, we derived the analytic equation for mesonic states and their exact mass spectrum. Calculating the meson mass difference directly from the spectrum, we found that interflavor QCD inequality of the mesonic sector almost always holds for gauged four–Fermi model, for which there is no rigorous proof of the inequality.

The other model is $\mathcal{N} = 1$ supersymmetric gauge theory with $U(1)\times U(1)'$ gauge group, which simulates $\mathcal{N} = 2$ supersymmetric QCD with one flavor perturbed by adjoint scalar mass. We obtained an exact solution of BPS domain wall junction of the model. Using the exact solution as concrete example, we discussed general properties of BPS domain wall junctions. Especially, we worked out explicitly massless Nambu-Goldstone modes on the BPS domain wall junction. We find that their wave functions extend along the wall to infinity (not localized) and are not normalizable. It is also argued that this feature is a generic phenomenon of Nambu–Goldstone modes on domain wall junctions in the bulk flat space in any dimensions. Nambu–Goldstone fermions exhibit a chiral structure in accordance with unitary representations of $(1, 0)$ supersymmetry algebra where fermion and boson with the same mass come in pairs except massless modes which can appear singly.

Contents

Chapter 1

Introduction

At present it is known that there are four fundamental interactions between elementary particles, the electromagnetic interaction, the weak interaction, the strong interaction and the gravitational interaction. Three of them are known to be described by a special class of quantum field theories, renormalizable gauge theories.

The electromagnetic and weak interactions are unified to a gauge theory with $SU(2) \times U(1)$ gauge symmetry, the so–called Weinberg–Salam model [1, 2]. The crucial point of this theory is spontaneously broken gauge symmetry, which gives masses to vector fields without spoiling the renormalizability. The weakness of the weak interaction is the result of massive gauge bosons. So far the Weinberg–Salam model has been well confirmed by various experiments, although there remain some mysteries in the Higgs sector.

The strong interaction is believed to be described by QCD, which is a non–abelian gauge theory with unbroken $SU(3)$ color gauge symmetry. A conspicuous character in strong interaction is *asymptotic freedom*, which was discovered by experiments of deep inelastic scattering; constituents of hadrons, which is now believed to be quarks, behave as if they were free particles at high energies. Historically it was the discovery of asymptotic freedom in non–abelian gauge theories that elevated QCD into the leading theory of the strong interactions [3, 4]. Since the gauge coupling constant becomes small at high energy, the behavior of quarks at high energy is well described in the framework of ordinary perturbation theory.

In contrast, it seems to us that the strong interaction becomes strong enough to confine quarks inside hadrons at low energy. This picture is well matched with the fact that the fractionally charged quarks were never discovered in any scattering experiment. However it is difficult to describe the low energy phenomena such as color confinement and dynamical chiral symmetry breaking directly from QCD, because gauge coupling is large and

perturbation theory becomes unreliable. Therefore nonperturbative methods are indispensable for deriving low energy dynamics of QCD.

Until now many methods have been exploited to investigate the nonperturbative effects in gauge theories: lattice gauge theory[5]–[8], large N expansion[19, 26], extension to those with supersymmetry[106], considering effective theories on various types of branes of superstring theories[9, 10] (so-called brane configuration[11], MQCD[12], AdS/CFT correspondence[13]–[18]), and so on.

In this thesis, using two of these methods, large N expansion and supersymmetry, we will obtain *exact solutions* of models having common properties with QCD, and derive some nonperturbative features which are unclear without exact solutions.

The basic idea of the large N expansion, introduced by 't Hooft[19], is to extend ordinary QCD to non–abelian gauge theory with gauge group $SU(N)$ and take the limit of $N \to \infty$ with g^2N fixed (g: gauge coupling constant). Naively, the more the number of colors N increases, the more complex the theory becomes. However, in the large N limit, only the *planar* diagrams appear in the theory, and one can add up all the diagrams explicitly to obtain nonperturbative effects. 't Hooft considered two dimensional QCD in the large N limit and derive the analytic bound state equation for mesonic states, from which the exact meson mass spectrum and wave function can be obtained [20]. There is no continuum state in the spectrum, which indicates that the confinement of quarks occurs.

Another crucial feature of QCD is dynamical chiral symmetry breaking. A natural explanation for the fact that the pion mass is much smaller than those of the other hadrons is that pion is the so–called Nambu–Goldstone boson accompanied with spontaneously broken chiral symmetry. In contrast to the Weinberg–Salam model, there are no elementary scalar fields in QCD. Therefore the chiral symmetry breaking must be caused *dynamically*; the composite scalar particles have some vacuum expectation value to cause symmetry breaking.

The Gross–Neveu model is a two dimensional model of fermions interacting through four–Fermi couplings[22], which was originally considered to investigate dynamical chiral symmetry breaking in a simple toy model having common properties with QCD, especially asymptotic freedom. The Gross–Neveu model is only known asymptotic free field theory other than four dimensional non–abelian gauge theories. In the large N limit, it has been shown to cause dynamical chiral symmetry breaking. Recently, various types of the Gross–Neveu models have been used to reveal the dynamics of quantum field theories, with finite temperature [47]–[50], with finite densities[51]–[54] , in the constant curvature[55]–[59], in the external field[60], and so on.

Since the Gross–Neveu model is defined in the large N limit, it can also be analyzed by using the 't Hooft's method. From this point of view, we considered the massive Gross–Neveu model, which is a more interesting model describing relatively small but nonzero pion mass, and derived the bound state equation from the Bethe–Salpeter approach. We confirmed that it is consistent with the ordinary approach with auxiliary scalar fields and investigated the physics of the massive Gross–Neveu model such as wave function, bound (resonance) state, chiral limit, and so on[32]. Analyzing the Gross–Neveu model in detail gives not only better understanding of the model itself but also some insight and nontrivial consistency check to more general model considered later.

Motivated by the fact that four–Fermi couplings become renormalizable in $1+1$ dimensions, we considered the gauged four–Fermi model, which combines and extends the 't Hooft and the Gross–Neveu model. These two models are realized as special limits of the gauged four–Fermi model. This model not only clarifies the dynamics of more complicated field theory model, but also has some application to phenomenological models such as top quark condensation models[42]–[46]. Using somewhat extended version of the 't Hooft's methods, we derived analytic bound state equation for mesonic states. In contrast to the Gross–Neveu model, we need to solve an integral equation for the gauged four–Fermi model. We developed systematic methods for solving the bound state equation and derived various results on the physical properties of the model[32, 79].

As one of the applications of our exact solution for the mesonic states, we considered so–called QCD inequalities. QCD inequalities are inequalities between the various types of hadrons; mesons, baryons, glueballs, exotic states, and so on[71]. These inequalities can be obtained relatively easily without solving the spectrum in detail. Roughly speaking, there are two approaches for the QCD inequalities; one of them is the euclidean path integral approach based on the quantum field theories, and the other is the Hamiltonian variational approach based on effective quantum mechanical description. In the path integral approach, the key point of the proof is the positivity of effective measure of gauge fields obtained after integrating out the fermionic degrees of freedom, which can be easily proved for vector–like gauge theories such as QCD. From this approach the well–known fact that the pion is the lightest meson, can be easily proved without solving the spectrum exactly[61]. Furthermore QCD inequalities give more informations about the QCD vacuum, because in general symmetry structure is closely related to the massless sector of the physical spectrum. Using the positivity of the effective measure and some plausible assumptions, Vafa and Witten proved that the vector symmetries of fermions are all unbroken, while the axial vector (chiral) sym-

metries are all spontaneously broken in the zero–mass limit in the vector–like gauge theories. These results are also useful for composite models such as technicolor models[73]–[77].

In this thesis we focus on a QCD inequality between the mesonic states; $\mu_{ab} \geq \frac{1}{2}(\mu_{aa} + \mu_{bb})$ (a, b are quark flavors and μ_{ab} etc. denote mesons of ab channel.), which we call the "mass inequality". Within the two dimensional models mentioned above, the mass inequality is proved for the 't Hooft model from the field theory point of view, but not for the other models. The mass inequality can be proved if the positivity of the effective measure is guaranteed. There are some cases other than vector–like gauge theories such as self–interacting scalar models, in which the positivity is guaranteed. However, in general, the Yukawa couplings spoil the positivity and the Gross–Neveu model is known to be equivalent to the model including Yukawa couplings. This is why the mass inequality cannot be easily proved for the Gross–Neveu model and its extension, gauged four–Fermi model.

On the other hand, from the point of view of the effective quantum mechanical description, the mass inequality always seems to be proved, if one assume that interactions between quarks do not depend on their flavor. Although quantum field theories can be regarded as quantum mechanical systems with infinite degrees of freedom, there are some crucial differences between them such as spontaneous symmetry breaking. Therefore it may be possible that the mass inequality is broken in the case of quantum field theories. Though it is difficult to extend the proof of the mass inequality to more general field theory models, our exact meson spectrum enables us to calculate the mass inequality (difference) directly to see whether the mass inequality is broken or not. From this point of view, we examined the mass inequality of the gauged four–Fermi model with the most general coupling constants, for which the mass inequality may be broken. As a result, we found that the mass inequality is *not* broken for almost every case [79].

Another direction to derive the nonperturbative effects in field theories is to extend models to those with supersymmetry, which relates fermions and bosons. (The phenomenological motivation of this symmetry is to explain the lightness of the Higgs fields from the chiral symmetry of their fermionic counterparts.) Naively, it seems that the theory becomes more complicated because each particle is accompanied by its superpartner of the other statistics. However, since supersymmetry imposes rather strong constraints on the model, sometimes exact results can be derived from the symmetry. Especially, various exact results for supersymmetric gauge theories have been obtained, which shed light on the dynamics of them [106]. The key ingredients in analyzing nonperturbative properties of supersymmetric gauge theories are *holomorphy, duality* and *BPS states*.

The holomorphic properties of supersymmetric field theories can be powerful tool in deriving exact results about them[86]– [89]; in $\mathcal{N} = 1$ supersymmetric theories, the superpotential is holomorphic and exact results can be obtained[89]–[92]. Furthermore, in the case of $\mathcal{N} = 2$ supersymmetric theories, the Kähler potential is also constrained by holomorphy and its exact form can be determined[93].

With the help of duality and BPS states, Seiberg and Witten obtained the exact solution of $\mathcal{N} = 2$ supersymmetric gauge theories for the first time in four dimensional gauge theories in the strong coupling region[107, 108]. BPS states, such as monopoles, saturate Bogomol'nyi bound given by topological charges, and they are stable for topological reasons[100, 101]. In the $\mathcal{N} = 2$ supersymmetric theories, it is known that BPS states preserve part of the supersymmetry and the Bogomol'nyi bound is given by central charges that appear in the $\mathcal{N} = 2$ supersymmetry algebra [102]. The $\mathcal{N} = 2$ supersymmetry algebra has "large" representation with sixteen states and "small" ones with only four states, to which BPS states belong. Since the number of degrees of freedom is different between them, the BPS states are believed to remain BPS after including the quantum corrections. Therefore the masses of these BPS states are given exactly as $M_{\rm BPS} = \sqrt{2}|Z_{\mathcal{N}=2}|$, where $Z_{\mathcal{N}=2}$ is the central charge that is a linear combination of conserved charges. The duality transformation maps the fundamental fields such as electron in the strong coupling region to the solitonic states such as monopole in the weak coupling region, which enables us to investigate the physics in the strong coupling region from the analysis of dual theories in the weak coupling region. Taking the advantage of these ideas, Seiberg and Witten determined the mass of the stable particles, the low energy effective actions[1] , and the metric on the quantum moduli space in the supersymmetric Yang–Mills theory[107] and supersymmetric QCD [108]. In addition, adding mass term to break the $\mathcal{N} = 2$ supersymmetry down to $\mathcal{N} = 1$, they derived analytically the nonperturbative effects of N=1 supersymmetric theories such as confinement[107] and chiral symmetry breaking[108] for the first time.

In contrast, there is no particle like BPS states for $\mathcal{N} = 1$ supersymmetric theories, because no central extension appears in $\mathcal{N} = 1$ supersymmetry algebra. However, if the translational invariance is broken under the nontrivial boundary condition, some central charges emerge[103, 104, 127, 128, 134, 136, 137] and correspondingly extended BPS states such as BPS strings[112]–[115], [138], BPS domain walls[99],[127]–[134], and BPS domain

[1]The word "(supersymmetric) gauge theories" is often used to refer to the non–abelian gauge theories that are asymptotically free. These theories are in the strong coupling region at low energy.

wall junctions[136]–[138] may appear.

We devote the latter half of this thesis to obtaining an exact solution of BPS domain wall junction and investigating general properties of BPS junctions in $\mathcal{N} = 1$ supersymmetric theories.

Domain walls interpolate between degenerate discrete minima of a potential and spread over two spatial dimensions, which appear in many areas of physics such as condensed matter physics and cosmology. These degenerate vacua arise naturally in four-dimensional $\mathcal{N} = 1$ supersymmetric field theories [99],[127]–[133]. It has been found that domain walls in supersymmetric theories can saturate the Bogomol'nyi bound [100, 101]. Such a domain wall preserves half of the original supersymmetry and is called 1/2 BPS state [102]. It has also been noted that these BPS states possess a topological charge which becomes a central charge Z of the supersymmetry algebra [103, 104, 127, 128, 134].

Investigating BPS domain walls not only deepens our understanding of them, but also gives some information about nonperturbative effects of $\mathcal{N} = 1$ supersymmetric gauge theories. For instance, let us consider the $\mathcal{N} = 1$ supersymmetric gluodynamics with $SU(N)$ gauge group in the large N limit. This theory is known to have N degenerate vacua[94]. The tension of BPS walls interpolating adjacent vacua is obtained exactly and it is of order N[132, 133]. Using the fact that the tensions of BPS walls are given by the difference of the superpotential between the two vacua and that the superpotential is proportional to the gaugino condensation[106], the gaugino condensation, which is essentially nonperturbative effect, should be of order N in the large N limit. In the case of $\mathcal{N} = 1$ supersymmetric QCD, BPS walls have been investigated and much information about their dynamics has been obtained [129]–[131].

Domain wall junctions are solitonic configurations such that some of the domain walls intersect one another. If three or more different discrete vacua occur in separate region of space, segments of domain walls separate each pair of the neighboring vacua. If the two spatial dimensions of all of these domain walls have one dimension in common, these domain walls meet at a one-dimensional junction. The solitonic configuration for the junction can preserve a quarter of supersymmetry. It has also been found that a new topological charge Y can appear for such a 1/4 BPS state [136] [137] [138]. There have been general considerations of junctions [136] [137] as well as more concrete numerical results [139]–[140]. Some information about the BPS domain walls and junctions, such as tension, central charges and conserved supercharges, can be obtained from the boundary conditions. However, exact junction solutions are needed if one wants to know other detailed information, such as energy (charge) densities, configuration near the center of junctions

and modes on the junction backgrounds. While some exact solutions of BPS domain walls have been obtained [99, 134], there is no analytic exact solution of BPS domain wall junction other than ours. Using a toy model simulating the $\mathcal{N} = 2$ supersymmetric QCD with one flavor perturbed by adjoint scalar mass, we obtained an exact analytic solution of BPS domain wall junction for the first time[141]. Using our exact solution as a concrete example, we investigate some general properties of BPS domain wall junctions[159, 160]. Especially, we reached the conclusion that the central charge Y peculiar to junction configurations contributes negatively to their mass. Thus we should not consider the central charge Y alone as a physical mass of the junction at the center. Various other aspects of the domain wall junctions have been also studied[144]–[158].

Recently, BPS domain walls and junctions have attracted much attention from the phenomenological point of view; an interesting idea has been advocated to regard our world as a domain wall embedded in higher dimensional space–time [116, 117]. Most of the particles in the standard model should be realized as modes localized on the wall. Phenomenological implications of the idea have been extensively studied from many aspects. Another fascinating possibility has also been proposed to consider walls in the bulk spacetime which has negative cosmological constant [118, 119]. The model can give large mass hierarchy or can give massless graviton localized on the wall. Subsequently a great deal of research activity has been performed to study and extend the proposal [123]–[126].

Since walls typically have co-dimension one, it is desirable to consider intersections and/or junctions of walls in order to obtain our four dimensional world from a spacetime with much higher dimensions. The model with the bulk cosmological constant has been extended to produce an intersection of walls [120]–[122].

In order to investigate localization of modes, we define mode equations and demonstrate explicitly that fermion and boson with the same mass have to come in pairs except massless modes. We work out explicitly massless Nambu-Goldstone (NG) modes on the BPS domain wall junction. We find that their wave functions extend along the wall to infinity (not localized) and are not normalizable. It is argued that this feature is a generic phenomenon of NG modes on domain wall junctions in the bulk flat space in any dimensions. NG fermions exhibit a chiral structure in accordance with unitary representations of $(1, 0)$ supersymmetry algebra where fermion and boson with the same mass come in pairs except massless modes which can appear singly[159].

So far nothing special is found about the nonperturbative effects of $\mathcal{N} = 1$ supersymmetric gauge theories from the knowledge of BPS domain wall

junctions. We hope it gives some clues to solve the low energy dynamics of supersymmetric and nonsupersymmetric gauge theories in the future.

The organization of this thesis is as follows: In **chapter 2** we review large N expansion and method by which 't Hooft succeeded in deriving the analytic equation describing the mesonic states. In **chapter 3**, we review the Gross–Neveu model, mainly about its properties shared with QCD. In **chapter 4**, we solve the bound state problem of the massive Gross–Neveu model by using the Bethe–Salpeter approach exploited by 't Hooft. We also discuss physical properties of the model, such as chiral limit, bound states, resonance states, and so on. In **chapter 5**, we consider the gauged four–Fermi model which combines and extends the 't Hooft model and the Gross–Neveu model. Using somewhat extended method from the 't Hooft's one, we derive the analytic bound state equation for the mesonic states of the model. We also give systematic ways for solving the equation and obtain the meson mass spectrum and wave functions. In **chapter 6**, we review QCD inequalities and comment on their applications to symmetry structure of QCD. In **chapter 7**, we focus on one of the QCD inequalities, which we call "mass inequality". In the case of the vector–like gauge theories such as the 't Hooft model, the mass inequality is proved rigorously, while not for the Gross–Neveu model and the gauged four–Fermi model. Rather than giving some proof for these models, we calculate mass difference directly from the exact mass spectrum obtained in chapter 5 to see the possibilities of broken mass inequalities.

In **chapter 8** and later, we move on to the models with supersymmetry which often enable us to obtain exact nonperturbative effects. The main results of the latter half of this thesis is revealing some properties of BPS domain wall junctions, which are BPS states in four dimensional $\mathcal{N} = 1$ supersymmetric theories. In **chapter 8**, we review supersymmetric gauge theories, especially those with $\mathcal{N} = 2$ supersymmetry for which exact solutions have been obtained by Seiberg and Witten[107, 108]. In **chapter 9**, we derive the BPS equation of $\mathcal{N} = 1$ (abelian) gauge theories from the condition that BPS states preserve part of the supersymmetry. Using the exact solution of a toy model simulating the Seiberg–Witten theory, we discuss fundamental properties of (BPS) domain walls. In **chapter 10**, we construct the extended version of the toy model in chapter 9, and obtain an exact solution of BPS domain wall junction. Using our exact solution as a concrete example, we discuss general properties of BPS domain wall junction in four dimensional supersymmetric theories, such as the relation between boundary conditions and conserved charges. In **chapter 11**, we especially focus on modes on BPS domain wall junction and discuss the possibility of localization of (zero) modes on junctions, which is crucial in constructing

phenomenological models. Finally in **chapter 12**, we end with conclusion and some discussions. In **appendix**, we summarize some relations useful for calculation, notation, comments, and so on.

Chapter 2

The 't Hooft model

In this chapter we shall review the methods 't Hooft used to derive analytic equation for mesonic states and fundamental properties of the 't Hooft model.

2.1 The large N expansion

The 't Hooft model is $1+1$ dimensional non-abelian gauge theory, whose gauge group is $SU(N)$. The Lagrangian of the model is

$$\mathcal{L} = -\frac{1}{2}\,\mathrm{tr}\,(F_{\mu\nu}F^{\mu\nu}) + \sum_{f=1}^{N_f} \overline{\psi}_f (i\not{D} - m_f)\psi_f. \tag{2.1}$$

The covariant derivative is defined as $D_\mu \equiv \partial_\mu - igA_\mu$, where g is the gauge coupling constant. The color indices have been suppressed.

Feynman diagrams can be characterized by the quantity $r = g^{V_3+2V_4}N^I$, where V_n and I denote the number of vertices and index loops respectively. Introducing F, P, V and L, which are the number of faces, internal lines, vertices and quark loops respectively, the following relations can be obtained,

$$F = L + I \tag{2.2}$$

$$V = \sum_n V_n = V_3 + V_4 \tag{2.3}$$

$$2P = \sum_n nV_n = 3V_3 + 4V_4. \tag{2.4}$$

The Euler theorem says

$$V - P + F = 2 - 2H \quad (H : \text{genus}). \tag{2.5}$$

Using these relations, we can rewrite r as

$$r = (g^2 N)^{\frac{1}{2}(V_3+2V_4)} N^{2-2H-L}, \tag{2.6}$$

where we assume $L \geq 1, H \geq 0$ for the purpose of treating the mesonic states. If we take the limit of $N \to \infty$ with $g^2 N$ fixed, the leading diagrams are those with $L = 1, H = 0$: thus in the limit of $N \to \infty$, the leading contributions come from the *planar diagrams*.

2.2 The light cone gauge fixing

Although the discussion in section 2.1 is valid for any dimensional space–time, we restrict ourselves to $1+1$ dimensional space–time dimension, from here on. Following the method used by 't Hooft, we will use the light–cone coordinates defined by $x^{\pm} = x_{\pm} = \frac{1}{\sqrt{2}}(x^0 \pm x^1)$, and correspondingly the gamma matrices become simple in the chiral basis

$$\gamma^+ = \begin{pmatrix} 0 & 0 \\ \sqrt{2} & 0 \end{pmatrix} \qquad \gamma^- = \begin{pmatrix} 0 & \sqrt{2} \\ 0 & 0 \end{pmatrix} \qquad \gamma_5 = \begin{pmatrix} 1 & 0 \\ 0 & -1 \end{pmatrix}. \tag{2.7}$$

These gamma matrices satisfy the relations; $(\gamma^+)^2 = (\gamma^-)^2 = 0, \{\gamma^+, \gamma^-\} = 2 \times \mathbf{1}$. As long as we treat $1+1$ dimensional field theory, we will use the metric $(+,-)$ [1].

In general, when we quantize the systems with gauge symmetries, we must perform gauge–fixing by breaking the gauge symmetry temporarily. Since the gauge fields have only two physical degrees of freedom in $1+1$ dimensional space-time, there is no classical degree of freedom after gauge–fixing is performed. Though there are many ways of gauge–fixing, Coulomb gauge, covariant gauge,...and so on, here we will use the light–cone gauge:

$$A_- = A^+ = \frac{1}{\sqrt{2}}(A_0 - A_1) = 0. \tag{2.8}$$

The merits of using the light–cone gauge are

- no ghost field appears.
- there exists no self interaction of the gauge fields peculiar to non–abelian gauge theories.

[1] Notice that we will use the well–known convention of the ref.[105] in the case of the $1+3$ dimensional supersymmetric field theories (see appendix D).

Under the light–cone gauge (2.8), the Lagrangian (2.1) takes much simpler form

$$\mathcal{L} = -\,\mathrm{tr}\ (\partial_- A_+)^2 + \sum_{f=1}^{N_f} \overline{\psi}_f (i\partial\!\!\!/ - m_f)\psi_f + \sum_{f=1}^{N_f} g\overline{\psi}_f \gamma^+ A_+ \psi_f. \tag{2.9}$$

From this form of the Lagrangian, it is found that gauge fields A_+ have no term with time component (x^+) derivative and that they are merely auxiliary fields which have no dynamical degree of freedom. In this respect the 't Hooft model does not seem to reflect all the dynamics of real four–dimensional QCD, however, it is known that some $1+1$ dimensional models such as the 't Hooft model have physical behavior resembling those of higher dimensions and have played an important role in understanding them.

2.3 The Schwinger–Dyson equation

In this section, we will derive full propagators of the quark fields including all the quantum corrections by solving the Schwinger–Dyson equation.

Full (dressed) propagators of quarks $S_d(p)$ can be obtained by summing up all the series of self–energy parts $\Gamma(p)$, (see Fig. 2.1). To the lead-

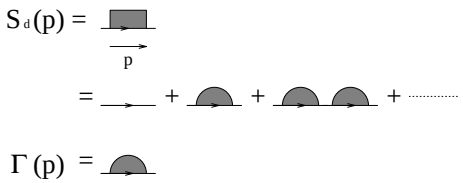

Figure 2.1: Full propagators of quarks can be obtained by summing up all the series of self–energy parts.

ing order of the large N expansion, Feynman graphs for self–energy part of quarks becomes "rainbow–type" graphs, as depicted in Fig. 2.2, where we

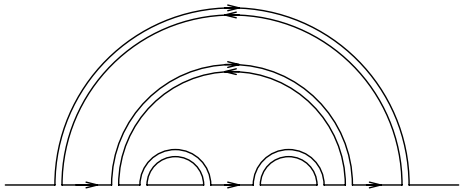

Figure 2.2: An example of "rainbow" type graphs for self–energy of quark fields.

used so–called double–line notation[2]. The self–energy parts can be obtained by solving the Schwinger–Dyson equation depicted in Fig. 2.3. Since the

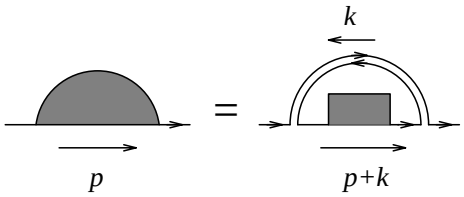

Figure 2.3: The Schwinger–Dyson equation.

full propagators are put between the quark–gluon interactions including only γ^+, $\Gamma(p)$ should be proportional to γ^+, therefore we can set $\Gamma(p) \equiv \gamma^+\Gamma_+(p)$. Summing up all the series of self–energy parts, full quark propagator is obtained

$$S_d(p) = (-i)\frac{m\mathbf{1} + [p_+ - i\Gamma_+(p)]\,\gamma^+ + p_-\gamma^-}{m^2 - 2p_-\,[p_+ - i\Gamma_+(p)] - i\epsilon}, \tag{2.10}$$

where $\Gamma_+(p)$ satisfies the Schwinger–Dyson equation

$$\Gamma_+(p) = \frac{2g^2N}{(2\pi)^2 i}\int_{-\infty}^{\infty}\frac{dk_+dk_-}{k_-^2}\frac{(-i)(p_- + k_-)}{m^2 - 2(p_- + k_-)\,[p_+ + k_+ - i\Gamma_+(p+k)] - i\epsilon}. \tag{2.11}$$

Shifting $k_+ + p_+ \to k_+$, we find that $\Gamma(p)$ depends only on p_- to obtain

$$\Gamma_+(p_-) = -\frac{g^2N}{2\pi^2}\int_{-\infty}^{\infty}dk_-\frac{(p_- + k_-)}{k_-^2}\int_{-\infty}^{\infty}\frac{dk_+}{m^2 - 2(p_- + k_-)k_+ + 2i\Gamma_+(p_- + k_-) - i\epsilon}. \tag{2.12}$$

The last integral includes ultra–violet divergence, which is known to appear as a result of our singular gauge condition (2.8). Fortunately, the divergence is only logarithmic and a symmetric ultra–violet cut–off removes the infinity and the second integral of the eq.(2.12) becomes $\frac{\pi i}{2|p_- + k_-|}$. After the k_+ integral is performed, there still remains infra–red divergence in $\Gamma_+(p_-)$. Here we shall take $\lambda_- < |k_-| < \infty$ as integral region and postpone the limit $\lambda_- \to 0$ until it makes sense. It will be found that the final results are completely independent of λ_-. [3] Finally we obtain the full propagator

$$S_d(p; m_f) = (-i)\frac{m_f + \gamma^+\,[p_+ - i\Gamma_+(p_-)] + \gamma^- p_-}{m_f^2 - 2p_-\,[p_+ - i\Gamma_+(p_-)] - i\epsilon}, \tag{2.13}$$

[2]It is convenient to represent the propagator by a double line with opposite arrows[19](*i.e.* viewing the adjoint representation as a direct product of fundamental and antifundamental representations).

[3]Cancellation of the infra–red divergence plays more important role when we consider more complicated models such as gauged four–Fermi model (see chapter 5).

where

$$\Gamma_+(p_-) = -\frac{g^2 N i}{4\pi}\int_{-\infty}^{\infty}\frac{dk_-}{k_-^2}\mathrm{sgn}(p_- + k_-) = -\frac{g^2 N i}{2\pi}\left(\frac{\mathrm{sgn(p_-)}}{\lambda_-} - \frac{1}{p_-}\right). \tag{2.14}$$

We find that the pole of this propagator is shifted towards $p_+ \to \infty$ in the limit of $\lambda_- \to 0$, and we conclude that there is no physical single quark state. This will also be confirmed in the next section by solving the spectrum, which has no continuum corresponding to a state with two free quarks.

2.4 The Bethe–Salpeter equation

To the leading order of the large N expansion, Feynman graphs which describe quark–antiquark bound states are "ladder-type" graphs as depicted in Fig. 2.4. These "ladder"graphs satisfy the Bethe–Salpeter equation depicted

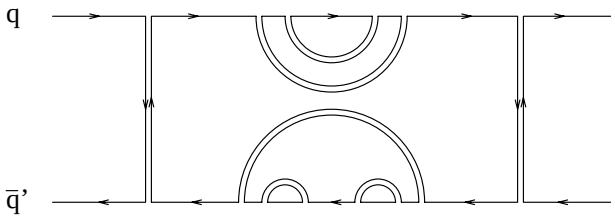

Figure 2.4: An example of "ladder" graphs describing quark–antiquark bound states.

in Fig. 2.5 [4]. Let $\psi_{\alpha\beta}(p,r)$ stand for the blob in the left hand side of the

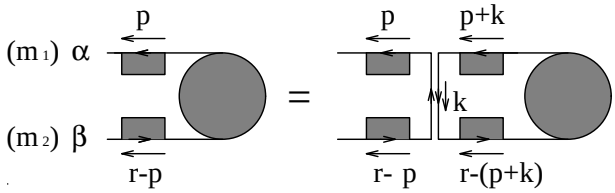

Figure 2.5: The Bethe-Salpeter equation.

Fig.2.5, the Bethe–Salpeter equation is written as

$$\psi_{\alpha\beta}(p,r) = S_d(p;m_1)_{\alpha 2}S_d(p-r;m_2)_{1\beta}\frac{2g^2N}{(2\pi)^2 i}\int_{-\infty}^{\infty}d^2k\frac{\psi_{12}(p+k,r)}{k_-^2}, \tag{2.15}$$

[4]Exactly speaking, the ladder graphs as in Fig. 2.4 satisfy inhomogeneous types of Bethe–Salpeter equation. Since we are interested in bound states of quarks here, we take only homogeneous part into consideration. Full quark–antiquark scattering amplitudes, which satisfy inhomogeneous type equation, were considered in ref.[21].

where α and β denote spinor indices, which run 1 and 2. Noticing that the p_+ integral is completely separated, which reflects the fact that gauge interactions become nonlocal instantaneous force after the light–cone gauge fixing, we can perform p_+ integral separately to obtain

$$\varphi_{\alpha\beta}(p_-,r)=\left(\int_{-\infty}^{\infty}dp_+S_d(p;m_1)_{\alpha 2}S_d(p-r;m_2)_{1\beta}\right)\frac{2g^2N}{(2\pi)^2i}\int_{-\infty}^{\infty}dk_-\frac{\varphi_{12}(p_-+k_-,r)}{k_-^2} \tag{2.16}$$

where we defined $\varphi_{\alpha\beta}(p_-,r)\equiv\int_{-\infty}^{\infty}dp_+\psi_{\alpha\beta}(p,r)$. Since the second integral of the eq.(2.16) has infra–red divergence, we introduce the infra–red cut–off λ_- as in section 2.3 to obtain

$$\int_{-\infty}^{\infty}dk_-\frac{\varphi_{12}(p_-+k_-,r)}{k_-^2}=\frac{2}{\lambda_-}\varphi_{12}(p_-,r)+P\int_{-\infty}^{\infty}dk_-\frac{\varphi_{12}(p_-+k_-,r)}{k_-^2} \tag{2.17}$$

where $P\int$ denotes the principal part integral.

Performing the integral $\int_{-\infty}^{\infty}dp_+S_d(p;m_1)_{\alpha 2}S_d(p-r;m_2)_{1\beta}$ (see appendix A), we obtain the bound state equations for the components as

$$\begin{aligned}&\left(\mu^2-\frac{2r_-}{\lambda_-}-\frac{\beta_1-1}{x}-\frac{\beta_2-1}{1-x}\right)\varphi_{11}(x)\\&\quad=\frac{m_2}{\sqrt{2}r_-(1-x)}\left(\frac{2r_-}{\lambda_-}\varphi_{12}(x)+P\int_0^1dy\frac{\varphi_{12}(y)}{(x-y)^2}\right)\end{aligned} \tag{2.18}$$

$$\begin{aligned}&\left(\mu^2-\frac{2r_-}{\lambda_-}-\frac{\beta_1-1}{x}-\frac{\beta_2-1}{1-x}\right)\varphi_{22}(x)\\&\quad=-\frac{m_1}{\sqrt{2}r_-x}\left(\frac{2r_-}{\lambda_-}\varphi_{12}(x)+P\int_0^1dy\,\frac{\varphi_{12}(y)}{(x-y)^2}\right)\end{aligned} \tag{2.19}$$

$$\left(\mu^2-\frac{\beta_1-1}{x}-\frac{\beta_2-1}{1-x}\right)\varphi_{12}(x)=-P\int_0^1dy\frac{\varphi_{12}(y)}{(x-y)^2} \tag{2.20}$$

$$\begin{aligned}&\left(\mu^2-\frac{2r_-}{\lambda_-}-\frac{\beta_1-1}{x}-\frac{\beta_2-1}{1-x}\right)\varphi_{21}(x)\\&\quad=\frac{m_1m_2}{2r_-^2x(1-x)}\left(\frac{2r_-}{\lambda_-}\varphi_{12}(x)+P\int_0^1dy\frac{\varphi_{12}(y)}{(x-y)^2}\right).\end{aligned} \tag{2.21}$$

Here we defined

$$\beta_i\equiv\pi\frac{m_i^2}{g^2N},\quad \mu^2\equiv\frac{\pi 2r_+r_-}{g^2N},\quad x\equiv\frac{p_-}{r_-},\quad y\equiv\frac{k_-}{r_-}. \tag{2.22}$$

Notice that in eq.(2.20) the infra–red cut–off λ_- is automatically cancelled and this equation is just the equation for mesonic states originally derived by 't Hooft in ref.[20]. On the other hand there remains the infra–red cut–off λ_- in the other three equations (2.18), (2.19) and (2.21). Here we require the cancellation of the cut–off to obtain the following conditions

$$\begin{aligned}\varphi_{11}(x) &= \frac{-m_2}{\sqrt{2}r_-(1-x)}\varphi_{12}(x), \qquad \varphi_{22}(x) = \frac{m_1}{\sqrt{2}r_- x}\varphi_{12}(x), \\ \varphi_{21}(x) &= -\frac{m_1 m_2}{2r_-^2 x(1-x)}\varphi_{12}(x). \end{aligned} \tag{2.23}$$

Inserting these relations into (2.18), (2.19) and (2.21), they reduce to the eq.(2.20) [5] . In this sense all the equation (2.18)–(2.21) are equivalent and the bound state equation for meson states is

$$\begin{aligned}\mu^2\varphi(x) &\equiv H\varphi(x) \\ &= \left(\frac{\beta_1 - 1}{x} + \frac{\beta_2 - 1}{1-x}\right)\varphi(x) - P\int_0^1 dy \frac{\varphi(y)}{(x-y)^2}. \end{aligned} \tag{2.24}$$

2.5 The bound states of quarks and the Regge trajectory

Unfortunately we can not solve the bound state equation (2.24) analytically, however, much can be said about the spectrum without solving the spectrum explicitly.

The wave functions should vanish at the boundary $x = 0, 1$ so that the Hamiltonian matrix element

$$\begin{aligned}(\psi, H\varphi) &= \int_0^1 dx \left(\frac{\beta_1}{x} + \frac{\beta_2}{1-x}\right)\varphi(x)\psi^*(x) \\ &+ \frac{1}{2}\int_0^1 dx \int_0^1 dy \frac{(\varphi(x) - \varphi(y))(\psi^*(x) - \psi^*(y))}{(x-y)^2} \end{aligned} \tag{2.25}$$

becomes finite and Hermitian. In addition, if we assume $\varphi(x)$ behave as x^γ at the boundary, γ_i $(i = 1, 2)$ can be determined by the relation

$$\beta_i - 1 + \pi\gamma_i \cot(\pi\gamma_i) = 0 \qquad (i = 1, 2). \tag{2.26}$$

[5] In ref.[20], eq.(2.24) was derived more directly by using the fact that the gauge interactions are proportional to γ^+ and only a part of quark propagators including γ^- can survive. Here we derive it in a roundabout way, however this observation gives important hints in deriving the bound state equation in more complicated models.

A rough approximation for the eigenstates can be obtained as follows. In the principal part integral in eq.(2.24), the main contribution comes from the region where y has almost the same value as x. Therefore we can approximate

$$P\int_0^1 \frac{e^{i\omega y}}{(x-y)^2}dy \approx P\int_{-\infty}^{\infty} \frac{e^{i\omega y}}{(x-y)^2}dy = -\pi|\omega|e^{i\omega x} \tag{2.27}$$

for a periodic function. In the case of $\beta_i \sim 1 \quad (i = 1, 2)$ the eigenfunctions can be approximated by

$$\varphi^k(x) \approx \sin k\pi x, \quad k = 1, 2, \ldots, \tag{2.28}$$

with eigenvalues

$$\mu_k^2 \approx \pi^2 k. \tag{2.29}$$

This approximation is valid for large k and eq.(2.29) shows that the asymptotic behavior of the spectrum exhibits "Regge trajectory" and there is no continuum in the spectrum.

For small k, numerical analysis is needed because deviations from the Regge behavior are expected as a consequence of the finiteness of the integral region and the contribution from the mass terms. Since the 't Hooft model can be regarded as special limit of extended models that will be considered later, we will not comment on numerical calculation here (see chapter 5).

Chapter 3

The Gross–Neveu model

The Gross–Neveu model shares lots of interesting features with QCD. It is particularly important in that it is the only known asymptotically free theory except for non–abelian gauge theories in four dimensions. In fact it was originally considered for the purpose of investigating dynamical chiral symmetry breaking, which is believed to occur in QCD, by more simple model than QCD. In this chapter we briefly review fundamental properties of the Gross–Neveu model.

3.1 The Gross–Neveu model with discrete chiral symmetry

In this section we consider the Gross–Neveu model with discrete chiral symmetry, which is originally discussed in ref.[22], and review the properties shared by various types of the Gross–Neveu models; asymptotic freedom, dynamical chiral symmetry breaking, dimensional transmutation, and so on. The Lagrangian of the model is given by

$$\mathcal{L} = \overline{\psi}^j i\partial\!\!\!/ \psi_j + \frac{a^2}{2}\left(\overline{\psi}^j \psi_j\right)^2 \qquad j = 1, 2 \ldots, N. \tag{3.1}$$

which is invariant under the discrete chiral transformation

$$\psi \rightarrow \gamma_5 \psi, \quad \bar{\psi} \rightarrow -\bar{\psi}\gamma_5. \tag{3.2}$$

Notice that the Lagrangian (3.1) can not have mass terms because of the discrete chiral symmetry and that four–Fermi couplings are renormalizable in $1+1$ dimensions in contrast to the Nambu–Jona–Lasinio model defined in $1+3$ dimensions[39].

3.1.1 Asymptotic freedom

The Lagrangian (3.1) can be rewritten by using an auxiliary field $\sigma(x)$ as

$$\mathcal{L} = \overline{\psi}^j i\partial\!\!\!/ \psi_j - \frac{1}{2}\sigma^2 + a\overline{\psi}^j \sigma \psi_j. \tag{3.3}$$

Then the discrete chiral transformation becomes eq.(3.2) and $\sigma \to -\sigma$. According to the original work [22], we perform large N expansion by taking the limit of $N \to \infty$ with $a^2 N$ fixed.

We can compute the full propagator of the σ field

$$\begin{aligned} D_\sigma(p^2) &= \frac{-i}{1 + i\pi(p^2)} \\ \pi(p^2) &= -a^2 N \int_{-\infty}^{\infty} \frac{d^2k}{(2\pi)^2} \frac{\mathrm{tr}[\not{k}(\not{k} - \not{p})]}{k^2(k-p)^2} = \frac{ia^2N}{2\pi}\int_0^1 dx \left[\ln\left(\frac{-\Lambda^2}{x(1-x)p^2}\right) - 2\right] \end{aligned} \tag{3.4}$$

where $\pi(p^2)$ denotes one–particle irreducible part of the propagator and x, Λ are Feynman parameter and ultraviolet cut–off. Renormalizing the four–Fermi coupling constant under the renormalization condition, $D_\sigma^{(R)}(p^2) = -i \quad \text{at} \quad p^2 = -\mu^2$, we obtain renormalized full propagator

$$D_\sigma^{(R)}(p^2, \mu^2) = \frac{-i}{1 + \frac{a^2N}{2\pi}\ln\left(-\frac{p^2}{\mu^2}\right)} \tag{3.5}$$

Since the renormalization scale μ can be chosen arbitrarily, the renormalized propagator $D_\sigma^{(R)}(p^2, \mu^2)$ satisfies the renormalization group equation

$$\begin{aligned} \left[\mu\frac{\partial}{\partial\mu} + \beta(a)\frac{\partial}{\partial a} + 2\gamma_\sigma(a)\right] D_\sigma^{(R)}(p^2, \mu^2) &= 0 \\ \beta(a) = \mu\frac{\partial a}{\partial\mu}|_{a_b,\Lambda:\text{fixed}}, \qquad \gamma_\sigma(a) &= \frac{1}{2}\mu\frac{\partial}{\partial\mu}(\ln Z_\sigma), \end{aligned} \tag{3.6}$$

where Z_σ is wave function renormalization constant of σ field and a_b denotes the bare coupling constant. Using the relation $a = a_b\sqrt{Z_\sigma}$, we can relate the beta function with the anomalous dimension as

$$\beta(g) = \mu\frac{\partial a}{\partial\mu}|_{a_b,\Lambda:\text{fixed}} = a_b\mu\frac{\partial}{\partial\mu}\sqrt{Z_\sigma} = a\gamma_\sigma(a). \tag{3.7}$$

Inserting the eqs.(3.5) and (3.7) into eq.(3.6), we obtain

$$\beta(a) = -\frac{a^3N}{2\pi}(< 0), \qquad \left(\gamma_\sigma(a) = -\frac{a^2N}{2\pi}\right). \tag{3.8}$$

Thus the Gross–Neveu model considered here has asymptotic freedom, which is a common property of various types of the Gross–Neveu models.

If we define $\bar{a}(a,t)$ as effective coupling constant renormalized at $p^2 = -\mu^2 e^{2t}$, it satisfies

$$\frac{d\bar{a}(a,t)}{dt} = \beta(\bar{a}), \qquad \bar{a}(a,0) = a. \tag{3.9}$$

Solving the eq.(3.9), we obtain

$$\bar{a}^2(a,t) = \frac{a^2}{1 + \frac{a^2 N}{\pi} t}. \tag{3.10}$$

As $t \to \infty$, the effective coupling constant $\bar{a}(a,t)$ decreases, which also indicates that the Gross–Neveu model has asymptotic freedom.

3.1.2 Dynamical chiral symmetry breaking

From eq.(3.10) we find that there is a tachyonic pole at

$$t = -\frac{\pi}{a^2 N} \qquad p^2 = -\mu^2 e^{-\frac{2\pi}{a^2 N}}, \tag{3.11}$$

for any value of coupling constant $a^2 N$. This indicates that we have constructed the theory about the *wrong* vacuum state and the pole in $\bar{a}^2$ is simply the signal for spontaneous symmetry breaking [1] .

In order to examine whether chiral symmetry is spontaneously broken or not we calculate the effective potential of the σ field. The effective potential is given by

$$V(\sigma) = \sum_{n=1}^{\infty} \frac{1}{n!} \Gamma^{(n)}(0, \cdots, 0) \sigma^n \tag{3.12}$$

where $\Gamma^{(n)}(0, \cdots, 0)$ is the sum of all one–particle irreducible Green's functions with n external σ lines carrying zero momentum. The leading terms for large N are given by the tree graphs plus all one–loop graphs. Summing up all the graphs in Fig. 3.1, we obtain

$$\begin{aligned} V(\sigma) &= \frac{1}{2}\sigma^2 - iN \sum_{n=1}^{\infty} \int_{-\infty}^{\infty} \frac{d^2k}{(2\pi)^2} \frac{1}{2n} \frac{(a_b^2 \sigma^2)^n}{(k^2 + i\epsilon)^n} \\ &= \frac{1}{2}\sigma^2 - \frac{a_b^2 N}{4\pi} \sigma^2 [\ln\Lambda^2 + 1 - \ln(a_b \sigma)^2], \end{aligned} \tag{3.13}$$

[1] This interpretation is correct only for the asymptotically free theories. In the case of infra–red stable theories such as ϕ^4 theory, they are simply nonsense at least in leading order of large N expansion.

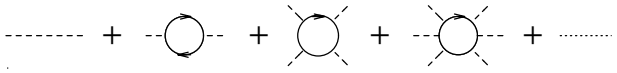

Figure 3.1: Feynman graphs which contribute to $V(\sigma)$ in leading order of large N expansion.

where Λ is an ultraviolet cut–off. Renormalizing under the condition $\frac{\partial^2 V^{(R)}}{\partial \sigma^2}|_{\sigma=\sigma_0} = 1$, the renormalized effective potential $V^{(R)}(\sigma)$ is obtained as

$$V^{(R)}(\sigma) = \frac{1}{2}\sigma^2 + \frac{a^2 N}{4\pi}\left[\ln\left(\frac{\sigma}{\sigma_0}\right)^2 - 3\right]. \tag{3.14}$$

By minimizing the potential, we have two candidate vacua $\sigma = \pm\sigma_0 \exp(1 - \frac{\pi}{a^2 N}) \equiv \pm\sigma_m$ ($V^{(R)}(\pm\sigma_m) = -\frac{a^2 N}{4\pi}\sigma_m^2$ (< 0)), which are *not* invariant under the chiral transformation $\sigma \to -\sigma$ (see Fig. 3.2) . Thus we see that the reason

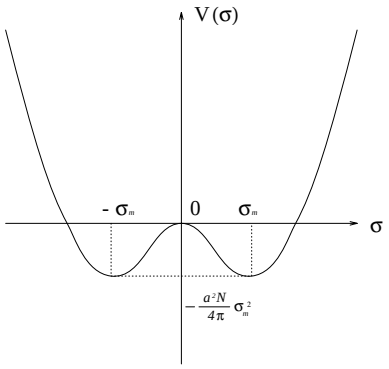

Figure 3.2: $V(\sigma)$ to leading order of large N expansion: Choosing one of the two minima, symmetry under $\sigma \to -\sigma$ is broken.

why we found a tachyon pole previously was that we were perturbing about a maximum of the potential. If we shift the σ field by nonvanishing vacuum expectation value, say $-\sigma_m$, the discrete chiral symmetry is broken and the fermion acquires a mass $M = a\sigma_m = a\sigma_0 \exp\left(1 - \frac{\pi}{a^2 N}\right)$. This spontaneous breaking of the discrete chiral symmetry occurs for any value of coupling constant a.

3.1.3 Dimensional transmutation

In the Lagrangian (3.1) there is only one dimensionless parameter a. The renormalization scale σ_0 is arbitrary and one convenient choice is to choose

σ_0 to coincide with the value of σ_m. In this case the fermion mass and four–Fermi coupling constant become

$$M = a\sigma_0 = \left(\frac{\pi}{N}\right)^{\frac{1}{2}} \sigma_0, \tag{3.15}$$

$$a^2 N = \pi. \tag{3.16}$$

With this choice of σ_0 it is manifest that the theory contains only one free parameter, say M or σ_0. We start with a theory of massless fermions which is determined by one dimensionless parameter a and end up with a theory determined by one dimensionful parameter σ_0 or M. This phenomenon is called dimensional transmutation, which is originally discovered in scalar QED [23].

3.2 The Gross–Neveu model with continuous chiral symmetry

In this section we consider the Gross–Neveu model with continuous chiral symmetry whose Lagrangian is given by

$$\mathcal{L} = \overline{\psi}^j i\partial\!\!\!/ \psi_j + \frac{a^2}{2}\left[\left(\overline{\psi}^j \psi_j\right)^2 - \left(\overline{\psi}^j \gamma_5 \psi_j\right)^2\right] \qquad j = 1, 2 \ldots, N. \tag{3.17}$$

The Lagrangian (3.17) is invariant under the continuous chiral transformation; $\psi \to e^{i\gamma_5\theta}\psi, \quad \bar{\psi} \to \bar{\psi} e^{i\gamma_5\theta}$.

Introducing auxiliary fields $\pi(x), \sigma(x)$, we can rewrite eq.(3.17) as

$$\mathcal{L} = \overline{\psi}^j i\partial\!\!\!/ \psi_j - \frac{1}{2}\left(\sigma^2 + \pi^2\right) + a\overline{\psi}^j \left(\sigma + i\pi\gamma_5\right)\psi_j \qquad j = 1, 2 \ldots, N. \tag{3.18}$$

In this form the continuous chiral transformation becomes

$$\psi \to e^{i\gamma_5\theta}, \quad \bar{\psi} \to \bar{\psi} e^{i\gamma_5\theta} \tag{3.19}$$

$$\begin{pmatrix} \sigma(x) \\ \pi(x) \end{pmatrix} \to \begin{pmatrix} \cos 2\theta & \sin 2\theta \\ -\sin 2\theta & \cos 2\theta \end{pmatrix} \begin{pmatrix} \sigma(x) \\ \pi(x) \end{pmatrix}. \tag{3.20}$$

The basic features of this model are common with those of the discrete model that we discussed in section 3.1. Here we comment on some additional features whose origin is in continuous symmetries.

3.2.1 Spontaneous breaking of continuous symmetry and Goldstone theorem

As in section 3.1.2, we calculate the effective potential of σ and π field to examine whether continuous chiral symmetry is broken or not.

Owing to the chiral symmetry we have only to replace σ^2 by $\rho^2(\equiv \sigma^2+\pi^2)$. The effective potential is

$$V^{(R)}(\rho) = \frac{1}{2}\rho^2 + \frac{a^2 N}{4\pi}\left[\ln\left(\frac{\rho}{\rho_0}\right)^2 - 3\right]. \tag{3.21}$$

Here we renormalize the potential under the renormalization condition $\frac{\partial^2 V^{(R)}}{\partial \rho^2}|_{\rho=\rho_0} = 1$. By minimizing the potential (3.21) we obtain continuum of vacua (σ_m, π_m), $\sigma_m^2 + \pi_m^2 = \rho_0^2 \exp\left(2 - \frac{2\pi}{a^2 N}\right) \equiv \rho_m^2$, where the potential has its minimum $V^{(R)}(\rho^2 = \rho_m^2) = -\frac{a^2 N}{4\pi}\rho_m^2 (< 0)$. The chiral symmetry is broken spontaneously by choosing one out of the continuous vacua (see Fig. 3.3). Choosing the π field to remain with vanishing vacuum expectation

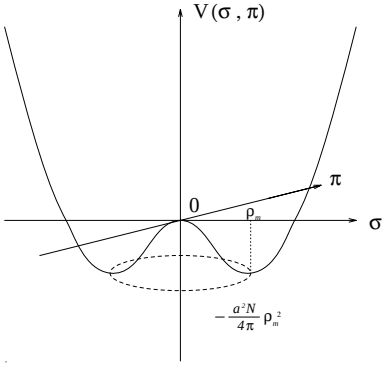

Figure 3.3: The effective potential to leading order in large N expansion; by choosing a vacuum, symmetry under the rotation in (σ, π) plane is broken.

value, the ground state can be taken as

$$\sigma = -\rho_0 \exp\left(1 - \frac{\pi}{a^2 N}\right), \quad \pi = 0, \tag{3.22}$$

and perturbation theory can be derived by shifting the σ field by this amount. The fermion dynamically acquires a mass $M = a\rho_0 \exp\left(1 - \frac{\pi}{a^2 N}\right)$ again.

According to the Goldstone theorem[72], there should be massless particles in the physical spectrum if some continuous symmetry is spontaneously broken. It will be seen that there exists a massless particle in pseudoscalar channel, which just corresponds to "pion" (see section 3.2.3, 4.3 and 7.3).

3.2.2 Some remarks on the Coleman theorem

In general, it is known as Coleman theorem that due to the untamable infrared divergences associated with massless particles in $(1+1)$ dimensions a sensible theory cannot possess Goldstone bosons; thus continuous symmetry cannot be broken spontaneously in two dimensional systems[24]. The existence of the massless π field seems to contradict the Coleman theorem, however in fact it is true if we were to calculate to higher order in large N expansion.

Here we are of the opinion that the model discussed above exhibits features of dynamical symmetry breaking that would be present in four–dimensional models particularly asymptotically free ones like QCD. In fact it is well known that $1+1$ dimensional models in large N expansion shows similar physical behavior with those in higher dimensions. It was argued in [25] that analysis with large N expansion is valid in the two dimensional Gross–Neveu model ($SU(N)$ Thirring model).

3.2.3 The bound state of the massless Gross–Neveu model

In the next chapter and section 7.3 we will discuss the bound state problem of more general type of the Gross–Neveu model. Information on the bound state of the original Gross–Neveu model can be obtained as some special limit of more general model. Hence we only comment on the well-known fact here.

In the case of the massless Gross–Neveu model, there are two bound states that are called σ and π. The π is just the massless Nambu–Goldstone boson accompanied with spontaneously broken chiral symmetry, while the mass of the σ is at the threshold; *i.e.* $\mu_\sigma^2 = 4M^2$. If no pseudoscalar coupling exists as in section 3.1, only the σ bound state exists[22, 26, 27].

Chapter 4

The Massive Gross-Neveu model: the Bethe-Salpeter approach

In this chapter we will discuss the massive Gross–Neveu model, which gives more realistic model describing "pion" with relatively small but nonzero mass. Inspired by the fact that the large N expansion is used for both the 't Hooft and Gross–Neveu models, we will analyze the bound states of the massive Gross–Neveu model by solving the Bethe-Salpeter equation[32].

4.1 The equation for the "meson" bound states

The Lagrangian of the Massive Gross–Neveu model is given by

$$\mathcal{L} = \overline{\psi}^j \left(i\partial\!\!\!/ - m\right)\psi_j + \frac{a^2}{2}\left[\left(\overline{\psi}^j\psi_j\right)^2 - \left(\overline{\psi}^j\gamma_5\psi_j\right)^2\right] \qquad j = 1, 2\ldots, N. \quad (4.1)$$

This is equivalent to the following Lagrangian written using the auxiliary real scalar fields σ, π,

$$\mathcal{L} = \overline{\psi}^j i\partial\!\!\!/\psi_j - \frac{1}{2}\left(\sigma^2+\pi^2\right) + a\overline{\psi}^j\left(\sigma + i\pi\gamma_5\right)\psi_j - \frac{m}{a}\sigma \qquad j = 1, 2\ldots, N. \quad (4.2)$$

The Gross–Neveu model has the global symmetry $SU(N)_V \times U(1)_L \times U(1)_R$ when $m = 0$. The symmetry transformations act on the fields as [denoting $\psi_{L,R} \equiv \frac{1}{2}\left(1 \pm \gamma_5\right)\psi$]

$$\begin{aligned} \psi_{Lj} &\mapsto e^{i\alpha_L} U^k_j \psi_{Lk}, \qquad \psi_{Rj} \mapsto e^{i\alpha_R} U^k_j \psi_{Rk}, \\ \left(\sigma + i\pi\right) &\mapsto e^{i(\alpha_R - \alpha_L)}\left(\sigma + i\pi\right), \qquad \alpha_{L,R} \in \mathbf{R}, \quad U \in SU(N). \end{aligned} \quad (4.3)$$

When $m \neq 0$, the axial $U(1)$ symmetry does not exist and the model has the symmetry $SU(N)_V \times U(1)_V$. Chiral symmetry, when it exists, is spontaneously broken in the full quantum theory, as we shall see below. The index j runs over the fermion "flavors" in this model; however, since this "flavor" group will be gauged in the sequel, we shall reserve the term "flavor" for a different purpose.

From the interactions in the Lagrangian (4.1) we obtain a self consistent equation for the propagator in the large N limit. As is clear from the interactions, these corrections do *not* have any momentum dependence. Therefore, it can be effectively summarized in a mass parameter, which we shall call M. The fermions in this model are physical particles and the parameter M is the physical mass of these fermions, which will be determined self consistently. Using the full propagator, we may straightforwardly obtain the

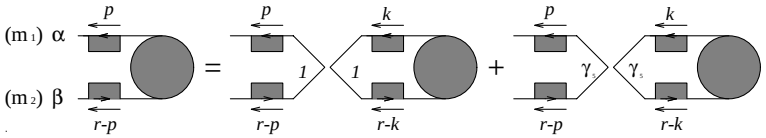

Figure 4.1: Bound state equation for the fermion–antifermion system in the Gross–Neveu model.

Bethe–Salpeter equation for what we shall call the "meson wavefunction", $\tilde{\psi}_{\alpha\beta}$, from the contributions graphically represented in Fig. 4.1 as:

$$\begin{aligned}\tilde{\psi}_{\alpha\beta}(p,r) &= 2a_b^2 N S_{\alpha 1}(p) S_{1\beta}(p-r) \int \frac{d^2k}{(2\pi)^2}\, \tilde{\psi}_{22}(k,r) \\ &\quad + 2a_b^2 N S_{\alpha 2}(p) S_{2\beta}(p-r) \int \frac{d^2k}{(2\pi)^2}\, \tilde{\psi}_{11}(k,r). \qquad (4.4)\end{aligned}$$

$S(p)$ is the full fermion propagator in this model, which is none other than the tree–level propagator with the mass m replaced by M. a_b denotes the *bare* four–Fermi coupling. Following 't Hooft, we integrate over one component of the momentum p_+ and define $\tilde{\varphi}_{\alpha\beta} \equiv \int dp_+ \tilde{\psi}_{\alpha\beta}$. Then, after some computation (see appendix A), the equations for the meson wavefunction $\tilde{\psi}_{\alpha\beta}$ reduce to the following equations for the components:

$$\begin{aligned}\frac{2\pi}{a_b^2 N}\left[\tilde{\mu}^2 - \frac{1}{x(1-x)}\right]\tilde{\varphi}_{11}(x) = &-\frac{1}{2(1-x)}\left[\tilde{\mu}^2 - \frac{1}{x} + \frac{1}{1-x}\right]\int_0^1 dy \tilde{\varphi}_{11}(y) \\ &+ \frac{1}{x(1-x)}\int_0^1 dy\, \tilde{\varphi}_{22}(y)\end{aligned}$$

$$\frac{2\pi}{a_b^2 N}\left[\tilde{\mu}^2-\frac{1}{x(1-x)}\right]\tilde{\varphi}_{22}(x)=-\frac{1}{2x}\left[\tilde{\mu}^2+\frac{1}{x}-\frac{1}{1-x}\right]\int_0^1 dy\,\tilde{\varphi}_{22}(y)$$
$$+\frac{1}{x(1-x)}\int_0^1 dy\,\tilde{\varphi}_{11}(y)$$
$$\frac{2\pi}{a_b^2 N}\frac{M}{\sqrt{2}r_-}\left[\tilde{\mu}^2-\frac{1}{x(1-x)}\right]\tilde{\varphi}_{12}(x)=\frac{1}{1-x}\int_0^1 dy\,\tilde{\varphi}_{11}(y)-\frac{1}{x}\int_0^1 dy\,\tilde{\varphi}_{22}(y)$$
$$\frac{2\pi}{a_b^2 N}\frac{\sqrt{2}r_-}{M}\left[\tilde{\mu}^2-\frac{1}{x(1-x)}\right]\tilde{\varphi}_{21}(x)=-\frac{1}{2x(1-x)}\left[\tilde{\mu}^2-\frac{1}{x}+\frac{1}{1-x}\right]\int_0^1 dy\tilde{\varphi}_{11}(y)$$
$$+\frac{1}{2x(1-x)}\left[\tilde{\mu}^2+\frac{1}{x}-\frac{1}{1-x}\right]\int_0^1 dy\tilde{\varphi}_{22}(y). \tag{4.5}$$

Here, we defined the momentum fraction of the incoming antifermion $x \equiv p_-/r_-$ and the mass squared of the bound state in units of the fermion mass squared as $\tilde{\mu}^2 = 2r_+r_-/M^2$. Without any loss of generality, we may define $\int dx\tilde{\varphi}_{11} = 1$, $\int dx\tilde{\varphi}_{22} = C$, where C is to be determined later. Then all the meson wavefunctions $\tilde{\varphi}_{\alpha\beta}$ may be solved algebraically using the equations (4.5) as follows. The consistency with the normalization of $\tilde{\varphi}_{11}$ requires that

$$\frac{4\pi}{a_b^2 N} = \int_0^1 dx\,\frac{\frac{\tilde{\mu}^2}{2}-2C-2+\frac{1}{2x(1-x)}}{1-\tilde{\mu}^2 x(1-x)}. \tag{4.6}$$

The compatibility of this with the normalization condition for $\tilde{\varphi}_{22}$ requires that $C = \mp 1$. These two cases correspond to the meson states π and σ respectively. We obtain the equations determining the masses of π and σ as

$$\pi : \frac{4\pi}{a^2 N} = \int_0^1 dx\,\frac{\tilde{\mu}_\pi^2}{1-\tilde{\mu}_\pi^2 x(1-x)}, \quad \sigma : \frac{4\pi}{a^2 N} = \int_0^1 dx\,\frac{\tilde{\mu}_\sigma^2-4}{1-\tilde{\mu}_\sigma^2 x(1-x)}. \tag{4.7}$$

Here, we renormalized the coupling constant as

$$\frac{4\pi}{a^2 N} = \frac{4\pi}{a_b^2 N} - \frac{1}{2}\int_0^1 dx\,\frac{1}{x(1-x)}. \tag{4.8}$$

The integral needs to be regularized at the endpoints $0, 1$ which is not explicitly expressed here. The same renormalization was employed in the light front Hamiltonian approach in ref.[29]. This regularization is effectively an ultraviolet cutoff, which will become clear below. The meson wavefunctions for π, σ can also be obtained algebraically as

$$\pi : \tilde{\varphi}_{12}^{\pi}(x) = \text{const.}\times\frac{1}{1-\tilde{\mu}_\pi^2 x(1-x)}, \quad \sigma : \tilde{\varphi}_{12}^{\sigma}(x) = \text{const.}\times\frac{1-2x}{1-\tilde{\mu}_\sigma^2 x(1-x)}. \tag{4.9}$$

The component $\tilde{\varphi}_{12}$ is shown here since it corresponds to the relevant component of the meson wavefunction in the 't Hooft model [19, 20] and will also be the essential component in our analysis of the gauged four–Fermi model (see section 5.2.2). The wavefunction for π is consistent with the results obtained using light front Hamiltonian methods [29, 30]. Other components of the wavefunction can also be computed algebraically using eqs.(4.5).

4.2 The analysis of the Gross–Neveu model using scalars and its relation to the Bethe–Salpeter equation

In this section, we clarify the relation between the results obtained above using the Bethe–Salpeter equation and the results obtained from using the auxiliary scalar fields σ, π as in the Lagrangian (4.2). Calculating the one–particle irreducible graph with only one fermion loop, and summing up all the series, we obtain full propagator for scalar fields. (This calculation is essentially the same with that in section 3.1.1 except that the fermionic fields have physical mass M.)

The full propagators for the σ, π fields are [22]

$$\begin{aligned} \sigma: \qquad D_\sigma^{-1}(p^2) &= 1 + \frac{a_b^2 N}{2\pi}\left[\ln\frac{M^2}{\Lambda^2} + B(p^2, M^2)\right] \\ \pi: \qquad D_\pi^{-1}(p^2) &= 1 + \frac{a_b^2 N}{2\pi}\left[\ln\frac{M^2}{\Lambda^2} + \frac{1}{1-4M^2/p^2}B(p^2, M^2)\right] \end{aligned} \tag{4.10}$$

where the a_b is the bare coupling and Λ is the ultraviolet momentum scale cutoff. (There is a mild abuse of notation here; this bare coupling is in principle not the same as the one in the previous section since the regularization methods are different.) The function $B(p^2, M^2)$ is defined as

$$\begin{aligned} B(p^2, M^2) &\equiv \sqrt{1-4M^2/p^2}\ln\frac{\sqrt{1-4M^2/p^2}+1}{\sqrt{1-4M^2/p^2}-1} \\ &= 2\sqrt{4M^2/p^2-1}\cot^{-1}\sqrt{4M^2/p^2-1}. \end{aligned} \tag{4.11}$$

The renormalized coupling a defined in eq.(4.8) is related to the bare coupling a_b here as

$$\frac{2\pi}{a^2 N} = \frac{2\pi}{a_b^2 N} + \ln\frac{M^2}{\Lambda^2}. \tag{4.12}$$

We find that the equations for the poles in the propagators for σ, π in (4.10) indeed agree with the equations (4.7) in this renormalization scheme. The

propagators have cuts for $p^2 > 4M^2$ corresponding to the production of physical fermion–antifermion pair of mass M each.

As in section 3.1.2 and section 3.2.1 the effective potential for the scalars may be obtained by computing the contributions from the fermion loops in the large N limit as

$$V(\sigma,\pi) = \frac{1}{2}\left(\sigma^2+\pi^2\right) - \frac{m}{a_b}\sigma + \frac{a_b^2 N}{4\pi}\left(\sigma^2+\pi^2\right)\left(\ln\frac{a_b^2\left(\sigma^2+\pi^2\right)}{\Lambda^2} - 1\right). \quad (4.13)$$

By minimizing the potential, we obtain a vacuum expectation value $\langle\sigma\rangle$ for σ. The physical mass is related to the vacuum expectation value simply as $M = a_b\langle\sigma\rangle$, without loss of generality. We obtain a relation between the bare and the renormalized parameters

$$\frac{M}{a^2 N} = \frac{m}{a_b^2 N}. \quad (4.14)$$

Since the mass is dynamically generated in the Gross–Neveu model even when $m = 0$, the chiral limit corresponds to $a^2 N \to \infty$.

4.3 Physics of the Gross–Neveu model

Here, we briefly summarize the physics of the Gross–Neveu model, in particular, emphasizing the salient features and its underlying physics which will be useful later on. The Lagrangian (4.1) has two parameters, m and a. Due to dimensional transmutation, the model is determined essentially by only one parameter. We can solve the equations (4.7) or the pole equations of the propagators (4.10) to obtain the masses of the scalars σ, π. We plot the spectrum of σ, π against the inverse coupling in Fig. 4.2. We understand the various regions in the coupling constant as follows:

1. $1/a^2 N = 0$: The chiral point. Here, the masses for σ and π are respectively $2M$ and zero. The wavefunction for π, $\tilde{\varphi}^{\pi}_{12}(x)$, is a constant in this limit, similarly to the 't Hooft model. π is the "Nambu–Goldstone" boson of the theory. Strictly speaking, Nambu–Goldstone boson does not exist in $(1+1)$ dimensions (see section 3.2.2 and ref.[24]), yet it is well known that many physical aspects of the higher dimensional theories are also seen in $(1+1)$ dimensional theories, especially in the large N limit. A similar massless boson bound state exists in the 't Hooft model in the chiral limit.

   The status of the σ particle is interesting; while the σ particle is usually said to exist, its wavefunction $\tilde{\varphi}^{\sigma}_{12}(x)$ approaches const./$(1-2x)$ and

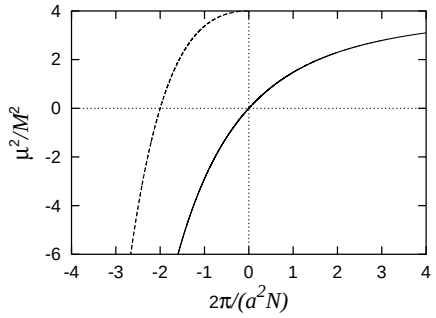

Figure 4.2: Mass squared of π (solid) and σ (dashed) in units of M^2 versus the inverse coupling $2\pi/(a^2N)$.

is singular in the limit $1/a^2N \to 0$. Physical decay into a fermion and an antifermion becomes kinematically allowed in this limit $\mu^2 \to 4M^2$ and the singular behavior is due to this. Similar behavior is also seen for π in the limit $\mu^2 \to 4M^2$. The wavefunction is well behaved when $a^2N < 0$, yet in this region, the vacuum is not physically stable, as explained below.

2. $a^2N > 0$: This region is physically consistent. The mass of π is between zero and $2M$. The meson wavefunction has a singular limit $\tilde{\varphi}^{\pi}_{12} \to$const.$\times(1-2x)^{-2}$ as $1/a^2N \to \infty$. The pole in the σ propagator (4.7) that exists for $a^2N \leq 0$ ceases to exist in this regime and there is no bound state corresponding to σ. Poles corresponding to resonance states also do not exist, unlike the Gross–Neveu model in $(2+1)$–dimensions[27].

3. $a^2N \leq -\pi$: While σ scalar has a finite mass, π is tachyonic. From the potential, we may understand this as follows; we are at an unstable vacuum where the potential is locally a minimum in the σ direction yet *maximal* in the π direction. Choosing the physically sensible vacuum reduces this case to the previous physically consistent case.

4. $-\pi < a^2N < 0$: We again have chosen an unstable vacuum. this vacuum is unstable in both σ and π directions so that both σ, π are tachyonic. Had the correct vacuum been chosen, the theory reduces to the $a^2N > 0$ case above.

We plot the potential for these various cases in Fig. 4.3 along the plane $\pi = 0$.

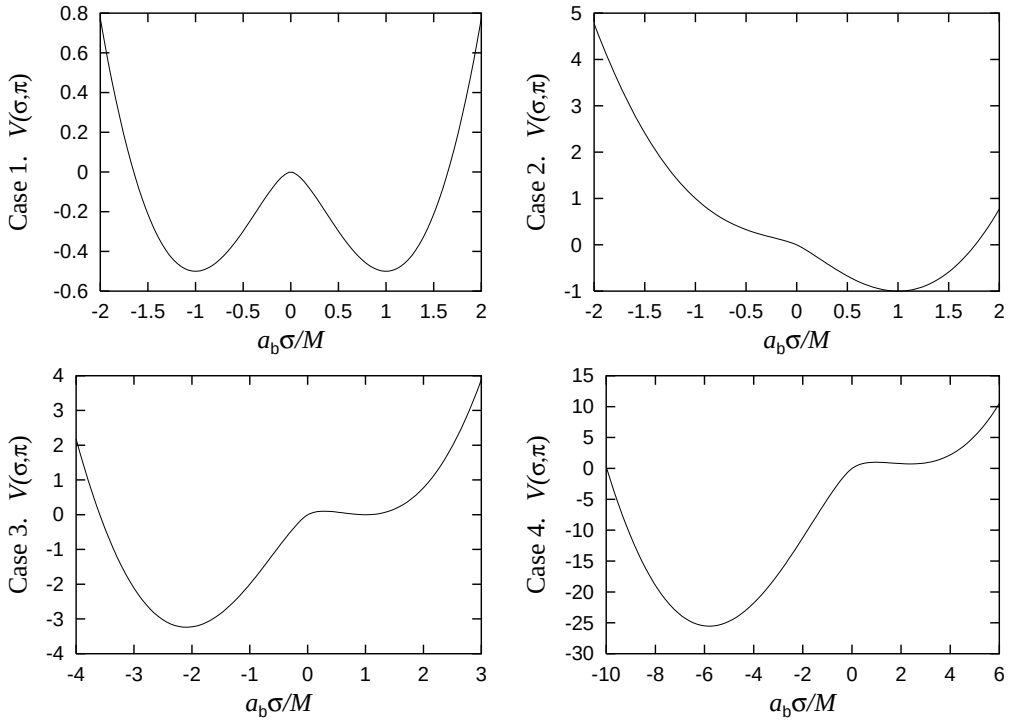

Figure 4.3: The potential for the massive Gross–Neveu model in the σ–plane. $a_b\sigma = M$ is the "vacuum" we choose. An example is given for the each of the four cases 1—4 explained in the text. The values chosen are $(2\pi)/a^2N = 0, 1, -1$ and -3, respectively. Vertical scale is in units of $NM^2/2\pi$.

Chapter 5

The gauged four-Fermi model

In this chapter, we will deal with the gauged four-Fermi model[32, 79]. Naively this model combines and generalizes the 't Hooft model and the Gross–Neveu model and it reduces to them as a special limit of the parameter space. As in the previous chapters, we will use the Bethe–Salpeter approach to derive analytic equations for the mesonic states. Then methods are presented in detail for solving the mesonic state equations systematically. Using these methods, we derive various results on the physical properties of the model.

5.1 The model

The Lagrangian of the model is given by

$$\begin{aligned}\mathcal{L} &= -\frac{1}{2}\,\mathrm{tr}\,(F_{\mu\nu}F^{\mu\nu}) + \sum_{f=1}^{N_f}\overline{\psi}_f(i\not{D} - m_f)\psi_f \\ &\quad + \frac{a^2}{2}\sum_{f,f'=1}^{N_f}(\overline{\psi_{f'}}\psi_f)(\overline{\psi_f}\psi_{f'}) - \frac{a_5^2}{2}\sum_{f,f'=1}^{N_f}(\overline{\psi_{f'}}\gamma_5\psi_f)(\overline{\psi_f}\gamma_5\psi_{f'}). \qquad (5.1)\end{aligned}$$

The $SU(N)$ symmetry in the Gross–Neveu model (4.1), (4.2) has been gauged and the covariant derivative is defined as $D_\mu \equiv \partial_\mu - igA_\mu$, where g is the gauge coupling constant. The color couplings in the four–Fermi terms are identical to those in the Gross–Neveu model and the color indices have been suppressed in the formula. Index f is the "flavor" index with a flavor coupling such that color singlets need *not* be flavor singlets. Flavor has been incorporated into the model since we shall consider bound states involving fermions of different masses. The motivations for such a generalization is obvious when we want to

apply the model to more realistic situations (for example, see chapter 7). Had the flavor summation been in the same channel as in the color summation, all color singlets would have been flavor singlets, which would have lead to a less interesting model for our purposes. The Lagrangian generically respects the global flavor symmetry $[U(1)_V]^N$, which is enlarged to $SU(N)_V \times U(1)_V$ when all the fermion masses m_f are the same. This symmetry is further enlarged to the chiral flavor symmetry $SU(N)_L \times U(1)_L \times SU(N)_R \times U(1)_R$ when all $m_f = 0$.

We obtain the 't Hooft model with both of the four–Fermi couplings off. The Gross–Neveu model we dealt with in the previous chapter corresponds to the case when there is no gauge coupling, only a single flavor type and $a^2 = a_5^2$.

Both the Gross–Neveu model and the 't Hooft model have been used extensively in the literature to understand the physical behavior of real systems, such as QCD. A model that combines the two models should be quite useful for understanding the dynamics of various field theories. In one direction, the four– Fermi coupling has been used to model strong interaction dynamics involving dynamical symmetry breaking for quite some time [39, 40, 41]. By interpolating between these two models, we intend to shed more light on the relation between the physical behavior of these two theories. Furthermore, when dynamical symmetry breaking scales are widely separated, in the intermediate energy range, the theory effectively becomes a gauged four–Fermi model. Such situations can occur quite generally where the lower energy scale is the QCD scale or some technicolor scale. These types of theories are of phenomenological interest and have been studied actively, for instance, in the so called "top quark condensation" models [39]–[46]. Admittedly, the model we studied is a $(1+1)$ dimensional toy model version of such theories. Historically, however, $(1+1)$ dimensional theories have played an important role in understanding of the corresponding higher dimensional theories and we hope this will also be true in the future.

5.2 The derivation of the bound state equation

5.2.1 The Schwinger–Dyson equation

First, we obtain the full propagator self consistently from the Schwinger–Dyson equation as in section 2.3. The situation is somewhat more complicated than that in section 2.3 because of the additional four–Fermi interactions. Diagrammatically, the Schwinger–Dyson equation may be ex-

pressed as in Fig. 5.1 in the large N limit. Only one flavor contributes

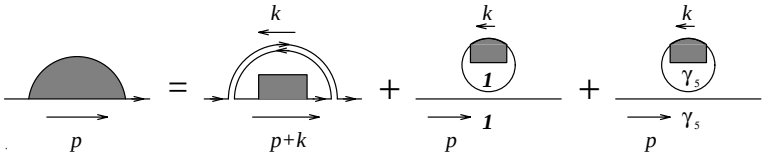

Figure 5.1: The self consistent equation for the propagator in the gauged four–Fermi model.

to the equation due to the manner the fermions of the different flavor are coupled in eq.(5.1). From the form of the interactions we can write the self–energy part $\Gamma(p)$, which appears in the left–hand side of the Fig. 5.1, as $\Gamma(p)\equiv\gamma^+\Gamma_+(p) + \mathbf{1}\Gamma_1(p) + \gamma_5\Gamma_5(p)$. Summing up all the series of the self–energy parts the full propagator $S(p)$ is obtained

$$S(p) = (-i)\frac{(m + i\Gamma_1(p))\,\mathbf{1} + \gamma^+\,(p_+ - i\Gamma_+(p)) + \gamma^- p_- i - \gamma_5\Gamma_5(p)}{(m + i\Gamma_1(p))^2 - 2p_-\,(p_+ - i\Gamma_+(p)) + \Gamma_5(p)^2 - i\epsilon}, \quad (5.2)$$

where $\Gamma_1(p)$, $\Gamma_5(p)$ and $\Gamma_+(p)$ satisfy the following equations;

$$\begin{aligned}
\Gamma_1(p)=&-2a^2N\int_{-\infty}^{\infty}\frac{d^2k}{(2\pi)^2}\frac{m + i\Gamma_1(k)}{(m + i\Gamma_1(k))^2 - 2k_-\,(k_+ - i\Gamma_+(k)) + \Gamma_5(k)^2 - i\epsilon}\\
\Gamma_5(p)=&2a_5^2N\int_{-\infty}^{\infty}\frac{d^2k}{(2\pi)^2}\frac{-i\Gamma_5(k)}{(m + i\Gamma_1(k))^2 - 2k_-\,(k_+ - i\Gamma_+(k)) + \Gamma_5(k)^2 - i\epsilon}\\
\Gamma_+(p)=&-\frac{2g^2N}{(2\pi)^2}\int_{-\infty}^{\infty}\frac{d^2k}{k_-^2}\\
&\times\frac{p_- + k_-}{(m+i\Gamma_1(p+k))^2 - 2\,(p_- + k_-)(p_+ + k_+ - i\Gamma_+(p+k)) + \Gamma_5(p+k)^2 - i\epsilon}.
\end{aligned} \quad (5.3)$$

Solving the equation (5.3), the self–energy parts are obtained as

$$\Gamma_1(p) = \text{const}, \quad \Gamma_5(p) = 0, \quad \Gamma_+(p_-) = -\frac{g^2Ni}{2\pi}\left(\frac{\text{sgn}(p_-)}{\lambda} - \frac{1}{p_-}\right), \quad (5.4)$$

where we introduced a cutoff λ_- for the infrared divergence in p_- integral. Finally we obtain the full propagator $S(p; M_f)$ as

$$S^{-1}(p; M_f) = -i\left[\not{p} - M_f + i\epsilon + \frac{g^2N}{2\pi}\left(\frac{\text{sgn}(p_-)}{\lambda_-} - \frac{1}{p_-}\right)\gamma^+\right], \quad (5.5)$$

where M_f is the mass of quarks containing the quantum corrections as in the case of the Gross–Neveu models.

5.2.2 The Bethe–Salpeter equation

The bound state equation for fermion–antifermion bound state may be derived in the large N limit, which is diagrammatically depicted in Fig. 5.2. Denoting the wavefunction of the bound state as $\psi_{\alpha\beta}(p,r)$, the Bethe–

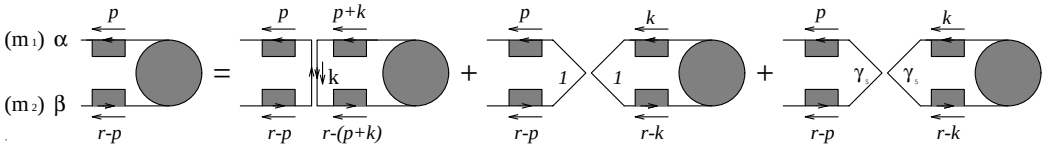

Figure 5.2: The bound state equation for the fermion–antifermion system in the gauged four–Fermi model.

Salpeter equation can be derived as the following matrix equation in the large N limit

$$\begin{aligned}
\psi(p,r) &= -i2g^2 N\, S(p;M_1)\gamma^+ \int \frac{d^2k}{(2\pi)^2}\,\psi(p+k,r)\gamma^+ S(p-r;M_2)\frac{1}{k_-^2} \\
&- ia_b^2 N\, S(p;M_1)S(p-r;M_2)\int \frac{d^2k}{(2\pi)^2}\ \mathrm{tr}\,\psi(k,r) \\
&+ ia_{5b}^2 N S(p;M_1)\gamma_5 S(p-r;M_2)\int \frac{d^2k}{(2\pi)^2}\ \mathrm{tr}\ (\gamma_5\psi(k,r))\,. \qquad (5.6)
\end{aligned}$$

The suffix b on the couplings indicates that these couplings are bare parameters. We define, as in section 2.4, $\varphi_{\alpha\beta}(p_-,r)\equiv\int_{-\infty}^{\infty} dp_+\psi_{\alpha\beta}(p,r)$. Integrating the eq.(5.6) over the p_+ space, (see appendix A) the bound state equations may be obtained for the components as

$$\begin{aligned}
&\left(\mu^2 - \frac{2r_-}{\lambda_-} - \frac{\beta_1-1}{x} - \frac{\beta_2-1}{1-x}\right)\varphi_{11}(x) \\
&= \frac{M_2}{\sqrt{2}r_-(1-x)}\left(\frac{2r_-}{\lambda_-}\varphi_{12}(x) + P\int_0^1 dy\frac{\varphi_{12}(y)}{(x-y)^2}\right) \\
&\quad + \frac{a_b^2 N}{2\pi}\frac{1}{4x(1-x)}\left[2\sqrt{\beta_1\beta_2} - x\left(\mu^2 - \frac{2r_-}{\lambda_-} - \frac{\beta_1-1}{x} - \frac{-\beta_2-1}{1-x}\right)\right] \\
&\qquad \times\int_0^1 dy[\varphi_{11}(y)+\varphi_{22}(y)] \\
&\quad - \frac{a_{5b}^2 N}{2\pi}\frac{1}{4x(1-x)}\left[2\sqrt{\beta_1\beta_2} + x\left(\mu^2 - \frac{2r_-}{\lambda_-} - \frac{\beta_1-1}{x} - \frac{-\beta_2-1}{1-x}\right)\right] \\
&\qquad \times\int_0^1 dy[\varphi_{11}(y)-\varphi_{22}(y)] \qquad (5.7)
\end{aligned}$$

$$
\begin{aligned}
&\left(\mu^2-\frac{2r_-}{\lambda_-}-\frac{\beta_1-1}{x}-\frac{\beta_2-1}{1-x}\right)\varphi_{22}(x)\\
&\quad=-\frac{M_1}{\sqrt{2}r_-x}\left(\frac{2r_-}{\lambda_-}\varphi_{12}(x)+P\int_0^1 dy\,\frac{\varphi_{12}(y)}{(x-y)^2}\right)\\
&+\frac{a_b^2N}{2\pi}\frac{1}{4x(1-x)}\left[2\sqrt{\beta_1\beta_2}-(1-x)\left(\mu^2-\frac{2r_-}{\lambda_-}-\frac{-\beta_1-1}{x}-\frac{\beta_2-1}{1-x}\right)\right]\\
&\qquad\qquad\times\int_0^1 dy\,[\varphi_{11}(y)+\varphi_{22}(y)]\\
&+\frac{a_{5b}^2N}{2\pi}\frac{1}{4x(1-x)}\left[2\sqrt{\beta_1\beta_2}+(1-x)\left(\mu^2-\frac{2r_-}{\lambda_-}-\frac{-\beta_1-1}{x}-\frac{\beta_2-1}{1-x}\right)\right]\\
&\qquad\qquad\times\int_0^1 dy\,[\varphi_{11}(y)-\varphi_{22}(y)]
\end{aligned}
\tag{5.8}
$$

$$
\begin{aligned}
&\left(\mu^2-\frac{\beta_1-1}{x}-\frac{\beta_2-1}{1-x}\right)\varphi_{12}(x)\\
&\quad=-P\int_0^1 dy\frac{\varphi_{12}(y)}{(x-y)^2}-\frac{M_1(1-x)-M_2x}{2\sqrt{2}x(1-x)}\frac{a_b^2r_-}{g^2}\int_0^1 dy\,[\varphi_{11}(y)+\varphi_{22}(y)]\\
&\quad+\frac{M_1(1-x)+M_2x}{2\sqrt{2}x(1-x)}\frac{a_{5b}^2r_-}{g^2}\int_0^1 dy\,[\varphi_{11}(y)-\varphi_{22}(y)]
\end{aligned}
\tag{5.9}
$$

$$
\begin{aligned}
&\left(\mu^2-\frac{2r_-}{\lambda_-}-\frac{\beta_1-1}{x}-\frac{\beta_2-1}{1-x}\right)\varphi_{21}(x)\\
&\quad=\frac{M_1M_2}{2r_-^2x(1-x)}\left(\frac{2r_-}{\lambda_-}\varphi_{12}(x)+P\int_0^1 dy\frac{\varphi_{12}(y)}{(x-y)^2}\right)\\
&\quad+\frac{a_b^2N}{2\pi}\frac{1}{4\sqrt{2}x(1-x)}\Big[-\left(\mu^2-\frac{2r_-}{\lambda_-}-\frac{\beta_1-1}{x}-\frac{-\beta_2-1}{1-x}\right)\frac{M_1}{r_-}\\
&\qquad+\left(\mu^2-\frac{2r_-}{\lambda_-}-\frac{-\beta_1-1}{x}-\frac{\beta_2-1}{1-x}\right)\frac{M_2}{r_-}\Big]\int_0^1 dy\,[\varphi_{11}(y)+\varphi_{22}(y)]\\
&\quad-\frac{a_{5b}^2N}{2\pi}\frac{1}{4\sqrt{2}x(1-x)}\Big[\left(\mu^2-\frac{2r_-}{\lambda_-}-\frac{\beta_1-1}{x}-\frac{-\beta_2-1}{1-x}\right)\frac{M_1}{r_-}\\
&\qquad+\left(\mu^2-\frac{2r_-}{\lambda_-}-\frac{-\beta_1-1}{x}-\frac{\beta_2-1}{1-x}\right)\frac{M_2}{r_-}\Big]\int_0^1 dy\,[\varphi_{11}(y)-\varphi_{22}(y)]\,.
\end{aligned}
\tag{5.10}
$$

Here we defined

$$
\beta_i\equiv\pi\frac{M_i^2}{g^2N},\quad \mu^2\equiv\frac{\pi 2r_+r_-}{g^2N},\quad x\equiv\frac{p_-}{r_-},\quad y\equiv\frac{k_-}{r_-},
\tag{5.11}
$$

and $P\int$ denotes the principal part integral. When the four–Fermi couplings a^2, a_5^2 are absent, the equation (5.9) is the 't Hooft equation (2.24), which is a closed equation by itself. Here, all the equations are coupled and they need to be disentangled in a more sophisticated manner.

Superficially, we have as many equations as the unknowns — the meson wavefunctions, $\varphi_{\alpha\beta}$'s. However, we expect the infrared cutoff λ_- to decouple from these physical equations, so that these equations are possibly over–constrained. It may be shown that all these equations consistently reduce to the following equations (5.12)—(5.14) and (5.9). These equations do *not* involve the infrared cutoff but are yet to be renormalized:

$$\varphi_{11}(x) = \frac{-M_2}{\sqrt{2}r_-(1-x)}\varphi_{12}(x) - \frac{1}{4(1-x)}\frac{a_b^2 N}{2\pi}\int_0^1 dy[\varphi_{11}(y)+\varphi_{22}(y)] - \frac{1}{4(1-x)}\frac{a_{5b}^2 N}{2\pi}\int_0^1 dy[\varphi_{11}(y)-\varphi_{22}(y)] \tag{5.12}$$

$$\varphi_{22}(x) = \frac{M_1}{\sqrt{2}r_- x}\varphi_{12}(x) - \frac{a_b^2 N}{2\pi}\frac{1}{4x}\int_0^1 dy\,[\varphi_{11}(y)+\varphi_{22}(y)] + \frac{a_{5b}^2 N}{2\pi}\frac{1}{4x}\int_0^1 dy\,[\varphi_{11}(y)-\varphi_{22}(y)] \tag{5.13}$$

$$\varphi_{21}(x) = -\frac{M_1 M_2}{2r_-^2 x(1-x)}\varphi_{12}(x) - \frac{M_1-M_2}{4\sqrt{2}r_- x(1-x)}\frac{a_b^2 N}{2\pi}\int_0^1 dy[\varphi_{11}(y)+\varphi_{22}(y)] - \frac{M_1+M_2}{4\sqrt{2}r_- x(1-x)}\frac{a_{5b}^2 N}{2\pi}\int_0^1 dy[\varphi_{11}(y)-\varphi_{22}(y)]. \tag{5.14}$$

From these equations we may derive the following closed equation for $\varphi_{12}(\equiv \varphi)$, whose suffix we shall omit for brevity from now on.

$$\begin{aligned}\mu^2\varphi(x) &\equiv H\varphi(x)\\ &= \left(\frac{\beta_1-1}{x}+\frac{\beta_2-1}{1-x}\right)\varphi(x) - P\int_0^1 dy\frac{\varphi(y)}{(x-y)^2}\\ &\quad - \frac{\sqrt{\beta_1}(1-x)-\sqrt{\beta_2}x}{x(1-x)}\frac{\int_0^1 dy\frac{\sqrt{\beta_1}(1-y)-\sqrt{\beta_2}y}{y(1-y)}\varphi(y)}{\frac{4\pi}{a_b^2 N}+\frac{1}{2}\int_0^1\frac{dx}{x(1-x)}}\\ &\quad - \frac{\sqrt{\beta_1}(1-x)+\sqrt{\beta_2}x}{x(1-x)}\frac{\int_0^1 dy\frac{\sqrt{\beta_1}(1-y)+\sqrt{\beta_2}y}{y(1-y)}\varphi(y)}{\frac{4\pi}{a_{5b}^2 N}+\frac{1}{2}\int_0^1\frac{dx}{x(1-x)}}.\end{aligned} \tag{5.15}$$

We shall often refer to H as the Hamiltonian. It is clear that this equation reduces to the 't Hooft equation (2.24) when $a^2 = a_5^2 = 0$ and that it reduces to the Gross–Neveu model case obtained in the previous section when $g = 0$, $\beta_1 = \beta_2$ and $a^2 = a_5^2$. Even when the gauge coupling is zero, this model is more general than the massive Gross–Neveu model in that it incorporates different four–Fermi couplings a, a_5 and fermions of different masses. This equation describes the properties of the mesons in the gauged four–Fermi model. When the fermion masses are equal, $\beta_1 = \beta_2 (\equiv \beta)$, the equation takes a substantially simpler form;

$$\begin{aligned}\mu^2\varphi(x) &= \frac{\beta-1}{x(1-x)}\varphi(x) - P\int_0^1 dy \frac{\varphi(y)}{(x-y)^2} \\ &\quad - \frac{\beta}{x(1-x)} \frac{\int_0^1 dy \frac{\varphi(y)}{y(1-y)}}{\frac{4\pi}{a_b^2 N} + \frac{1}{2}\int_0^1 \frac{dx}{x(1-x)}} - \frac{\beta(1-2x)}{x(1-x)} \frac{\int_0^1 dy \frac{1-2y}{y(1-y)}\varphi(y)}{\frac{4\pi}{a_{5b}^2 N} + \frac{1}{2}\int_0^1 \frac{dx}{x(1-x)}}.\end{aligned} \tag{5.16}$$

When the fermion masses are equal, $\beta_1 = \beta_2$, *and* when the couplings are equal, $a^2 = a_5^2$, the bound state equation for the mesons in the gauged four–Fermi model (5.15) reduces to the equation given by Burkardt [29]. Burkardt obtained a renormalized form of the equation when the meson wavefunction is an even function of the momentum fraction by using an operator identity involving the divergence of the axial current. In contrast, below, we will renormalize the more general bound state equation (5.15) and reduce the equations to its renormalized form without using any further identities.

5.2.3 Renormalization and boundary condition

The equations derived in the previous section (5.12)–(5.15) are expressed in terms of bare quantities. The equation for the meson wavefunction should be expressible in terms of renormalized quantities and the Hamiltonian matrix elements between physical states should be finite. From these conditions, we may derive the renormalization for the couplings and the boundary conditions for the meson wavefunction. The coupling constants are renormalized as follows

$$\frac{4\pi}{a^2 N} = \frac{4\pi}{a_b^2 N} - \frac{1}{2}\int_0^1 dx \, \frac{1}{x(1-x)}, \qquad \frac{4\pi}{a_5^2 N} = \frac{4\pi}{a_{5b}^2 N} - \frac{1}{2}\int_0^1 dx \, \frac{1}{x(1-x)}. \tag{5.17}$$

From here on, we shall use the notation $G \equiv a^2 N/(4\pi)$, $G_5 = a_5^2 N/(4\pi)$ to avoid cluttering the formulas. As in the Gross–Neveu model, these integrals have been regularized which is not explicitly denoted here. It should be noted

here that this generalizes the renormalization of the coupling constant in the Gross–Neveu model (4.8). The mass parameter M needs no renormalization. This is again consistent with the renormalization in both the Gross–Neveu model and the 't Hooft model. We expand the meson wavefunction as

$$\varphi(x) = \varphi^{(0)} + \varphi^{(1)}(1-2x) + \hat{\varphi}(x), \tag{5.18}$$

where $\varphi^{(0)}, \varphi^{(1)}$ are constants and $\hat{\varphi}(x)/\left[x(1-x)\right]$ is integrable at $x = 0, 1$. Then, the boundary conditions for the meson wavefunction are

$$\begin{pmatrix} b_+ & (1+4G_5)b_- \\ b_- & (1+4G)b_+ \end{pmatrix}\begin{pmatrix} \varphi^{(0)} \\ \varphi^{(1)} \end{pmatrix} = \int_0^1 dx \frac{\hat{\varphi}(x)}{x(1-x)} \begin{pmatrix} G_5 & 0 \\ 0 & G \end{pmatrix}\begin{pmatrix} b_+ & b_- \\ b_- & b_+ \end{pmatrix}\begin{pmatrix} 1 \\ 1-2x \end{pmatrix}. \tag{5.19}$$

Here, we defined $b_\pm \equiv \left(\sqrt{\beta}_1 \pm \sqrt{\beta}_2\right)/2$. In particular, when the coupling constants are equal, $G = G_5$, *or* when the masses are equal, $\beta_1 = \beta_2$, the boundary conditions simplify to

$$\begin{pmatrix} \varphi^{(0)} \\ \varphi^{(1)} \end{pmatrix} = \int_0^1 dx \, \frac{\hat{\varphi}(x)}{x(1-x)} \begin{pmatrix} G_5 \\ \frac{G(1-2x)}{1+4G} \end{pmatrix}. \tag{5.20}$$

The meson wavefunction does *not* vanish at the boundaries. This property is similar to that of the Gross–Neveu model but *unlike* that of the 't Hooft model. When the Gross–Neveu couplings are zero, the wavefunction *does* vanish at the boundaries, thereby recovering the boundary conditions of 't Hooft. Also, it is instructive to check that the equation for the meson wavefunction (5.15) and the boundary conditions (5.20) for $\beta_1 = \beta_2$ reduce exactly to the equations (4.7) in the Gross–Neveu model for σ and π scalars when $\varphi^{(0)} = 0$ and $\varphi^{(1)} = 0$, respectively.

The equation for the meson states is now reduced to

$$\begin{aligned} H\varphi(x) &= \mu^2\varphi(x) \\ &= \left(\frac{\beta_1 - 1}{x} + \frac{\beta_2 - 1}{1-x}\right)\hat{\varphi}(x) - P\int_0^1 dy \, \frac{\hat{\varphi}(y)}{(y-x)^2} \\ &\qquad + 2\varphi^{(1)}\left(-\beta_1 + \beta_2 + \ln\frac{1-x}{x}\right). \end{aligned} \tag{5.21}$$

subject to the boundary conditions (5.19). It is straightforward to check that the Hamiltonian is Hermitian under the given boundary condition. The *explicit* dependence on the coupling constants is contained in the non–trivial boundary conditions. The problem has been reduced to that of solving a well defined integral equation. For later purposes, we also derive the matrix elements of the "Hamiltonian", H, in the most general case, when the couplings

and the masses are arbitrary:

$$
\begin{aligned}
(\varphi', H\varphi) &= \left[\frac{\beta_1+\beta_2}{4}\left(\frac{1}{G}+\frac{1}{G_5}\right)+\frac{1}{2}\sqrt{\beta_1\beta_2}\left(\frac{1}{G_5}-\frac{1}{G}\right)\right]\overline{\varphi^{(0)\prime}}\varphi^{(0)} \\
&\quad +\frac{\beta_1-\beta_2}{4}\left(\frac{1}{G}+\frac{1}{G_5}\right)\left(\overline{\varphi^{(0)\prime}}\varphi^{(1)}+\overline{\varphi^{(1)\prime}}\varphi^{(0)}\right) \\
&\quad +\left[\frac{\beta_1+\beta_2}{4}\left(\frac{1}{G}+\frac{1}{G_5}+8\right)+2+\frac{1}{2}\sqrt{\beta_1\beta_2}\left(\frac{1}{G}-\frac{1}{G_5}\right)\right]\overline{\varphi^{(1)\prime}}\varphi^{(1)} \\
&\quad +\int_0^1 dx\,\left(\frac{\beta_1-1}{x}+\frac{\beta_2-1}{1-x}\right)\overline{\hat{\varphi}'(x)}\hat{\varphi}(x)-P\int_0^1\int_0^1\frac{dx\,dy}{(x-y)^2}\,\overline{\hat{\varphi}'(x)}\hat{\varphi}(y) \\
&\quad +\int_0^1 dx\,2\left(-\beta_1+\beta_2+\ln\frac{1-x}{x}\right)\left(\overline{\varphi^{(1)\prime}}\hat{\varphi}(x)+\overline{\hat{\varphi}'(x)}\varphi^{(1)}\right). \qquad (5.22)
\end{aligned}
$$

5.3 Systematic methods for solving the meson bound state equation

In this section, we show how the meson bound state equation (5.15) may be solved systematically utilizing a finite dimensional system of algebraic equations. We will give explicit formulas for two approaches, namely a variational method using polynomials of the momentum fraction and a method of working with the equation directly using a sinusoidal basis. These methods will be used in the next section to investigate some physical properties of the gauged four–Fermi model.

5.3.1 Variational method

Here, we shall use a variational method using polynomials of the momentum fraction x that satisfy the boundary condition (5.19). In the 't Hooft model, a similar method was employed in ref.[33].

We choose the basis functions $\{\varphi_j|\ j=2,3,\ldots\}$ as

$$
\begin{aligned}
\varphi_{2k}(x) &= c_{11}+c_{21}(1-2x)+\frac{[x(1-x)]^k}{B(k,k)} \\
\varphi_{2k+1}(x) &= c_{12}+c_{22}(1-2x)+\frac{(2k+1)(1-2x)\,[x(1-x)]^k}{B(k,k)} \quad (k=1,2\ldots).
\end{aligned} \qquad (5.23)
$$

The normalization factor was chosen so as to make the matrix elements be of order one. c_{ij}'s need to be determined to satisfy the boundary conditions

(5.19) as

$$\begin{pmatrix} c_{11} & c_{12} \\ c_{21} & c_{22} \end{pmatrix} = \begin{pmatrix} b_+ & (1+4G_5)b_- \\ b_- & (1+4G)b_+ \end{pmatrix}^{-1} \begin{pmatrix} G_5 & 0 \\ 0 & G \end{pmatrix} \begin{pmatrix} b_+ & b_- \\ b_- & b_+ \end{pmatrix} = \frac{1}{d} \times$$
$$\begin{pmatrix} \frac{1}{4}(G_5-G)(\beta_1+\beta_2)+\left(\frac{G_5+G}{2}+4G_5G\right)\sqrt{\beta_1\beta_2} & \frac{1}{4}(G_5-G)(\beta_1-\beta_2) \\ -\frac{1}{4}(G_5-G)(\beta_1-\beta_2) & -\frac{1}{4}(G_5-G)(\beta_1+\beta_2)+\frac{1}{2}(G_5+G)\sqrt{\beta_1\beta_2} \end{pmatrix} \tag{5.24}$$

where we set

$$d \equiv (1+4G)b_+^2 - (1+4G_5)b_-^2 = (G-G_5)(\beta_1+\beta_2) + (1+2G_5+2G)\sqrt{\beta_1\beta_2}. \tag{5.25}$$

In the variational method, the problem of obtaining the meson states is reduced to solving an eigenvalue problem:

$$(\mu^2 N_{kl} - H_{kl})w_l = 0, \quad H_{kl} \equiv (\varphi_k, H\varphi_l)\,, \ N_{kl} \equiv (\varphi_k, \varphi_l) \qquad k,l = 2,3,4\ldots. \tag{5.26}$$

We will approximate the solution by using basis elements up to a certain number and check the convergence by varying this number.

With some work, the matrix elements can be computed to be

$$\begin{aligned} N_{2k,2l} &= c_{11}^2 + \frac{c_{21}^2}{3} + \frac{c_{11}}{2}\left(\frac{k}{2k+1} + \frac{l}{2l+1}\right) \\ &\quad + \frac{k+l}{2(2k+2l+1)} \frac{B(k+l,k+l)}{B(k,k)B(l,l)} \\ N_{2k+1,2l+1} &= c_{12}^2 + \frac{c_{22}^2}{3} + \frac{c_{22}}{2}\left(\frac{k}{2k+3} + \frac{l}{2l+3}\right) \\ &\quad + \frac{(k+l)(2k+1)(2l+1)}{2(2k+2l+1)(2k+2l+3)} \frac{B(k+l,k+l)}{B(k,k)B(l,l)} \\ N_{2k,2l+1} &= N_{2l+1,2k} = c_{11}c_{12} + \frac{1}{3}c_{21}c_{22} + \frac{k}{2(2k+1)}c_{12} + \frac{l}{2(2l+3)}c_{21} \end{aligned} \tag{5.27}$$

$$\begin{aligned} H_{2k,2l} &= \frac{1}{d}\sqrt{\beta_1\beta_2}\left[\frac{1}{4}(G+G_5+8GG_5)(\beta_1+\beta_2) - \frac{1}{2}(G-G_5)\sqrt{\beta_1\beta_2}\right] \\ &\quad + 2c_{12}^2 + (\beta_1-\beta_2)c_{12}\left(2c_{11} + \frac{k}{2k+1} + \frac{l}{2l+1}\right) \\ &\quad + \left(\frac{\beta_1+\beta_2}{2} - 1\right)\frac{B(k+l,k+l)}{B(k,k)B(l,l)} + \frac{kl}{2(k+l)} \\ H_{2k+1,2l+1} &= \frac{1}{d}\sqrt{\beta_1\beta_2}\left[\frac{1}{4}(G+G_5)(\beta_1+\beta_2) + \frac{1}{2}(G-G_5)\sqrt{\beta_1\beta_2}\right] \end{aligned} \tag{5.28}$$

$$+2c_{22}\left[c_{22}-(\beta_1-\beta_2)c_{12}\right]+c_{22}\left(\frac{k}{k+1}+\frac{l}{l+1}\right)$$
$$+\left(\frac{\beta_1+\beta_2}{2}-1\right)\frac{(2k+1)(2l+1)}{2k+2l+1}\frac{B(k+l,k+l)}{B(k,k)B(l,l)}+\frac{kl(2k+1)(2l+1)}{2(k+l)(k+l+1)}$$
$$H_{2k,2l+1}=H_{2l+1,2k}=\frac{1}{4d}\sqrt{\beta_1\beta_2}(\beta_1-\beta_2)(G+G_5)-2c_{12}\left(c_{22}-(\beta_1-\beta_2)c_{12}\right)$$
$$-c_{12}\frac{l}{l+1}-c_{22}(\beta_1-\beta_2)\frac{k}{2k+1}+\frac{1}{2}(\beta_1-\beta_2)\frac{(2l+1)B(k+l,k+l)}{(2k+2l+1)B(k,k)B(l,l)}.$$

When $\beta_1=\beta_2$, the even and the odd sectors completely decouple.

5.3.2 Multhopp's method

Rather than using a variational method, we may choose to work with the equation (5.21) directly. By a clever choice of basis, this singular integral equation may be brought into an algebraic equation. The method we use here generalizes the methods used to numerically analyze the 't Hooft equation previously [34]-[38],[31, 32, 79].

Defining $x\equiv(1+\cos\theta)/2$, the wave function can be expanded in a manner consistent with the boundary conditions as

$$\varphi(x)=2\pi\left(c_{11}\sum_{n:\text{odd}}v_n-c_{12}\sum_{n:\text{even}}v_n\right)-2\pi\left(c_{21}\sum_{n:\text{odd}}v_n-c_{22}\sum_{n:\text{even}}v_n\right)\cos\theta$$
$$+\sum_{n=1}v_n\sin n\theta, \tag{5.29}$$

where c_{ij}'s were defined in eq.(5.24). This reduces the Bethe–Salpeter equation (5.21) to

$$\sum_n\left[\mu^2\hat{P}_n(\theta)-\hat{M}_n(\theta)\right]v_n=0, \tag{5.30}$$

where

$$\hat{P}_n(\theta) \equiv \sin n\theta+2\pi\begin{cases}c_{11}-c_{21}\cos\theta & n:\text{ odd}\\ -c_{12}+c_{22}\cos\theta & n:\text{ even}\end{cases} \tag{5.31}$$
$$\hat{M}_n(\theta) \equiv 2\left(\frac{\beta_1-1}{1+\cos\theta}+\frac{\beta_2-1}{1-\cos\theta}\right)\sin n\theta+2\pi\frac{n\sin n\theta}{\sin\theta}$$
$$+4\pi\left(\beta_1-\beta_2+\ln\frac{1+\cos\theta}{1-\cos\theta}\right)\times\begin{cases}-c_{21} & n:\text{ odd}\\ c_{22} & n:\text{ even}\end{cases}.$$

The above equation (5.30) is still a functional equation, with the dependence on the parameter θ.

This can be further reduced to a generalized matrix eigenvalue problem

$$\left(\mu^2 P - M\right) v = 0. \tag{5.32}$$

The matrices are defined as

$$P_{mn} \equiv \sum_{l=1}^{K} g_m(\theta_l)\hat{P}_n(\theta_l), \quad M_{mn} \equiv \sum_{l=1}^{K} g_m(\theta_l)\hat{M}_n(\theta_l), \qquad \theta_j \equiv \pi\frac{j}{K+1}. \tag{5.33}$$

The function $g_m(\theta)$ is arbitrary, but using functions with the property $g_m(\theta_l) = (-1)^{m+1} g_m(\theta_{K+1-l})$ simplifies the matrix elements. With this condition, the matrix elements are

$$\begin{aligned}
P_{mn} &= \sum_{l=1}^{K} g_m(\theta_l)\sin\theta_{nl} + 2\pi\sum_{l=1}^{K} g_m(\theta_l)\begin{cases} c_{11} & (m,n\text{: odd}) \\ c_{22}\cos\theta_l & (m,n\text{: even}) \end{cases} \\
P_{mn} &= -2\pi\sum_{l=1}^{K} g_m(\theta_l)\begin{cases} c_{12} & (m\text{: odd},n\text{: even}) \\ c_{21}\cos\theta_l & (m\text{: even},n\text{: odd}) \end{cases}
\end{aligned} \tag{5.34}$$

$$\begin{aligned}
M_{mn} &= \sum_{l=1}^{K} g_m(\theta_l)\left[2\frac{(\beta_1+\beta_2-2)}{\sin^2\theta_l} + \frac{2\pi n}{\sin\theta_l}\right]\sin\theta_{nl} \\
&\qquad +4\pi\sum_{l=1}^{K} g_m(\theta_l)\begin{cases} (-c_{21})(\beta_1-\beta_2) & (m,n\text{: odd}) \\ c_{22}\ln\frac{1+\cos\theta_l}{1-\cos\theta_l} & (m,n\text{: even}) \end{cases} \\
M_{mn} &= -2(\beta_1-\beta_2)\sum_{l=1}^{K} g_m(\theta_l)\frac{\cos\theta_l\sin\theta_{nl}}{\sin^2\theta_l} \\
&\qquad +4\pi\sum_{l=1}^{K} g_m(\theta_l)\begin{cases} c_{22}(\beta_1-\beta_2) & (m\text{: odd},n\text{: even}) \\ (-c_{21})\ln\frac{1+\cos\theta_l}{1-\cos\theta_l} & (m\text{: even},n\text{: odd}) \end{cases}.
\end{aligned} \tag{5.35}$$

In what follows, we adopt $g_m(\theta) = 2\sin m\theta/(K+1)$ as was done so for the 't Hooft model [34]-[38],[31, 32, 79]. Unlike the variational method, the approximate solution obtained by truncating to finite dimensional solution space needs *not* be an upper bound on the true solution and in general will not be.

5.4 Physics of the gauged four–Fermi model

In this section we investigate the physical properties of the gauged four–Fermi model. In this section we restrict ourselves to the case of scalar and pseudoscalar couplings being equal, $G = G_5$, for simplicity.

First, we would like to determine the parameter region where the behavior of the system is physically reasonable. In particular, the meson bound state should *not* be tachyonic. Here, we will perform the analysis for fermions of equal mass since we expect tachyonic mesons in the flavor singlet channel *if* tachyonic mesons exist at all. Using the variational method for the meson wavefunction in a manner similar to the previous section,

$$\varphi_\gamma(x) \equiv G + B(\gamma,\gamma)^{-1}\left[x(1-x)\right]^\gamma \qquad \gamma > 0, \tag{5.36}$$

we obtain an upper bound μ_γ^2 for the meson mass squared for each $\gamma > 0$.

$$\mu_\gamma^2 = \frac{(\varphi_\gamma, H\varphi_\gamma)}{(\varphi_\gamma,\varphi_\gamma)} = \frac{G\beta + \frac{\gamma}{4} + (\beta-1)\frac{B(2\gamma,2\gamma)}{B(\gamma,\gamma)^2}}{G^2 + G\frac{\gamma}{2\gamma+1} + \frac{\gamma}{4\gamma+1}\frac{B(2\gamma,2\gamma)}{B(\gamma,\gamma)^2}} \sim \begin{cases} \frac{\beta}{G} & \gamma \sim 0 \\ 2\sqrt{2\pi\gamma} & \gamma \sim \infty \end{cases}. \tag{5.37}$$

This immediately establishes that when $\beta G < 0$ tachyonic mesons will appear. While it is *logically* possible from this analysis that the region with both $\beta < 0$ and $G < 0$ may be physically consistent, it is unreasonable to expect so; in practice, we find that tachyonic mesons appear for this case also, when we have a large enough variational space. Therefore, we henceforth interest ourselves in the region $G > 0$ and $\beta > 0$.

Using the methods explained in the previous section, we may obtain the spectrum and the meson wavefunctions. We plot the spectrum and the wave functions for some typical cases below in figures Fig. 5.3, Fig. 5.4 and Fig. 5.5. We have added a brief note on the convergence of the numerical data in appendix B. As in the 't Hooft model, the fermions are confined and the following Regge–type behavior is observed for the highly massive mesons, similarly to the 't Hooft model (see section 2.5):

$$\mu^2 \sim \pi^2 k \qquad k \gg 1,\ \beta. \tag{5.38}$$

This Regge behavior is shown in Fig. 5.6. We may understand the behavior of the spectrum in the various limits of the model as follows: when we turn off the Gross–Neveu coupling a^2, the spectrum reduces to that of the 't Hooft model. As we take the gauge coupling to zero, which effectively is the limit $\beta \to \infty$, the splitting between the higher levels disappear. We have explicitly checked that the mass of the lightest meson approaches to the Gross–Neveu model value plotted in Fig. 4.2 in this limit. For the higher levels, μ^2 approaches 4β in this Gross–Neveu limit. The chiral limit may be identified as the limit G (or a^2N) $\to \infty$, similarly to the Gross–Neveu model case. In the spectrum, mass of the meson states decrease as we approach the chiral limit and it is clear that $\mu^2 \to 0$ for the lightest meson bound state in the limit

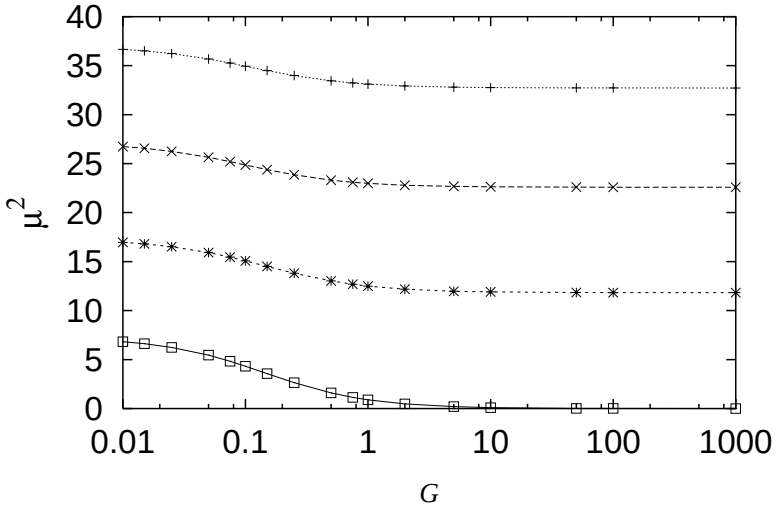

Figure 5.3: Mass squared of the lightest four meson states versus the coupling G for $\beta = 1$.

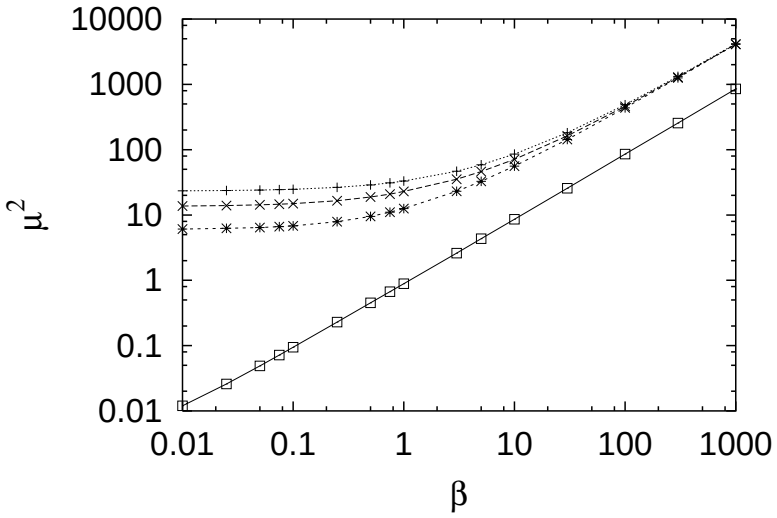

Figure 5.4: Mass squared of the lightest four meson states versus the fermion mass squared β for the coupling $G = 1$.

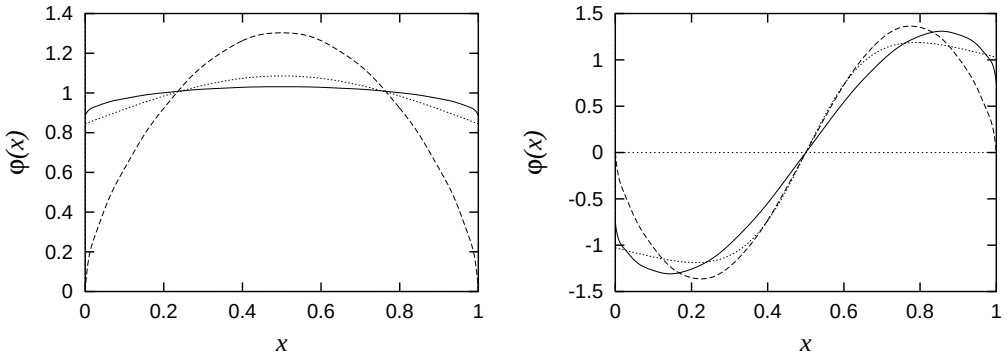

Figure 5.5: The meson wavefunctions for the gauged four–Fermi model (solid), the 't Hooft model (long dashes) and the Gross–Neveu model (short dashes). The functions are plotted for the lightest two meson states. The parameters chosen for the gauged four–Fermi model is $G = 1, \beta = 1$ for both mesons. For the 't Hooft model $\beta = 1$ also. For the Gross–Neveu model, in the lightest meson case, the meson mass was chosen to agree with that of the gauged four–Fermi model. In the next lightest meson case, $\mu^2/\beta = 3$ was chosen.

$G \to \infty$. When the limit $\beta \to \infty$ is taken in addition, it may be explicitly checked that the next lightest meson satisfies $\mu^2/M^2 \to 4$ corresponding the the σ mass in the Gross–Neveu model.

As β becomes large, the meson masses behave linearly with the quark masses, as is expected from the naive constituent quark picture. This picture is supposedly valid for highly massive quarks. The lightest meson behaves in a qualitatively different manner from the other meson states in the theory. This is a feature of the gauged four–Fermi model; such a behavior does *not* occur in the 't Hooft model. The Gross–Neveu coupling affects the lightest meson state relatively more than the other meson states. This disparate behavior is a necessary consequence of the Gross–Neveu limit where μ^2/β of π and the other mesons approach the corresponding value $\tilde{\mu}^2$ in the Gross–Neveu model and 4. In the 't Hooft model, μ^2/β for the lightest meson also approaches 4 for large β.

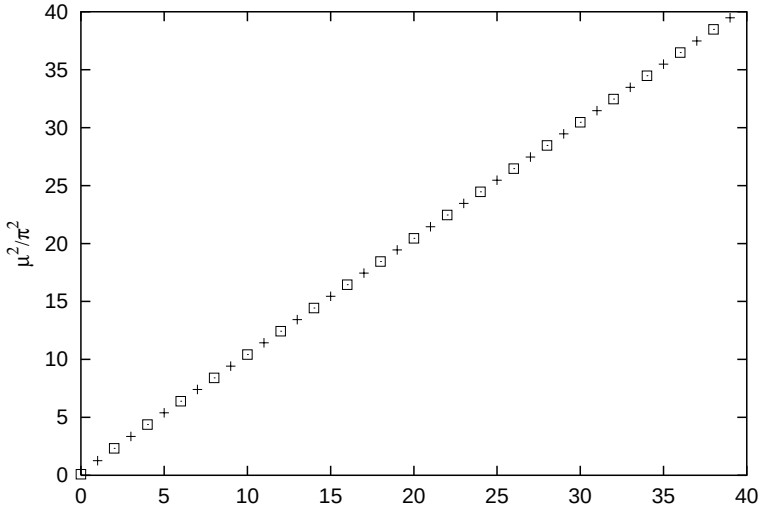

Figure 5.6: Mass squared normalized by π^2 of the meson states versus the "level number" for the case $\beta = 1$, $G = 1$. $\Box$ (+)'s denote states whose wavefunctions are even (odd) under $x \leftrightarrow 1 - x$,

Chapter 6

A brief review of QCD inequalities

In this chapter we briefly review QCD inequalities, which have a wide area of applications mainly in the theory of strongly interacting particles (see a recent review [71]). Here we will focus on the inequalities used in chapter 7 and one of the applications, the Vafa–Witten theorem on symmetry breaking patterns [62], which is cited most often.

6.1 What are QCD inequalities?

QCD inequalities are inequalities between hadronic masses or other hadronic matrix elements (observables), which are deduced directly from QCD Lagrangian and from its Hamiltonian counterpart (with possible additional assumptions). For example, by comparing the two–point functions of some currents, one can obtain the following relations;

$$m^{(0)}(\text{any meson}) \geq m_\pi, \qquad m^{(0)}(\text{any baryon}) \geq m_\pi, \tag{6.1}$$

where the suffix (0) implies the lowest state. These inequalities reflect the well–known fact that the pion is the lightest hadron.

In general it is difficult to perform quantitative computations of hadron matrix elements and the hadronic spectrum, however QCD inequalities can be derived more easily by comparing expressions for different correlation functions or the energies of different hadronic systems *without* requiring explicit evaluation. We only need to assume that an appropriate regularization scheme and gauge fixing have been devised to make the path integral or the Schrödinger problem well defined.

QCD inequalities not only describe the well–known relations as eqs.(6.1) but also have more profound implications for the phase structure of QCD. In general the symmetry structure of a field theory is closely tied in with the zero mass sector; for example

- spontaneous breaking of global symmetries implies the existence of massless scalar Nambu–Goldstone bosons via Goldstone theorem [72].
- spontaneous breaking of axial global symmetries implies Nambu–Goldstone massless pseudoscalars [39].
- an unbroken axial symmetry requires massless fermions in the physical spectrum.

Evidently mass relations such as eqs.(6.1) between baryons (fermions) and scalar and/or pseudoscalar mass could restrict some of these possibilities and dictate the patterns of global symmetry realization in QCD and other vectorial theories such as technicolor models[73]–[77].

The QCD inequality we discuss from here on is

$$\mu_{ab} \geq \frac{1}{2}\left(\mu_{aa} + \mu_{bb}\right), \tag{6.2}$$

where index a, b denote quark flavor and μ_{ab} is the lightest (pseudoscalar) meson mass of ab channel.

Comparing the inequality (6.2) with particle data[80], it seems to hold in any case (see Table I)[1].

In the next two sections we will derive the QCD inequality (6.2), which we call (meson) mass inequality, by using two different methods, rigorous Euclidean path integral approach (see section 6.2) and Hamiltonian variational approach (see section 6.3).

[1]The comparison made here is based on the Hamiltonian variational approach (see section 6.3 and [71] for further details). For the iso–singlet pseudoscalars the strong coupling to the gluonic channel due to the $U(1)$ anomaly, which in particular accounts for the massive η' meson [81]–[83], suggests strong mixing between the two iso–singlet states that are made of light quarks, $\frac{1}{\sqrt{2}}\left(u\bar{u} + d\bar{d}\right)$, and the $s\bar{s}$ state. Hence one can set $|s\bar{s}\rangle = \alpha|\eta\rangle + \beta|\eta'\rangle$. The reasonable expectation that the eigenstates η, η' are the $SU(3)$ flavor octet $\frac{1}{\sqrt{6}}\left(u\bar{u} + d\bar{d} - 2s\bar{s}\right)$ and singlet $\frac{1}{\sqrt{3}}\left(u\bar{u} + d\bar{d} + s\bar{s}\right)$ [84] implies $\alpha = \sqrt{2/3}, \beta = \sqrt{1/3}$. Therefore one can expect $\mu_{s\bar{s}} = \left(\alpha\langle\eta| + \beta\langle\eta'|\right) H_{\rm QCD}\left(\alpha|\eta\rangle + \beta|\eta'\rangle\right) = \alpha^2\mu_\eta + \beta^2\mu_{\eta'} \cdots \approx \frac{2}{3}\mu_\eta + \frac{1}{3}\mu_{\eta'}$. (For a review of $\eta\eta'$ mixing, see ref.[85].)

For the $b\bar{b}$ channel, we used the mass of the vectorial state μ_Υ, instead of the as yet unknown μ_{η_b}. The fact that the lowest state is pseudoscalar meson (*i.e.* $\mu_\Upsilon \geq \mu_{\eta_b}$) [61] indicates that the original inequality is satisfied.

TABLE I. Comparison with particle data (MeV)

$u\bar{s}$ sector	$\mu_K \geq \frac{1}{2}\left(\mu_\pi + \frac{2}{3}\mu_\eta + \frac{1}{3}\mu_{\eta'}\right)$	495.009	$\geq$	411.08
$u\bar{c}$ sector	$\mu_D \geq \frac{1}{2}\left(\mu_\pi + \mu_{\eta_c}\right)$	1867.7	$\geq$	1558.9
$u\bar{b}$ sector	$\mu_B \geq \frac{1}{2}\left(\mu_\pi + \mu_\Upsilon\right)$	5279.0	$\geq$	4799.2
$s\bar{c}$ sector	$\mu_{D_S} \geq \frac{1}{2}\left(\frac{2}{3}\mu_\eta + \frac{1}{3}\mu_{\eta'} + \mu_{\eta_C}\right)$	1968.5	$\geq$	1832.0
$s\bar{b}$ sector	$\mu_{B_S^0} \geq \frac{1}{2}\left(\frac{2}{3}\mu_\eta + \frac{1}{3}\mu_{\eta'} + \mu_\Upsilon\right)$	5369.3	$\geq$	5072.2
$c\bar{b}$ sector	$\mu_{B_C^\pm} \geq \frac{1}{2}\left(\mu_{\eta_C} + \mu_\Upsilon\right)$	6400	$\geq$	6219.6

6.2 The rigorous euclidean path integral approach

In this section we will derive the mass inequality (6.2) directly from the euclidean version of the QCD Lagrangian,

$$\mathcal{L}_{QCD} = \sum_{f=1}^{N_f} \bar{\psi}_f \left(\not{D} + m_f\right) \psi_f + \frac{1}{2}\mathrm{tr}\left(F_{\mu\nu}\right)^2 . \tag{6.3}$$

Here we consider ordinary QCD in four space–time dimensions and with no CP–violating vacuum angle θ, however the derivation is also valid for another choice of space–time dimensions as long as they are vector–like gauge theories.

Outline of the proof

The euclidean correlation functions of color singlet local operators $O_{a_i}(x)$ are given by the functional path integral

$$\begin{aligned} W_{a_1\ldots a_n}(x_1,\cdots,x_n) &= \langle 0\,|O_{a_1}(x_1)\cdots O_{a_n}(x_n)|\,0\rangle \\ &= \int \mathcal{D}A_\mu \int \mathcal{D}\psi \int \mathcal{D}\bar{\psi} O_{a_1}(x_1)\cdots O_{a_n}(x_n) \exp\left(-\int d^4x \mathcal{L}_{QCD}(x)\right), \end{aligned} \tag{6.4}$$

where $\int \mathcal{D}A_\mu \int \mathcal{D}\psi \int \mathcal{D}\bar{\psi}$ denotes the functional integral over the ordinary gauge field and fermionic degrees of freedom. By analytically continuing the corresponding momentum space correlations $W_{a_1\ldots a_n}(p_1,\cdots,p_n)$, all hadronic scattering amplitudes can be determined.

The simplest two–point functions are particularly useful. The spectral representation for such functions

$$W_a(x,y) = \langle 0 \left| J_a(x) J_a^\dagger(y) \right| 0 \rangle = \int d(\mu^2) \sigma_a(\mu^2) e^{-\mu|x-y|} \tag{6.5}$$

yields information on the hadronic states in the channel with J_a quantum numbers. The lowest state of mass $m_a^{(0)}$ dominates the asymptotic behavior as

$$\langle 0 \left| J_a(x) J_a^\dagger(y) \right| 0 \rangle \to e^{m_a^{(0)}|x-y|} \qquad \text{as} \quad |x-y| \to \infty. \tag{6.6}$$

A key ingredient in deriving relations between correlation functions is the *positivity of the effective measure* $\mathcal{D}\mu(A)$ obtained after integrating out the fermionic degrees of freedom. In fact the fermionic bilinear part $\sum_{f=1}^{N_f} \bar{\psi}_f \left(\not{D} + m_f \right) \psi_f$ yields the determinant factor $\prod_{f=1}^{N_f} \mathrm{Det}(\not{D} + m_f)$, which can be shown to be positive–definite for *any* background fields $A_\mu(x)$ in vectorial (non-chiral) theories.

If the integrand of one correlation function is greater than that of another correlation function in any background fields $A_\mu(x)$, the positivity of path integral measure guarantees that the inequality between the two correlation functions also holds after integrated over the gauge fields. As a result we can obtain a rigorous inequality between the two correlation functions.

And if an inequality $\langle 0 \left| J_a(x) J_a^\dagger(y) \right| 0 \rangle \geq \langle 0 | J_b(x) J_b^\dagger(y) | 0 \rangle$ hold, we obtain the reversed inequality $m_a^{(0)} \leq m_b^{(0)}$ for the lowest mass states with the quantum numbers of $J_a(x)$ and $J_b(x)$ via the relation (6.6).

Positivity of the effective measure

An important element of the proof is the positivity of the effective measure $\mathcal{D}\mu(A) \equiv e^{-S_{\rm YM}(A)} \prod \mathrm{Det}(\not{D}_A + m_f) \mathcal{D}A_\mu(x)$, which follows from the positivity of the determinant factor[2] $\prod \mathrm{Det}(\not{D}_A + m_f)$. To show the positivity of the determinant factor, let us consider the eigenmodes $\psi_A(\lambda_A)$ of the hermitian operator $i\not{D}_A$ satisfying

$$i \not{D}_A \psi_\lambda^A = \lambda(A) \psi_\lambda^A \tag{6.7}$$

with real eigenvalues $\lambda(A)$. The γ_5 anticommutation $\gamma_5 \gamma_\mu \gamma_5 = -\gamma_\mu$ implies the relation $\not{D}_A = -\gamma_5 \not{D}_A \gamma_5$. This relation forces all nonzero eigenvalues of $\not{D}_A$ to appear in *complex conjugate pairs*. Indeed from the eq.(6.7) and the γ_5 anticommutation,

$$i \not{D}_A \left(\gamma_5 \psi_\lambda \right) = \gamma_5^2 i \not{D}_A \gamma_5 \psi_\lambda = -\gamma_5 \left(i \not{D}_A \right) \psi_\lambda = -\lambda(A) \gamma_5 \psi_\lambda, \tag{6.8}$$

[2]Here the suffix A implies that $\not{D}$ includes any given background configuration $A_\mu(x)$.

so that $\gamma_5\psi_\lambda$ is the eigenfunction corresponding to eigenvalues $-\lambda(A)$. Thus we have explicitly positive determinants[3]

$$\mathrm{Det}\left(\not{D}_A + m\right) = \prod_{\lambda>0}\left[i\lambda(A)+m\right]\left[-i\lambda(A)+m\right] = \prod_{\lambda>0}\left[\lambda^2(A)+m^2\right], \quad (6.9)$$

and hence $\mathcal{D}\mu(A) \geq 0$ for all given $A_\mu(x)$.

It is important to notice that the above argument applies only for vectorial, non–chiral models including quarks as Dirac fermions. If $\gamma_5\psi_\lambda$ is not a distinct new spinor (as is the case for chiral fermions) then the positivity argument breaks down. And also notice that we have set all vacuum angle θ to zero; otherwise the measure contains a complex factor $\exp\left(\frac{i\theta}{16\pi^2}\int d^4x \mathrm{Tr} F_{\mu\nu}\tilde{F}^{\mu\nu}\right)$, and above argument would be also invalid.

In the case of models with some scalar fields, as long as the scalars do *not* have Yukawa couplings to fermions, the above argument is valid, because the euclidean space action for scalars with renormalizable self–interactions and gauge couplings only is real. However, *Yukawa couplings* generally invalidate the arguments. With scalar couplings the euclidean Dirac operator has the form $\left(\not{D} + m + g\phi\right)$. In the ϕ integral one encounters a region of field space where $m + g\phi \approx 0$. With pseudoscalar Yukawa couplings, the Dirac operator becomes $\left(\not{D} + m + ig\gamma_5\phi\right)$ and the determinant of that operator is no longer real.

Derivation of the mass inequality

Let a and b be two quark flavors. It has been shown that a pseudoscalar meson is the lightest of all mesons with $a\bar{b}$ quantum numbers[61]. Following the Witten's work [65], consider the pseudoscalar currents such as $\bar{\psi_a} i\gamma_5\psi_b(x)$. The two–point function of these pseudoscalar currents is

$$\langle 0 \left| \bar{\psi_a} i\gamma_5\psi_b(x)\bar{\psi_b} i\gamma_5\psi_a(y) \right| 0\rangle = \int \mathcal{D}\mu(A) \mathrm{Tr}\gamma_5 S_A\left(x,y;m_a\right)\gamma_5 S_A\left(y,x;m_b\right), \quad (6.10)$$

where $S_A\left(x,y;m\right)$ is the full euclidean fermionic propagator in the background field $A_\mu(x)$ and the trace refers to both spinor and color indices. The full propagator satisfies the equation $\left(\not{D}_A + m\right) S_A\left(x,y;m\right) = \delta\left(x-y\right)$, and it is formally given by $S_A\left(x,y;m\right) = \langle x\left|\left(\not{D}_A + m\right)^{-1}\right|y\rangle$.

[3]In addition there may be unpaired zero eigenvalues, not indicated here. They contribute factors of m to the determinant. If $m > 0$ (which corresponds to $\theta = 0$) the fermion determinant is still positive.

Setting $U \equiv S_A(x,y;m_a)$ and $V \equiv S_A(x,y;m_b)$ and using the relation

$$\begin{aligned}\gamma_5 S_A(x,y;m)\gamma_5 &= \langle x|\gamma_5\left(\not{D}_A+m\right)^{-1}\gamma_5|y\rangle = \langle x|\left(-\not{D}_A+m\right)^{-1}|y\rangle \\ &= \langle x|\left[\left(\not{D}_A+m\right)^{-1}\right]^{\dagger}|y\rangle = S_A^{\dagger}(y,x;m), \end{aligned} \tag{6.11}$$

we can rewrite the eq.(6.10) as

$$\langle 0\left|\bar{\psi}_a i\gamma_5\psi_b(x)\bar{\psi}_b i\gamma_5\psi_a(y)\right|0\rangle = \int \mathcal{D}\mu \mathrm{Tr}UV^{\dagger}, \tag{6.12}$$

where dagger refers to the conjugate matrix in color and spinor space. Similarly we can also write the pseudoscalar currents for $a\bar{a}$ and $b\bar{b}$ channels as follows;

$$\begin{aligned}\langle 0\left|\bar{\psi}_a i\gamma_5\psi_a(x)\bar{\psi}_a i\gamma_5\psi_a(y)\right|0\rangle &= \int \mathcal{D}\mu(A)\mathrm{Tr}\gamma_5 S_A(x,y;m_a)\gamma_5 S_A(y,x;m_a) \\ &= \int \mathcal{D}\mu \mathrm{Tr}UU^{\dagger} \\ \langle 0\left|\bar{\psi}_b i\gamma_5\psi_b(x)\bar{\psi}_b i\gamma_5\psi_b(y)\right|0\rangle &= \int \mathcal{D}\mu \mathrm{Tr}VV^{\dagger}. \end{aligned} \tag{6.13}$$

By the Cauchy–Schwarz inequality

$$\left|\int \mathcal{D}\mu \mathrm{Tr}UV^{\dagger}\right|^2 \leq \int \mathcal{D}\mu \mathrm{Tr}UU^{\dagger}\int \mathcal{D}\mu \mathrm{Tr}VV^{\dagger}, \tag{6.14}$$

we can obtain an inequality between the two–point functions;

$$\begin{aligned}&\left|\langle 0\left|\bar{\psi}_a i\gamma_5\psi_b(x)\bar{\psi}_b i\gamma_5\psi_a(y)\right|0\rangle\right|^2 \\ &\qquad \leq \langle 0\left|\bar{\psi}_a i\gamma_5\psi_a(x)\bar{\psi}_a i\gamma_5\psi_a(y)\right|0\rangle\langle 0\left|\bar{\psi}_b i\gamma_5\psi_b(x)\bar{\psi}_b i\gamma_5\psi_b(y)\right|0\rangle. \end{aligned} \tag{6.15}$$

From the asymptotic behavior of these correlation functions;

$$\begin{aligned}\langle 0\left|\bar{\psi}_a i\gamma_5\psi_b(x)\bar{\psi}_b i\gamma_5\psi_a(y)\right|0\rangle &\rightarrow \exp\left(-\mu_{ab}|x-y|\right) \\ \langle 0\left|\bar{\psi}_a i\gamma_5\psi_a(x)\bar{\psi}_a i\gamma_5\psi_a(y)\right|0\rangle &\rightarrow \exp\left(-\mu_{aa}|x-y|\right) \\ \langle 0\left|\bar{\psi}_b i\gamma_5\psi_b(x)\bar{\psi}_b i\gamma_5\psi_b(y)\right|0\rangle &\rightarrow \exp\left(-\mu_{bb}|x-y|\right) \\ &\qquad \text{as} \quad |x-y|\rightarrow\infty, \end{aligned} \tag{6.16}$$

we obtain the mass inequality (6.2).

Finally we should comment on the validity of the eqs.(6.13). In deriving the eqs.(6.13), we supposed that gluon intermediate states could be neglected in the $a\bar{a}$ or $b\bar{b}$ channels. This is true in the case listed below.

- in the large N limit. (We will consider this case in the chapter 7)
- for any N with sufficiently large m_a, m_b.
- weakly coupled vector–like theories such as quantum electrodynamics.
- with two distinct quarks a, a' of essentially equal mass (such as up and down quark).

6.3 The Hamiltonian variational approach

In this section we will derive the mass inequality (6.2) from the Hamiltonian variational approach exploited by Nussinov[66]. In the approach we consider the Hamiltonian counterpart of the QCD Lagrangian $\mathcal{L}_{\rm QCD}$. Then the hadronic spectrum can be obtained via the Schrödinger equation

$$H_{\rm QCD}\Psi = \mu\Psi, \tag{6.17}$$

with Ψ a wave function describing the degrees of freedom of the valence quarks and any number of additional quark–antiquark pairs and gluons. The complexity of the physical state in eq.(6.17) impedes quantitative computations of hadronic mass spectrum[4]. However the comparison of masses of meson or baryons differing just by flavor may be easier than direct computations of hadronic mass spectrum. Using a variational principle for the ground state masses and assuming *flavor symmetric* ground state wave functions we can also obtain the inequality (6.2).

Here we will review the basic idea of the Hamiltonian variational approach by using a simple potential toy model, which contains some features of the full–fledged QCD. It is assumed that the interactions –represented by the potentials– are flavor independent and all flavor dependence is in the kinetic terms only. Let us consider a two–body system described by the Hamiltonian

$$H_{12} = K_1 + K_2 + V_{12}. \tag{6.18}$$

For a nonrelativistic Schrödinger equation, the kinetic terms are $K_1 = \vec{p_1}^{\,2}/2m_1, K_2 = \vec{p_2}^{\,2}/2m_2$ with $m_i (i = 1, 2)$ the masses of particles 1 and 2. We assume that the potential V depends only on the relative coordinate

[4]In the case of two dimensional models, we can obtain the bound state equations of the form of eq.(6.17) directly from *first principles*, and determine the mass spectrum exactly in the large N limit, although they include only mesonic sectors. In the next chapter we will explicitly calculate the mass difference of models, for which we have no rigorous proof of the mass inequality, to examine whether the mass inequality holds or not.

$\vec{r} = \vec{r_1} - \vec{r_2}$ and is rotationally invariant *i.e.* $V = V(|\vec{r}|) = V(r)$. We can separate the motion of the center of mass;

$$\begin{aligned} \psi &= e^{i\vec{P}\cdot\vec{R}}\psi_{12}(\vec{r}) \\ \vec{R} &= \frac{m_1\vec{r_1} + m_2\vec{r_2}}{m_1 + m_2}, \quad \vec{r} = \vec{r_1} - \vec{r_2}, \end{aligned} \tag{6.19}$$

and rewrite H_{12} as

$$H_{12} = \frac{\vec{P}^{\,2}}{2M} + \frac{\vec{p}^{\,2}}{2m_{12}} + V_{12}(r) \equiv \frac{\vec{P}^{\,2}}{2M} + h_{12} \tag{6.20}$$

with $\vec{P} = \vec{p_1} + \vec{p_2}$, $\vec{p} = \vec{p_1} - \vec{p_2}$, $M = m_1 + m_2$ and $m_{12} = \frac{m_1 m_2}{m_1+m_2}$. For the subsequent discussion we will specialize to the center of mass system with $\vec{P} = 0$. We are interested in the bound states of h_{ab} which satisfies

$$\begin{aligned} h_{ab}\psi_{ab} &= \epsilon_{ab}\psi_{ab} \\ h_{ab} = \frac{\vec{p}^{\,2}}{2m_{ab}} + V_{ab}(r) &= \frac{\vec{p}^{\,2}}{2m_a} + \frac{\vec{p}^{\,2}}{2m_b} + V_{ab}(r) \equiv \frac{\vec{p}^{\,2}}{2m_a} + \frac{\vec{p}^{\,2}}{2m_b} + V(r) \end{aligned} \tag{6.21}$$

where $\psi_{ab} = \psi_{ab}(r)$ is normalizable state; *i.e.* $\int d^3r \, |\psi_{ab}(\vec{r})|^2 = 1$. (We assume that such bound states exist.)

We can next consider other two systems with identical potentials $V_{aa}(r) = V_{bb}(r) = V(r)$ (*flavor symmetric assumption*), whose Hamiltonians are given by

$$\begin{aligned} h_{aa} &= \vec{p}^{\,2}\left(\frac{1}{2m_a} + \frac{1}{2m_a} + V(r)\right) \\ h_{bb} &= \vec{p}^{\,2}\left(\frac{1}{2m_b} + \frac{1}{2m_b} + V(r)\right). \end{aligned} \tag{6.22}$$

From the eq.(6.21) and (6.22) the operator identity

$$h_{ab} = \frac{1}{2}\left(h_{aa} + h_{bb}\right) \tag{6.23}$$

is obtained. Let $\epsilon^{(0)}_{ab}, \epsilon^{(0)}_{aa}, \epsilon^{(0)}_{bb}$ be the groundstate energy for the three Hamiltonians h_{12} which satisfy $h_{12}\psi^{(0)}_{12} = \epsilon^{(0)}_{12}\psi^{(0)}_{12}$, and consider the expectation value of the identity (6.23) with the ground state $\psi^{(0)}_{ab}$, we obtain

$$\langle\psi^{(0)}_{ab}\,|h_{ab}|\,\psi^{(0)}_{ab}\rangle = \epsilon^{(0)}_{ab} = \frac{1}{2}\left(\langle\psi^{(0)}_{ab}\,|h_{aa}|\,\psi^{(0)}_{ab}\rangle + \langle\psi^{(0)}_{ab}\,|h_{bb}|\,\psi^{(0)}_{ab}\rangle\right). \tag{6.24}$$

By the variational principle each of the expectation values on the right–hand side exceeds $\epsilon^{(0)}_{aa}$ and $\epsilon^{(0)}_{bb}$ respectively, which are minima of $\langle\psi|h_{aa}|\psi\rangle$ and $\langle\psi|h_{bb}|\psi\rangle$ with $\psi = \psi^{(0)}_{aa}$ and $\psi = \psi^{(0)}_{bb}$. Thus we obtain $\epsilon^{(0)}_{ab} \geq \frac{1}{2}\left(\epsilon^{(0)}_{aa} + \epsilon^{(0)}_{bb}\right)$. In the center of mass frame with $\vec{P} = 0$, we can obtain an inequality for the total masses of the bound states by adding the rest mass $m_1 + m_2$ to the binding energy $\epsilon^{(0)}_{12}$;

$$\mu^{(0)}_{ab} \geq \frac{1}{2}\left(\mu^{(0)}_{aa} + \mu^{(0)}_{bb}\right), \tag{6.25}$$

which is essentially the same with the inequality (6.2). While the above discussion is in the framework of nonrelativistic Schrödinger equation, the result (6.25) holds in a far more general context. The particular form of the kinetic energy $K_i = \vec{p}^{\,2}/2m_i$ did not play any role in deriving the operator relation (6.23). Hence K_i could have an arbitrary $\vec{p}$ dependence. In particular, we can take $K_i = \sqrt{\vec{p}^{\,2} + m_i^2}$, the expression appropriate for relativistic motion.

Finally we make some comments on our work that will be discussed in the next chapter. The Hamiltonian variational approach describes bound state problem of two valence quarks, which is essentially quantum mechanical system. It seems to us that the mass inequality (6.25) holds in almost every quantum mechanical system under the *flavor symmetric assumption* (see also section 7.2). Quantum field theories can be regarded as quantum mechanical systems with infinite degrees of freedom. However there exists essential difference between them such as spontaneous symmetry breaking, whose origin is in the infinite degrees of freedom. So the mass inequality may be broken in the case of more complicated field theory models such as the Gross–Neveu model. This is one of the motivations of our work[79].

6.4 The Vafa–Witten theorem

In this section we briefly review the Vafa–Witten work[62], which is most cited of the topics in QCD inequalities.

An outstanding problem about strongly interacting gauge theories is to determine which global symmetries are spontaneously broken and which are unbroken. For these theories there is definite conventional wisdom: the vector symmetries of fermions are all unbroken, while the axial vector (chiral) symmetries are all spontaneously broken in the zero–mass limit.

Imposing some highly plausible technical assumptions, Vafa and Witten showed that the first part of the conventional wisdom is true: *in vector–like gauge theories, vector symmetries are not spontaneously broken.* Given the validity of the first part of the conventional wisdom, the 't Hooft anomaly

matching condition [78] strongly suggests that the second part is also valid in most or all cases.

As in the case of the path integral approach to the mass inequality (see section 6.2), the important point is the positivity of the effective measure. Let X be some observable whose vacuum expectation value we wish to evaluate. Let $\langle X\rangle^A$ be the expectation value of X in a given gauge field A–after integrating out the fermions but before integrating over the gauge field A. Suppose it is known that for any A, $|\langle X\rangle^A| \leq K$ with some constant K that is independent of A. Then the vacuum expectation value of X obeys the same inequality

$$|\langle X\rangle| = \frac{1}{Z}\left|\int \mathcal{D}\mu \langle X\rangle^A\right| \leq K, \tag{6.26}$$

since the average of a function with respect to a real and positive measure is equal to or less than the maximum value of the function. (If the measure $\mathcal{D}\mu$ were not real and positive, eq.(6.26) would not be true in general.)

There are two approaches to show that isospin breaking does not occur in vector–like theories. Here we roughly review these two approaches.

An instructive approach

Let us consider a fermion q of bare mass m in a world volume V. We calculate the space–time average of the vacuum expectation value of $\bar{q}q$ in a background gauge field. This can be written in terms of the trace of fermion Green function in the background field:

$$\langle \bar{q}q\rangle^A = \frac{1}{V}\int d^4x \langle \bar{q}q(x)\rangle^A = \frac{1}{V}\int d^4x \langle x|\frac{1}{\not{D}+m}|x\rangle = \frac{1}{V}\mathrm{Tr}\frac{1}{\not{D}+m}. \tag{6.27}$$

If we let $\rho(\lambda)$ be the density of eigenvalues of hermitian operator $i\not{D}$ per unit space–time volume, we have

$$\langle \bar{q}q\rangle^A = \int d\lambda \rho(\lambda)\frac{1}{m-i\lambda}. \tag{6.28}$$

If we wish to discuss chiral symmetry breaking, we may want to investigate $\lim_{m\to 0}\langle \bar{q}q\rangle$. To this end we note that $\lim_{m\to 0}\frac{1}{m-i\lambda} = iP\frac{1}{\lambda} + \pi\delta(\lambda)$ (P is the principal value symbol), so

$$\langle \bar{q}q\rangle^A = iP\int d\lambda \rho(\lambda)\frac{1}{\lambda} + \pi\rho(0). \tag{6.29}$$

Since the Dirac eigenvalues appear in pairs (see section 6.2), $\rho(\lambda)$ satisfies the relation $\rho(\lambda) = \rho(-\lambda)$. Therefore $\frac{\rho(\lambda)}{\lambda}$ is totally a odd function of λ and

the integral in eq.(6.29) vanishes and we find

$$\langle \bar{q}q \rangle^A = \pi\rho(0). \tag{6.30}$$

So chiral symmetry breaking occurs if $\rho(0) \neq 0$.

For the case of the isospin breaking, let us consider two fermions u and d with bare mass m_u and m_d and show that $\langle \bar{u}u \rangle - \langle \bar{d}d \rangle \to 0$ as $m_u \to m_d$ keeping $m_u, m_d \neq 0$. By analogy to the case of chiral symmetry, we have

$$\begin{aligned} \langle \bar{u}u - \bar{d}d \rangle^A &= \int d\lambda \rho(\lambda) \left(\frac{1}{m_u - i\lambda} - \frac{1}{m_d - i\lambda} \right) \\ &= (m_d - m_u) \int_{-\infty}^{\infty} \frac{d\lambda\rho(\lambda)}{(m_u - i\lambda)(m_d - i\lambda)}. \end{aligned} \tag{6.31}$$

On the right–hand side of eq.(6.31), the explicit factor $m_d - m_u$ vanishes as $m_u \to m_d$. The integral should remain non–singular as $m_d - m_u \to 0$ with $m_u, m_d \neq 0$ because the integral is on the real λ axis while the poles are off this axis at $\lambda = -im_u,\ -im_d$. Hence in the limit $m_d - m_u \to 0$, $\langle \bar{u}u - \bar{d}d \rangle^A$ vanishes for any A. It is plausible that this result survives after averaging over A with positive measure.

The approach used here has the advantage of drawing a clear contrast between chiral symmetry and isospin, but it has several disadvantages. It assumes the order parameter to be a fermion bilinear and does not generalize easily to other possibilities. A bilinear is a suitable order parameter for a non–abelian symmetry like isospin, but for abelian symmetry like baryon number there is no suitable bilinear order parameter.

Another approach

Let $J(x)$ be any operator with a non–zero isospin or baryon number (or any other conserved quantity carried by fermions but not by gauge bosons). We wish to study the expectation value $\langle J(x)J^*(0) \rangle^A$ in a given background field A.

To discuss more concretely, consider the isospin current $J(x) = \bar{q}\gamma_\mu \tau q(x)$($\tau$: Pauli matrices) as an example. In this case $\langle J(x)J^*(0) \rangle^A$ can be written in terms of the fermion propagator in the external field:

$$\langle J^a_\mu(x) J^b_\nu(0) \rangle^A = -\mathrm{Tr}\gamma_\mu \tau^a S_A(x, 0; m) \gamma_\nu \tau^b S_A(0, x; m) \tag{6.32}$$

Here $S_A(x, y; m)$ is the fermion propagator defined in the section 6.2.

Vafa and Witten have shown that there is a bound of type [5]

$$|S_A(x,y;m)| \leq \alpha \exp\left(-\beta|x-y|\right) \tag{6.33}$$

where constants α, β are independent of the gauge field A and $|S|$ denotes the norm of the matrix S. Given the bound (6.33), it would follow from eq.(6.32) that the two–point function of the isospin current in a given background field would be bounded above by $\alpha^2 \mathrm{Tr}(\tau^\alpha)^2 \exp(-2\beta|x|)$. Such an upper bound would survive after averaging over A with a positive measure.

If there were a massless particle $|\chi\rangle$ with non–zero isospin, there would be an isospin bearing operator $J(x)$ creating $|\chi\rangle$ from the vacuum: $\langle 0|J(x)|\chi\rangle \neq 0$. If so, the two-point function $\langle J(x)J^*(0)\rangle$ would not exhibit exponential fall–off. The isospin current J^a_μ is an isospin bearing operator to which above discussion applies. Therefore exponential fall–off of $\langle J^a_\mu(x)J^b_\nu(0)\rangle$ indicates that there is no Goldstone boson in this channel and isospin is not spontaneously broken.

In the case of the baryon number, the situation is more subtle since the baryon number current is a neutral operator to which above discussion does not apply. After some consideration they concluded that there is no order parameter which indicates spontaneous breakdown of baryon number.

In this chapter, we have discussed some examples of QCD inequalities and their applications to symmetry breaking. There are many works on other type of inequalities and symmetry breaking; baryon–meson inequality[61], inequality for glueballs[67], inequalities in the continuum meson–meson sector and for exotic states[68], no spontaneous breaking of parity in QCD[63]. Furthermore QCD–type inequalities are still useful in supersymmetric theories, though in the $m_{\text{Higgsino}} \to \infty$ limit[69]. It has been shown from the Vafa–Witten inequalities that parity is conserved in supersymmetric theories[70].

[5]Exactly speaking, they established a suitable analog of this bound which leads to the same conclusion. Here we will not discuss in detail because its derivation is somewhat complicated and it is not our aim.

Chapter 7

Mass inequalities in $1+1$ dimensional field theories

As shown in the previous chapter it has been proved that the mass inequalities hold in vector–like gauge theories such as 't Hooft model. The key ingredient in the proof is the positivity of the effective measure.

On the other hand we can say nothing about whether mass inequalities hold for more general theories, especially those with Yukawa coupling like the Gross–Neveu models. Though it is difficult to give a general proof for the mass inequalities, the meson mass spectrum solved in chapter 5 enables us to calculate the mass differences directly. In this chapter we investigate whether the mass inequalities in the gauged four–Fermi model, for which no rigorous proof exists for lack of positivity of the effective measure, hold or not by evaluating the meson mass differences directly[79].

7.1 The meson mass susceptibility

In studying the mass inequalities quantitatively, we need a quantitative measure of how "large" the inequality is. This encodes information, intuitively speaking, on how strong the interactions in the theory are. The mass inequality we consider is

$$\delta\mu_{ab} \equiv \mu_{ab} - \frac{(\mu_{aa} + \mu_{bb})}{2}, \tag{7.1}$$

which is known to be positive for vector–like theories (see chapter 6). Here, denoting the constituents q's, μ_{ab} is the mass of the meson that overlaps with the $\overline{q_a}q_b$ state, and so on.

This quantity is dimensionful and depends not only on the model, but also on the difference of the masses of the constituents. The quantity may be made

dimensionless trivially by taking the ratio of the inequality with a meson mass, but this inequality may still become large just because the constituent mass difference is large. In fact, if we consider the field theory space to be parameterized by the couplings of the model, including the masses, the mass inequality is *not* a local quantity in the parameter space. It is more natural to define a local parameter in the field theory space. Let us define the mass squared of the constituents to be

$$M_a^2 = M^2(1+\Delta), \qquad M_b^2 = M^2(1-\Delta). \tag{7.2}$$

The meson mass difference $\delta\mu_{ab}$ is even under the interchange of M_a and M_b and is therefore an even function of Δ.

We shall characterize the inequality by a parameter we refer to as the "meson mass susceptibility", for the lack of a better name. This quantity is defined by

$$\mathcal{R} \equiv \lim_{\Delta\to 0} \frac{\delta\mu_{ab}}{\mu_{ab}\Delta^2} = \lim_{\Delta\to 0} \frac{2\mu_{ab} - (\mu_{aa}+\mu_{bb})}{2\mu_{ab}\Delta^2} \tag{7.3}$$

7.2 Mass inequalities in quantum mechanics

In this section, we briefly discuss mass inequalities in quantum mechanics. While the discussion is not necessary for computing mass inequalities in relativistic field theories, we feel that it is nonetheless quite instructive and provides a broader perspective on mass inequalities in quantum theories. Also, the mass inequalities in relativistic field theories should reduce to that of quantum mechanics in the non–relativistic limit.

In quantum mechanics, the problem of two body bound states under a local potential reduces to a model with the Hamiltonian

$$H = \frac{p^2}{2M_{12}} + V(x), \tag{7.4}$$

where M_{12} denotes the reduced mass, $1/M_{12} = 1/M_1 + 1/M_2$. We will analyze one dimensional models, but similar analysis can be applied to higher dimensional models.

Infinitely deep square well potential

The potential of the model is

$$V(x) = \begin{cases} 0 & (0 \le x \le L) \\ \infty & (x < 0, x > L) \end{cases}. \tag{7.5}$$

The spectrum of the bound states is known to be $E_{12,n} = \frac{\pi^2}{2M_{12}L^2}n^2$, $(n = 1, 2, \ldots)$. This is somewhat trivial but an interesting case. The susceptibility $\mathcal{R} = 0$ and this we can understand as the signature of the model being free within the well.

Delta function potential

The delta function potential

$$V(x) = -V_0\delta(x) \qquad (V_0 > 0) \tag{7.6}$$

has a bound state with the binding energy $-M_{12}V_0^2/2$. The mass inequality is

$$\delta\mu_{ab} = E_{ab} - \frac{E_{aa} + E_{bb}}{2} = \frac{V_0^2}{8}\frac{(M_a - M_b)^2}{(M_a + M_b)}. \tag{7.7}$$

This leads to the susceptibility

$$\mathcal{R} = \frac{V_0^2}{32\,(1 - V_0^2/8)} > 0. \tag{7.8}$$

In the non-relativistic limit, $V_0 \ll 1$.

Monomial potentials

Let us also discuss potentials whose behavior is governed by a monomial

$$V(x) = A\,x^\gamma, \qquad A\gamma > 0, \tag{7.9}$$

where γ needs not be an integer but $\gamma > -2$ needs to be satisfied for sensible physics behavior. $A\gamma > 0$ needs to be imposed for the existence of bound states. $\gamma = 2, -1$ corresponds to the harmonic oscillator and the three dimensional Coulomb case.

We can use the uncertainty principle to crudely estimate the bound state energy as

$$E_{12} \simeq \left(\frac{\gamma}{2} + 1\right) A \left(\frac{1}{\gamma A M_{12}}\right)^{\frac{\gamma}{\gamma+2}}. \tag{7.10}$$

We can obtain the susceptibility from this energy as

$$\mathcal{R} \simeq \frac{1}{8(\gamma + 2)} \left(\frac{\gamma A}{2}\right)^{\frac{2}{\gamma+2}} M^{-\frac{2(\gamma+1)}{\gamma+2}} > 0 \tag{7.11}$$

in the non–relativistic limit. While the derivation is not rigorous, the susceptibilities agrees with those obtained exactly, in the harmonic oscillator and the Coulomb cases.

Relation between the mass inequality and the susceptibility

Here we comment on the relation between the mass inequality $\delta\mu_{ab}$ and the meson mass susceptibility $\mathcal{R}$.

Let us consider the monomial potential case. The binding energy can be rewritten as

$$E_{12} \simeq \left(\frac{\gamma}{2}+1\right) A \left(\frac{M_1^{-1}+M_2^{-1}}{\gamma A}\right)^{\frac{\gamma}{\gamma+2}} \equiv F\left(\frac{M_1^{-1}+M_2^{-1}}{2}\right), \tag{7.12}$$

where we define $F(x) \equiv \left(\frac{\gamma}{2}+1\right) A \left(\frac{2x}{\gamma A}\right)^{\frac{\gamma}{\gamma+2}}$. Then the mass inequality can be written as

$$\delta\mu_{ab} = F\left(\frac{M_a^{-1}+M_b^{-1}}{2}\right) - \frac{F\left(M_a^{-1}\right)+F\left(M_b^{-1}\right)}{2}. \tag{7.13}$$

Mathematically, this problem is reduced to the problem of *convex analysis*. Thus, if the $F(x)$ is a concave (convex) function, the mass inequality $\delta\mu_{ab}$ is always positive (negative) [1].

On the other hand, the susceptibility $\mathcal{R}$ can be written as

$$\mathcal{R} = -\frac{1}{8M^2[2M+F(M^{-1})]} F''(M^{-1}) \approx -\frac{F''(M^{-1})}{16M^3}, \tag{7.14}$$

where we have used the fact that the binding energy is negligible in the non–relativistic limit. This formula clarifies that the mass susceptibility $\mathcal{R}$ is proportional to $-F''(M^{-1})$ and if $\mathcal{R}$ is positive for any value of M, $F(x)$ is a concave function, which indicates that the mass inequality is unbroken.

Here we took the monomial potential case as a concrete example. It is not difficult to verify that this argument is valid for the other quantum mechanical systems discussed above.

Unfortunately, in the case of quantum field theories, the situation is more complicated and above discussion cannot be easily extended to them. However we believe that this relation between the mass inequality and susceptibility is also valid for quantum field theories.

[1] **definition of concave (convex) functions**: Here we have used the following definition. If the real function $F(x)$ satisfies the inequality $F\left(\frac{x+y}{2}\right) \leq \frac{1}{2}\left(F(x)+F(y)\right)$, $F(x)$ is a convex function. And if $-F(x)$ is a convex function, then $F(x)$ is a concave function.

The necessary and sufficient condition for the concavity (convexity) of a function $F(x)$ is $F''(x) \leq 0$ ($F''(x) \geq 0$) for any x.

7.3 Mass inequalities in the generalized Gross-Neveu model

In this section, we analyze the mass inequalities in the generalized Gross–Neveu models, described by the Lagrangian

$$\mathcal{L} = \sum_{f=1}^{N_F} \overline{\psi}_f (i\partial\!\!\!/ - m_f)\psi_f + \frac{a^2}{2} \sum_{f,f'=1}^{N_F} (\overline{\psi_{f'}}\psi_f)(\overline{\psi_f}\psi_{f'}) - \frac{a_5^2}{2} \sum_{f,f'=1}^{N_F} (\overline{\psi_{f'}}\gamma_5\psi_f)(\overline{\psi_f}\gamma_5\psi_{f'}). \tag{7.15}$$

In addition to the flavor indices f, f' denoted explicitly in the above formula, the fermions carry an additional internal space index, the 'color' index $(1, 2, \ldots N)$ which has been suppressed in the notation. This index should not be confused with the flavor index. We take the large N limit while keeping $a^2 N, a_5^2 N$ fixed. When $m_f = 0, a_5^2 = 0$, the model reduces to the original Gross–Neveu model with discrete chiral symmetry (see section 3.1) and when $m_f = 0, a^2 = a_5^2$, the model reduces to the Gross–Neveu model with continuous chiral symmetry (see section 3.2). We need to consider multiple flavors for the analysis of the mass inequalities.

This class of models is included in the gauged four–Fermi models we dealt with in chapter 5 and the analytic methods discussed there can be applied here also. However, the generalized Gross–Neveu models can be solved completely analytically using different methods than the gauged four–Fermi model case, so we shall discuss it separately.

The generalized Gross–Neveu models were solved in chapter 4(see also ref.[32]). Here, in general, we shall need the spectrum in *the most general case* when two flavors have different masses, $m_1^2 \neq m_2^2$, and $a^2 \neq a_5^2$, which was not solved explicitly there. We shall present the spectrum and analyze the mass inequalities.

Let us consider a meson bound state of constituents with masses, M_1, M_2. These constituent masses are physical fermion masses that include the effects of spontaneous chiral symmetry breaking that occurs dynamically in the Gross–Neveu model. We dispense with the derivation here, but the Bethe–Salpeter equation for the meson state can be solved algebraically to obtain the meson "wave function", $\varphi(x)$ as

$$\varphi(x) = \varphi^{(0)} + \varphi^{(1)}(1-2x) + \hat{\varphi}(x), \qquad (0 \leq x \leq 1) \tag{7.16}$$

$$\hat{\varphi}(x) = \frac{\mu_{12}^2 \left(\varphi^{(0)} + \varphi^{(1)}(1-2x)\right) + 2\left(M_1^2 - M_2^2\right)\varphi^{(1)}}{-\mu_{12}^2 + \frac{M_1^2}{x} + \frac{M_2^2}{1-x}}, \tag{7.17}$$

where $\varphi^{(0)}, \varphi^{(1)}$ are constants and $\hat{\varphi}(x)/\left[x(1-x)\right]$ is integrable at $x = 0, 1$.

The meson wave function satisfies the following boundary conditions

$$\begin{pmatrix} M_+ & (1{+}4G_5)M_- \\ M_- & (1{+}4G)M_+ \end{pmatrix}\begin{pmatrix} \varphi^{(0)} \\ \varphi^{(1)} \end{pmatrix}=\int_0^1 dx\frac{\hat{\varphi}(x)}{x(1{-}x)}\begin{pmatrix} G_5 & 0 \\ 0 & G \end{pmatrix}\begin{pmatrix} M_+ & M_- \\ M_- & M_+ \end{pmatrix}\begin{pmatrix} 1 \\ 1{-}2x \end{pmatrix}. \tag{7.18}$$

Here, we used the notation $G \equiv a^2N/(4\pi)$, $G_5 \equiv a_5^2N/(4\pi)$ for the *renormalized* couplings and defined $M_\pm \equiv (M_1 \pm M_2)/2$. When the coupling constants are equal, $a^2 = a_5^2$, or when the masses are equal, $M_1 = M_2$, the two boundary condition equations simply decouple, but do *not* in the general case.

The boundary conditions lead to a secular equation

$$\begin{vmatrix} \mu^2 J_{12} - \frac{1}{2G_+} - \frac{1}{G_-}\frac{M_1^2+M_2^2}{4M_1M_2} & (M_1^2-M_2^2)J_{12} + \ln\frac{M_1^2}{M_2^2} - \frac{1}{G_-}\frac{M_1^2-M_2^2}{4M_1M_2} \\ -(M_1^2-M_2^2)J_{12} + \ln\frac{M_1^2}{M_2^2} + \frac{1}{G_-}\frac{M_1^2-M_2^2}{4M_1M_2} & (\mu^2-2M_1^2-2M_2^2)J_{12} - \frac{1}{2G_+} + \frac{1}{G_-}\frac{M_1^2+M_2^2}{4M_1M_2} \end{vmatrix} = 0. \tag{7.19}$$

Here, we defined $\frac{1}{G_\pm} \equiv \frac{1}{G_5} \pm \frac{1}{G}$ and

$$J_{12} \equiv \int_0^1 \frac{dx}{-\mu^2 x(1-x) + M_1^2(1-x) + M_2^2 x}. \tag{7.20}$$

It should be noted that since the couplings G, G_5 are dimensionless, the overall mass scale M can always be scaled out of the problem and only the relative masses have a physical meaning. The physical parameters of this quantum field theory are the two dimensionless renormalized couplings G and G_5.

Before we analyze the behavior of the mass inequalities, we first need to understand the behavior of the spectrum when the masses of the constituents are the same. In this case, the secular equation (7.19) splits into two independent equations for the pseudo–scalar and scalar bound states, π and σ:

$$\pi: \qquad \frac{1}{G_5} = \int_0^1 dx\, \frac{(\mu_\pi/M)^2}{1-(\mu_\pi/M)^2 x(1-x)} = \frac{4}{\sqrt{4(M/\mu_\pi)^2-1}} \tan^{-1}\left(\frac{1}{\sqrt{4(M/\mu_\pi)^2-1}}\right) \tag{7.21}$$

$$\sigma: \qquad \frac{1}{G} = \int_0^1 dx \frac{(\mu_\sigma/M)^2-4}{1-(\mu_\sigma/M)^2 x(1-x)} \tag{7.22}$$

σ exists as a non–tachyonic bound state only for $G < -1/4$. It is not clear whether the theory is unitary for negative G and we shall consider the region $G \geq 0$, so we shall not have much more to say on σ. The original Gross–Neveu model corresponds to $G \to -\infty$ in our scheme and in this limit, $\mu_\sigma^2 \to 4M^2$.

π exists as a bound state for any $G_5 \geq 0$ and $0 \leq \mu_\pi \leq 4M^2$. The dependence of the bound state mass on the coupling is plotted in Fig. 7.1. This is the only bound state in the model for $G, G_5 > 0$ and corresponds to the Nambu–Goldstone like particle when the constituent masses are zero[22, 39], as in the Gross–Neveu model with continuous chiral symmetry. It is the dependence of this meson state on the constituent masses that we shall investigate. As a side note, there is an intriguing possibility when $G_5 \geq 0$ and $G < -1/4$, in some cases, the π mass can be larger than the σ mass. We do not know whether this can be achieved in a physically consistent situation. Another comment is perhaps appropriate; in the literature, the Gross–Neveu model ($G \neq 0, G_5 = 0$) is often used as a prototypical simple model with a bound state. However, the original Gross–Neveu model has no binding energy for the meson and has barely a bound state. It seems to us that in fact, the simplest theory that may be considered in this family that is useful in analyzing bound state dynamics is $G_5 \neq 0, G = 0$ case. In this case, we have a bound state whose mass depends on the coupling.

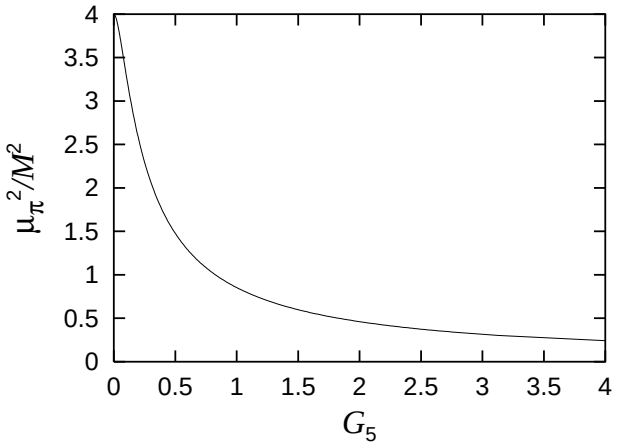

Figure 7.1: The behavior of the π meson mass, μ_π^2/M^2 with respect to the coupling, G_5.

The meson mass susceptibility may be obtained by perturbing the equation (7.19) in the mass difference parameter Δ. After some computation, we derive

$$\mathcal{R} = \left(\zeta - \frac{1}{4}\right)\left\{\frac{1}{2} - \frac{1}{\left(1+\frac{\zeta}{G_5}\right)\left[\left(\zeta-\frac{1}{4}\right)\frac{1}{G_5}+\frac{1}{4G}\right]}\right\} \tag{7.23}$$

(see appendix A). We defined $\zeta \equiv M^2/\mu_0^2$, where μ_0^2 is the mass of the meson

in the unperturbed case, when $\Delta = 0$. The susceptibility is independent of the mass scale since it can be scaled out of the problem. The susceptibility may be shown to be *positive for any* $G, G_5 > 0$.

It is interesting to check the asymptotic behavior of the susceptibility for small and large couplings. For small coupling

$$\mathcal{R} = \frac{\pi^2 G_5^2}{2}\left[1 - 8G_5(1+4G) + \mathcal{O}(G_5^2)\right]. \tag{7.24}$$

This behavior is consistent with that for the δ function problem discussed in section 7.2. For large couplings,

$$\mathcal{R} = \frac{G_5}{2(4G+1)} - \frac{1}{24(4G+1)^2} + \mathcal{O}\left(G_5^{-1}\right). \tag{7.25}$$

The behavior of the susceptibility with respect to G_5 is shown for $G = 0, 0.1, 1, 10$ in Fig. 7.2. The dependence on G is not strong; this is because the properties of the bound state π is governed mostly by the pseudo–scalar coupling G_5. The asymptotic behavior of the susceptibility can be seen in the plot.

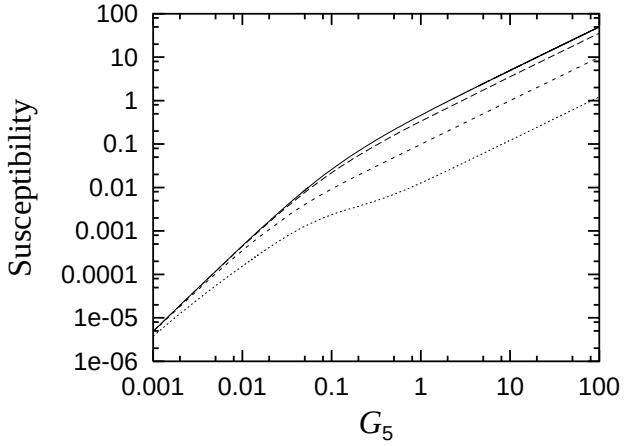

Figure 7.2: The behavior of the meson mass susceptibility $\mathcal{R}$ with respect to the coupling G_5 for the generalized Gross–Neveu models. The lines represent, from top to bottom, $\mathcal{R}$ for $G = 0, 0.1, 1, 10$ respectively.

7.4 Mass inequalities in the gauged four-Fermi model

In the generalized Gross–Neveu model, the spectrum could be obtained by just solving an ordinary equation, albeit an transcendental one. In contrast, for the gauged four–Fermi model, we need to solve an integral equation which is technically more involved. Of course, this is to be expected, since the usual 't Hooft model, which is a simpler model, is solved in terms of an integral equation. To solve the integral equation (5.21), we have employed two methods (see section 5.3). With either of the two methods, we can solve for the spectrum and the wavefunctions of the meson states for arbitrary combinations of masses and couplings in the gauged four–Fermi model. By using the two different methods simultaneously, we are able to obtain a better control over the error in the results which inevitably arise when we solve the integral equation numerically.

Let us move on to the behavior of meson mass susceptibilities. To compute the susceptibilities, we may just use the methods explained in section 5.3 and obtain the susceptibility as the limiting case of small mass differences going to zero. We can refine the method by perturbing in the mass difference analytically and obtain the mass susceptibilities directly. However, the standard perturbation formulas are *not* applicable to either of the two methods explained in section 5.3. While this should be of use to further study, since this is technical and somewhat involved we have chosen to describe the methods concretely in appendix C. We have computed the susceptibility from both methods and have checked that the results do agree.

The parameters of the gauged four–Fermi model are β, G, G_5 and we expect G to play a not so dominant role in determining the properties of the lightest meson state. G_5 is the pseudo–scalar coupling that strongly affects the lightest meson. β is in fact the strength of the gauge coupling; when β is large, the gauge coupling is small and vice versa.

For $G = G_5$ and $\beta = 0$, we can show analytically that the susceptibility is zero.

For the other values of parameters, numerical calculation is needed and here we plot the meson mass susceptibility in some cases. For $\beta \gg 1$, the susceptibilities approach those of the generalized Gross–Neveu model as expected, since the gauge coupling is weak. It can be seen from comparison of Fig. 7.3 and Fig. 7.2. Furthermore we found that $\mathcal{R}$ does hardly change for $\beta \gtrsim 1$ (see Fig. 7.4 and Fig. 7.5). This indicates that the gauged four–Fermi model is reduced to the Gross–Neveu model for $\beta \gtrsim 1$. And it can be also seen from the Fig. 7.4 and Fig. 7.5 that $\mathcal{R}$ increases linearly for

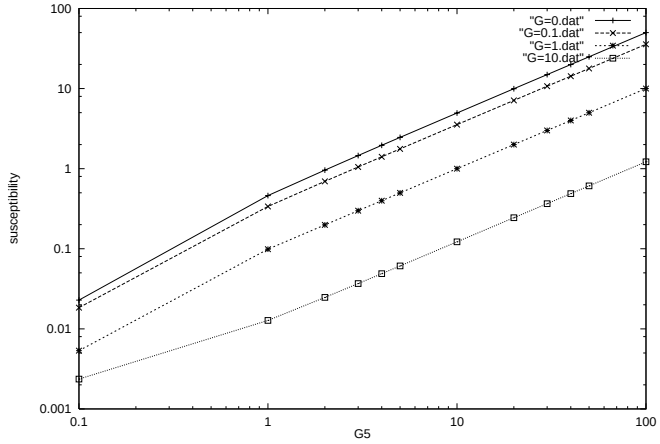

Figure 7.3: The behavior of the meson mass susceptibility $\mathcal{R}$ with respect to the coupling G_5 for $\beta = 1 \times 10^4$ case. This case is considered to correspond to the Gross–Neveu limit and it has the similar behavior with Fig. 7.2 The lines represent, from top to bottom, $\mathcal{R}$ for $G = 0, 0.1, 1, 10$ respectively.

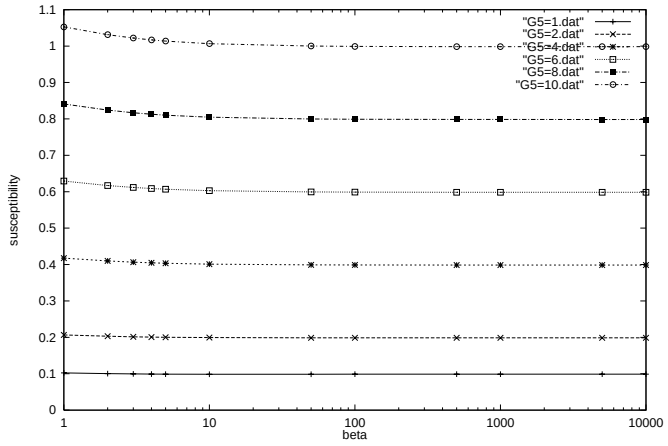

Figure 7.4: The behavior of the meson mass susceptibility $\mathcal{R}$ with respect to the coupling β for some values of G_5 ($G_5 = 1, 2, 4, 6, 8, 10$). We found that $\mathcal{R}$ does not change for $\beta \gg 1$ and increases linearly with respect to G_5.

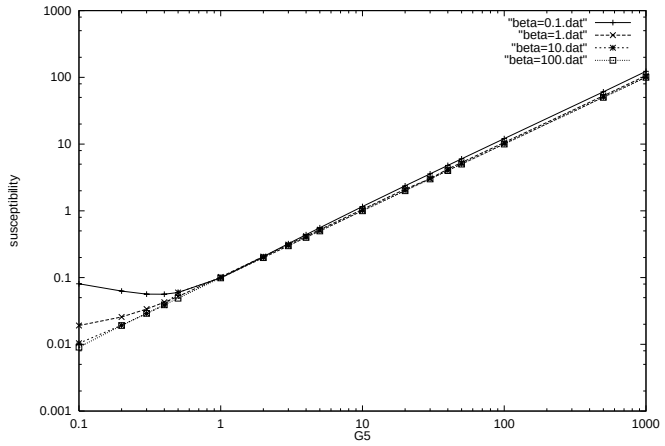

Figure 7.5: The behavior of the meson mass susceptibility $\mathcal{R}$ with respect to the coupling G_5 for some values of β ($\beta = 0.1, 1, 10, 100$). For sufficiently large G_5 ($G_5 \gg 1$), $\mathcal{R}$ increase linearly.

large G_5, which is consistent with the behavior of the Gross–Neveu model (see eq.(7.25)).

We have investigated throughout the parameter space to find that the mass inequality holds in *almost all the region* of the parameter space[2]. In the case of Gross–Neveu models, we have already shown analytically that the mass inequality is *not* broken for any combinations of four–Fermi couplings (G, G_5) despite its equivalence to the model with Yukawa couplings (see section 7.3). For the 't Hooft model there is a rigorous proof that the mass inequality is unbroken (see chapter 6). Taking these things into consideration, it seems unnatural that the mass inequality is broken after combining two models, for which it is unbroken.

[2]Strictly speaking, we found some loopholes in the strong coupling region ($\beta \sim 0, G \sim G_5$), where the mass inequality *may* be broken. Unfortunately, in such a region, the convergence of numerical solutions is not good enough to determine whether it is really broken or not. (For further details, see ref.[79] and also appendix B.)

Chapter 8

Supersymmetric gauge theories in four dimensions

8.1 Overview

In the previous chapters we have discussed nonperturbative properties of 1+1 dimensional (gauge) theories which have asymptotic freedom. In analyzing these models, the large N expansion plays an important role; it enables us to add up all the diagrams and to obtain the spectrum and wave functions of bound states of quarks.

Another direction to derive nonperturbative effects exactly is extending the gauge theories to those with supersymmetry. In the rest of this thesis, we will focus on nonperturbative properties in four dimensional supersymmetric gauge theories [1].

From the supersymmetric point of view, the ordinary QCD corresponds to, as it were $\mathcal{N} = 0$ supersymmetric gauge theory. In general the more the number of supersymmetry $\mathcal{N}$ increases, the more constraints are imposed on the theories. For example, in $\mathcal{N} = 1$ supersymmetric theories, flavor symmetries and holomorphy determine the form of the effective superpotential exactly, and we can explore their phase structure and the mechanism of phase transitions[106]. Unfortunately, no such constraints apply to the effective Kähler potential and it is not fully determined. However the situation is under much better control for $\mathcal{N} = 2$ supersymmetric gauge theories where the Kähler potential follows from a holomorphic pre-potential and the entire low–energy effective Lagrangian can be completely determined. Furthermore in $\mathcal{N} = 2$ theories, central charge appears in the supersymmetric algebra[102], which gives Bogomol'nyi, Prasad Sommerfield bound[100, 101].

[1] From here on, we will use the notation in appendix D.

The mass of any state satisfies

$$M \geq \sqrt{2}|Z_{\mathcal{N}=2}|, \tag{8.1}$$

where $Z_{\mathcal{N}=2}$ is the central charge of the $\mathcal{N}=2$ algebra, involving the gauge and global quantum numbers of the states. The BPS saturated states, for which the inequality (8.1) is saturated, are some of the stable states in the spectrum. Since $Z_{\mathcal{N}=2}$ is a holomorphic object, it can often be exactly determined; eq.(8.1) then yields the exact mass spectrum for some of the stable states. Using the BPS states and duality, which transforms elementary fields in strong coupling into solitonic BPS states in weak coupling, we can exactly determine the low energy effective action of $\mathcal{N}=2$ supersymmetric gauge theories (see section 8.2).

In the case of $\mathcal{N}=1$ supersymmetric theories, no central term appears in the superalgebra and correspondingly no particle–like BPS state exists. However, if the translational invariance is broken, the $\mathcal{N}=1$ superalgebra also receives contributions from central charges (see section 9.2) and extended types of BPS states such as BPS domain walls appear. In the rest of this thesis we will discuss the BPS domain walls and BPS domain wall junctions in $\mathcal{N}=1$ supersymmetric theories.

In this chapter we briefly review the Seiberg–Witten theories, toy models of which enable us to obtain exact solution of BPS domain walls and BPS domain wall junctions.

8.2 The Seiberg–Witten theory: $\mathcal{N}=2$ pure super Yang–Mills theory

Seiberg and Witten derived the exact solution for the first time in four dimensional gauge field theories in the strong gauge coupling region. The key ingredients in solving the problem are holomorphy, duality, and BPS states. In this section we briefly review how the exact solution of $\mathcal{N}=2$ supersymmetric gauge theories can be obtained by using models with $SU(2)$ gauge symmetry originally considered by Seiberg and Witten.

8.2.1 $\mathcal{N}=2$ $SU(2)$ pure super Yang–Mills theory

Firstly we consider $\mathcal{N}=2$ pure super Yang–Mills theory with $SU(2)$ gauge group, in which only $\mathcal{N}=2$ vector multiplet exists. In terms of $\mathcal{N}=1$ supersymmetry, an $\mathcal{N}=2$ vector multiplet is composed of an $\mathcal{N}=1$ vector superfield $W_\alpha^a(A_\mu^a, \lambda^a)$ and an $\mathcal{N}=1$ chiral superfield $\Phi^a(\psi^a, \phi^a)$ in

the adjoint representation of the gauge group($a = 1, 2, 3$). The Lagrangian of the theory is

$$\begin{aligned}\mathcal{L} &= \frac{1}{2\pi}\mathrm{Im}\left[\tau_{\mathrm{cl}}\int d^2\theta d^2\bar{\theta}\mathrm{tr}\Phi^\dagger e^{-2V}\Phi + \tau_{\mathrm{cl}}\int d^2\theta\frac{1}{2}\mathrm{tr}WW\right] \\ &= \mathrm{tr}\Bigg\{\frac{2}{g^2}\Bigg(-\frac{1}{4}F^{\mu\nu}F_{\mu\nu} - \bar{\lambda}i\bar{\sigma}^\mu\mathcal{D}_\mu\lambda - \bar{\psi}i\bar{\sigma}^\mu\mathcal{D}_\mu\psi - \mathcal{D}_\mu\phi\mathcal{D}^\mu\phi^\dagger \\ &\qquad + i\sqrt{2}\phi[\bar{\lambda},\bar{\psi}] + i\sqrt{2}\phi^\dagger[\lambda,\psi] - \frac{1}{2}[\phi,\phi^\dagger]^2\Bigg) \\ &\qquad - i\frac{\theta}{32\pi^2}\epsilon^{\mu\nu\alpha\beta}F_{\mu\nu}F_{\alpha\beta}\Bigg\}. \end{aligned} \tag{8.2}$$

Here τ_{cl} is the classical (complex) gauge coupling constant; more concretely it can be written with the gauge coupling g and the vacuum angle θ as $\tau_{\mathrm{cl}} = \theta/2\pi + i4\pi/g^2$.

The beta function of $SU(2)$ $\mathcal{N} = 2$ gauge theory is obtained by 1 loop approximation as

$$\beta = -\frac{g^3}{16\pi^2}\left(4 - N_f\right), \tag{8.3}$$

where N_f denotes the number of hypermultiplets. In the case of $\mathcal{N} = 2$ supersymmetric theories, no higher loop correction exists and eq.(8.3) is exact. In this section we consider the case with no hypermultiplet ($N_f = 0$), where the model is asymptotic free. As is the case of the Gross–Neveu model, the classical Lagrangian (8.2) contains only a dimensionless parameter g, however in the quantum theory dimensional transmutation occurs and dimensionful mass scale Λ appears (see section 3.1.3).

8.2.2 The classical moduli space

From the Lagrangian (8.2) the classical potential for scalar components is

$$V(\phi) = \frac{1}{g^2}\mathrm{Tr}\left[\phi,\phi^\dagger\right]^2, \tag{8.4}$$

where $\phi = \sum_{a=1}^{3}\phi^a\sigma^a$. The classical theory therefore has a family of vacuum states, which is labeled by, for instance, $\phi = \frac{1}{2}a\sigma^3$ with a complex parameter a. The gauge symmetry is broken to $U(1)$ with nonzero value of a, which is restored only if the complex parameter a becomes zero.

The classical moduli space of vacua is parameterized by gauge invariant quantity

$$u = \mathrm{Tr}\phi^2 = \frac{1}{2}a^2 \qquad (u \in \mathbf{C}). \tag{8.5}$$

Classically, there is a singularity at $u = 0$, where full $SU(2)$ gauge symmetry is restored and more fields become massless.

8.2.3 The low energy effective Lagrangian

For sufficiently large $|u|$ ($|u| \gg \Lambda$), the theory is in weak coupling region and semiclassical approximation is useful. Let us consider the low energy effective action for light fields. In the weak coupling region W_α^a and Φ^a ($a = 1, 2$) are highly massive and low energy theory contains only a single $\mathcal{N} = 2$ vector multiplet, which we call (A, W_α) in terms of $\mathcal{N} = 1$ superfields. As mentioned before, the low energy effective Lagrangian is completely determined from a holomorphic prepotential $\mathcal{F}(A)$ as

$$\mathcal{L} = \frac{1}{4\pi}\mathrm{Im}\left[\int d^2\theta d^2\bar{\theta}\frac{\partial\mathcal{F}(A)}{\partial A}\bar{A} + \int d^2\theta\frac{1}{2}\frac{\partial^2\mathcal{F}(A)}{\partial A^2}W_\alpha W^\alpha\right]. \tag{8.6}$$

And the Kähler potential can be written with the prepotential

$$K(A,\bar{A}) = \mathrm{Im}\left(\frac{\partial\mathcal{F}(A)}{\partial A}\bar{A}\right) = \frac{1}{2i}\left(\frac{\partial\mathcal{F}(A)}{\partial A}\bar{A} - \frac{\partial\bar{\mathcal{F}}(\bar{A})}{\partial\bar{A}}A\right) \tag{8.7}$$

In the classical theory, the prepotential $\mathcal{F}$ can be read off from the tree level Lagrangian of the $SU(2)$ gauge theory; $\mathcal{F}_{\mathrm{cl}}(A) = \frac{1}{2}\tau_{\mathrm{cl}}A^2$.

The classical relation $\tau_{\mathrm{cl}} = \frac{\partial^2\mathcal{F}_{\mathrm{cl}}(a)}{\partial a^2}$ is extended to the effective coupling constant in quantum theory

$$\tau(a) = \frac{\partial^2\mathcal{F}(a)}{\partial a^2}, \qquad \tau(a) = \frac{\theta_{\mathrm{eff}}(a)}{2\pi} + i\frac{4\pi}{g^2(a)}. \tag{8.8}$$

The quantum corrections to $\mathcal{F}$ were analyzed in ref.[93]. The tree level and one–loop corrections add up to

$$\mathcal{F}_{1\mathrm{loop}}(A) = \frac{i}{2\pi}A^2\log\frac{A^2}{\Lambda^2} \tag{8.9}$$

and higher order perturbative corrections are absent. In addition there are nonperturbative instanton contributions

$$\mathcal{F}_{\mathrm{instanton}}(A) = \sum_{k=1}^{\infty}\mathcal{F}_k\left(\frac{\Lambda}{A}\right)^{4k}A^2, \tag{8.10}$$

where the k–th terms arises as a contribution of k instantons. Adding eqs.(8.9) and (8.10), the prepotential in the weak coupling region is

$$\mathcal{F}(A) = \frac{i}{2\pi}A^2\log\frac{A^2}{\Lambda^2} + \sum_{k=1}^{\infty}\mathcal{F}_k\left(\frac{\Lambda}{A}\right)^{4k}A^2. \tag{8.11}$$

Differentiating eq.(8.7), we obtain the Kähler metric

$$\frac{\partial^2 K}{\partial a \partial \bar{a}} = \frac{1}{2i}\left(\frac{\partial^2 \mathcal{F}}{\partial a^2} - \frac{\partial^2 \bar{\mathcal{F}}}{\partial \bar{a}^2}\right) = \mathrm{Im}\frac{\partial^2 \mathcal{F}}{\partial a^2} = \mathrm{Im}\tau(a). \tag{8.12}$$

Thus the metric on the moduli space becomes

$$(ds)^2 = \mathrm{Im}\tau(a) da d\bar{a} \tag{8.13}$$

and $\mathrm{Im}\tau(a)$ is required to be positive definite. However, if $\mathrm{Im}\tau(a)$ is globally defined, it cannot be positive definite as the harmonic function $\mathrm{Im}\tau$ cannot have a minimum. This indicates that the above discussion of the metric must be valid only locally. If we define $a_D \equiv \frac{\partial \mathcal{F}}{\partial a}$, then the metric (8.13) can be rewritten

$$(ds)^2 = \mathrm{Im} da_D d\bar{a} = \frac{1}{2i}\left(da_D d\bar{a} - da d\bar{a}_D\right). \tag{8.14}$$

This formula is completely symmetric in a and a_D, so if we use a_D as a local parameter, the metric will be in the same general form as eq.(8.13) with a different harmonic function replacing $\mathrm{Im}\tau$. As we will see presently, a_D can be regarded as dual Higgs field of a and exchanging these fields corresponds to the electric–magnetic duality.

8.2.4 Duality

In order to investigate the physics in the strong coupling region $|u| \sim \Lambda$, we can use duality transformation which maps the original field theory in the strong coupling region into the weak coupling theory of dual fields. To see this concretely, let us examine how duality works in the Lagrangian (8.6).

Consider the second term of the eq.(8.6); $\frac{1}{8\pi}\mathrm{Im}\int d^2\theta \tau(A) W^2$, in which we treat W_α as an independent chiral field. The superspace Bianchi identity is $\mathrm{Im}DW = 0$, where D is supercovariant derivative. This identity can be implemented by a real vector superfield V_D which acts as a Lagrange multiplier. Adding the constraint term

$$\begin{aligned}\frac{1}{4\pi}\mathrm{Im}\int d^4x d^2\theta d^2\bar{\theta} V_D DW &= \frac{1}{4\pi}\mathrm{Re}\int d^4x d^2\theta d^2\bar{\theta} i D V_D W \\ &= -\frac{1}{4\pi}\mathrm{Im}\int d^4x d^2\theta W_D W \end{aligned} \tag{8.15}$$

to the action and performing the Gaussian integral over W, we obtain an equivalent Lagrangian

$$\frac{1}{8\pi}\mathrm{Im}\int d^2\theta \frac{-1}{\tau(A)} W_D^2. \tag{8.16}$$

Notice that in the Lagrangian (8.16), effective coupling constant is inversed; $\tau \to \frac{-1}{\tau}$. We call this transformation "S–transformation".

To proceed further, we need to transform the $\mathcal{N}=1$ chiral supermultiplet A to A_D. If we define

$$h(A) \equiv \frac{\partial \mathcal{F}}{\partial A} = A_D, \quad h_D(A_D) \equiv -A = h_D(h(A)), \tag{8.17}$$

the kinetic term of the classical multiplet is transformed as

$$\begin{aligned} \mathrm{Im} \int d^2\theta d^2\bar{\theta} \left(\frac{\partial \mathcal{F}}{\partial A} \bar{A} \right) &= \mathrm{Im} \int d^2\theta d^2\bar{\theta} h(A) \bar{A} \\ &= -\mathrm{Im} \int d^2\theta d^2\bar{\theta} A_D \bar{h}_D(A_D) = \mathrm{Im} \int d^2\theta d^2\bar{\theta} h_D(A_D) \bar{A}_D. \end{aligned} \tag{8.18}$$

Thus it is invariant under the duality transformation (8.17). Furthermore by using the relation (8.17),

$$\frac{-1}{\tau(A)} = \frac{-1}{\frac{\partial^2 \mathcal{F}}{\partial A^2}} = \frac{-1}{\frac{\partial h}{\partial A}} = \frac{\partial h_D}{\partial A_D} = \tau_D(A_D), \tag{8.19}$$

which is consistent with the kinetic term (8.16).

On the other hand, the vacuum angle θ should be periodic under the shift $\theta \to \theta + 2\pi$. In terms of the effective coupling constant, it corresponds to $\tau \to \tau + 1$, which we call "T–transformation". Combining the S and T–transformations, $SL(2, \mathbf{Z})$ transformation is generated, by which τ transforms as

$$\tau \to \frac{a\tau + b}{c\tau + d}, \tag{8.20}$$

where $ad - bc = 1$ and $a, b, c, d \in \mathbf{Z}$. In this form the S and T–transformation is given by

$$S = \begin{pmatrix} 0 & 1 \\ -1 & 0 \end{pmatrix}, \qquad T = \begin{pmatrix} 1 & 1 \\ 0 & 1 \end{pmatrix} \tag{8.21}$$

respectively.

8.2.5 The BPS mass formula

The $SU(2)$ gauge theory under discussion has electrically and magnetically charged solitonic states whose masses satisfy

$$M^2 = 2|Z^{\mathrm{cl}}_{\mathcal{N}=2}|^2 \qquad Z^{\mathrm{cl}}_{\mathcal{N}=2} = a(n_e + \tau_{\mathrm{cl}} n_m), \tag{8.22}$$

where n_e and n_m are the electric and magnetic charges [102]. The $Z^{\mathrm{cl}}_{\mathcal{N}=2}$ is the (classical) central charge which appears in $\mathcal{N}=2$ supersymmetric algebra,

from which we obtain the Bogomol'nyi bound; $M \geq \sqrt{2}|Z^{\rm cl}_{\mathcal{N}=2}|$. The solitonic states which saturate this equality (or equivalently whose masses are given by the eq.(8.22)) are called BPS–saturated states. Those BPS states belong to the *small* representation of the $\mathcal{N} = 2$ supersymmetric algebra, which has four helicity states in contrast to the *large* representation with sixteen states. Since the number of the degrees of freedom of the small representation and large representation is different, the BPS saturated states are believed to remain BPS after undergoing the quantum corrections. Taking this into consideration, Seiberg and Witten assumed that the classical mass formula (8.22) is also valid in the quantum theory and quantum mass formula is given by

$$M = \sqrt{2}\,|an_e + a_D n_m|\,. \tag{8.23}$$

Notice that the formula (8.23) has manifest duality and reduces to classical formula (8.22) in the classical limit.

8.2.6 Structure of the quantum moduli space

In section 8.2.3, we found that the local framework (8.6) can not satisfactorily describe the low energy effective Lagrangian globally because the metric on the moduli space of vacua could not be positive definite. Instead, the global structure should involve certain monodromies, which is easily shown to exist from semiclassical approximation at infinity.

Singularity at infinity

Due to the asymptotic freedom, the renormalization group corrected classical formula (8.9) gives for large a,

$$a_D = \frac{\partial \mathcal{F}}{\partial a} \approx \frac{2ia}{\pi} \ln \frac{a}{\Lambda} + \frac{ia}{\pi}, \tag{8.24}$$

which indicates that a_D is not a single–valued function of a for large a. Noticing the semiclassical relation $u = \frac{1}{2}a^2$, we can determine the monodromy as follows; under a circuit of the u plane at large u, one has the relation $\ln u \to \ln u + 2\pi i$ and $\ln a \to \ln a + \pi i$, therefore the transformation of a_D and a are

$$\begin{aligned} a_D &\to -a_D + 2a \\ a &\to -a. \end{aligned} \tag{8.25}$$

Thus, there exists a non–trivial monodromy at infinity in the u plane,

$$M_\infty = PT^{-2} = \begin{pmatrix} -1 & 2 \\ 0 & -1 \end{pmatrix}, \tag{8.26}$$

where $P = -\mathbf{1}$ and T defined in eqs.(8.21) are elements of SL(2,$\mathbf{Z}$).

Singularities at strong coupling

The monodromy at infinity means that there must be an additional singularity. And the absence of the global framework also requires that there should be at least two more singularities on the u plane. Here we assume that the number of singularities is minimal, in other words, there are precisely two more singularities at $u = \pm\Lambda^2$. (Here we used the fact that u has mass dimension 2 and there is a symmetry which acting on the u plane as $u \to -u$, whose origin is in the $U(1)_R$ symmetry.) This assumption is satisfied by the fact that it leads to a unique and elegant solution that pass many tests.

The most natural physical interpretation of singularities in the u plane is that some additional massless particles are appearing at a particular value of u. Such a phenomenon is also observed in $\mathcal{N} = 1$ theories[90]. We assume that the singularities came from massive particles of spin $\leq \frac{1}{2}$. The possibilities are severely restricted by the structure of $\mathcal{N} = 2$ supersymmetry: a massive multiplet of particles of spins $\leq \frac{1}{2}$ must be hypermultiplet that saturates the BPS bound. In the semiclassical approximation the only such hypermultiplets in the $\mathcal{N} = 2$ gauge theory are the monopoles and dyons. We will interpret the needed singularities as arising when these particles become massless.

Firstly we will analyze the behavior of the effective Lagrangian near the point $u = \Lambda^2$ where we assume a monopole to be massless; $a_D(\Lambda^2) = 0$. Since the monopoles couple in a non–local way to the original photon, we cannot use that photon in our effective Lagrangian. Instead, we should perform a duality transformation and write the effective Lagrangian in terms of the dual vector multiplet (A_D, W_D^α). The low energy theory is therefore an abelian gauge theory with matter (an $\mathcal{N} = 2$ version of QED).

The dominant effect on the low energy gauge coupling constant is due to loops of light fields, which are the light monopoles in our case. The low energy theory is not asymptotically free and therefore its gauge coupling constants becomes smaller as the mass of the monopoles becomes smaller. Since the mass is proportional to a_D, the low energy coupling goes to zero as $u \to \Lambda^2$. (The electric coupling constant which is the inverse of the magnetic one diverges at that point.) Using the one–loop beta function, the magnetic coupling is

$$\tau_D \approx -\frac{i}{\pi} \ln a_D \tag{8.27}$$

near the point $u = \Lambda^2$ where $a_D = 0$. Since a_D is a good coordinate near

that point, a_D can be written as

$$a_D \approx c_0 \left(u - \Lambda^2\right) \tag{8.28}$$

with some constant c_0. Using the relations $\tau_D = \frac{dh_D}{da_D}$ and (8.17), we obtain

$$a(u) = -h_D(u) \approx a_0 + \frac{i}{\pi} a_D \ln a_D \approx a_0 + \frac{i}{\pi} c_0 \left(u - \Lambda^2\right) \ln \left(u - \Lambda^2\right) \tag{8.29}$$

for some nonzero constant $a_0 = a\left(u = \Lambda^2\right)$. Now we can read off the monodromy; when u circles around Λ^2, so $\ln\left(u - \Lambda^2\right) \to \ln\left(u - \Lambda^2\right) + 2\pi i$, one has

$$\begin{aligned} a_D &\to a_D \\ a &\to a - 2a_D. \end{aligned} \tag{8.30}$$

Correspondingly the monodromy matrix is

$$M_{\Lambda^2} = ST^2S^{-1} = \begin{pmatrix} 1 & 0 \\ -2 & 1 \end{pmatrix} \tag{8.31}$$

where S and T are defined by eqs.(8.21).

The monodromy around the third singularity $u = -\Lambda^2$ is obtained in the same way. Near the point $u = -\Lambda^2$, a_D and a behave as

$$a_D - a \approx c_0' \left(u + \Lambda^2\right), \qquad a \approx a_0' + \frac{i}{\pi} c_0' \left(u + \Lambda^2\right) \ln \left(u + \Lambda^2\right), \tag{8.32}$$

and the monodromy matrix is given by

$$M_{-\Lambda^2} = (TS)T^2(TS)^{-1} = \begin{pmatrix} -1 & 2 \\ -2 & 3 \end{pmatrix}. \tag{8.33}$$

Since encircling the infinity counterclockwise is equivalent to encircling counterclockwise the point $u = -\Lambda^2$ and $u = \Lambda^2$ consecutively, the monodromy matrix (8.26) should be the product of the matrices (8.31) and (8.33). In fact the relation $M_\infty = M_{\Lambda^2} M_{-\Lambda^2}$ can be easily verified.

If one arranges the charges as a row vector $q = (n_m, n_e)$, then the massless particle that produces a monodromy M has $qM = q$. For instance, monodromy M_{Λ^2} arises from a massless monopole of charge vector $q_{\Lambda^2} = (1, 0)$, and from the eq.(8.31) we can verify the relation $q_{\Lambda^2} M_{\Lambda^2} = q_{\Lambda^2}$. Upon setting $q_{-\Lambda^2} = (1, -1)$, we get $q_{-\Lambda^2} M_{-\Lambda^2} = q_{-\Lambda^2}$, hence the monodromy $M_{-\Lambda^2}$ arises from vanishing mass of dyon with charges $(1, -1)$.

8.2.7 The exact solution of the model

We found that the moduli space of quantum vacua is the complex u plane with three singularities at $u = \pm\Lambda^2, \infty$. Near these singularities, $(a_D(u), a(u))$ behave as eqs.(8.24), (8.28), (8.29) and (8.32). At the other point of the moduli space, $(a_D(u), a(u))$ are holomorphic and determined from the theory of elliptic function; thus $(a_D(u), a(u))$ are related to the two cycles of the elliptic curve

$$y^2 = \left(x + \Lambda^2\right)\left(x - \Lambda^2\right)(x - u)\,. \tag{8.34}$$

Let γ_1, γ_2 refer to the cycle which encloses the branch points Λ^2, u and $-\Lambda^2, \Lambda^2$ respectively, $(a_D(u), a(u))$ is given by

$$\begin{aligned} a_D(u) &= \oint_{\gamma_1} \lambda = \frac{\sqrt{2}}{\pi}\int_{\Lambda^2}^{u} \frac{dx\sqrt{x-u}}{\sqrt{x^2-\Lambda^4}} \\ a(u) &= \oint_{\gamma_2} \lambda = \frac{\sqrt{2}}{\pi}\int_{-\Lambda^2}^{\Lambda^2} \frac{dx\sqrt{x-u}}{\sqrt{x^2-\Lambda^4}}, \end{aligned} \tag{8.35}$$

where $\lambda = \frac{\sqrt{2}}{2\pi}\frac{dx\sqrt{x-u}}{\sqrt{x^2-\Lambda^4}}$. Inversely solving the relation $a_D = \frac{d\mathcal{F}(a)}{da}$, the exact form of the prepotential $\mathcal{F}(a)$ can be obtained; thus the coefficients of eq.(8.11) are determined as follows: $\mathcal{F}_1 = \frac{1}{2^5}, \mathcal{F}_2 = \frac{5}{2^{14}}, \mathcal{F}_3 = \frac{3}{2^{18}}, \mathcal{F}_4 = \frac{1469}{2^{31}}, \mathcal{F}_5 = \frac{4471}{2^{34}.5}, \mathcal{F}_6 = \frac{40397}{2^{43}} \ldots$.

The effective coupling constant τ can be rewritten as

$$\tau = \frac{d^2\mathcal{F}}{da^2} = \frac{da_D}{da} = \frac{\frac{da_D}{du}}{\frac{da}{du}} = \frac{\int_{\Lambda^2}^{u}\frac{dx}{y}}{\int_{-\Lambda^2}^{\Lambda^2}\frac{dx}{y}}. \tag{8.36}$$

The right hand side is just the ratio of the two periods of elliptic integrals, whose imaginary part is known to be positive. Thus the positivity of the metric (8.13) is automatically satisfied.

8.2.8 Breaking $\mathcal{N} = 2$ to $\mathcal{N} = 1$: the monopole condensation and confinement

As mentioned above, a $\mathcal{N} = 2$ vector multiplet consists of a vector multiplet W_α and a chiral multiplet Φ in terms of $\mathcal{N} = 1$ superfields. If one adds a superpotential $\mathcal{W} = m\mathrm{Tr}\Phi^2$, which gives a bare mass to Φ, $\mathcal{N} = 2$ supersymmetry is broken down to $N = 1$ and the low energy theory is reduced to a pure $\mathcal{N} = 1$ gauge theory.

The $\mathcal{N} = 1$ pure super Yang–Mills theory with $SU(2)$ gauge group is known to have the following properties, which are shared with nonsupersymmetric QCD,

- there is a mass gap
- electric charges are confined
- $\mathbf{Z}_4$ chiral symmetry is broken to $\mathbf{Z}_2$.

Furthermore, there is no vacuum degeneracy except what is produced by the symmetry breaking. Thus there are precisely two vacuum states[94], which are just the singularities where monopole and dyon becomes massless (see section 8.2.6). In short, all the vacua other than singularities are lifted by the superpotential and two singularities remain as vacua.

Since there are two degenerate vacua which is related by discrete symmetry, one can expect domain wall configurations interpolating these vacua. In the next chapter we consider a toy model of $\mathcal{N} = 2$ pure Yang–Mills theories perturbed by a mass term, which enables us to obtain an exact solution of BPS domain wall.

In order to realize mass gap for gauge fields, one has to introduce light monopole fields which cause a (magnetic) Higgs mechanism. Near the point at which there are massless monopoles, the monopoles can be represented in an $\mathcal{N} = 1$ language by ordinary (local) chiral superfields $\mathcal{M}$ and $\tilde{\mathcal{M}}$, as long as one describes the gauge field by the dual to the original photon. The superpotential is

$$\hat{\mathcal{W}} = \sqrt{2} A_D \mathcal{M} \tilde{\mathcal{M}} + m U(A_D), \tag{8.37}$$

where the first term is required by $\mathcal{N} = 2$ invariance of the $m = 0$ theory, and the second term is the effective contribution to the superpotential induced by the microscopic perturbation $m\mathrm{Tr}\Phi^2$.

From the superpotential (8.37), we can obtain the low energy vacuum structure; at the vacuum

$$a_D = 0, \qquad \mathcal{M} = \tilde{\mathcal{M}} = \left(-\frac{m u'(0)}{\sqrt{2}} \right)^{\frac{1}{2}}. \tag{8.38}$$

Since monopole fields has vacuum expectation values, gauge field gets a mass by the Higgs mechanism. Condensation of monopoles will induce confinement of electric charge (dual Meissner effect)[96, 97, 98]. This for the first time gives a real relativistic field theory model in which confinement of charge is expected in the long–suspected fashion.

8.3 The Seiberg–Witten theory: $\mathcal{N} = 2$ $SU(2)$ SQCD case

In section 8.2.8, we have seen that there are two degenerate vacua in $\mathcal{N} = 2$ pure Yang–Mills theory perturbed by adjoint scalar mass term. In the following chapters, we will discuss domain walls and domain wall junction configurations. Naively, it seems to us that at least three degenerate vacua are needed, if one wants to construct a *stable* domain wall junction. In fact, it is known that the simplest junction with two degenerate vacua, which consists out of four sectors separated by spokes intersecting $\frac{\pi}{2}$ angles, is unstable against local perturbations and decay into a configuration with three domains separated by two domain walls[144].

In this section we comment on $\mathcal{N} = 2$ supersymmetric QCD with one fundamental quark. When the adjoint scalar mass term is added to break $\mathcal{N} = 2$ to $\mathcal{N} = 1$, it has three distinct vacua and toy model of which enables us to obtain an exact analytic solution of BPS domain wall junction (see chapter 10).

8.3.1 Classical moduli space of SQCD

In this case, there is an additional quark field, which is a hypermultiplet in the fundamental representation. This hypermultiplet contains a Dirac fermion and four real scalars. In terms of $\mathcal{N} = 1$ superfields, the hypermultiplet contains two chiral superfields $\mathcal{Q}_a$ and $\tilde{\mathcal{Q}}_a (a = 1, 2$ is color index.). The superpotential for these chiral superfields is

$$\mathcal{W} = \sqrt{2}\tilde{\mathcal{Q}}\Phi\mathcal{Q} + m_1\mathcal{Q}\tilde{\mathcal{Q}} \tag{8.39}$$

with color indices suppressed. There is always a flat direction with non zero ϕ. Along this direction the gauge symmetry is broken to $U(1)$ and quark field becomes massive. Since the quark field cannot have any vacuum expectation value, there is no Higgs branch and only Coulomb branch exists in the moduli space.

8.3.2 The BPS mass formula

Since the global symmetry includes an abelian continuous symmetry, it can contribute to the central extension in the algebra. As a result the BPS mass formula (8.23) is modified to be

$$M = \sqrt{2}|Z_{\mathcal{N}=2}|, \qquad Z_{\mathcal{N}=2} = n_e a + n_m a_D + S\frac{m_1}{\sqrt{2}}, \tag{8.40}$$

where S is the global $SO(2)$ charge. The appearance of the extra term can be deduced from the fact that the hypermultiplet is in "small" representations. It follows from eq.(8.40) that for $a = \pm\frac{m}{\sqrt{2}}$, the quark field becomes massless.

8.3.3 The quantum moduli space

Starting with massless $N_f = 3$ theory and making some quarks heavy, one can obtain the information on the quantum moduli space. After integrating out two quarks successively, one can obtain the massless $N_f = 1$ theory and its quantum moduli space is obtained as follows: the global symmetry of the u plane is $\mathbf{Z}_3$ and there are three singularities related by this symmetry with massless states $(n_m, n_e) = (1, 0),\ (1, 1)$ and $(1, 2)$.

Furthermore if we take the limit $m_1 \to \infty$ with $\Lambda_0^4 = m_1\Lambda_1^3$ fixed, one of the singularities moves to infinity and the other two remain.(Λ_0, Λ_1 is dynamical scale of pure super Yang–Mills theory and super QCD with one flavor respectively.) This is just the moduli space we obtained in section 8.2.6.

The light states near all the singularities are photon multiplet and some charged fields. Using the duality transformation, the low energy theory near any of the singularities is an abelian gauge theory with some light hypermultiplet. The low energy theories in all the singularities have flat directions of the a field along which all the hypermultiplets acquire a mass. As such they are connected smoothly to the semiclassical picture. In the case of $N_f = 1$ there is a single hypermultiplet at every singularities and therefore no other flat directions. This is consistent with the absence of Higgs branches in the moduli space of the original theory.

8.3.4 Breaking $\mathcal{N} = 2$ to $\mathcal{N} = 1$

As in the section 8.2.8, we break $\mathcal{N} = 2$ supersymmetry to $\mathcal{N} = 1$ by adding mass term $m\mathrm{Tr}\Phi^2$ to the tree level superpotential (8.39).

When $m \gg \Lambda$, the $\mathcal{N} = 1$ chiral multiplet in the adjoint representation Φ is heavy and can be integrated out. The resulting theory is $\mathcal{N} = 1$ supersymmetric gauge theory with gauge group $SU(2)$ and 2 chiral doublets $\mathcal{Q}^r$ $(r = 1, 2)$, whose dynamical scale is given by $\tilde{\Lambda}_1$ ($\tilde{\Lambda}_1^5 = m^2\Lambda_1^3$). As $m \to \infty$ with $\tilde{\Lambda}_1$ fixed, we should recover the known results of $\mathcal{N} = 1$ theory[90].

For small m one can use the low energy effective theory. The mass term is represented as a term mU in the superpotential. Since it has no critical points as a function of U, the only reason that there are any supersymmetric ground states at all is that new degrees of freedom become light and have to be included near the singularities. As in section 8.2.8, the matter fields

$\mathcal{M}$ and $\tilde{\mathcal{M}}$ acquire expectation values breaking the $U(1)$ gauge symmetry. Since these are magnetic monopoles, this means confinement of the original charges. Therefore the continuum of vacua has disappeared and the surviving ground states are at the singularities.

8.3.5 The exact solution

As is the case of $\mathcal{N} = 2$ pure Yang–Mills theory, the exact solution for the low energy effective action, metric on the moduli space and particle masses are obtained by introducing a suitable family of elliptic curves and interpreting (a_D, a) as a periods of an appropriate family of meromorphic one–forms.

Here we only summarize the results. The elliptic curve of massless $N_f = 1$ theory is given by

$$y^2 = x^2(x - u) + t\Lambda_1^6 \qquad (t : \text{const}). \tag{8.41}$$

For the massive theory, the elliptic curve is

$$y^2 = x^2(x - u) + \frac{1}{4}m_1\Lambda_1^3 - \frac{1}{64}\Lambda_1^6. \tag{8.42}$$

Chapter 9

BPS domain wall

Domain walls arise in many areas of physics. They occur as solutions of scalar field theories whenever the potential has isolated degenerate minima. There are two circumstances in which this happens naturally. One is when a discrete symmetry is spontaneously broken; in this case the degeneracy is due to the symmetry. The other is when the field theory is supersymmetric.

Domain wall solutions are stable for topological reasons. In the case of supersymmetric field theories, the stability can also be deduced from the fact that a static domain wall partially preserves the supersymmetry of the vacuum. This condition for partially unbroken supersymmetry leads to BPS equation and equivalently the domain wall solution saturates BPS bound. In the rest of this thesis we mainly discuss the properties of BPS domain walls and BPS domain wall junctions.

9.1 Domain wall: a simple example

Before discussing BPS domain walls, we will illustrate fundamental properties of domain walls by using a simple model. Consider a model whose Lagrangian is given by

$$\mathcal{L} = -\frac{1}{2}\partial_\mu\phi\partial^\mu\phi - V(\phi), \tag{9.1}$$

where the potential $V(\phi)$ is

$$V(\phi) = \frac{\lambda}{4}\left(\phi^2 - \phi_0^2\right)^2 \qquad \left(\phi_0^2 \equiv \frac{\mu^2}{\lambda}\right). \tag{9.2}$$

The Lagrangian (9.1) is symmetric under the transformation $\phi \to -\phi$. However the potential has two degenerate vacua $\phi = \pm\phi_0$, and if we choose one

of the vacua, the symmetry is spontaneously broken. The Hamiltonian is

$$H \equiv \int d^3x \mathcal{H} = \int d^3x \left(\frac{1}{2} \left[(\partial_t \phi)^2 + (\nabla \phi)^2 \right] + V(\phi) \right). \tag{9.3}$$

If we assume that wall configurations depend only on x^1 and they spread over the x^2, x^3 directions; *i.e.* $\phi = \phi(x_1)$, then the Hamiltonian (9.3) takes more simple form

$$H \propto \int dx^1 \left[\frac{1}{2} (\partial_1 \phi)^2 + V(\phi) \right]. \tag{9.4}$$

Mathematically, minimizing the energy (9.4) is equivalent to solving the motion of classical particle in a potential $-V(x)$. From this analog we obtain the relation $\frac{1}{2} (\partial_1 \phi)^2 - V(\phi) = 0$ under the boundary condition $|\phi| \to \phi_0$ at $|x| \to \infty$. Solving this equation, we obtain domain wall configurations

$$\phi(x) = \pm \phi_0 \tanh \left(\frac{\mu}{\sqrt{2}} x \right) \tag{9.5}$$

where we imposed the condition $\phi(0) = 0$. The sign $\pm$ corresponds to so–called *kink* and *anti-kink* type solution.

The energy density $\mathcal{H}$ of the wall is obtained as $\mathcal{H} = 2V(\phi) = (\partial_1 \phi)^2 = \frac{\mu^4}{2\lambda \cosh^4 \left(\frac{\mu}{\sqrt{2}} x \right)}$, from which we found that the energy is concentrated in a finite region of space $x \sim 0$. The tension of the wall T_{wall} is defined by energy per unit area and by using the solutions (9.5) we obtain

$$T_{\text{wall}} \equiv \int dx^1 \mathcal{H} = 2 \int dx^1 V(\phi) = \int dx^1 (\partial_1 \phi)^2 = \frac{2\sqrt{2}\mu^3}{3\lambda}. \tag{9.6}$$

The domain wall solutions (9.5) have an interesting topological property which makes these solutions stable. If we define a topological current by $j_\mu(x) = \frac{1}{2\phi_0} \epsilon_{\mu\nu} \partial^\nu \phi(x)$, it is automatically conserved and corresponding conserved charge (per unit area in (x^2, x^3) plane) $\mathcal{Q}_{\text{top}}$ is

$$\mathcal{Q}_{\text{top}} = \int_{-\infty}^{\infty} j_0(x) dx^1 = \frac{1}{2\phi_0} \int_{-\infty}^{\infty} \partial_1 \phi dx^1 = \frac{1}{2\phi_0} \left[\phi(\infty) - \phi(-\infty) \right]. \tag{9.7}$$

The topological charge of the kink type and anti–kink type walls are ± 1 respectively, and in the case of the ordinary vacuum it is zero. Thus there is no transition between kink (or anti–kink) solutions and groundstates, therefore they are stable. This conservation law, usually called the *topological conservation law*, has a different origin from the usual Noether conservation laws coming from the symmetry of the theory in that it holds independently of the equations of motion.

9.2 BPS states and Bogmonl'nyi bounds

From now on, we mainly consider $\mathcal{N} = 1$ supersymmetric theories. In the case of the supersymmetric theories, BPS states not only saturate the Bogomol'nyi bounds but also conserve part of the supercharges. And the Bogomol'nyi bounds can be also derived from the point of view of the conservation of supercharges. In this section, we will derive the Bogomol'nyi bounds from such a viewpoint to obtain (candidate) conserved charges and BPS equations [141].

From here on we use two-component spinors following the convention of ref.[105] except that the four dimensional indices are denoted by Greek letters $\mu, \nu = 0, 1, 2, 3$ instead of roman letters m, n. Using the convention of ref.[105], we denote the left-handed and right-handed supercharges of the $\mathcal{N} = 1$ supersymmetric four-dimensional field theory as Q_α, $\bar{Q}_{\dot{\alpha}}$. It is known that if the translational invariance is broken as is the case for domain walls and/or junctions, the $\mathcal{N} = 1$ superalgebra in general receives contributions from central charges [127]–[143]. The anti-commutator between two left-handed supercharges has central charges Z_k, $k = 1, 2, 3$

$$\{Q_\alpha, Q_\beta\} = 2i(\sigma^k \bar{\sigma}^0)_\alpha{}^\gamma \epsilon_{\gamma\beta} Z_k. \tag{9.8}$$

The anti-commutator between left- and right-handed supercharges receives a contribution from central charges Y_k, $k = 1, 2, 3$

$$\{Q_\alpha, \bar{Q}_{\dot{\alpha}}\} = 2(\sigma^\mu_{\alpha\dot{\alpha}} P_\mu + \sigma^k_{\alpha\dot{\alpha}} Y_k), \tag{9.9}$$

where P_μ, $\mu = 0, \cdots, 3$ are the energy-momentum four-vector of the system. Hermiticity of supercharges dictates that the central charges Z_k are complex, and that Y_k are real: $(Y_k)^* = Y_k$.

These central charges come from the total divergence and are non-vanishing when there are nontrivial differences in asymptotic behavior in different region of spatial infinity as is the case of domain walls and junctions. Therefore these charges are topological in the sense that they are determined completely by the boundary conditions at infinity.

For instance, we can take a general Wess-Zumino model with an arbitrary number of chiral superfields Φ^i, an arbitrary superpotential $\mathcal{W}$ and an arbitrary Kähler potential $K(\Phi^i, \Phi^{*j})$

$$\mathcal{L} = \int d^2\theta d^2\bar{\theta} K(\Phi^i, \Phi^{*j}) + \left[\int d^2\theta \mathcal{W}(\Phi^i) + \text{h.c.} \right], \tag{9.10}$$

and compute the anticommutators (9.8), (9.9) to find the central charges. The contributions to these central charges from bosonic components of chiral

superfields are given [1]by [137]

$$Z_k = 2\int d^3x\, \partial_k \mathcal{W}^*(A^*), \tag{9.11}$$

$$Y_k = i\epsilon^{knm}\int d^3x\, K_{ij^*}\partial_n(A^{*j}\partial_m A^i), \qquad \epsilon^{123}=1, \tag{9.12}$$

where A^i is the scalar component of the i-th chiral superfield Φ^i and $K_{ij^*} = \partial^2 K(A^*, A)/\partial A^i \partial A^{*j}$ is the Kähler metric.

We see that the central charge Z_k is completely determined by the difference of values of the superpotential $\mathcal{W}$ at spatial infinities where different discrete vacua are chosen for different directions. Since single domain wall has a field configuration which is nontrivial only in one dimension, one can see from eq.(9.12) that the central charge Y_k vanishes whereas the central charge Z_k is non-vanishing. The central charge Y_k can be non-vanishing, if the field configuration at infinity is nontrivial in two-dimensions. This situation occurs when three or more different vacua occur at infinity as is the case for the domain wall junctions (see chapter 10).

To examine the lower bound for the energy due to the hermiticity of the supercharges, we consider a hermitian linear combination of operators Q and $\bar{Q}$ with an arbitrary complex two-vector β^α and its complex conjugate $\bar{\beta}^{\dot{\alpha}} = (\beta^\alpha)^*$ as coefficients

$$K = \beta^\alpha Q_\alpha + \bar{\beta}^{\dot{\alpha}}\bar{Q}_{\dot{\alpha}}. \tag{9.13}$$

We treat β^α as c-numbers rather than the Grassmann numbers. Since K is hermitian, the expectation value of the square of K over any state is non-negative definite

$$\langle S|K^2|S\rangle \equiv (\beta^1, \beta^2, \bar{\beta}^{\dot{1}}, \bar{\beta}^{\dot{2}})\hat{K}^2 \begin{pmatrix} \beta^1 \\ \beta^2 \\ \bar{\beta}^{\dot{1}} \\ \bar{\beta}^{\dot{2}} \end{pmatrix} \geq 0. \tag{9.14}$$

The equality holds if and only if the linear combination of supercharges K is preserved by the state $|S\rangle$;*i.e.* $K|S\rangle = 0$ and the states $|S\rangle$ are called **BPS states**. Since we are interested in field configurations at rest, we obtain $P^k = 0, (k = 1, 2, 3)$ and the matrix $\hat{K}^2$ in terms of the central charges Z_k,

[1]The central charge Y_k also receives contributions from fermionic components of chiral superfields which is given in appendix E.

Y_k and the hamiltonian H explicitly

$$\hat{K}^2 = \begin{pmatrix} \langle -Z_2 - iZ_1\rangle & \langle iZ_3\rangle & \langle H + Y_3\rangle & \langle Y_1 - iY_2\rangle \\ \langle iZ_3\rangle & \langle -Z_2 + iZ_1\rangle & \langle Y_1 + iY_2\rangle & \langle H - Y_3\rangle \\ \langle H + Y_3\rangle & \langle Y_1 + iY_2\rangle & \langle -Z_2^* + iZ_1^*\rangle & \langle -iZ_3^*\rangle \\ \langle Y_1 - iY_2\rangle & \langle H - Y_3\rangle & \langle -iZ_3^*\rangle & \langle -Z_2^* - iZ_1^*\rangle \end{pmatrix}. \tag{9.15}$$

For simplicity, let us assume that field configuration is at most two-dimensional, for instance, depends on x^1, x^2 only. Then we obtain $\langle Z_3\rangle = \langle Y_1\rangle = \langle Y_2\rangle = 0$. The inequality (9.14) implies in this case that for any β and any state

$$\langle H\rangle \geq \frac{-1}{|\beta^1|^2 + |\beta^2|^2}\Big\{(|\beta^1|^2 - |\beta^2|^2)\langle Y_3\rangle + \mathrm{Re}\left[(\beta^1)^2\langle -Z_2 - iZ_1\rangle\right] + \mathrm{Re}\left[(\beta^2)^2\langle -Z_2 + iZ_1\rangle\right]\Big\}. \tag{9.16}$$

The minimum energy is achieved at the larger one of vanishing eigenvalues of the matrix $\hat{K}^2$

$$\det(\hat{K}^2) = (\langle H+Y_3\rangle^2 - |\langle -iZ_1 - Z_2\rangle|^2)(\langle H-Y_3\rangle^2 - |\langle iZ_1 - Z_2\rangle|^2) = 0. \tag{9.17}$$

Thus the BPS bound becomes $\langle H\rangle \geq \max\{H_{\rm I}, H_{\rm II}\}$ where $H_{\rm I}$ and $H_{\rm II}$ are two solutions of eq.(9.17)

$$H_{\rm I} \equiv |\langle -iZ_1 - Z_2\rangle| - \langle Y_3\rangle, \quad H_{\rm II} \equiv |\langle iZ_1 - Z_2\rangle| + \langle Y_3\rangle. \tag{9.18}$$

The corresponding eigenvectors are given by

- $\bar{\beta}^{\dot{1}} = \beta^1\langle iZ_1 + Z_2\rangle/|\langle iZ_1 + Z_2\rangle|$, $\beta^2 = \bar{\beta}^{\dot{2}} = 0$ for $\langle H\rangle = H_{\rm I}$
- $\beta^1 = \bar{\beta}^{\dot{1}} = 0$, $\bar{\beta}^{\dot{2}} = \beta^2\langle -iZ_1 + Z_2\rangle/|\langle -iZ_1 + Z_2\rangle|$ for $\langle H\rangle = H_{\rm II}$.

Here we obtained two candidate supercharges corresponding to two eigenvalues listed above. Since $\langle Z_k\rangle$ and $\langle Y_k\rangle$ are given by total divergence as shown in eqs.(9.11) and (9.12), whether these candidate charges are really conserved or not depends on the boundary condition of the solitonic states:

1. $H_{\rm I} > H_{\rm II}$ **case**; then supersymmetry can only be preserved at $\langle H\rangle = H_{\rm I}$ and the only one combination of supercharges is conserved

$$\left(Q_1 + \frac{\langle iZ_1 + Z_2\rangle}{|\langle iZ_1 + Z_2\rangle|}\bar{Q}_{\dot{1}}\right)|\mathrm{BPS}\rangle = 0. \tag{9.19}$$

2. $H_{\rm II} > H_{\rm I}$ **case**; then supersymmetry can only be preserved at $\langle H\rangle = H_{\rm II}$ and the only one combination of supercharges is conserved

$$\left(Q_2 + \frac{\langle -iZ_1 + Z_2\rangle}{|\langle -iZ_1 + Z_2\rangle|}\bar{Q}_{\dot{2}}\right)|{\rm BPS}\rangle = 0. \tag{9.20}$$

These two cases correspond to the 1/4 **BPS** state.

3. $H_{\rm I} = H_{\rm II}$ **case**; both two combinations of supercharges (9.19) and (9.20) are conserved. This case corresponds to 1/2 **BPS** state at $H = H_{\rm I} = H_{\rm II}$.

From the candidate conserved charges discussed above, we can derive the BPS equations for the solitonic field configurations. Here we take abelian gauge fields into consideration for the purpose of solving our toy model.

The BPS equations for chiral superfields

- $H = H_{\rm I}$ **case**: the condition of supercharge conservation (9.19) for $H = H_{\rm I}$ applied to chiral superfield $\Phi^i = (A^i, \psi^i, F^i)$ gives after eliminating the auxiliary field F^i

$$2iK_{ij^*}\frac{\langle iZ_1 + Z_2\rangle}{|\langle iZ_1 + Z_2\rangle|}\mathcal{D}_{\bar{z}}A^i = -\frac{\partial \mathcal{W}^*}{\partial A^{*j}}, \tag{9.21}$$

where complex coordinates $z = x^1 + ix^2, \bar{z} = x^1 - ix^2$, gauge covariant derivatives $\mathcal{D}_\mu$, $\mathcal{D}_{\bar{z}} = \frac{1}{2}(\mathcal{D}_1 + i\mathcal{D}_2)$ and $\mathcal{D}_z = \frac{1}{2}(\mathcal{D}_1 - i\mathcal{D}_2)$ are introduced.

- $H = H_{\rm II}$ **case**: the condition of supercharge conservation (9.20) for $H = H_{\rm II}$ applied to chiral superfield gives after eliminating the auxiliary field

$$2iK_{ij^*}\frac{\langle iZ_1 - Z_2\rangle}{|\langle iZ_1 - Z_2\rangle|}\mathcal{D}_{z}A^i = -\frac{\partial \mathcal{W}^*}{\partial A^{*j}}. \tag{9.22}$$

The BPS equations for vector superfields

- $H = H_{\rm I}$ **case**: The BPS condition (9.19) applied to $U(1)$ vector superfield in the Wess-Zumino gauge $V = (v_\mu, \lambda, D)$ gives after eliminating the auxiliary field D

$$v_{12} = -D = \frac{1}{2}\sum_j A^{*j}e_j A^j, \quad v_{03} = 0, \quad v_{01} = v_{31}, \quad v_{23} = -v_{02}, \tag{9.23}$$

where $v_{\mu\nu} \equiv \partial_\mu v_\nu - \partial_\nu v_\mu$ and e_j is the charge of the field A^j.

- $H = H_{\rm II}$ **case**: The BPS condition (9.20) applied to $U(1)$ vector superfield in the Wess-Zumino gauge gives

$$v_{12} = D = -\frac{1}{2}\sum_j A^{*j} e_j A^j, \quad v_{03} = 0, \quad v_{01} = -v_{31}, \quad v_{23} = v_{02}. \tag{9.24}$$

Here we derived the BPS equations for the abelian gauge fields. A similar condition holds in the case of non–abelian gauge group. These BPS conditions (9.21) and (9.23) for $H = H_{\rm I}$ and (9.22) and (9.24) for $H = H_{\rm II}$ ensure that the configuration is BPS saturated.

9.3 BPS domain wall in supersymmetric theories

Supersymmetry has been useful to achieve stability of solitonic solutions such as domain walls. Domain walls in supersymmetric theories can saturate the Bogomol'nyi bound [100, 101]. Such a domain wall preserves half of the original supersymmetry and is called a 1/2 BPS state [102]. It has also been noted that these BPS states possess a topological charge which becomes a central charge Z of the supersymmetry algebra [103] [127, 128]. Thanks to the topological charge, these BPS states are guaranteed to be stable under arbitrary local fluctuations. Various properties of domain walls in $\mathcal{N} = 1$ supersymmetric field theories in four dimensions have been extensively studied [129]–[133].

Investigating (BPS) domain walls gives not only a better understanding of themselves but also some information about nonperturbative properties of (supersymmetric) gauge theories. For example, consider $\mathcal{N} = 1$ supersymmetric gluodynamics in the large N limit[2], whose action is given by

$$S = \frac{1}{g^2}\int d^4x \left[-\frac{1}{4}G^a_{\mu\nu}G^{a\mu\nu} + i\lambda^{a\alpha}D_{\alpha\dot\beta}\bar\lambda^{a\dot\beta}\right], \tag{9.25}$$

where $D_{\alpha\dot\beta} \equiv \sigma^\mu_{\alpha\dot\beta}D_\mu$. The superpotential for a given vacuum is known to be proportional to the gluino condensation; $\mathcal{W} = N\langle {\rm Tr}\lambda\lambda\rangle$[106].

[2]In this thesis we have used large N expansion and supersymmetry separately. Needless to say, one can use both of them simultaneously. There are many works in which both of the techniques are used and meaningful results are obtained (for example see the recent work[95]).

On the other hand the tension of minimal BPS domain wall T_D, which interpolates adjacent vacua, is known to be of order N in the large N limit[133];

$$T_D \sim N\Lambda^3, \tag{9.26}$$

where Λ is dynamical scale. Since the domain wall configuration is BPS, the tension (9.26) remains unchanged after including quantum corrections. Therefore the gluino condensation should be of the form

$$\langle \mathrm{Tr}\lambda\lambda \rangle_k \sim N e^{\frac{2\pi i}{N}k}, \qquad (k = 1, 2, \ldots, N), \tag{9.27}$$

so that it is consistent with the superpotential.

In contrast to BPS domain wall junctions, exact solutions of BPS domain walls are known in several cases, for example $\mathcal{N} = 1$ supersymmetric QCD with $SU(2)$ gauge group[134].

In the next section we discuss the toy model originally considered by Kaplunovsky *et.al.*[99], because it gives an exact solution of BPS domain wall and we can also obtain an exact solution of BPS domain wall junction of extended model of it[141, 159, 160].

9.4 A toy model with $U(1) \times U(1)'$ gauge symmetry

In this section we consider the BPS domain wall of a toy model with $U(1) \times U(1)'$ gauge symmetry, which is an analogue of the $\mathcal{N} = 1$ supersymmetric Yang–Mills theory, and derive the exact solution of BPS domain wall[99].

In general, $\mathcal{N} = 1$ supersymmetric QCD with $SU(N_c)$ gauge group and N_f flavors has $N_c - N_f$ discrete supersymmetric vacua [106], and can have domain wall solutions [127]–[133]. This model can also be obtained from the $\mathcal{N} = 2$ supersymmetric QCD by perturbing with a mass term for the adjoint chiral superfield. It reduces to the $\mathcal{N} = 1$ supersymmetric gauge theory in the infinite mass limit, whereas it ends up at the singular points of moduli space of the $\mathcal{N} = 2$ supersymmetric gauge theory in the limit of vanishing adjoint mass. The moduli space of the $\mathcal{N} = 2$ $SU(2)$ supersymmetric Yang-Mills theory has two singularities where monopole or dyon becomes massless respectively [107] (see section 8.2).

In order to discuss the model in a simpler setting, Kaplunovsky *et. al.* have proposed a toy model which can be treated as a local field theory [99]. They introduced two pairs of chiral superfields $\mathcal{M}, \tilde{\mathcal{M}}$ and $\mathcal{D}, \tilde{\mathcal{D}}$ simulating the monopole, anti-monopole and the dyon, anti-dyon of the Seiberg-Witten theory respectively. Instead of the modulus u of the Seiberg-Witten

theory, they introduced a linearized analogue T as a neutral chiral superfield. The gauge group was chosen as $U(1)\times U(1)'$ simulating electric and magnetic gauge group and the quantum number of these chiral superfields are given by

$$\begin{array}{cccccc} & \mathcal{M} & \tilde{\mathcal{M}} & \mathcal{D} & \tilde{\mathcal{D}} & T \\ U(1) & 0 & 0 & 1 & -1 & 0 \\ U(1)' & 1 & -1 & 1 & -1 & 0 \end{array} \tag{9.28}$$

To mimic a massless monopole at $T=\Lambda$ and a massless dyon at $T=-\Lambda$, they consider a superpotential

$$\mathcal{W} = (T-\Lambda)\mathcal{M}\tilde{\mathcal{M}} + (T+\Lambda)\mathcal{D}\tilde{\mathcal{D}} - h^2 T, \tag{9.29}$$

where the coupling parameter h^2 replaces the effect of the mass for the adjoint chiral superfield. Since the action is invariant under the two global $U(1)$ transformations

$$\mathcal{M}\to e^{i\delta_1}\mathcal{M}, \quad \tilde{\mathcal{M}}\to e^{-i\delta_1}\tilde{\mathcal{M}}, \quad \mathcal{D}\to e^{i\delta_2}\mathcal{D}, \quad \tilde{\mathcal{D}}\to e^{-i\delta_2}\tilde{\mathcal{D}}, \tag{9.30}$$

we can choose the vacuum configuration to be

$$\begin{aligned} &\text{Vac.1}: T=\Lambda, \quad \mathcal{M}=\tilde{\mathcal{M}}=h, \quad \mathcal{D}=\tilde{\mathcal{D}}=0, \quad \mathcal{W}_1=-h^2\Lambda, \\ &\text{Vac.2}: T=-\Lambda, \quad \mathcal{D}=\tilde{\mathcal{D}}=h, \quad \mathcal{M}=\tilde{\mathcal{M}}=0, \quad \mathcal{W}_2=h^2\Lambda. \end{aligned} \tag{9.31}$$

Here we assume the domain wall configuration depends only on x^1 and we impose the boundary condition as follows: the domain wall configuration approaches Vac.2 as $x^1\to-\infty$ and Vac.1 as $x^1\to\infty$. From the boundary condition the central charges and energy of the domain wall are obtained

$$\begin{aligned} \langle Z_1\rangle = -4h^2\Lambda\int dx^2dx^3, \quad \langle Z_2\rangle = \langle Y_3\rangle = 0, \\ H = H_I = H_{II} = 4h^2\Lambda\int dx^2dx^3. \end{aligned} \tag{9.32}$$

Since H_I and H_{II} are equal, both of the candidate supercharges

$$\frac{1}{\sqrt{2}}\left(e^{i\frac{\pi}{4}}Q_1 + e^{-i\frac{\pi}{4}}Q_{\dot{1}}\right), \qquad \frac{1}{\sqrt{2}}\left(e^{-i\frac{\pi}{4}}Q_2 + e^{i\frac{\pi}{4}}Q_{\dot{2}}\right) \tag{9.33}$$

are conserved and the BPS domain wall is a 1/2 BPS state. The BPS equations (9.21) and (9.22) become the same one $\frac{dA^i}{dx^1} = -\frac{\partial\mathcal{W}^*}{\partial A^{*i}}$, and in this case we obtain

$$\begin{aligned} \frac{d\mathcal{M}}{dx^1} &= -\left(T-\Lambda\right)^*\tilde{\mathcal{M}}^*, \qquad \frac{d\tilde{\mathcal{M}}}{dx^1} = -\left(T-\Lambda\right)^*\mathcal{M}^* \\ \frac{d\mathcal{D}}{dx^1} &= -\left(T+\Lambda\right)^*\tilde{\mathcal{D}}^*, \qquad \frac{d\tilde{\mathcal{D}}}{dx^1} = -\left(T+\Lambda\right)^*\mathcal{D}^* \\ \frac{dT}{dx^1} &= -\left(\mathcal{M}\tilde{\mathcal{M}} + \mathcal{D}\tilde{\mathcal{D}} - h^2\right)^*, \end{aligned} \tag{9.34}$$

where we used the fact that the BPS equations for vector fields (9.23) and (9.24) are satisfied by $v_\mu = D = 0$. Noticing that (9.31) and (9.34) are invariant under the following global phase changes of parameters, fields and coordinate x^1

$$\begin{aligned} h \to e^{i\beta}h, \quad \mathcal{M} \to e^{i\beta}\mathcal{M}, \quad \tilde{\mathcal{M}} \to e^{i\beta}\tilde{\mathcal{M}}, \\ \mathcal{D} \to e^{i\beta}\mathcal{D}, \quad \tilde{\mathcal{D}} \to e^{i\beta}\tilde{\mathcal{D}}, \\ \Lambda \to e^{i\gamma}\Lambda, \quad T \to e^{i\gamma}T, \quad x^1 \to e^{2i\beta+i\gamma}x^1, \end{aligned} \tag{9.35}$$

arbitrary complex parameters h and Λ can be obtained from real-positive h and Λ by these phase changes. Therefore we shall take h and Λ to be real-positive in the following without loss of generality. The BPS equations for vectorsuperfields (9.23) and (9.24) also requires $|\mathcal{M}(x^1)| = |\tilde{\mathcal{M}}(x^1)|$ and $|\mathcal{D}(x^1)| = |\tilde{\mathcal{D}}(x^1)|$. Inspired by this condition, we wish to find a solution assuming

$$\mathcal{M}(x^1) = \tilde{\mathcal{M}}(x^1), \quad \mathcal{D}(x^1) = \tilde{\mathcal{D}}(x^1), \quad T(x^1) = T^*(x^1) \tag{9.36}$$

and that all of them are real-positive. Now the BPS equations (9.34) becomes

$$\begin{aligned} \frac{d\ln\mathcal{M}}{dx^1} &= -\left(T-\Lambda\right), \qquad \frac{d\ln\mathcal{D}}{dx^1} = -\left(T+\Lambda\right) \\ \frac{dT}{dx^1} &= -\left(\mathcal{M}^2+\mathcal{D}^2-h^2\right) \end{aligned} \tag{9.37}$$

The first equations of the eq.(9.37) can be solved by

$$\begin{aligned} \mathcal{M}(x^1) &= h\exp\left[\frac{1}{2}\xi(x^1)+\Lambda x^1\right], \quad \mathcal{D}(x^1) = h\exp\left[\frac{1}{2}\xi(x^1)-\Lambda x^1\right] \\ \frac{d\xi(x^1)}{dx^1} &= -2T(x^1) \end{aligned} \tag{9.38}$$

Inserting eq.(9.38) into the third equation of the eq. (9.37), the differential equation for $\xi(x^1)$ is obtained

$$\frac{d^2\xi(x^1)}{d(x^1)^2} = -2h^2\left[1-2e^{\xi(x^1)}\cosh\left(2\Lambda x^1\right)\right]. \tag{9.39}$$

If h^2 has special value, more concretely $h^2 = 2\Lambda^2$, we can obtain the analytic solution of eq.(9.39) as $\xi(x^1) = -2\ln\left(\cosh\left(\Lambda x^1\right)\right)$. Then the exact solutions of the model are

$$\begin{aligned} \mathcal{M}(x^1) &= \frac{\sqrt{2}\Lambda}{1+e^{-2\Lambda x^1}}, \quad \mathcal{D}(x^1) = \frac{\sqrt{2}\Lambda}{1+e^{2\Lambda x^1}} \\ T(x^1) &= \Lambda\tanh\left(\Lambda x^1\right). \end{aligned} \tag{9.40}$$

The profile of the BPS domain wall is depicted in Fig. 9.1.

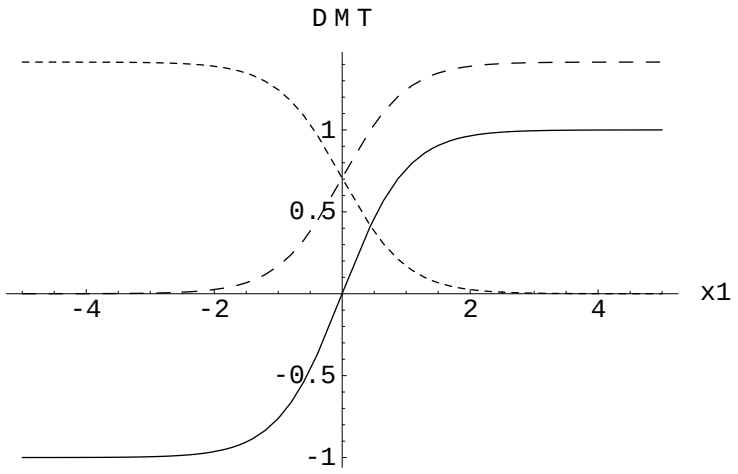

Figure 9.1: The BPS domain wall configuration of T (solid line), $\mathcal{M}$ (long dashed line) and $\mathcal{D}$ (short dashed line). In the figure we take the unit of $\Lambda = 1$.

The tension and energy density

The energy of the BPS domain wall is given by

$$\begin{aligned} H &= |\langle Z_1 \rangle| = |2 \int d^3x \partial_1 \mathcal{W}^*| = 2 \left| \mathcal{W}^*(x^1 = \infty) - \mathcal{W}^*(x^1 = -\infty) \right| \int dx^2 dx^3 \\ &= 4h^2\Lambda \int dx^2 dx^3 = 8\Lambda^3 \int dx^2 dx^3, \end{aligned} \tag{9.41}$$

and the tension of the wall, which is defined by energy per unit area, is $4h^2\Lambda (= 8\Lambda^3)$.

The energy density of the domain wall is obtained from the solution (9.40)

$$\mathcal{H}(x^1) = \frac{96\Lambda^4 e^{4\Lambda x^1}}{\left(1 + e^{2\Lambda x^1}\right)^4}. \tag{9.42}$$

The 3D plot of $\mathcal{H}(x^1)$ is in Fig. 9.2 from which we can see the energy (domain wall) is localized along the x^1 direction and extended along x^2 (and x^3) direction.

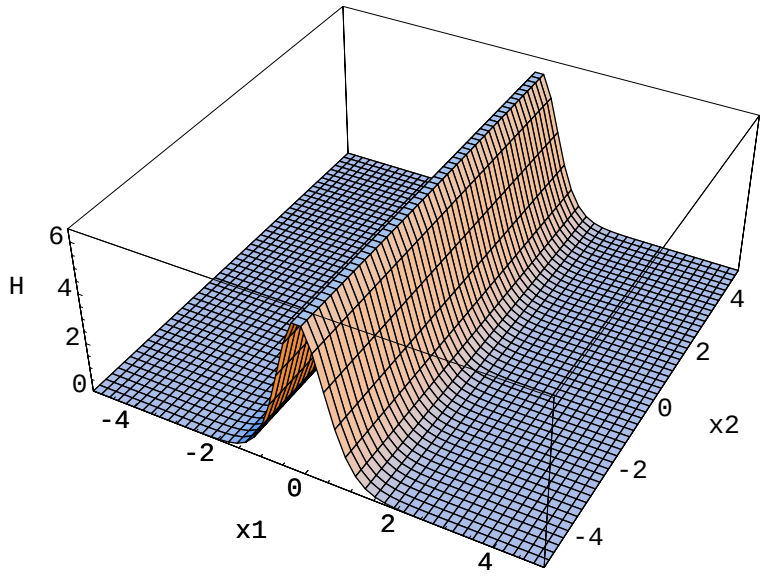

Figure 9.2: 3D plot of the energy density of the wall. the energy (domain wall) is localized along the x^1 direction and extended along x^2 (and x^3) direction. In the figure we take the unit of $\Lambda = 1$.

Chapter 10

BPS domain wall junction

10.1 Domain wall junction

As described in chapter 9, domain walls occur in interpolating two degenerate vacua in separate region of space. If three or more different discrete vacua occur in separate region of space, segments of domain walls separate each pair of the neighboring vacua. If the two spatial dimensions of all of these domain walls have one dimension in common, these domain walls meet at a one-dimensional junction. In the case of supersymmetric theories, the solitonic configuration for the junction can preserve a quarter of supersymmetry (see section 9.2). It has also been found that a new topological charge Y can appear for such a 1/4 BPS state [136] [137] [138]. There have been a number of numerical simulations which indicate the existence of the domain wall junction solutions [139, 140, 144]. In order to make progress in understanding these solitonic objects, it is quite useful to have exact solutions which allows us to investigate closely the behavior of these solitons and to evaluate explicitly the central charges Y besides Z. In this respect, an exact solution offers informations complementary to general considerations and numerical studies.

In the next section we will consider a toy model and present an exact solution of BPS domain wall junction[141]. This is the first and only known exact analytic solution of BPS domain wall junction. As mentioned before, some of the properties of BPS domain walls and junctions such as tension and conserved supercharges are determined without solving their profile explicitly. However, with exact analytic solution, we can obtain more concrete informations of those BPS objects, structure near the center of junctions, energy densities and modes on junction backgrounds, and so on[159, 160].

10.2 A toy model with $U(1)\times U(1)'$ gauge symmetry

In this section we consider BPS domain wall junction of a toy model motivated by the $\mathcal{N}=2$ supersymmetric $SU(2)$ gauge theory with one flavor broken to $\mathcal{N}=1$ by the mass of the adjoint chiral superfield.

If we add a single flavor of quarks in the fundamental representation in the $\mathcal{N}=2$ $SU(2)$ gauge theory, we obtain three singularities in the moduli space. For large bare mass of the quark, the additional singularity corresponds to the situation where the effective mass of quark vanishes, whereas the Z_3 symmetry among three singularities is realized in the limit of vanishing bare quark mass [108] (see also section 8.3). These three singularities become three discrete vacua of $\mathcal{N}=1$ gauge theory when perturbed by the adjoint scalar mass [109]. In view of these features, we extend the $U(1)\times U(1)'$ model of ref.[99] (see section 9.4) by adding an additional pair of chiral superfields $\mathcal{Q}, \tilde{\mathcal{Q}}$ corresponding to the quark and anti-quark.

The model and its vacua

The model has the following chiral superfields with the charge assignment for the $U(1)\times U(1)'$ gauge group

$$\begin{array}{cccccccc} & \mathcal{M} & \tilde{\mathcal{M}} & \mathcal{D} & \tilde{\mathcal{D}} & \mathcal{Q} & \tilde{\mathcal{Q}} & T \\ U(1) & 0 & 0 & 1 & -1 & 1 & -1 & 0 \\ U(1)' & 1 & -1 & 1 & -1 & 0 & 0 & 0 \end{array} \tag{10.1}$$

,where $\mathcal{Q}, \tilde{\mathcal{Q}}$ are new fields added here. To make the quark massless at $T=m$ where m is the bare mass parameter for the quark $\mathcal{Q}$, the superpotential (9.29) is extended as

$$\mathcal{W} = (T-\Lambda)\mathcal{M}\tilde{\mathcal{M}} + (T+\Lambda)\mathcal{D}\tilde{\mathcal{D}} + (T-m)\mathcal{Q}\tilde{\mathcal{Q}} - h^2 T. \tag{10.2}$$

This simple modification produces a model which possesses three distinct $\mathcal{N}=1$ supersymmetric vacua and allows us to obtain an exact solution for junctions. Since the action is invariant under the three global $U(1)$ transformations

$$\begin{aligned} &\mathcal{M}\to e^{i\delta_1}\mathcal{M}, \quad \tilde{\mathcal{M}}\to e^{-i\delta_1}\tilde{\mathcal{M}}, \quad \mathcal{D}\to e^{i\delta_2}\mathcal{D}, \quad \tilde{\mathcal{D}}\to e^{-i\delta_2}\tilde{\mathcal{D}}, \\ &\mathcal{Q}\to e^{i\delta_3}\mathcal{Q}, \quad \tilde{\mathcal{Q}}\to e^{-i\delta_3}\tilde{\mathcal{Q}}, \end{aligned} \tag{10.3}$$

we can choose the vacuum configuration to be

$$\text{Vac.1}: T=\Lambda, \quad \mathcal{M}=\tilde{\mathcal{M}}=h, \quad \mathcal{Q}=\tilde{\mathcal{Q}}=\mathcal{D}=\tilde{\mathcal{D}}=0, \quad \mathcal{W}_1=-h^2\Lambda,$$

$$\begin{aligned}
&\text{Vac.2} : T = m, \quad \mathcal{Q} = \tilde{\mathcal{Q}} = h, \quad \mathcal{M} = \tilde{\mathcal{M}} = \mathcal{D} = \tilde{\mathcal{D}} = 0, \quad \mathcal{W}_2 = -h^2 m, \\
&\text{Vac.3} : T = -\Lambda, \quad \mathcal{D} = \tilde{\mathcal{D}} = h, \quad \mathcal{Q} = \tilde{\mathcal{Q}} = \mathcal{M} = \tilde{\mathcal{M}} = 0, \quad \mathcal{W}_3 = h^2 \Lambda.
\end{aligned} \tag{10.4}$$

The boundary condition and conserved supercharges

We will consider a field configuration which is static and translationally invariant along x^3 direction and take the boundary condition in (x^1, x^2) where the wall 1 extends along the negative x^2 axis separating the vacuum 1 ($x^1 > 0$) and 3 ($x^1 < 0$) as shown in Fig. 10.1.

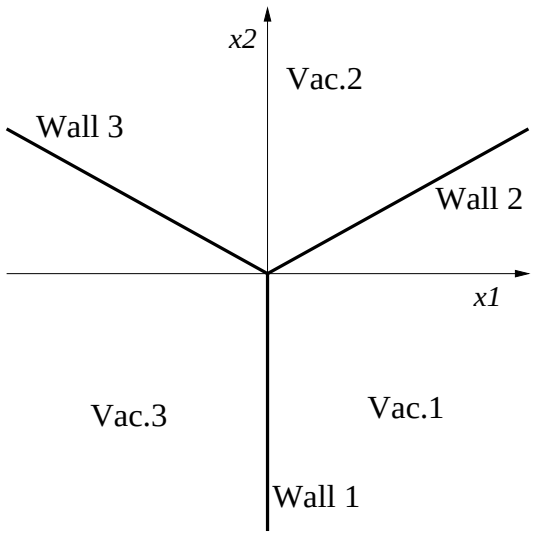

Figure 10.1: Boundary condition in the (x^1, x^2) space we take here.

Since conserved supercharges are determined solely by the boundary condition at spatial infinity (see Fig. 10.1), we evaluate them on a large cylindrical region with a disk of large radius R ($R \gg \Lambda^{-1}$) centered at $z = 0$ and a height L_3. Field configurations on the surface of the large cylinder approaches a step-function across domain walls. In this approximation, the central charges can be evaluated as

$$\langle Z_1 \rangle = -12\Lambda^3 R L_3, \quad \langle Z_2 \rangle = i12\Lambda^3 R L_3, \quad \langle Y_3 \rangle = -2\sqrt{3}\Lambda^2 L_3, \tag{10.5}$$

with corrections suppressed exponentially as $R \to \infty$. Therefore we obtain

$$\begin{aligned}
H_{\rm I} &= |\langle -iZ_1 - Z_2 \rangle| - \langle Y_3 \rangle = 2\sqrt{3}\Lambda^2 L_3, \\
H_{\rm II} &= |\langle iZ_1 - Z_2 \rangle| + \langle Y_3 \rangle = 24\Lambda^3 R L_3 - 2\sqrt{3}\Lambda^2 L_3.
\end{aligned} \tag{10.6}$$

We see that $H_{\rm II} > H_{\rm I}$ and the conserved charge is $\frac{1}{\sqrt{2}}(\mathrm{e}^{-i\frac{\pi}{4}}Q_2 + \mathrm{e}^{i\frac{\pi}{4}}\overline{Q}_{\dot{2}})$ and that the solitonic state satisfying the boundary condition in Fig. 10.1 is 1/4 BPS state as expected. Correspondingly we have to choose the BPS equations (9.22) and (9.24).

Another derivation of the conserved charges

We can also derive the conserved charge of junction from the view point of the domain walls composing the junction. Far from the origin of the (x^1, x^2) space where the center of the junction (hub) is located, the junction configuration approaches those of isolated domain walls. If we have only the wall 1, we obtain the central charge Z_k (vanishing Y_k) and find the two conserved supercharges from eqs.(9.19) and (9.20) as

$$Q^{(1)} = \frac{1}{\sqrt{2}}(\mathrm{e}^{-i\frac{\pi}{4}}Q_2 + \mathrm{e}^{i\frac{\pi}{4}}\overline{Q}_{\dot{2}}), \qquad Q^{(2)} = \frac{1}{\sqrt{2}}(\mathrm{e}^{i\frac{\pi}{4}}Q_1 + \mathrm{e}^{-i\frac{\pi}{4}}\overline{Q}_{\dot{1}}). \tag{10.7}$$

The other two walls have also two conserved supercharges

$$\begin{aligned} &\text{at wall 2} \quad Q^{(3)} = \tfrac{1}{\sqrt{2}}(\mathrm{e}^{-i\frac{\pi}{12}}Q_1 + \mathrm{e}^{i\frac{\pi}{12}}\overline{Q}_{\dot{1}}), \quad Q^{(1)} = \tfrac{1}{\sqrt{2}}(\mathrm{e}^{-i\frac{\pi}{4}}Q_2 + \mathrm{e}^{i\frac{\pi}{4}}\overline{Q}_{\dot{2}}), \\ &\text{at wall 3} \quad Q^{(4)} = \tfrac{1}{\sqrt{2}}(\mathrm{e}^{-i\frac{5\pi}{12}}Q_1 + \mathrm{e}^{i\frac{5\pi}{12}}\overline{Q}_{\dot{1}}), \quad Q^{(1)} = \tfrac{1}{\sqrt{2}}(\mathrm{e}^{-i\frac{\pi}{4}}Q_2 + \mathrm{e}^{i\frac{\pi}{4}}\overline{Q}_{\dot{2}}). \end{aligned} \tag{10.8}$$

When these three half walls coexist, we can have only one common conserved supercharge $Q^{(1)} = (\mathrm{e}^{-i\frac{\pi}{4}}Q_2 + \mathrm{e}^{i\frac{\pi}{4}}\overline{Q}_{\dot{2}})/\sqrt{2}$, which is the same one we have already derived above. In fact we find that the domain wall junction configuration conserves precisely this single combination of supercharges, even though it has also another central charge Y_k contributing.

Exact solution of the junction

From here on we assume a canonical Kähler metric $K_{ij^*} = \delta_{ij}$ for simplicity. The BPS equation (9.24) for $U(1) \times U(1)'$ vector superfields can be satisfied trivially[1] by $v_\mu = 0$ and $D = 0$. The other BPS equation (9.22) becomes

$$2K_{ij^*}\frac{\partial A^i}{\partial z} = \Omega_- \frac{\partial W^*}{\partial A^{*j}}, \quad \Omega_- = -i\frac{\langle iZ_1^* + Z_2^* \rangle}{|\langle iZ_1^* + Z_2^* \rangle|}. \tag{10.9}$$

[1]The Z_3 symmetric case of the vanishing bare quark mass in the Seiberg-Witten theory yields a different charge assignment for the third singularity $(n_m, n_e) = (1, 2)$ instead of $(n_m, n_e) = (0, 1)$ [108] (see section 8.3.3). Even if we use this charge assignment for the Q field, The vanishing D term condition gives the same result.

We will look for a solution of this partial differential equation. We observe that the phase of Ω_- can be absorbed by a rotation of field configuration, since the BPS equation (10.9) is invariant under a phase rotation : $\Omega_- \to \mathrm{e}^{i\delta}\Omega_-,\ z \to \mathrm{e}^{-i\delta}z$. From the boundary condition we chose above we should take $\Omega_- = -1$.

Since we assume a canonical Kähler metric $K_{ij*} = \delta_{ij}$, the BPS eqs. (10.9) become for our model

$$\begin{aligned}
2\frac{\partial \mathcal{M}}{\partial z} &= \Omega_- \tilde{\mathcal{M}}^*(T-\Lambda)^*, \qquad 2\frac{\partial \tilde{\mathcal{M}}}{\partial z} = \Omega_- \mathcal{M}^*(T-\Lambda)^*, \\
2\frac{\partial \mathcal{D}}{\partial z} &= \Omega_- \tilde{\mathcal{D}}^*(T+\Lambda)^*, \qquad 2\frac{\partial \tilde{\mathcal{D}}}{\partial z} = \Omega_- \mathcal{D}^*(T+\Lambda)^*, \\
2\frac{\partial \mathcal{Q}}{\partial z} &= \Omega_- \tilde{\mathcal{Q}}^*(T-m)^*, \qquad 2\frac{\partial \tilde{\mathcal{Q}}}{\partial z} = \Omega_- \mathcal{Q}^*(T-m)^*, \\
2\frac{\partial T}{\partial z} &= \Omega_- \left(\mathcal{M}\tilde{\mathcal{M}} + \mathcal{D}\tilde{\mathcal{D}} + \mathcal{Q}\tilde{\mathcal{Q}} - h^2\right)^*.
\end{aligned} \tag{10.10}$$

Eqs. (10.4) and (10.10) are invariant under the following global phase changes of parameters, fields and complex coordinate z

$$\begin{aligned}
h \to e^{i\beta}h, \quad \mathcal{M} \to e^{i\beta}\mathcal{M}, \quad \tilde{\mathcal{M}} \to e^{i\beta}\tilde{\mathcal{M}}, \\
\mathcal{D} \to e^{i\beta}\mathcal{D}, \quad \tilde{\mathcal{D}} \to e^{i\beta}\tilde{\mathcal{D}}, \quad \mathcal{Q} \to e^{i\beta}\mathcal{Q}, \quad \tilde{\mathcal{Q}} \to e^{i\beta}\tilde{\mathcal{Q}}, \\
\Lambda \to e^{i\gamma}\Lambda, \quad T \to e^{i\gamma}T, \quad , m \to e^{i\gamma}mz \to e^{2i\beta+i\gamma}z.
\end{aligned} \tag{10.11}$$

Arbitrary complex parameters h and Λ can be obtained from real-positive h and Λ by these phase changes. Therefore we shall take h and Λ to be real-positive in the following without loss of generality. The BPS condition $D = 0$ yields $|\mathcal{M}(z,\bar{z})| = |\tilde{\mathcal{M}}(z,\bar{z})|$, $|\mathcal{D}(z,\bar{z})| = |\tilde{\mathcal{D}}(z,\bar{z})|$, and $|\mathcal{Q}(z,\bar{z})| = |\tilde{\mathcal{Q}}(z,\bar{z})|$. Inspired by this condition, we wish to find a solution assuming

$$\mathcal{M}(z,\bar{z}) = \tilde{\mathcal{M}}(z,\bar{z}), \quad \mathcal{D}(z,\bar{z}) = \tilde{\mathcal{D}}(z,\bar{z}), \quad \mathcal{Q}(z,\bar{z}) = \tilde{\mathcal{Q}}(z,\bar{z}). \tag{10.12}$$

and that all of them are real-positive in the entire complex plane. We shall see that this Ansatz gives a consistent solution.

We note that the model acquires a Z_3 symmetry if we choose the bare mass m of $\mathcal{Q}$ as

$$m = i\sqrt{3}\Lambda. \tag{10.13}$$

In order to obtain the exact analytic solution of the domain wall junction, we specialize to this case, and shift the field T as $T' = T - i\frac{1}{\sqrt{3}}\Lambda$ to make $T' = 0$ as the origin of the Z_3 rotation $T' \to \mathrm{e}^{\pm i\frac{2\pi}{3}}T'$. The three vacua (10.4)

and BPS equations (10.10) take manifestly Z_3 symmetric forms

$$\begin{aligned}
&\text{Vac.1} : T' = \frac{2}{\sqrt{3}} e^{-i\frac{1}{6}\pi}\Lambda, \quad \mathcal{M} = \tilde{\mathcal{M}} = h, \quad \mathcal{Q} = \tilde{\mathcal{Q}} = \mathcal{D} = \tilde{\mathcal{D}} = 0, \\
&\text{Vac.2} : T' = \frac{2}{\sqrt{3}} e^{i\frac{1}{2}\pi}\Lambda, \quad \mathcal{Q} = \tilde{\mathcal{Q}} = h, \quad \mathcal{M} = \tilde{\mathcal{M}} = \mathcal{D} = \tilde{\mathcal{D}} = 0, \\
&\text{Vac.3} : T' = \frac{2}{\sqrt{3}} e^{-i\frac{5}{6}\pi}\Lambda, \quad \mathcal{D} = \tilde{\mathcal{D}} = h, \quad \mathcal{Q} = \tilde{\mathcal{Q}} = \mathcal{M} = \tilde{\mathcal{M}} = 0,
\end{aligned} \tag{10.14}$$

$$\begin{aligned}
2\frac{\partial}{\partial z}\ln q_M &= \Omega_- \left(T'^* - \frac{2}{\sqrt{3}} e^{i\frac{1}{6}\pi}\Lambda \right), \\
2\frac{\partial}{\partial z}\ln q_D &= \Omega_- \left(T'^* - \frac{2}{\sqrt{3}} e^{i\frac{5}{6}\pi}\Lambda \right), \\
2\frac{\partial}{\partial z}\ln q &= \Omega_- \left(T'^* - \frac{2}{\sqrt{3}} e^{-i\frac{1}{2}\pi}\Lambda \right), \\
2\frac{\partial}{\partial z} T' &= \Omega_- \, h^2 \left(q_M^2 + q_D^2 + q^2 - 1 \right),
\end{aligned} \tag{10.15}$$

where we have normalized the scalar fields by the nonzero expectation value h at vacua

$$\mathcal{M}(z,\bar{z}) = h\, q_M(z,\bar{z}), \quad \mathcal{D}(z,\bar{z}) = h\, q_D(z,\bar{z}), \quad \mathcal{Q}(z,\bar{z}) = h\, q(z,\bar{z}). \tag{10.16}$$

The first of eq.(10.15) can be rewritten as

$$q_M = C(\bar{z}) \exp\left(\frac{1}{2}\eta - \frac{1}{\sqrt{3}} \Omega_- e^{i\frac{1}{6}\pi}\Lambda z \right), \tag{10.17}$$

$$\frac{\partial}{\partial z}\eta(z,\bar{z}) = \Omega_- \, T'^*(z,\bar{z}), \tag{10.18}$$

where the unknown function $C(\bar{z})$ is determined by the reality condition for q_M up to a constant which is absorbed into η

$$C(\bar{z}) = \exp\left(-\frac{1}{\sqrt{3}} \Omega_-^* e^{-i\frac{1}{6}\pi}\Lambda \bar{z} \right). \tag{10.19}$$

The remaining unknown function $\eta(z,\bar{z})$ should then be real. Consequently we obtain

$$q_M = \exp\left(\frac{1}{2}\eta + \frac{2}{\sqrt{3}} \Lambda \mathrm{Re}\left(-\Omega_- \, e^{i\frac{1}{6}\pi} z \right) \right), \quad \eta(z,\bar{z}) = \left(\eta(z,\bar{z})\right)^*. \tag{10.20}$$

By an exactly similar procedure, we solve the second and third equations and obtain

$$q_D = \exp\left(\frac{1}{2}\eta + \frac{2}{\sqrt{3}}\Lambda \mathrm{Re}\left(-\Omega_- e^{i\frac{5}{6}\pi} z\right) + C_D\right), \qquad C_D \in \mathbb{R}, \tag{10.21}$$

$$q = \exp\left(\frac{1}{2}\eta + \frac{2}{\sqrt{3}}\Lambda \mathrm{Re}\left(-\Omega_- e^{-i\frac{1}{2}\pi} z\right) + C\right), \qquad C \in \mathbb{R}, \tag{10.22}$$

where C_D and C are integration constants. Let us assume that the origin $z = 0$ is the center of the domain wall junction and is Z_3 symmetric. Therefore, $q_M = q_D = q$ at $z = 0$, which implies $C_D = C = 0$. Inserting eq.(10.18) to the complex conjugate of the last of eq.(10.15), we obtain

$$\begin{aligned} 2\frac{\partial^2}{\partial z \partial \bar{z}}\eta = -h^2\Bigg[1 - e^{\eta}\Bigg\{&\exp\left(\frac{4\Lambda}{\sqrt{3}}\mathrm{Re}\left(-\Omega_- e^{i\frac{1}{6}\pi} z\right)\right) \\ &+ \exp\left(\frac{4\Lambda}{\sqrt{3}}\mathrm{Re}\left(-\Omega_- e^{i\frac{5}{6}\pi} z\right)\right) + \exp\left(\frac{4\Lambda}{\sqrt{3}}\mathrm{Re}\left(-\Omega_- e^{-i\frac{1}{2}\pi} z\right)\right)\Bigg\}\Bigg]. \end{aligned} \tag{10.23}$$

For the special case of $h^2 = 2\Lambda^2$, eq. (10.23) can be solved analytically. Imposing the boundary conditions at infinity we obtain the solution

$$\begin{aligned} \eta(z,\bar{z}) = -2\ln\Bigg[&\exp\left(\frac{2\Lambda}{\sqrt{3}}\mathrm{Re}\left(-\Omega_- e^{i\frac{1}{6}\pi} z\right)\right) \\ &+ \exp\left(\frac{2\Lambda}{\sqrt{3}}\mathrm{Re}\left(-\Omega_- e^{i\frac{5}{6}\pi} z\right)\right) + \exp\left(\frac{2\Lambda}{\sqrt{3}}\mathrm{Re}\left(-\Omega_- e^{-i\frac{1}{2}\pi} z\right)\right)\Bigg]. \end{aligned} \tag{10.24}$$

Therefore we find solutions for scalar fields as

$$\begin{aligned} \mathcal{M}(z,\bar{z}) &= \tilde{\mathcal{M}}(z,\bar{z}) = \frac{\sqrt{2}\Lambda s}{s+t+u}, \\ \mathcal{D}(z,\bar{z}) &= \tilde{\mathcal{D}}(z,\bar{z}) = \frac{\sqrt{2}\Lambda t}{s+t+u}, \\ \mathcal{Q}(z,\bar{z}) &= \tilde{\mathcal{Q}}(z,\bar{z}) = \frac{\sqrt{2}\Lambda u}{s+t+u}, \\ T'(z,\bar{z}) &= \frac{2\Lambda}{\sqrt{3}}\frac{e^{-i\frac{1}{6}\pi}s + e^{-i\frac{5}{6}\pi}t + e^{i\frac{1}{2}\pi}u}{s+t+u}, \end{aligned} \tag{10.25}$$

$$s = \exp\left(\frac{2\Lambda}{\sqrt{3}}\mathrm{Re}\left(-\Omega_- e^{i\frac{1}{6}\pi} z\right)\right),$$

$$t = \exp\left(\frac{2\Lambda}{\sqrt{3}}\mathrm{Re}\left(-\Omega_- e^{i\frac{5}{6}\pi}z\right)\right),$$
$$u = \exp\left(\frac{2\Lambda}{\sqrt{3}}\mathrm{Re}\left(-\Omega_- e^{-i\frac{1}{2}\pi}z\right)\right). \tag{10.26}$$

The modulus of the field T' is plotted as a function of x^1 and x^2 in Fig. 10.2 where we can recognize three valleys corresponding to three domain walls.

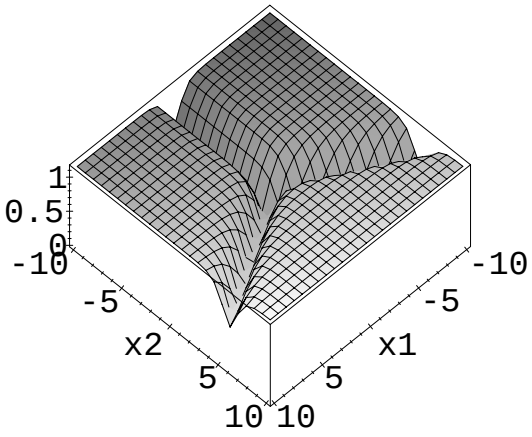

Figure 10.2: The modulus of the field T' as a function of x^1 and x^2. We set $\Lambda = 1$ for simplicity.

Domain wall limit

Here we examine the boundary conditions at spatial infinity $|z| \to \infty$ and behavior of the spokes far from the center of the junction. From eqs. (10.25) and (10.26), we find

$$\begin{aligned}
&\text{when} \quad -\tfrac{1}{2}\pi < \arg(z) < \tfrac{1}{6}\pi, \quad \text{then} \quad s \gg t, u, \quad T' \to \tfrac{2}{\sqrt{3}} e^{-i\frac{1}{6}\pi}\Lambda, \quad \text{(vac.1)} \\
&\text{when} \quad \tfrac{1}{6}\pi < \arg(z) < \tfrac{5}{6}\pi, \quad \text{then} \quad u \gg s, t, \quad T' \to \tfrac{2}{\sqrt{3}} e^{i\frac{1}{2}\pi}\Lambda, \quad \text{(vac.2)} \\
&\text{when} \quad \tfrac{5}{6}\pi < \arg(z) < \tfrac{3}{2}\pi, \quad \text{then} \quad t \gg s, u, \quad T' \to \tfrac{2}{\sqrt{3}} e^{-i\frac{5}{6}\pi}\Lambda, \quad \text{(vac.3).}
\end{aligned} \tag{10.27}$$

Secondly we examine the asymptotic behavior along the region between two neighboring vacua. In the limit $x^2 \to -\infty$ with fixed x^1, eq.(10.25) reduces to

$$\mathcal{M} \to \frac{\sqrt{2}\Lambda e^{\Lambda x^1}}{e^{\Lambda x^1} + e^{-\Lambda x^1}}, \quad \mathcal{D} \to \frac{\sqrt{2}\Lambda e^{-\Lambda x^1}}{e^{\Lambda x_1} + e^{-\Lambda x^1}}, \quad \mathcal{Q} \to 0,$$
$$T' \to \Lambda \tanh \Lambda x^1 - \frac{\Lambda}{\sqrt{3}} i, \qquad \left(T \to \Lambda \tanh \Lambda x^1\right). \tag{10.28}$$

Thus we recover the exact solution of BPS domain wall (9.40) (see section 9.4). By the Z_3 symmetry, we also obtain respective exact domain wall solutions at the asymptotic region $x^1 = \pm\sqrt{3}x^2$ correctly.

10.3 Some fundamental properties of BPS domain wall junction

In the rest of this chapter we give a more detailed study of the properties of the BPS domain wall junction in $\mathcal{N} = 1$ supersymmetric field theories by using our exact solution as a concrete example[159, 160].

10.3.1 Boundary conditions and BPS equations

For a 1/4 BPS state, there are two sets of BPS equations, eqs.(9.21), (9.23) and (9.22), (9.24), corresponding to the two kinds of BPS domain wall junctions. In this subsection we make explicit the relation between the boundary conditions and the choice of these BPS equations.

BPS domain wall junction is formed when nonparallel BPS walls meet at a junction. In regions far away from the junction, the configuration approaches to isolated walls asymptotically. BPS domain wall is a 1/2 BPS state and conserves two supercharges. These two supercharges are given, from Eqs.(9.19) and (9.20), in terms of central charges Z_1 and Z_2 for the wall. Let us take a general Wess-Zumino model in Eq.(9.10) and examine if a domain wall junction can be formed where N different vacua appear in asymptotic regions. These N vacua correspond to N points in the complex plane of superpotential $\mathcal{W}$. The field configuration of the junction at infinity is mapped to a straight line connecting these N vertices [137, 139, 140]. In order to have a balance of force, this polygon has to be convex [137]. We set the origin of the $\mathcal{W}$ space at an arbitrary point inside this BPS polygon and denote the value of the superpotential at the I-th vacuum as $\mathcal{W}_I$, for $I = 1, \ldots, N$, as illustrated in Fig. 10.3(b). Let us take the origin in x^1, x^2

space as the junction point of these BPS walls. If we denote θ_{IJ} the angle of the half wall separating two vacua, I and J, as illustrated in Fig. 10.3(a), the central charges Z_1 and Z_2 of this wall are given by eq.(9.11) as

$$\vec{Z}_{IJ} \equiv (Z_1, Z_2)_{IJ} = 2\,[\mathcal{W}_J^* - \mathcal{W}_I^*] \cdot \vec{\omega}_{IJ} \cdot (\text{Area}), \tag{10.29}$$

$$\vec{\omega}_{IJ} \equiv (\cos(\theta_{IJ} + \pi/2), \sin(\theta_{IJ} + \pi/2)). \tag{10.30}$$

Thus two supercharges conserved at this wall are

$$Q_1 + e^{i(-\alpha_{IJ} - \theta_{IJ})} \bar{Q}_{\dot{1}}, \qquad Q_2 + e^{i(-\alpha_{IJ} + \theta_{IJ})} \bar{Q}_{\dot{2}}, \tag{10.31}$$

where $\alpha_{IJ} = \arg(\mathcal{W}_J - \mathcal{W}_I)$.

BPS domain wall junction is a 1/4 BPS state and conserves only one supercharge. Let us consider the case of $H = H_{\rm II}$ where a linear combination of Q_2 and $\bar{Q}_{\dot{2}}$ is conserved as shown in eq.(9.20). This must be the common conserved supercharge for all the walls

$$\cdots = Q_2 + e^{i(-\alpha_{IJ} + \theta_{IJ})} \bar{Q}_{\dot{2}} = Q_2 + e^{i(-\alpha_{JK} + \theta_{JK})} \bar{Q}_{\dot{2}} = \cdots. \tag{10.32}$$

Then the relative angle of the two neighboring walls must be equal to the difference of two phases of the differences $\Delta\mathcal{W}$ of the superpotentials for the two walls

$$\cdots,\ \theta_{JK} - \theta_{IJ} = \alpha_{JK} - \alpha_{IJ},\ \cdots. \tag{10.33}$$

Moreover the field configuration at infinity should move counterclockwise in $\mathcal{W}$ space, as we go around the origin counterclockwise in x^1, x^2 space.

Similarly, a linear combination of Q_1 and $\bar{Q}_{\dot{1}}$ is the common conserved supercharge in the case of $H = H_{\rm I}$. We obtain in this case

$$\cdots,\ \theta_{JK} - \theta_{IJ} = -(\alpha_{JK} - \alpha_{IJ}),\ \cdots \tag{10.34}$$

and that the field configuration at infinity should move clockwise in $\mathcal{W}$ space, as we go around the origin counterclockwise in x^1, x^2 space.

Therefore we find that the BPS equations (9.22) and (9.24) for the case $H = H_{\rm II}$ should be used if the phase of the superpotential $\mathcal{W}$ increases as we go around the origin counterclockwise in x^1, x^2 space. If the phase of the superpotential $\mathcal{W}$ decreases as we go around the origin counterclockwise in x^1, x^2 space, the other BPS equations (9.21) and (9.23) for $H = H_{\rm I}$ should be used.

Negative contribution of central charge Y_3 to junction mass

Next we discuss the sign of the contribution of the central charge Y_3 to the mass of the junction configuration. We can use the Stokes theorem to obtain

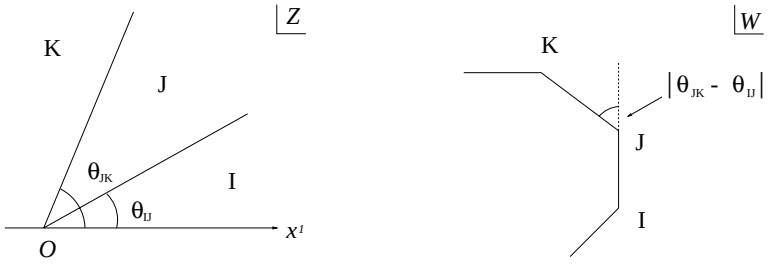

(a)Walls separating vacua I, J, K in x^1, x^2 space.

(b)BPS polygon in $\mathcal{W}$ space.

Figure 10.3: Walls in x^1, x^2 space and BPS polygon in $\mathcal{W}$ space.

an expression for the central charge Y_3 as a contour integral[137, 141]

$$Y_3 = \int dx^3\, i \int d^2x\, \left[\partial_1\left(K_i \partial_2 A^i\right) - \partial_2\left(K_i \partial_1 A^i\right)\right] = \int dx^3\, i \oint K_i dA^i, \tag{10.35}$$

where $K_i \equiv \partial K/\partial A^i$ is a derivative of the Kähler potential K. This contour integral in the field space should be done as a map from a counterclockwise contour in the infinity of $z = x^1 + ix^2$ plane. Only complex fields can contribute to Y_3. Let us assume for simplicity that there is only one field which can contribute to Y_3 as in our exact solution.

Eq.(10.35) shows that the central charge Y_3 becomes negative (positive), if the asymptotic counterclockwise contour in x^1, x^2 is mapped into a counterclockwise (clockwise) contour in field space. On the other hand, the sign of the contribution of the central charge Y_3 to the mass of the junction configuration is determined by the formula $H = H_{\rm II} = |\langle iZ_1 - Z_2\rangle| + \langle Y_3\rangle$, or $H = H_{\rm I} = |\langle -iZ_1 - Z_2\rangle| - \langle Y_3\rangle$. The choice of these mass formulas are in turn determined by the map of the asymptotic counterclockwise contour in x^1, x^2 space to a counterclockwise or clockwise contour in the superpotential space $\mathcal{W}$. Combining these two observations, we conclude that the contribution of the central charge Y_3 to the mass of the junction configuration is negative if the sign of rotations is the same in field space A^i and in superpotential space $\mathcal{W}$, and positive if the sign of rotations is opposite.

The field configuration moves counterclockwise in field space in our exact solution in (10.25) and then the central charge is negative in this solution. Since the exact solution satisfies the BPS equation for the case $H = H_{\rm II}$, the central charge contributes to the mass of the junction configuration negatively. Therefore we should not consider the central charge Y_3 alone as the

physical mass of the junction at the center. In the junction configuration, the junction at the center cannot be separated from the walls. We also can find a solution for the other case of $H = H_{\rm I}$ in our model. The solution is just a configuration obtained by a reflection $x^1 \to -x^1$. Then the central charge is positive, but the contribution to the mass $H = H_{\rm I}$ becomes again negative. In either solution, the rotation in field T space has the same sign as the rotation in superpotential $\mathcal{W}$ space. Therefore central charge Y_3 contributes negatively to the mass of the junction, irrespective of the choice of $H = H_{\rm I}$ or $H = H_{\rm II}$.

More recently this feature of negative contribution of Y_3 to the junction mass is studied from a different viewpoint and it is argued that this feature is valid in most situations except possibly in contrived models [146]. These models, if they exist, should correspond to the case of opposite sign of rotations in $\mathcal{W}$ space and field space.

10.3.2 Energy density and central charges

Charge densities

Our exact solution is useful to examine how the topological charges Z_k, Y_k and energy of the domain wall junction are distributed in x^1, x^2 space. We shall study their densities and integrated quantities in finite regions in this subsection.

Y charge density The Y_3 charge density $\mathcal{Y}_3 = i\epsilon^{3nm}\partial_n \left(T^* \partial_m T\right)$ is given in our exact solution by

$$\begin{aligned}\mathcal{Y}_3 &= -24\Lambda^4 \frac{e^{\sqrt{3}\Lambda x^2}}{\left[e^{\sqrt{3}\Lambda x^2} + 2\cosh\left(\Lambda x^1\right)\right]^3} \\ &= -24\Lambda^4 \frac{1}{\left[e^{\frac{2\Lambda r}{\sqrt{3}}\sin\theta} + e^{\frac{2\Lambda r}{\sqrt{3}}\sin\left(\theta+\frac{2\pi}{3}\right)} + e^{\frac{2\Lambda r}{\sqrt{3}}\sin\left(\theta-\frac{2\pi}{3}\right)}\right]^3},\end{aligned} \tag{10.36}$$

where the cylindrical coordinates r and θ is used to make Z_3 symmetry explicit. A bird's eye view of the $\mathcal{Y}_3$ is given in Fig. 10.4. Here and the following, we shall take the unit of $\Lambda \equiv 1$ in drawing figures. The density is localized near the origin and the Z_3 symmetry is manifest.

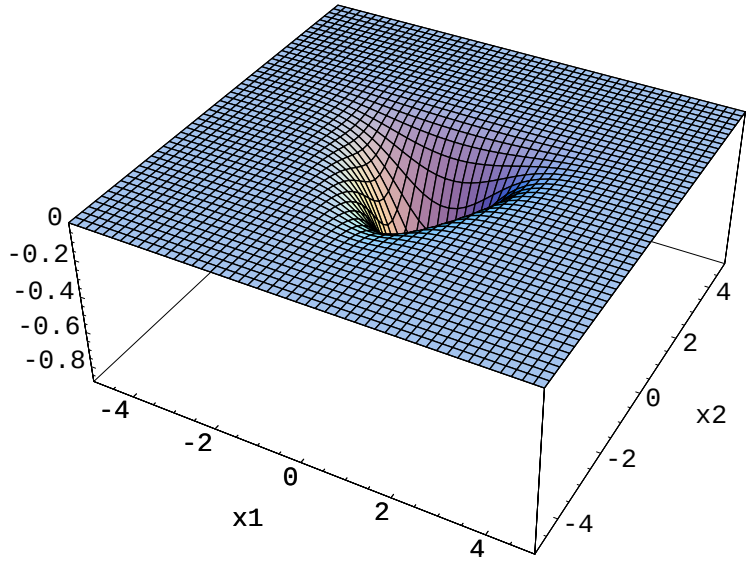

Figure 10.4: A bird's eye view of $\mathcal{Y}_3$.

Z charge density We obtain the superpotential as the function of x^1 and x^2, by inserting the solution (10.25)

$$\begin{aligned}
\mathrm{Re}\mathcal{W}^* &= -8\Lambda^3 \frac{\left(2+3e^{\sqrt{3}\Lambda x^2}\cosh\left(\Lambda x^1\right)+\cosh\left(2\Lambda x^1\right)\right)\sinh\left(\Lambda x^1\right)}{\left[e^{\sqrt{3}\Lambda x^2}+2\cosh\left(\Lambda x^1\right)\right]^3} \\
\mathrm{Im}\mathcal{W}^* &= 2\sqrt{3}\Lambda^3 \frac{e^{\sqrt{3}\Lambda x^2}\left[2+e^{2\sqrt{3}\Lambda x^2}+6e^{\sqrt{3}\Lambda x^2}\cosh\left(\Lambda x^1\right)\right]}{\left[e^{\sqrt{3}\Lambda x^2}+2\cosh\left(\Lambda x^1\right)\right]^3}.
\end{aligned} \tag{10.37}$$

The Z charge densities are given by $\mathcal{Z}_k = 2\partial_k \mathcal{W}^*, (k=1,2)$ and are found to be

$$\begin{aligned}
\mathrm{Re}\mathcal{Z}_1 &= -48\Lambda^4 \frac{2+e^{2\sqrt{3}\Lambda x^2}\cosh\left(2\Lambda x^1\right)+3e^{\sqrt{3}\Lambda x^2}\cosh\left(\Lambda x^1\right)}{\left[e^{\sqrt{3}\Lambda x^2}+2\cosh\left(\Lambda x^1\right)\right]^4} \\
\mathrm{Im}\mathcal{Z}_1 &= -\mathrm{Re}\mathcal{Z}_2 = -48\sqrt{3}\Lambda^4 \frac{e^{\sqrt{3}\Lambda x^2}\sinh\left(\Lambda x^1\right)\left(1+2e^{\sqrt{3}\Lambda x^2}\cosh\left(\Lambda x^1\right)\right)}{\left[e^{\sqrt{3}\Lambda x^2}+2\cosh\left(\Lambda x^1\right)\right]^4} \\
\mathrm{Im}\mathcal{Z}_2 &= 48\Lambda^4 \frac{e^{\sqrt{3}\Lambda x^2}\left[\cosh\left(\Lambda x^1\right)+e^{\sqrt{3}\Lambda x^2}\left(2+3\cosh\left(2\Lambda x^1\right)\right)\right]}{\left[e^{\sqrt{3}\Lambda x^2}+2\cosh\left(\Lambda x^1\right)\right]^4}.
\end{aligned} \tag{10.38}$$

We can define the effective value of the Z charge which contributes to the energy of the junction as $Z_{\text{eff}} = -\text{Re}Z_1 + \text{Im}Z_2$. Corresponding effective charge density is given by

$$\mathcal{Z}_{\text{eff}} = 96\Lambda^4 \frac{1 + 2e^{\sqrt{3}\Lambda x^2}\cosh(\Lambda x^1) + e^{2\sqrt{3}\Lambda x^2}(1 + 2\cosh(2\Lambda x^1))}{\left[e^{\sqrt{3}\Lambda x^2} + 2\cosh(\Lambda x^1)\right]^4}. \quad (10.39)$$

Let us note that the effective charge density is Z_3 symmetric, whereas individual charges $\mathcal{Z}_1, \mathcal{Z}_2$ are not.

Energy density Adding $\mathcal{Z}_{\text{eff}}$ and $\mathcal{Y}_3$ together, the energy density of the junction is obtained,

$$\mathcal{H} = 24\Lambda^4 \frac{4 + 6e^{\sqrt{3}\Lambda x^2}\cosh(\Lambda x^1) + e^{2\sqrt{3}\Lambda x^2}(3 + 8\cosh(2\Lambda x^1))}{\left[e^{\sqrt{3}\Lambda x^2} + 2\cosh(\Lambda x^1)\right]^4} \quad (10.40)$$

A bird's eye view of $\mathcal{H}$ is shown in Fig. 10.5. The energy density is Z_3

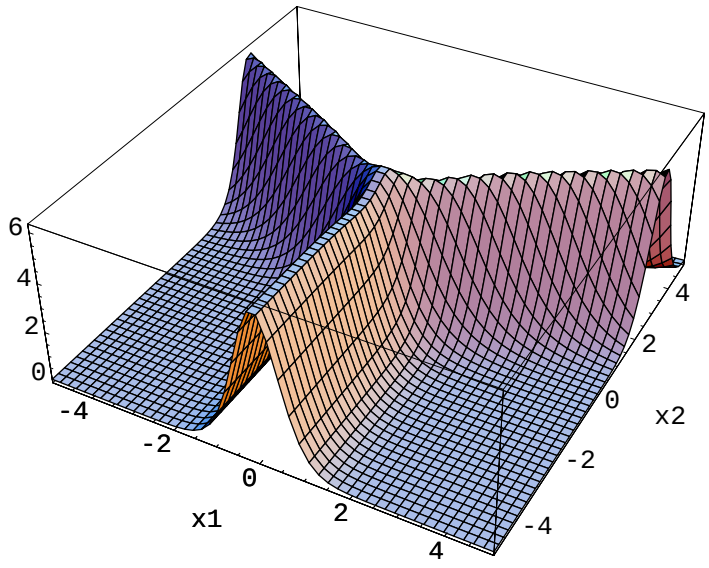

Figure 10.5: A bird's eye view of the energy density of the junction.

symmetric as expected.

A cross section of the densities, $\mathcal{H}, \mathcal{Z}_{\text{eff}}$ and $\mathcal{Y}_3$ along one of the walls (e.g. negative x^2 direction) is shown in Fig. 10.6. The Z_{eff} charge contributes

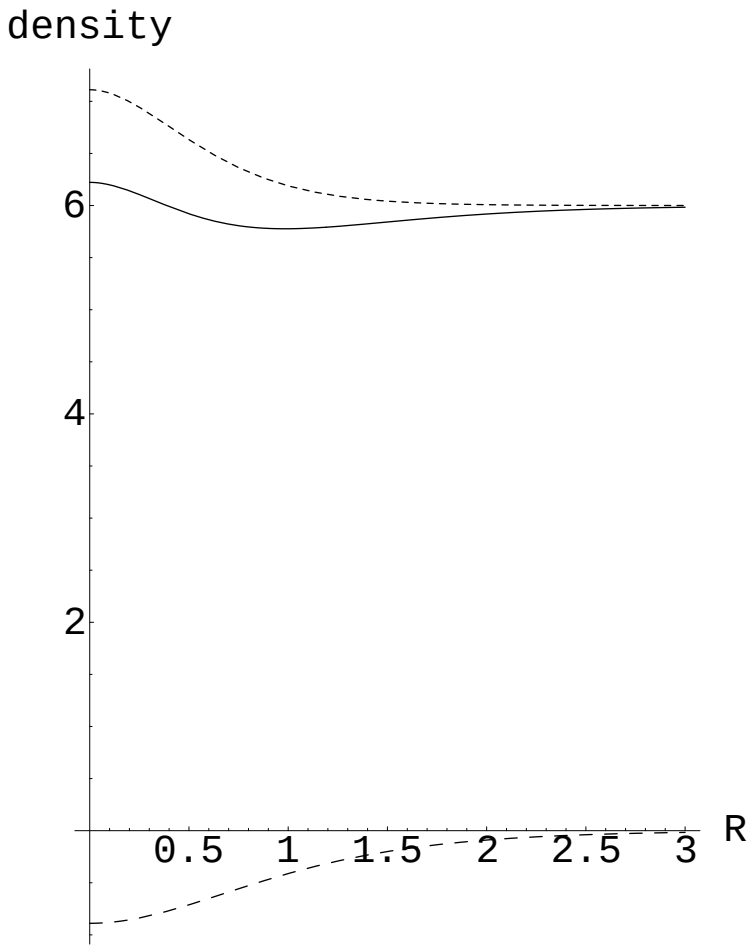

Figure 10.6: A cross section of the densities $\mathcal{H}$ (solid line), $\mathcal{Z}_{\text{eff}}$ (short dashed line) and $\mathcal{Y}_3$ (long dashed line) along the negative x^2 direction.

to the energy positively while Y_3 does negatively. Since the decrease of $\mathcal{Z}_{\rm eff}$ is faster than the increase of $\mathcal{Y}_3$, a small dip is found around $R\Lambda \sim 1$. Far from the origin there is practically no difference between $\mathcal{Z}_{\rm eff}$ and $\mathcal{H}$ because $\mathcal{Y}_3$ is localized near the origin.

10.3.3 Charge densities integrated over a region of finite radius

In this subsection we shall evaluate the central charge densities integrated over a triangular or circular region depicted in Fig. 10.7.

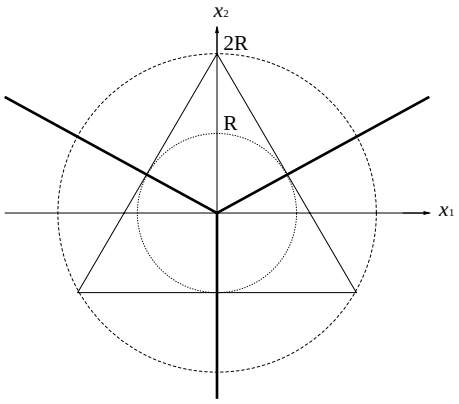

Figure 10.7: The domains of integration: triangle (solid line), inscribed circle (short dashed line) and circumscribed circle (long dashed line). The bold lines denote the domain walls forming a junction.

Y_3 charge Integrating $\mathcal{Y}_3$ over a triangle whose inscribed circle has a radius R as shown in Fig. 10.7, we obtain for large R ($R\Lambda \gg 1$)

$$Y_3^{\rm triangle}(R) = -2\sqrt{3}\Lambda^2 L_3 \left[1 - \frac{3\pi}{4} e^{-\sqrt{3}R\Lambda} + \mathcal{O}\left(e^{-2\sqrt{3}R\Lambda}\right)\right], \qquad (10.41)$$

where L_3 denotes the length along the x^3 direction. The leading term agrees with our previous evaluation by the step function approximation[141] (see also eq.(10.5)) and the subleading terms vanish exponentially as $R \to \infty$.

On the other hand, for small R ($R\Lambda \ll 1$), we obtain the Y_3 charge

$$Y_3^{\rm triangle}(R) = -\frac{8}{\sqrt{3}}\Lambda^2 L_3 \left[R^2\Lambda^2 - R^4\Lambda^4 - \frac{4\sqrt{3}}{45}R^5\Lambda^5 + \mathcal{O}\left(R^6\Lambda^6\right)\right]. \qquad (10.42)$$

Notice that the leading term comes from the density at the origin multiplied by the area of the triangle. Although there are no terms of the first or third degree in R, there is a fifth degree term.

We can also integrate the $\mathcal{Y}_3$ over a circle of radius R. In this case it is more convenient to use cylindrical coordinates (r, θ, and x^3), and the following surface integral formula obtained from the Stokes theorem,

$$Y_3^{\rm circle}(R) = \int_{-L_3/2}^{L_3/2} dx^3 \int_0^{2\pi} d\theta \left[iT'^* \frac{\partial}{\partial\theta} T' \right] = \frac{8R\Lambda^3 L_3}{\sqrt{3}} \tag{10.43}$$
$$\times \int_0^{2\pi} d\theta \frac{\sin\left(\theta - \frac{2\pi}{3}\right) e^{2R\Lambda\cos\theta} + \sin\theta e^{2R\Lambda\cos\left(\theta+\frac{2\pi}{3}\right)} + \sin\left(\theta+\frac{2\pi}{3}\right) e^{2R\Lambda\cos\left(\theta-\frac{2\pi}{3}\right)}}{\left[e^{\frac{2R\Lambda}{\sqrt{3}}\sin\left(\theta+\frac{2\pi}{3}\right)} + e^{\frac{2R\Lambda}{\sqrt{3}}\sin\left(\theta-\frac{2\pi}{3}\right)} + e^{\frac{2R\Lambda}{\sqrt{3}}\sin\theta} \right]^3}$$

where the Z_3 symmetry is manifest. Expanding the integrand for small R ($R\Lambda \ll 1$), we obtain

$$Y_3^{\rm circle}(R) = -\frac{8\pi}{9}\Lambda^2 L_3 \left[R^2\Lambda^2 - \frac{1}{2}R^4\Lambda^4 + \mathcal{O}(R^6\Lambda^6) \right]. \tag{10.44}$$

The leading term is again the density at the origin multiplied by the area of the circle. In contrast to the triangle case, there is no term of odd degree in R.

For large R ($R\Lambda \gg 1$), we have to perform numerical integration to evaluate the $Y_3^{\rm circle}(R)$. We compare the $Y_3(R)$ evaluated for triangle, inscribed and circumscribed circle in Fig. 10.8. In the limit of $R \to \infty$, $Y_3(R)$ for all the regions converge to $-2\sqrt{3}\Lambda^2 L_3$ as expected.

Z charges Since the Z_1 charge is given by a total derivative in x^1, we can rewrite the Z_1 charge as

$$Z_1(R) = 2\int dx^2 \int dx^1 \partial_1 \mathcal{W}^*(A^*) \tag{10.45}$$
$$= 2\int_{x^{2-}}^{x^{2+}} dx^2 \left[\mathcal{W}^*\left(x^{1+}\left(x^2\right), x^2\right) - \mathcal{W}^*\left(x^{1-}\left(x^2\right), x^2\right) \right], \tag{10.46}$$

where $x^{i\pm} (i = 1, 2)$ denote the upper and lower bound of the domain of integration. Since eq.(10.37) shows that ${\rm Im}\mathcal{W}^*(x^1, x^2)$ is even and ${\rm Re}\mathcal{W}^*(x^1, x^2)$ is odd in x^1, we obtain ${\rm Im}Z_1(R) = 0$ and ${\rm Re}Z_2(R) = 0$ for an integration region symmetric in x^1 which we shall use. Let us note that ${\rm Re}\mathcal{Z}_1$ (${\rm Im}\mathcal{Z}_2$) is negative (positive) definite.

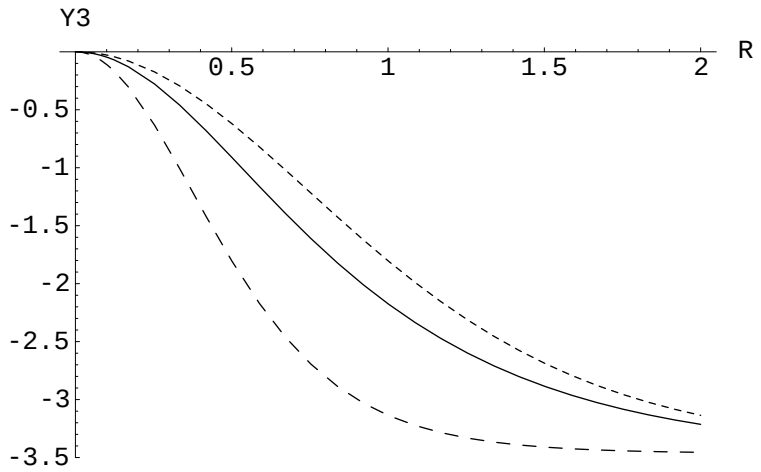

Figure 10.8: $Y_3(R)$ evaluated for the triangle (solid line), inscribed circle of radius R (short dashed line) and circumscribed circle (long dashed line).

Firstly we choose as a domain of integration the triangle region whose inscribed circle has a radius R. For large R ($R\Lambda \gg 1$), we obtain

$$\begin{aligned}
\mathrm{Re}Z_1^{\mathrm{triangle}}(R) &= -12\Lambda^2 L_3 \left[R\Lambda + \frac{\sqrt{3}\pi}{4} e^{-\sqrt{3}R\Lambda} + \mathcal{O}\left(e^{-2\sqrt{3}R\Lambda}\right) \right] \\
\mathrm{Im}Z_2^{\mathrm{triangle}}(R) &= 12\Lambda^2 L_3 \left[R\Lambda + \frac{\sqrt{3}}{3}\left(\frac{\pi}{8} - \frac{4}{3}\right) e^{-\sqrt{3}R\Lambda} + \mathcal{O}\left(e^{-2\sqrt{3}R\Lambda}\right) \right].
\end{aligned} \tag{10.47}$$

The leading linear term represents the contribution of charge density per unit length of the wall. It is interesting to observe that there are no constant terms. The exponentially suppressed terms represent the way the domain wall junction configuration converges to isolated walls as $R \to \infty$. The effective value of the Z charge becomes

$$\begin{aligned}
Z_{\mathrm{eff}}^{\mathrm{triangle}}(R) &= -\mathrm{Re}Z_1^{\mathrm{triangle}}(R) + \mathrm{Im}Z_2^{\mathrm{triangle}}(R) \\
&= 24\Lambda^3 L_3 R + \sqrt{3}\left(\frac{7\pi}{2} - \frac{16}{3}\right)\Lambda^2 L_3 e^{-\sqrt{3}R\Lambda} + \mathcal{O}\left(e^{-2\sqrt{3}R\Lambda}\right).
\end{aligned} \tag{10.48}$$

For small R ($R\Lambda \ll 1$), Z charges become

$$\mathrm{Re}Z_1^{\mathrm{triangle}}(R) = -\frac{32}{\sqrt{3}}\Lambda^2 L_3 \left[R^2\Lambda^2 + \frac{1}{2}R^4\Lambda^4 - \frac{2\sqrt{3}}{9}R^5\Lambda^5 + \mathcal{O}\left(R^6\Lambda^6\right) \right]$$

$$\mathrm{Im}Z_2^{\mathrm{triangle}}(R) = \frac{32}{\sqrt{3}}\Lambda^2 L_3 \left[R^2\Lambda^2 - \frac{1}{2}R^4\Lambda^4 + \frac{2\sqrt{3}}{9}R^5\Lambda^5 + \mathcal{O}\left(R^6\Lambda^6\right)\right]. \tag{10.49}$$

Notice that the leading term represents the density at the origin multiplied by the area of the triangle, and that there is no term of the first or third degree in R. The effective value of Z charge is

$$Z_{\mathrm{eff}}^{\mathrm{triangle}}(R) = \frac{64}{\sqrt{3}}R^2\Lambda^4 L_3 + \mathcal{O}\left(R^6\Lambda^6\right). \tag{10.50}$$

We can also choose a circle of radius R as a domain of integration. For small R ($R\Lambda \ll 1$) we obtain

$$\begin{aligned}\mathrm{Re}Z_1^{\mathrm{circle}}(R) &= -\frac{32\pi}{9}\Lambda^2 L_3 \left[R^2\Lambda^2 - \frac{1}{4}R^4\Lambda^4 + \mathcal{O}\left(R^6\Lambda^6\right)\right] \\ \mathrm{Im}Z_2^{\mathrm{circle}}(R) &= \frac{32\pi}{9}\Lambda^2 L_3 \left[R^2\Lambda^2 - \frac{1}{4}R^4\Lambda^4 + \mathcal{O}\left(R^6\Lambda^6\right)\right].\end{aligned} \tag{10.51}$$

The leading term is again given by the densities at the origin multiplied by the area of the circle. The effective value of the Z charge is

$$Z_{\mathrm{eff}}^{\mathrm{circle}}(R) = \frac{64\pi}{9}\Lambda^2 L_3 \left[R^2\Lambda^2 - \frac{1}{4}R^4\Lambda^4 + \mathcal{O}\left(R^6\Lambda^6\right)\right]. \tag{10.52}$$

A numerical evaluation is needed for large R. We compare the effective Z value evaluated for triangle, inscribed circle and circumscribed circle in Fig. 10.9. As $R \to \infty$, the asymptotic slope of $Z_{\mathrm{eff}}^{\mathrm{ins.circle}}(R)$ for inscribed circle converges to the same value as that for the triangle. In the case of the circumscribed circle, the Z_{eff} becomes twice as large as those of the other cases for large R, since the total length of the walls is twice as long as those of the other cases.

Energy of the junction Since our exact solution satisfies the BPS equation corresponding to $H = H_{\mathrm{II}}$, the energy of the junction is obtained by adding Y_3 and Z_{eff} together $H = Z_{\mathrm{eff}} + \mathrm{Y}_3 = -\mathrm{Re}Z_1 + \mathrm{Im}Z_2 + \mathrm{Y}_3$.

Firstly we choose the triangle region whose inscribed circle has radius R. For large R ($R\Lambda \gg 1$), the energy is

$$H_{\mathrm{triangle}}(R) = 24\Lambda^3 L_3 R - 2\sqrt{3}\Lambda^2 L_3 + \sqrt{3}\left(5\pi - \frac{16}{3}\right)\Lambda^2 L_3 e^{-\sqrt{3}R\Lambda} + \mathcal{O}\left(e^{-2\sqrt{3}R\Lambda}\right). \tag{10.53}$$

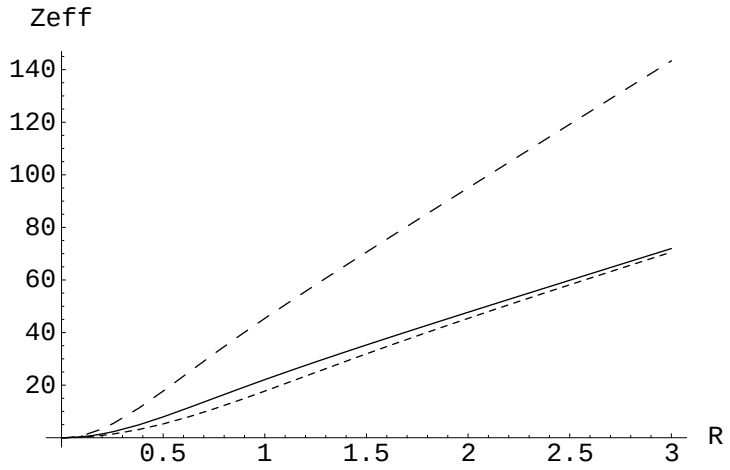

Figure 10.9: $Z_{\rm eff}(R)$ evaluated for the triangle (solid line), the inscribed circle of the radius R (short dashed line), and circumscribed circle (long dashed line).

The first linear term can be regarded as the contribution from the walls and the second constant term can be regarded as the contribution from the junction at the center. For small R ($R\Lambda \ll 1$), the energy is

$$H_{\rm triangle}(R) = \frac{56}{\sqrt{3}}\Lambda^2 L_3 \left[R^2\Lambda^2 + \frac{1}{7}R^4\Lambda^4 + \frac{4\sqrt{3}}{315}R^5\Lambda^5 + \mathcal{O}\left(R^6\Lambda^6\right) \right]. \tag{10.54}$$

In the case of the circle of radius R, the energy is given for small R ($R\Lambda \ll 1$) as

$$H_{\rm circle}(R) = \frac{56\pi}{9}\Lambda^2 L_3 \left[R^2\Lambda^2 - \frac{3}{14}R^4\Lambda^4 + \mathcal{O}\left(R^6\Lambda^6\right) \right]. \tag{10.55}$$

The energy of the triangle region is compared to those of inscribed and circumscribed circles in Fig. 10.10. For large R ($R\Lambda \gg 1$), the energy H reduces to $Z_{\rm eff}$.

Finally we plot the θ–dependence of the energy and charges that are obtained by integrating the densities from $r = 0$ to $r = R$ with θ fixed (see Fig. 10.11). In each figure the energy H (solid line) is the sum of the $Z_{\rm eff}$ (short dashed line) and Y_3 (long dashed line) and Z_3 symmetry is manifest in their θ–dependence. In Fig. 10.11(a), all the quantities are almost uniform in θ near the junction at the center, reflecting the fact that the junction is a string–like object and symmetric around the x^3 axis. As we move away from the origin, main contribution comes from the direction of the walls (in

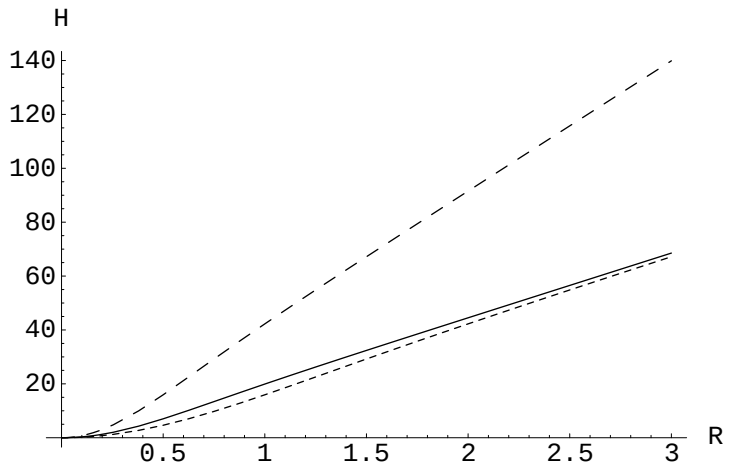

Figure 10.10: The energy of the junction configuration $H(R)$ evaluated for the triangle (solid), inscribed circle of radius R (short dashed line) and circumscribed circle (long dashed line).

our case $-\pi/2, \pi/6$, and $5\pi/6$) (see Fig. 10.11(b) and (c)). As R grows, Y_3 disappears and the energy H approaches Z_{eff} (see Fig. 10.11(d)).

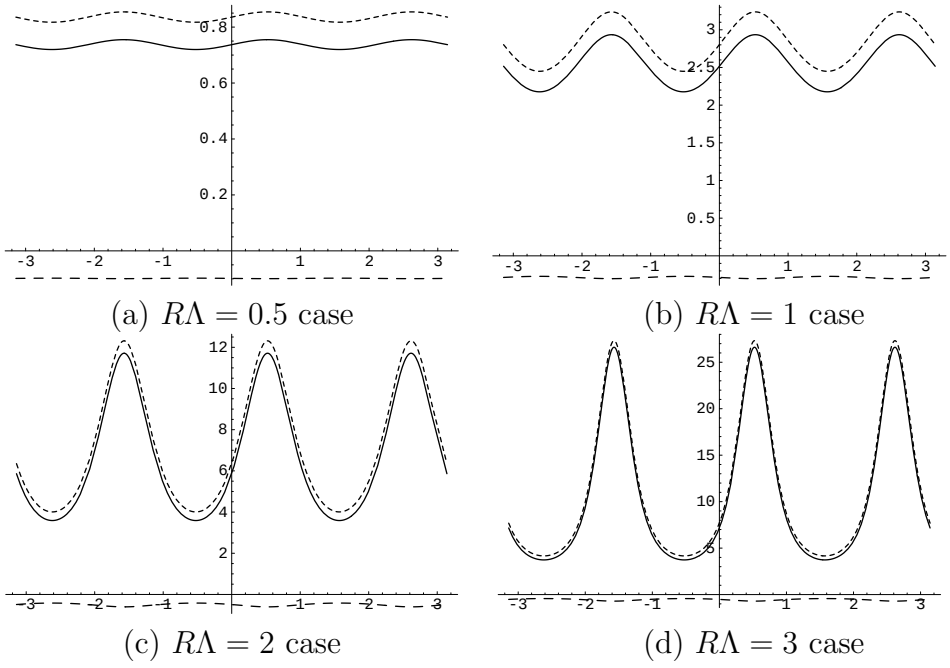

(a) $R\Lambda = 0.5$ case (b) $R\Lambda = 1$ case

(c) $R\Lambda = 2$ case (d) $R\Lambda = 3$ case

Figure 10.11: The θ–dependence of the energy and charges that are obtained by integrating the densities over the radial direction up to R with θ fixed. In each figure horizontal axis denotes θ, and solid, short dashed and long dashed lines correspond to H, $Z_{\rm eff}$ and Y_3 respectively.

Chapter 11

Modes on BPS domain wall junctions

In the previous two chapters we have discussed various properties of BPS domain walls and junctions. In this chapter we will focus on modes on the domain wall junction background[159, 160].

11.1 Modes on domain walls: a simple example

In this section we briefly discuss localization of (zero) modes on the domain wall of a simple model used in section 9.1.

The classical domain wall solution (9.5) provides a potential well, which is narrow along the x^1 direction if μ is sufficiently large.

Let us consider the quantum fluctuations $\phi'(x)$ around the classical solution (9.5) which we call $\phi_{\rm cl}(x^1)$. The equation of motion obtained from the Lagrangian (9.1) is

$$-\partial_\mu\partial^\mu\phi - \mu^2\phi + \lambda\phi^3 = 0. \tag{11.1}$$

Especially the classical solution $\phi_{\rm cl}(x^1)$ satisfies more simple equation $\frac{d^2\phi_{\rm cl}}{d(x^1)^2} = -\mu^2\phi_{\rm cl} + \lambda\phi_{\rm cl}^3$.

Perturbing $\phi(x) \equiv \phi_{\rm cl}(x^1) + \phi'(x^1)$ and retaining the first order of the fluctuations, we obtain the linearized equation for the scalar fluctuations

$$-\partial_\mu\partial^\mu\phi' - \mu^2\phi' + 3\lambda\phi_{\rm cl}^2\phi' = 0. \tag{11.2}$$

If we define mode equation by

$$\left(-\partial_1^2 - \mu^2 + 3\lambda\phi_{\rm cl}^2\right) u_n(x^1) = m_n^2 u_n(x^1), \tag{11.3}$$

the quantum fluctuation can be expanded by these mode functions $u_n(x^1)$ as $\phi'(x) = \sum_n a_n(x^0, x^2, x^3)u_n(x^1)$. The coefficients $a_n(x^0, x^2, x^3)$ satisfies the equation of motion of $2+1$ dimensional massive scalar fields

$$\left[\partial_0^2 - \partial_2^2 - \partial_3^2 + m_n^2\right] a_n(x^0, x^2, x^3) = 0. \tag{11.4}$$

We can obtain mode expansion by solving the mode equation (11.3). Especially it is not difficult to verify that the zero mode equation $(-\partial_1^2 - \mu^2 + 3\lambda\phi_{\rm cl}^2)\, u_0(x^1) = 0$ is satisfied by $\frac{d\phi_{\rm cl}}{dx^1}$, and we can obtain the zero mode wave function

$$\phi'(x) = \frac{d\phi_{\rm cl}}{dx^1} e^{i\left(k^2x^2 + k^3x^3 - k^0x^0\right)} = \frac{\mu^2}{\sqrt{2\lambda}} \frac{e^{i\left(k^2x^2 + k^3x^3 - k^0x^0\right)}}{\cosh^4\left(\frac{\mu}{\sqrt{2}}x^1\right)}. \tag{11.5}$$

From this wave function we can see that the zero mode is localized near the region $x^1 \sim 0$ and it can freely move along the x^2, x^3 direction.

Here we have seen the localization of scalar field. It is known that other types of fields such as fermionic fields and gauge fields are also localized on domain walls[127, 134, 135]. In the next sections we will consider the (zero) modes on the domain wall junction background.

11.2 Modes on domain wall junctions

In the rest of this chapter, we will study the modes on the background of the domain wall junction, especially the Nambu-Goldstone modes. We will use our exact solution as a concrete example and will extract the generic properties of modes on the BPS domain wall junctions. We define mode equations and demonstrate explicitly that fermion and boson with the same mass have to come in pairs except massless modes. Massless modes can appear singly without accompanying fields with opposite statistics. We also show that unitary representations of the surviving $(1, 0)$ supersymmetry are classified into doublets for massive modes and singlets for massless modes. We work out explicitly massless Nambu-Goldstone modes associated with the broken supersymmetry and translational invariance. We find that the Nambu-Goldstone fermions exhibit an interesting chiral structure in accordance with the surviving $(1, 0)$ supersymmetry algebra. However, we also find that any linear combinations of the Nambu-Goldstone modes associated with the junctions become a linear combination of zero modes on at least one of the domain walls asymptotically along these walls. Since their wave functions are extended along these walls without damping, they are not localized states on the junction. Therefore they are not normalizable, contrary to a

previous expectation [136]. This indicates that the resulting theory cannot be regarded as a genuine $1+1$ dimensional field theory with discrete particle spectrum even at zero energy. Although the remaining supersymmetry is just $(1,0)$ which is characteristic to $1+1$ dimensions, we have to keep in mind that the domain wall junction configuration is actually living in one more dimensions similarly to the domain wall itself. Zero modes on the junction turn out to have properties quite similar to those on the domain wall. The non-normalizability of Nambu-Goldstone modes on the junction configuration is not an accident in this particular model. We observe that the origin of this property can be traced back to the fact that the supersymmetry is broken by the coexistence of nonparallel walls. Therefore the fact that the Nambu-Goldstone modes on the BPS domain wall junction are not normalizable is a generic feature of supersymmetric field theories in the bulk flat space.

One should note that our conclusion need not apply to the case with negative cosmological constant in the bulk. In the presence of a bulk negative cosmological constant in six dimensions, five dimensional walls can intersect in Anti de Sitter space. If one demands a flat space at the four dimensional intersection, one has an Anti de Sitter space not only in the bulk but also even on the walls [120]–[122]. Since Anti de Sitter space does not have translational invariance, the wave function of the zero mode does not become constant along the wall asymptotically, contrary to our situation. If one approaches the intersection along the wall, one meets precisely the same situation as the wall in the five dimensional Anti de Sitter space. For instance graviton zero mode is exponentially suppressed away from the intersection along the wall direction to produce a normalizable wave function. Therefore the Anti de Sitter geometry along the wall plays an essential role to achieve the localization of the wave function on the intersection in models with cosmological constant.

11.3 Unitary representations of $(1,0)$ supersymmetry algebra

Let us examine states on the background of a domain wall junction from the point of view of surviving symmetry. In the case of the BPS states satisfying the BPS equation (9.22) corresponding to $H = H_{\rm II}$, we have only one surviving supersymmetry charge $Q^{(1)}$, two translation generators H, P^3, and one Lorentz generator J^{03}, out of the $\mathcal{N} = 1$ four dimensional super Poincaré generators. Since we are interested in excitation modes on the

background of the domain wall junction, we define the Hamiltonian $H' = H - \langle H \rangle$ measured from the energy $\langle H \rangle$ of the background configuration. By projecting from the supersymmetry algebra (9.8), (9.9) with central charges in four dimensions, we immediately find

$$\left(Q^{(1)}\right)^2 = H' - P^3. \tag{11.6}$$

We also obtain the Poincaré algebra in $1+1$ dimensions

$$\begin{aligned} [J^{03}, Q^{(1)}] = \frac{i}{2} Q^{(1)}, \qquad & [J^{03}, H' - P^3] = i(H' - P^3), \\ & [J^{03}, H' + P^3] = -i(H' + P^3). \end{aligned} \tag{11.7}$$

Other commutation relations are trivial

$$[H' - P^3, H' + P^3] = [H' - P^3, Q^{(1)}] = [H' + P^3, Q^{(1)}] = 0. \tag{11.8}$$

This is precisely the $(1,0)$ supersymmetry algebra on the domain wall junction as anticipated [136].

To obtain unitary representations, we can diagonalize H' and P^3

$$H'|E, p^3\rangle = E|E, p^3\rangle, \qquad P^3|E, p^3\rangle = p^3|E, p^3\rangle, \qquad E \geq |p^3|, \tag{11.9}$$

and combine them by means of $Q^{(1)}$. If $E - p^3 > 0$, we can construct bosonic state from fermionic state and vice versa by operating $Q^{(1)}$ on the state.

$$|B\rangle = \frac{1}{\sqrt{E - p^3}} Q^{(1)}|F\rangle, \qquad |F\rangle = \frac{1}{\sqrt{E - p^3}} Q^{(1)}|B\rangle. \tag{11.10}$$

Therefore we obtain a doublet representation $(|B\rangle, |F\rangle)$. If $E - p^3 = 0$, operating by $Q^{(1)}$ on the state gives an unphysical zero norm state

$$\left|Q^{(1)}|E, p^3\rangle\right|^2 = \langle E, p^3| \left(Q^{(1)}\right)^2 |E, p^3\rangle = \langle E, p^3|H' - P^3|E, p^3\rangle = E - p^3 = 0. \tag{11.11}$$

Then the massless right-moving state $|E, p^3 = E\rangle$ is a singlet representation. This singlet state can either be boson or fermion. Thus we find that there are only two types of representations of the $(1,0)$ supersymmetry algebra, doublet and singlet. We also find that massive modes should appear in pairs of boson and fermion, whereas the massless right-moving mode can appear singly without accompanying a state with opposite statistics. This provides an interesting possibility of a chiral structure for fermions.

If another BPS equation (9.21) corresponding to $H = H_{\rm I}$ is satisfied instead of eq. (9.22), we have $(0,1)$ supersymmetry and the left-moving massless states can appear as singlets.

11.4 Nambu-Goldstone and other modes on the junction

11.4.1 Mode equation on the junction

Since the vector superfields have no nontrivial field configurations, Nambu-Goldstone modes have no component of vector superfield. Moreover we can replace our model, if we wish, by another model with purely chiral superfields without spoiling the essential features including the solvability [1]. Consequently we shall neglect vector superfields and consider the general Wess-Zumino model in eq.(9.10) in the following. For simplicity we assume the minimal kinetic term here $K_{ij^*} = \delta_{ij^*}$.

Let us consider quantum fluctuations A'^i, ψ^i around a classical solution $A^i_{\rm cl}$ which satisfies the BPS equations (9.21) and (9.23) for $H = H_{\rm I}$ or (9.22) and (9.24) for $H = H_{\rm II}$.

$$A^i = A^i_{\rm cl} + A'^i. \tag{11.12}$$

We retain the part of the Lagrangian quadratic in fluctuations and eliminate the auxiliary fields F^i to obtain the linearized equation for the scalar fluctuations

$$-\partial_\mu\partial^\mu A'^{*i} + \frac{\partial^2\mathcal{W}}{\partial A^i_{\rm cl}\partial A^k_{\rm cl}}\frac{\partial^2\mathcal{W}^*}{\partial A^{*k}_{\rm cl}\partial A^{*j}_{\rm cl}}A'^{*j} + \frac{\partial^3\mathcal{W}}{\partial A^i_{\rm cl}\partial A^k_{\rm cl}\partial A^j_{\rm cl}}\frac{\partial\mathcal{W}^*}{\partial A^{*k}_{\rm cl}}A'^j = 0. \tag{11.13}$$

In order to separate variables in x^0, x^3 and x^1, x^2 we have to define mode equations on the background which has a nontrivial dependence in two dimensions, x^1, x^2. The bosonic modes $A'^i_n(x^1, x^2)$ can easily be defined in terms of a differential operator $\mathcal{O}_B$ in x^1, x^2 space

$$\mathcal{O}_B{}^i{}_j \equiv \begin{bmatrix} -\left(\partial_1^2+\partial_2^2\right)\delta^i_j + \frac{\partial^2\mathcal{W}}{\partial A^i_{\rm cl}\partial A^k_{\rm cl}}\frac{\partial^2\mathcal{W}^*}{\partial A^{*k}_{\rm cl}\partial A^{*j}_{\rm cl}} & \frac{\partial^3\mathcal{W}}{\partial A^i_{\rm cl}\partial A^k_{\rm cl}\partial A^j_{\rm cl}}\frac{\partial\mathcal{W}^*}{\partial A^{*k}_{\rm cl}} \\ \frac{\partial^3\mathcal{W}^*}{\partial A^{*i}_{\rm cl}\partial A^{*k}_{\rm cl}\partial A^{*j}_{\rm cl}}\frac{\partial\mathcal{W}}{\partial A^k_{\rm cl}} & -\left(\partial_1^2+\partial_2^2\right)\delta^i_j + \frac{\partial^2\mathcal{W}^*}{\partial A^{*i}_{\rm cl}\partial A^{*k}_{\rm cl}}\frac{\partial^2\mathcal{W}}{\partial A^k_{\rm cl}\partial A^j_{\rm cl}} \end{bmatrix} \tag{11.14}$$

[1] Our model is originally motivated by the softly broken $\mathcal{N} = 2$ $SU(2)$ gauge theory with one flavor. However, we can simplify the model without spoiling the solvability to obtain a Wess-Zumino model consisting of purely chiral superfields by the following procedure. The vector superfields actually serve to constrain chiral superfields to have the identical magnitude pairwise through $D = 0$ to satisfy the BPS equation (9.24) for vector superfields: $|\tilde{\mathcal{M}}| = |\mathcal{M}|, |\tilde{\mathcal{D}}| = |\mathcal{D}|, |\tilde{\mathcal{Q}}| = |\mathcal{Q}|$. Therefore we can eliminate the vector superfields and reduce the number of chiral superfields by identifying pairwise $\tilde{\mathcal{M}} = \mathcal{M}, \tilde{\mathcal{D}} = \mathcal{D}, \tilde{\mathcal{Q}} = \mathcal{Q}$. Correspondingly we should take the superpotential as $\mathcal{W} = \frac{1}{2}(T - \Lambda)\mathcal{M}^2 + \frac{1}{2}(T + \Lambda)\mathcal{D}^2 + \frac{1}{2}(T - i\sqrt{3}\Lambda)\mathcal{Q}^2 - \frac{h^2}{2}T$. This Wess-Zumino model has the same solution as ours by changing $h^2 \to h^2/2, \Lambda \to \sqrt{3}\Lambda/2$. A similar observation has also been made in ref.[146].

$$\mathcal{O}_B{}^i{}_j \begin{bmatrix} A'^{*j}_n \\ A'^j_n \end{bmatrix} = M_n^2 \begin{bmatrix} A'^{*i}_n \\ A'^i_n \end{bmatrix}, \tag{11.15}$$

where the eigenvalue M_n^2 has to be real from Majorana condition. The quantum fluctuation for scalar can be expanded in terms of these mode functions to obtain a real scalar field equation with the mass M_n for the coefficient bosonic field $a_n(x^0, x^3)$

$$A'^i(x^0, x^1, x^2, x^3) = \sum_n a_n(x^0, x^3) A'^i_n(x^1, x^2) \tag{11.16}$$

$$\left(\partial_0^2 - \partial_3^2 + M_n^2\right) a_n(x^0, x^3) = 0. \tag{11.17}$$

Similarly the linearized equation for fermions is given by

$$-i\bar{\sigma}^\mu \partial_\mu \psi^i - \frac{\partial^2 \mathcal{W}^*}{\partial A^{*i}_{\rm cl} \partial A^{*j}_{\rm cl}} \bar{\psi}^j = 0 \tag{11.18}$$

$$-i\sigma^\mu \partial_\mu \bar{\psi}^i - \frac{\partial^2 \mathcal{W}}{\partial A^i_{\rm cl} \partial A^j_{\rm cl}} \psi^j = 0. \tag{11.19}$$

To separate variables for fermion equations, it is more convenient to use a gamma matrix representation where direct product structure of 2×2 matrices for (x^0, x^3) and (x^1, x^2) space is manifest. We shall describe one such representation in appendix F. Transforming from such a representation to the Weyl representation which we are using, we can define the fermionic modes $\psi^i_{n\alpha}, \bar{\psi}^{i\beta}_n$ combining components of left-handed and right-handed spinors by means of the following operators

$$\mathcal{O}_1{}^i{}_j \equiv \begin{bmatrix} -\frac{\partial^2 \mathcal{W}^*}{\partial A^{*i}_{\rm cl} \partial A^{*j}_{\rm cl}} & -i\left(-\partial_1 + i\partial_2\right)\delta^i_j \\ -i\left(\partial_1 + i\partial_2\right)\delta^i_j & -\frac{\partial^2 \mathcal{W}}{\partial A^i_{\rm cl} \partial A^j_{\rm cl}} \end{bmatrix} \tag{11.20}$$

$$\mathcal{O}_2{}^i{}_j \equiv \begin{bmatrix} -\frac{\partial^2 \mathcal{W}}{\partial A^i_{\rm cl} \partial A^j_{\rm cl}} & -i\left(\partial_1 - i\partial_2\right)\delta^i_j \\ -i\left(-\partial_1 - i\partial_2\right)\delta^i_j & -\frac{\partial^2 \mathcal{W}^*}{\partial A^{*i}_{\rm cl} \partial A^{*j}_{\rm cl}} \end{bmatrix} \tag{11.21}$$

$$\mathcal{O}_1{}^i{}_j \begin{bmatrix} \bar{\psi}^{j\dot{1}}_n \\ \psi^j_{n2} \end{bmatrix} = -im_n^{(1)} \begin{bmatrix} \psi^i_{n1} \\ \bar{\psi}^{i\dot{2}}_n \end{bmatrix} \tag{11.22}$$

$$\mathcal{O}_2{}^i{}_j \begin{bmatrix} \psi^j_{n1} \\ \bar{\psi}^{j\dot{2}}_n \end{bmatrix} = im_n^{(2)} \begin{bmatrix} \bar{\psi}^{i\dot{1}}_n \\ \psi^i_{n2} \end{bmatrix}, \tag{11.23}$$

where the mass eigenvalues $m_n^{(1)}, m_n^{(2)}$ are real. Please note a peculiar combination of left- and right-handed spinor components to define eigenfunctions. We can expand ψ^i in terms of these mode functions

$$\psi^i_\alpha(x^0, x^1, x^2, x^3) = \sum_n \begin{pmatrix} b_n(x^0, x^3)\psi^i_{n1}(x^1, x^2) \\ c_n(x^0, x^3)\psi^i_{n2}(x^1, x^2) \end{pmatrix} \tag{11.24}$$

Since $\psi(x^0, x^1, x^2, x^3)$ is a Majorana spinor, the coefficient fermionic fields b_n, c_n are real. The linearized equations (11.18) (11.19) for the fermion gives a Dirac equation in 1+1 dimensions for the coefficient fermionic fields (c_n, ib_n) with two mass parameters $m_n^{(1)}, m_n^{(2)}$

$$\left[-i\left(\rho_1\partial_0 + i\rho_2\partial_3\right) - m_n^{(1)}\frac{1+\rho_3}{2} - m_n^{(2)}\frac{1-\rho_3}{2}\right]\begin{bmatrix} c_n(x^0, x^3) \\ ib_n(x^0, x^3)\end{bmatrix} = 0, \quad (11.25)$$

where we use Pauli matrices $\rho_a,\ a = 1, 2, 3$ to construct the 2×2 gamma matrices $\rho_1, i\rho_2$ in 1+1 dimensions. Since we have a Majorana spinor in 1+1 dimensions which does not allow chiral rotations, we have two distinct real mass parameters $m_n^{(1)}, m_n^{(2)}$.

To relate the mass eigenvalues of fermions and bosons, let us multiply two differential operators for fermions $\mathcal{O}_2$ to $\mathcal{O}_1$. In this ordering, we can use the BPS equation (9.22) corresponding to $H = H_{\rm II}$ to find the differential operator for bosons $\mathcal{O}_B$

$$\mathcal{O}^i_{2k}\mathcal{O}^k_{1j} = \begin{bmatrix} \mathrm{e}^{i\frac{\pi}{4}}\Omega_-^{\frac{1}{2}} & 0 \\ 0 & \mathrm{e}^{-i\frac{\pi}{4}}\Omega_-^{-\frac{1}{2}}\end{bmatrix}\mathcal{O}^i_{Bj}\begin{bmatrix} \mathrm{e}^{-i\frac{\pi}{4}}\Omega_-^{-\frac{1}{2}} & 0 \\ 0 & \mathrm{e}^{i\frac{\pi}{4}}\Omega_-^{\frac{1}{2}}\end{bmatrix}, \quad (11.26)$$

where $\Omega_- \equiv i\frac{\langle -iZ_1^* - Z_2^*\rangle}{|\langle -iZ_1^* - Z_2^*\rangle|}$. Therefore the BPS equation (9.22) corresponding to $H = H_{\rm II}$ guarantees that the existence of a solution $\bar\psi_n^{i\dot 1}, \psi^i_{n2}$ of fermionic mode equations implies the existence of a solution of bosonic mode equations with the mass squared $M_n^2 = m_n^{(1)}m_n^{(2)}$

$$A'^{*i}_n = \mathrm{e}^{-i\frac{\pi}{4}}\Omega_-^{-\frac{1}{2}}\bar\psi_n^{i\dot 1}, \qquad A'^i_n = \mathrm{e}^{i\frac{\pi}{4}}\Omega_-^{\frac{1}{2}}\psi^i_{n2}. \quad (11.27)$$

If another BPS equation (9.21) corresponding to $H = H_{\rm I}$ is valid, operator multiplication with different ordering gives the same bosonic operator whose rows and columns are interchanged

$$\mathcal{O}^i_{1k}\mathcal{O}^k_{2j} = \begin{bmatrix} 0 & \mathrm{e}^{i\frac{\pi}{4}}\Omega_+^{-\frac{1}{2}} \\ -\mathrm{e}^{-i\frac{\pi}{4}}\Omega_+^{\frac{1}{2}} & 0\end{bmatrix}\mathcal{O}^i_{Bj}\begin{bmatrix} 0 & -\mathrm{e}^{i\frac{\pi}{4}}\Omega_+^{-\frac{1}{2}} \\ \mathrm{e}^{-i\frac{\pi}{4}}\Omega_+^{\frac{1}{2}} & 0\end{bmatrix}, \quad (11.28)$$

where $\Omega_+ \equiv i\frac{\langle -iZ_1^* + Z_2^*\rangle}{|\langle -iZ_1^* + Z_2^*\rangle|}$. Therefore the BPS equation (9.21) corresponding to $H = H_{\rm I}$ guarantees that the existence of a solution $\bar\psi_n^{i\dot 2}, \psi^i_{n1}$ of fermionic mode equations implies the existence of a solution of bosonic mode equations with the mass squared $M_n^2 = m_n^{(1)}m_n^{(2)}$

$$A'^{*i}_n = -\mathrm{e}^{i\frac{\pi}{4}}\Omega_+^{-\frac{1}{2}}\bar\psi_n^{i\dot 2}, \qquad A'^i_n = \mathrm{e}^{-i\frac{\pi}{4}}\Omega_+^{\frac{1}{2}}\psi^i_{n1}. \quad (11.29)$$

Therefore we find that all massive states come in pairs of boson and fermion with the same mass squared $M_n^2 = m_n^{(1)}m_n^{(2)}$ in accordance with the result of the unitary representation of the $(1, 0)$ supersymmetry algebra.

11.4.2 Nambu-Goldstone modes

Since we are usually most interested in a low energy effective field theory, we wish to study massless modes here. If global continuous symmetries are broken spontaneously, there occur associated massless modes which are called the Nambu-Goldstone modes. To find the wave functions of the Nambu-Goldstone modes, we perform the associated global transformations and evaluate the transformed configuration by substituting the classical field. For supersymmetry we obtain nontrivial wave function by substituting the classical field $A^i_{\rm cl}(x^1, x^2)$ and $F^i_{\rm cl}(x^1, x^2)$ to the transformation of fermions by a Grassmann parameter ξ, since classical field configuration of fermion vanishes $\psi^i_{\rm cl} = 0$

$$\delta_\xi \psi^i = i\sqrt{2}\sigma^\mu \bar{\xi}\partial_\mu A^i_{\rm cl} + \sqrt{2}\xi F^i_{\rm cl}. \tag{11.30}$$

If the BPS equation (9.22) for the junction background is valid, we obtain

$$\delta_\xi \psi^i = \sqrt{2}\left[(i\sigma^1\bar{\xi} - \Omega^*_-\xi)\partial_1 A^i_{\rm cl} + (i\sigma^2\bar{\xi} + i\Omega^*_-\xi)\partial_2 A^i_{\rm cl}\right]. \tag{11.31}$$

We see that there is one conserved direction in the Grassmann parameter:

$$i\sigma^1\bar{\xi} = \Omega^*_-\xi \ \text{ and } \ \sigma^2\bar{\xi} = -\Omega^*_-\xi. \tag{11.32}$$

The other three real Grassmann parameters ξ correspond to broken supercharges. For our exact solution, for instance, we find it convenient to choose the three broken supercharges as the following real supercharges

$$\begin{aligned} Q_{\rm I} &= \frac{1}{\sqrt{2}}(e^{i\pi/4}Q_2 + e^{-i\pi/4}\bar{Q}_{\dot{2}}), \quad Q_{\rm II} = \frac{1}{\sqrt{2}}(e^{-i\pi/4}Q_1 + e^{i\pi/4}\bar{Q}_{\dot{1}}), \\ Q_{\rm III} &= \frac{1}{\sqrt{2}}(e^{i\pi/4}Q_1 + e^{-i\pi/4}\bar{Q}_{\dot{1}}). \end{aligned} \tag{11.33}$$

Then the corresponding massless mode functions are given by

$$\psi_0^{({\rm I})i}(x^1, x^2) = \begin{pmatrix} 4\partial_z A^i_{\rm cl}(x^1, x^2)e^{-i\pi/4} \\ 0 \end{pmatrix}, \tag{11.34}$$

$$\psi_0^{({\rm II})i}(x^1, x^2) = \begin{pmatrix} 0 \\ 2\partial_1 A^i_{\rm cl}(x^1, x^2)e^{i\pi/4} \end{pmatrix}, \tag{11.35}$$

$$\psi_0^{({\rm III})i}(x^1, x^2) = \begin{pmatrix} 0 \\ 2\partial_2 A^i_{\rm cl}(x^1, x^2)e^{i\pi/4} \end{pmatrix}. \tag{11.36}$$

Since the transformation parameter should correspond to the Nambu-Goldstone field with zero momentum and energy, the three transformation parameters ξ should be promoted to three real fermionic fields in x^0, x^3 space,

$b_0^{(\mathrm{I})}(x^0,x^3), c_0^{(\mathrm{II})}(x^0,x^3)$, and $c_0^{(\mathrm{III})}(x^0,x^3)$, to obtain the Nambu-Goldstone component of the mode expansion

$$\psi^i(x^0,x^1,x^2,x^3) = b_0^{(\mathrm{I})}(x^0,x^3)\psi_0^{(\mathrm{I})i}(x^1,x^2) + c_0^{(\mathrm{II})}(x^0,x^3)\psi_0^{(\mathrm{II})i}(x^1,x^2) + c_0^{(\mathrm{III})}(x^0,x^3)\psi_0^{(\mathrm{III})i}(x^1,x^2) + \sum_{n>0}\begin{pmatrix} b_n(x^0,x^3)\psi_{n1}^i(x^1,x^2) \\ c_n(x^0,x^3)\psi_{n2}^i(x^1,x^2)\end{pmatrix}. \tag{11.37}$$

We have explicitly displayed three massless Nambu-Goldstone fermion components distinguishing from the massive ones ($n > 0$). The Dirac equation for the coefficient fermionic fields (11.25) shows that $b_0^{(\mathrm{I})}(x^0 - x^3)$ is a right-moving massless mode, and $c_0^{(\mathrm{II})}(x^0 + x^3)$, and $c_0^{(\mathrm{III})}(x^0 + x^3)$ are left-moving modes.

We plot the absolute values of $|\psi_0^{(a)i=T}|$ of the $i = T$ component of the wave function of the Nambu-Goldstone fermions $a = \mathrm{I}, \mathrm{II}, \mathrm{III}$ in Fig. 11.1. We can see that Nambu-Goldstone fermions have wave functions which extend to infinity along three walls. They become identical to fermion zero modes on at least two of the walls asymptotically and hence they are not localized around the center of the junction. We can construct a linear combination of the Nambu-Goldstone fermions to have no support along one out of the three walls. However, no linear combination of these Nambu-Goldstone fermions can be formed which does not have support extended along any of the wall. Therefore these wave functions are not localized and are not normalizable. This fact means that the low energy dynamics of BPS junction cannot be described by a $1+1$ dimensional effective field theory with a discrete particle spectrum.

Similarly the Nambu-Goldstone bosons corresponding to the broken translation $P^a, a = 1, 2$ are given by

$$A_0^{(a)}(x^1,x^2) = \partial_a A_{\mathrm{cl}}^i(x^1,x^2), \qquad a = 1, 2. \tag{11.38}$$

These two bosonic massless modes consist of two left-moving modes and two right-moving modes. On the other hand, we have seen already that there are two left-moving massless Nambu-Goldstone fermions and one right-moving massless Nambu-Goldstone fermion. These two left-moving Nambu-Goldstone bosons and fermions form two doublets of the $(1, 0)$ supersymmetry algebra. The right-moving modes are asymmetric in bosons and fermions: two Nambu-Goldstone bosons and a single Nambu-Goldstone fermion. These three states are all singlets of the $(1, 0)$ supersymmetry algebra in accordance with our analysis in section 11.3. Therefore we obtained a chiral structure of Nambu-Goldstone fermions on the junction background configuration.

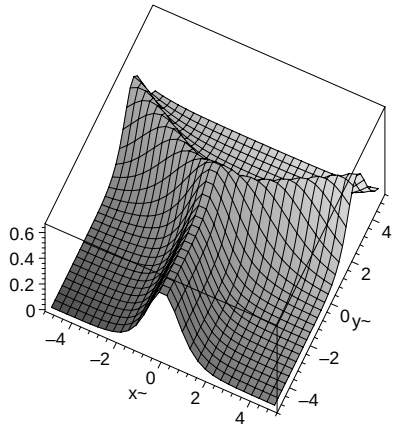

The wave function $\left|\psi_0^{(\mathrm{I})T}\right|$

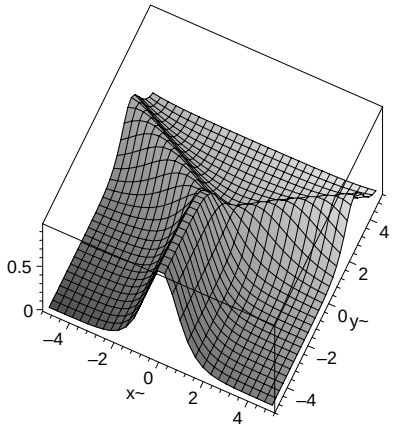

The wave function $\left|\psi_0^{(\mathrm{II})T}\right|$

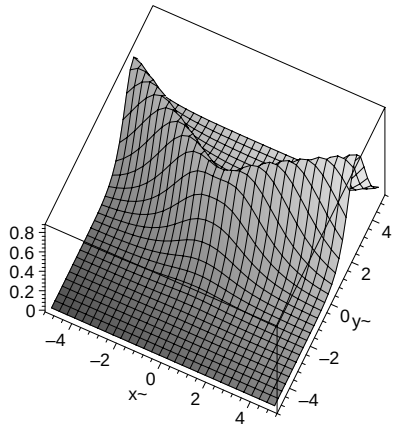

The wave function $\left|\psi_0^{(\mathrm{III})T}\right|$

Figure 11.1: The bird's eye view of the absolute value of the $i = T$ component of the wave functions of the Nambu-Goldstone fermions on the junction in the (x^1, x^2) space

11.4.3 Non-normalizability of the Nambu-Goldstone fermions

We would like to argue that our observation is a generic feature of the Nambu-Goldstone fermions on the domain wall junction in a flat space in the bulk: Nambu-Goldstone fermions are not localized at the junction and hence are not normalizable, if they are associated with the supersymmetry breaking due to the coexistence of nonparallel domain walls. The following observation is behind this assertion. A single domain wall breaks only a half of supercharges. Nonparallel wall also breaks half of supercharges, some of which may be linear combinations of the supercharges already broken by the first wall. If the junction configuration is a 1/4 BPS state, linearly independent ones among these two sets of broken supercharges of nonparallel walls become $\frac{3}{4}$ of the original supercharges.

To see in more detail, let us first note that the junction configuration reduces asymptotically to a wall if one goes along the wall, say the wall 1. On this first wall, a half of the original supersymmetry $(Q^{(1)}, \cdots, Q^{(N)})$ is broken. Denoting the number of original supercharges to be N, we call these broken supercharges as $Q^{(1)}, \cdots, Q^{(N/2)}$. Consequently we have Nambu-Goldstone fermions localized around the core of the wall and is constant along the wall. In the junction configuration, we have other walls which are not parallel to the first wall. Asymptotically far away along one of such walls, say wall 2, another half of the supersymmetry $Q'^{(1)}, \cdots, Q'^{(N/2)}$ is broken. If the junction is a 1/4 BPS state, a half of these, say $Q'^{(1)}, \cdots, Q'^{(N/4)}$, is a linear combination of $Q^{(1)}, \cdots, Q^{(N/2)}$ broken already on the wall 1. The other half, $Q'^{(\frac{N}{4}+1)}, \cdots, Q'^{(\frac{N}{2})}$ are unbroken on the wall 1. Altogether a quarter of the original supercharges remain unbroken. Consequently the Nambu-Goldstone fermions corresponding to $Q'^{(1)}, \cdots, Q'^{(N/4)}$ have a wave function which extends to infinity and approaches a constant profile along both the walls 1 and 2. Those modes corresponding to $Q'^{(\frac{N}{4}+1)}, \cdots, Q'^{(\frac{N}{2})}$ have support only along the wall 2, and those corresponding to the linear combinations of $Q^{(1)}, \cdots, Q^{(N/2)}$ orthogonal to $Q'^{(1)}, \cdots, Q'^{(N/4)}$ have support only along the wall 1. Thus we find that any linear combinations of the Nambu-Goldstone fermions have to be infinitely extended along at least one of the walls which form the junction configuration. Therefore the Nambu-Goldstone fermions associated with the coexistence of nonparallel domain walls are not localized at the junction and are not normalizable.

In our exact solution, domain wall junction configuration reduces asymptotically to the wall 1 at $x^2 \to -\infty$ with fixed x^1. On the wall, only two

supercharges in eq.(11.33) are broken

$$Q_{\rm I} = \frac{1}{\sqrt{2}}(e^{i\pi/4}Q_2 + e^{-i\pi/4}\overline{Q}_{\dot{2}}), \qquad Q_{\rm II} = \frac{1}{\sqrt{2}}(e^{-i\pi/4}Q_1 + e^{i\pi/4}\overline{Q}_{\dot{1}}), \quad (11.39)$$

and there are two corresponding Nambu-Goldstone fermions which become domain wall zero modes asymptotically

$$\begin{aligned}
\psi_0^{({\rm I})i}(x^1, x^2) &= \begin{pmatrix} 4\partial_z A^i_{\rm cl}(x^1, x^2)e^{-i\pi/4} \\ 0 \end{pmatrix} \to \begin{pmatrix} 2\partial_1 A^{i{\rm wall}}_{\rm cl}(x^1)e^{-i\pi/4} \\ 0 \end{pmatrix}, \\
\psi_0^{({\rm II})i}(x^1, x^2) &= \begin{pmatrix} 0 \\ 2\partial_1 A^i_{\rm cl}(x^1, x^2)e^{i\pi/4} \end{pmatrix} \to \begin{pmatrix} 0 \\ 2\partial_1 A^{i{\rm wall}}_{\rm cl}(x^1)e^{i\pi/4} \end{pmatrix} \quad (11.40)
\end{aligned}$$

These wave functions are localized on the core of the wall 1 in the x^1 direction and are constant along the wall. Along the other walls we find two broken supercharges one of which is identical to one of the broken supercharges, $Q_{\rm I}$. The other broken supercharge is $Q'_{\rm II}$ on the wall 2 and $Q''_{\rm II}$ on the wall 3. There are only two independent supercharges among $Q_{\rm II}$, $Q'_{\rm II}$, and $Q''_{\rm II}$. Together with $Q_{\rm I}$ we obtain three independent broken supercharges. We can construct a linear combination of the Nambu-Goldstone fermions to have no support along one out of the three walls. However, any linear combination has nonvanishing wave function which becomes fermion zero mode on at least one of the wall asymptotically. Therefore the associated Nambu-Goldstone fermions have support which is infinitely extended at least along two of the walls.

If a single wall is present, we can explicitly construct a plane wave solution propagating along the wall, which may be called a spin wave and is among massive modes on the wall background. Even if there are several walls forming a junction configuration, we can consider excitation modes which reduce to the spin wave modes along each wall. They should be a massive mode on the domain wall junction background. The Nambu-Goldstone mode on the domain wall junction is the zero wave number limit of such a spin wave mode. This physical consideration suggests that the massless Nambu-Goldstone fermion is precisely the vanishing wave number (along the wall) limit of the massive spin wave mode.

Let us note that our argument does not apply to models with the bulk cosmological constant. In such models, massless graviton is localized on the background of intersection of walls [120]–[122]. In that case, massless mode is a distinct mode different from the massless limit of the massive continuum, although the massless mode is buried at the tip of the continuum of massive modes. The normalizability of the massless graviton is guaranteed by the Anti de Sitter geometry away from the junction or intersection including the direction along the wall.

Chapter 12

Conclusion and Discussion

Throughout this thesis, we have discussed nonperturbative properties of quantum field theories, especially those having common properties with QCD, by using exact solutions. As described in chapter 1, many methods for deriving the nonperturbative effects have been exploited. In this thesis we have used two of them, large N expansion and supersymmetry.

In chapter 2, we reviewed the large N expansion and the 't Hooft model. In general, the more the number of colors increases, the more complex the model becomes. However in the limit of $N \to \infty$ with g^2N fixed, one has only to calculate *planar* Feynman diagrams. As a result one can add up all the diagrams and exactly determine nonperturbative effects, especially the bound state problem of mesonic states. In the large N limit, one can obtain the bound state equation analytically from the *first principle*.

In chapter 3 we have reviewed the Gross–Neveu model, which has common properties with QCD such as asymptotic freedom, dynamical chiral symmetry breaking, dimensional transmutation, and so on.

Since large N expansion is used to solve the Gross–Neveu model, it may also be solved from the Bethe–Salpeter approach used by 't Hooft. From this point of view, in chapter 4, we solved the bound state problem of the massive Gross–Neveu model from the Bethe–Salpeter approach and compared the analysis with the ordinary one. In contrast to the 't Hooft model and the gauged four–Fermi model, the bound state equation of the Gross–Neveu model can be solved analytically. Therefore investigating the Gross–Neveu model gives not only the better understanding of the model itself, but also nontrivial consistency check for numerical calculation performed for the gauged four–Fermi model. We also examine the physics of the Gross–Neveu model in detail.

In chapter 5, we dealt with the gauged four–Fermi model, which combines and extends the 't Hooft model and the Gross–Neveu model. Applying the 't

Hooft method, we derive the analytic equation for the mesonic bound states and give the systematic methods to analyze it. We investigated the physical properties of the bound states and verified that the 't Hooft model and the Gross–Neveu model are realized at the special limit of the parameter space.

In chapter 6, we reviewed QCD inequalities and some related topics. For vector–like gauge theories, rigorous proof for the mass inequality exists from the viewpoint of quantum field theories. The key ingredient for the proof is the positivity of the effective measure. While it can be easily shown for vector–like gauge theories, we can say nothing about the positivity for some models, especially those with *Yukawa couplings*.

We have also seen that mass inequality can be proved for almost every *quantum mechanical* systems with the flavor symmetry assumption (see section 6.3 and 7.2). Quantum field theories can be regarded as quantum mechanical system with infinite degrees of freedom. However there are some crucial differences between them such as spontaneous symmetry breaking. Therefore there may be some field theory models for which the mass inequality is broken. In this thesis, we calculate the mass inequality (difference) directly from the exact solution obtained in chapter 5 and examined whether the mass inequality is broken or not. In order to evaluate the mass difference by local quantity we have defined the meson mass susceptibility. If the susceptibility is positive for any values of parameters, the mass inequality is unbroken.

In section 7.3, we considered the generalized Gross–Neveu model with any combinations of four–Fermi couplings, which is equivalent with the model including Yukawa couplings. This is the case for which it is suspected that the mass inequality may be broken. In the case of the Gross–Neveu model we can derive the susceptibility *analytically* to find that the susceptibility is always positive, which indicates that the mass inequality is unbroken for any combinations of Yukawa couplings. As is the case of the 't Hooft model, numerical calculation is needed to evaluate the susceptibility for the gauged four–Fermi model. We have evaluated the meson susceptibility directly from the mass spectrum and using the perturbation formula (see appendix C) to check the results. For gauged four–Fermi model the mass susceptibility is almost always positive and the mass inequality holds for almost all the cases. Since it is proved for the 't Hooft model, taking the analytic results of the Gross–Neveu model into consideration, it seems natural that the mass inequality is almost always unbroken for gauged four–Fermi model, naively a combined model of them. To conclude, we could not show explicitly models for which the mass inequality is broken and it remains unclear whether or not the mass inequality is also valid for any field theory models.

In the second part of this thesis, we focus on nonperturbative effects in

supersymmetric gauge theories, especially BPS states which play an important role in determining nonperturbative effects exactly. We succeeded in obtaining *an exact analytic solution* of BPS domain wall junction for the first time and clarified some properties of BPS domain wall junctions which are unclear without concrete example.

In chapter 8, we reviewed the Seiberg–Witten theory, which determines physics in the strong coupling region of four dimensional gauge theories for the first time. In deriving nonperturbative effects exactly, restrictions from the supersymmetry, duality and BPS states play an important role. Simpler toy models of the Seiberg–Witten theories enable us to obtain exact solutions of BPS domain wall and junction.

In chapter 9, we briefly reviewed fundamental properties of (BPS) domain walls. Then we derived the BPS equation for $\mathcal{N} = 1$ supersymmetric (abelian) gauge theories from the condition that BPS objects such as BPS domain walls and junctions preserve some part of the supersymmetry. Applying the BPS condition to the toy model of the Seiberg–Witten theory, which is originally considered by Kaplunovsky *et. al.*[99], we obtain an exact solution of BPS domain wall and discuss some general properties of BPS walls.

In chapter 10, we extended the toy model considered in chapter 9 to one with three distinct vacua, which is a toy model of SQCD version of the Seiberg–Witten theory, and obtain an exact solution of BPS domain wall junction. In general, some information on the BPS domain walls and junctions such as their tension and conserved supercharges can be obtained from the boundary condition only, however exact solutions are needed to investigate their profiles near the center of junctions, energy densities, modes on them, and so on. From our exact junction solution, we investigate in detail its profile, charge densities and charges themselves. Furthermore, using our exact solution as concrete example we discussed some general properties of BPS domain wall junctions in four dimensional supersymmetric theories. Especially, we find that the new central charge Y_k associated with the junction gives a negative contribution to the mass of the domain wall junction, whereas the central charge Z_k gives a dominant positive contribution. Therefore one has to be cautious to identify the central charge Y_k alone as the mass of the center of the junction.

In chapter 11, we focus on modes on BPS domain wall junction background, especially Nambu–Goldstone modes, which are interesting from the phenomenological point of view. We defined mode functions and showed that they appear in a boson-fermion pair of identical mass for massive modes. Nambu-Goldstone fermions exhibit a chiral structure in accordance with $(1, 0)$ supersymmetry. We explicitly showed that the Nambu-Goldstone

fermions are not normalizable. Therefore modes on the junction does not reduce to a $1+1$ dimensional field theory with a discrete mass spectrum even for massless modes. These results are *not* specific to our exact solution of junction but a generic phenomenon of modes on domain wall junction in the flat bulk space in any dimension.

Our final goal is deriving the low energy dynamics of QCD, such as confinement and dynamical chiral symmetry breaking, explicitly from *first principles*. Unfortunately, we have not obtained direct hints toward them from the knowledge of BPS domain wall junctions. However we hope it will shed some light on them in the future.

Acknowledgment

I am very grateful to Profs. N. Sakai, Y. Kitazawa, K(atsushi) Ito, and K. Aoki for teaching me basic knowledge of particle physics and giving me much good advice.

The first part of this thesis consists of collaborations with Prof. K. Aoki. He not only had a discussion about our work but also gave me much advice since I was a student of the master course. I cannot be too grateful for his help and encouragement.

I am very grateful to Prof. N. Sakai, Dr. H. Oda and M. Naganuma for collaborations which are the bases of the second part of this thesis.

I am also grateful to the other members of our laboratory for lots of useful discussion and advice, especially to my senior Drs. Y. Mimura, T. Ichihara, T. Sakai, S. Kiyoura and M. Sato.

Finally, I am thankful to my parents and my sister for financial support and encouragement.

Appendix A

A chart of some integrals

For the Gross–Neveu model

$$\int_{-\infty}^{\infty} dp_+ S_d(p)_{\alpha\beta} S_d(p-r)_{\gamma\delta}$$
$$= \frac{\theta(p_-)\theta(r_- - p_-)}{4p_-(r_- - p_-)} 2\pi i \left[r_+ - \frac{M^2}{2p_-} - \frac{M^2}{2(r_- - p_-)} \right]^{-1}$$
$$\times \begin{cases} & (\alpha\beta\gamma\delta) \\ M^2 & (1111) \\ -\sqrt{2}M(r_- - p_-) & (1112) \\ \sqrt{2}Mp_- & (1211) \\ -2p_-(r_- - p_-) & (1212) \\ \left[r_+ + \frac{M^2}{2p_-} - \frac{M^2}{2(r_- - p_-)} \right] \times \frac{M}{\sqrt{2}} & (2111) \\ \left[r_+ + \frac{M^2}{2p_-} - \frac{M^2}{2(r_- - p_-)} \right] \times (-1)(r_- - p_-) & (2112) \\ \left[r_+ - \frac{M^2}{2p_-} + \frac{M^2 -}{2(r_- - p_-)} \right] \times (-\frac{M}{\sqrt{2}}) & (1121) \\ \left[r_+ - \frac{M^2}{2p_-} + \frac{M^2}{2(r_- - p_-)} \right] \times (-p_-) & (1221) \\ -\frac{M^2}{2p_-(r_- - p_-)} r_+ r_- + (\frac{M^2}{2p_-})^2 + (\frac{M^2}{2(r_- - p_-)})^2 & (2121) \end{cases} \tag{A.1}$$

For the gauged four–Fermi model

In the case of the pure 't Hooft model, almost the same results are obtained; thus we have only to replace M_i by m_i.

$$\int_{-\infty}^{\infty} dp_+ S_d(p)_{\alpha\beta} S_d(p-r)_{\gamma\delta}$$

$$= \frac{\theta(p_-)\theta(r_- - p_-)}{4p_-(r_- - p_-)} 2\pi i \left[r_+ - \frac{g^2 N}{\pi \lambda_-} - \frac{M_1^2 - \frac{g^2 N}{\pi}}{2p_-} - \frac{M_2^2 - \frac{g^2 N}{\pi}}{2(r_- - p_-)} \right]^{-1}$$

$$\times \begin{cases} & (\alpha\beta\gamma\delta) \\ M_1 M_2 & (1111) \\ -\sqrt{2} M_1 (r_- - p_-) & (1112) \\ \sqrt{2} M_2 p_- & (1211) \\ -2p_-(r_- - p_-) & (1212) \\ \left[r_+ - \frac{g^2 N}{\pi\lambda_-} - \frac{-M_1^2 - \frac{g^2 N}{\pi}}{2p_-} - \frac{M_2^2 - \frac{g^2 N}{\pi}}{2(r_- - p_-)} \right] \times \frac{M_2}{\sqrt{2}} & (2111) \\ \left[r_+ - \frac{g^2 N}{\pi\lambda_-} - \frac{-M_1^2 - \frac{g^2 N}{\pi}}{2p_-} - \frac{M_2^2 - \frac{g^2 N}{\pi}}{2(r_- - p_-)} \right] \times (-1)(r_- - p_-) & (2112) \\ \left[r_+ - \frac{g^2 N}{\pi\lambda_-} - \frac{M_1^2 - \frac{g^2 N}{\pi}}{2p_-} - \frac{-M_2^2 - \frac{g^2 N}{\pi}}{2(r_- - p_-)} \right] \times (-\frac{M_1}{\sqrt{2}}) & (1121) \\ \left[r_+ - \frac{g^2 N}{\pi\lambda_-} - \frac{M_1^2 - \frac{g^2 N}{\pi}}{2p_-} - \frac{-M_2^2 - \frac{g^2 N}{\pi}}{2(r_- - p_-)} \right] \times (-\frac{p_-}{2}) & (1221) \\ -(\frac{M_1^2}{2p_-} + \frac{M_2^2}{2(r_- - p_-)}) \left[r_+ - \frac{g^2 N}{\pi\lambda_-} + \frac{\frac{g^2 N}{\pi}}{2p_-} + \frac{\frac{g^2 N}{\pi}}{2(r_- - p_-)} \right] & \\ \quad + (\frac{M_1^2}{2p_-})^2 + (\frac{M_2^2}{2(r_- - p_-)})^2 & (2121) \end{cases} \tag{A.2}$$

Some integrals and derivation of $\mathcal{R}$ for the generalized Gross–Neveu model

$$\begin{aligned} J_0 \equiv \int_0^1 dx \frac{1}{-\mu_0^2 x(1-x) + M^2} &= \frac{4}{\mu_0^2 \sqrt{4\zeta - 1}} \tan^{-1}\left(\frac{1}{\sqrt{4\zeta - 1}} \right) \\ \int_0^1 dx \frac{x(1-x)}{\left(-\mu_0^2 x(1-x) + M^2\right)^2} &= \frac{1}{\mu_0^4} \left[\frac{2}{4\zeta - 1} + \frac{1 - 2\zeta}{4\zeta - 1} \mu_0^2 J_0 \right] \\ \int_0^1 dx \frac{(1-2x)^2}{\left(-\mu_0^2 x(1-x) + M^2\right)^3} &= \frac{1}{\mu_0^6} \left[\frac{-2\zeta + 1}{\zeta^2 (4\zeta - 1)} + \frac{2}{4\zeta - 1} \mu_0^2 J_0 \right] \\ \int_0^1 dx \frac{[x(1-x)]^2}{\left(-\mu_0^2 x(1-x) + M^2\right)^3} &= \frac{1}{\mu_0^6} \left[\frac{3(1-2\zeta)}{(4\zeta - 1)^2} + \frac{6\zeta^2 - 4\zeta + 1}{(4\zeta - 1)^2} \mu_0^2 J_0 \right], \end{aligned} \tag{A.3}$$

where $\zeta \equiv \frac{M^2}{\mu_0^2}$.

From the definition of the mass of quarks (7.2), we can expand $\mu_{aa} + \mu_{bb} = 2\mu_0 \left[1 - \frac{\Delta^2}{8} - \frac{5}{128}\Delta^4 + \mathcal{O}\left(\Delta^6\right) \right]$, where μ_0 is unperturbed meson mass (*i.e.* $\Delta = 0$). Noticing that $\mu_{ab} = \mu_{ba}$, μ_{ab} is even in Δ so that it has only

even powers in the perturbation. Therefore we can expand $\mu_{ab}^2 = \mu_0^2 + \mu_2^2\Delta^2 + \mu_4^4\Delta^4 + \mathcal{O}(\Delta^6)$. This leads to

$$\begin{aligned} &2\mu_{ab} - (\mu_{aa} + \mu_{bb}) \\ &\quad = 2\mu_0 \left[\left(\frac{\mu_2^2}{2\mu_0^2} + \frac{1}{8} \right) \Delta^2 + \left(-\frac{\mu_2^4}{8\mu_0^4} + \frac{\mu_4^2}{2\mu_0^2} + \frac{5}{128} \right) \Delta^4 + \mathcal{O}\left(\Delta^6\right) \right]. \end{aligned} \tag{A.4}$$

Computing the matrix elements of eq.(7.19), which we call $\mathcal{M}_{ij}$, we have

$$\begin{aligned} \mathcal{M}_{11} &= \Delta^2 \left[\mu_2^2 J_0 + \mu_0^2 J_2 - \frac{1}{4}\left(\frac{1}{G_5} - \frac{1}{G} \right) \right] + \mathcal{O}\left(\Delta^4\right) \\ \mathcal{M}_{12} &= 2\Delta \left[1 + M^2 J_0 - \frac{1}{4}\left(\frac{1}{G_5} - \frac{1}{G} \right) \right] + \mathcal{O}\left(\Delta^3\right) \\ \mathcal{M}_{21} &= 2\Delta \left[1 - M^2 J_0 + \frac{1}{4}\left(\frac{1}{G_5} - \frac{1}{G} \right) \right] + \mathcal{O}\left(\Delta^3\right) \\ \mathcal{M}_{22} &= \left(\mu_0^2 - 4M^2 \right) J_0 - \frac{1}{G} + \mathcal{O}\left(\Delta^2\right). \end{aligned} \tag{A.5}$$

Here we have used the relation $\mu_0^2 J_0 = \frac{1}{G_5}$ and set J_{12} as follows;

$$\begin{aligned} J_{12} &= \int_0^1 \frac{dx}{-\mu_{12}^2 x(1-x) + M^2(1+\Delta)(1-x) + M^2(1-\Delta)x} \\ &\equiv J_0 + J_2\Delta^2 + \mathcal{O}\left(\Delta^4\right). \end{aligned} \tag{A.6}$$

Thus

$$J_2 \equiv \mu_2^2 \int_0^1 dx \frac{x(1-x)}{\left(-\mu_0^2 x(1-x) + M^2\right)^2} + M^4 \int_0^1 dx \frac{(1-2x)^2}{\left(-\mu_0^2 x(1-x) + M^2\right)^3}. \tag{A.7}$$

From the definition (7.3), we can obtain $\mathcal{R} = \frac{\mu_2^2}{2\mu_0^2} + \frac{1}{8}$. Using the relations (A.3) and (A.7), the bound state equation $\mathcal{M}_{11}\mathcal{M}_{22} - \mathcal{M}_{12}\mathcal{M}_{21} = 0$ gives the relation

$$\frac{2\mu_2^2}{\mu_0^2} = (2\zeta - 1) - \frac{4\zeta - 1}{\left(1 + \frac{\zeta}{G_5}\right)\left[\frac{\zeta}{G_5} + \frac{1}{4}\left(\frac{1}{G} + \frac{1}{G_5}\right)\right]}. \tag{A.8}$$

Inserting this relation into the $\mathcal{R} = \frac{\mu_2^2}{2\mu_0^2} + \frac{1}{8}$, the meson mass susceptibility (7.23) is obtained.

Appendix B

A brief note on the convergence of numerical solutions

The convergence of the numerical solutions depends on the parameters (G, G_5, β). When $\beta \gtrsim 1$, it is relatively easy to achieve a relative accuracy of $\sim 10^{-4}$ in the meson mass at least using both the variational method (dimension ~ 10) and Multhopp's method (dimension ~ 400). For $\beta \lesssim 1$, more effort is needed to achieve the same level of convergence. The difficulties in the variational method using polynomials of the momentum fraction (section 5.3.1) arise because of the round off errors since the eigenvalues in the normalization matrix (5.27) tend to become small. Analytically choosing an orthonormal basis or using some other basis appropriate for the parameter region in question might alleviate this problem. In Multhopp's method (section 5.3.2), the limitations arise due to the necessary computational time when using larger space of functions. Choice of $g_m(\theta)$ may speed up the convergence process in some parameter regions.

In the parameter regions where the convergence is slow, extrapolation in the data can be effective. We have found that trial functions of the type $x + aK^b$ fit the data quite well. Here x is the extrapolated value, K is the dimension of the space spanned by the basis and a, b are parameters. Extrapolation can sometimes be misleading so checks on the results are desirable. In our case, we compare the extrapolation values from both the variational method and Multhopp's method and we confirm that they are consistent within the errors of the fit. An example of such an extrapolation is shown in Fig.B.1.

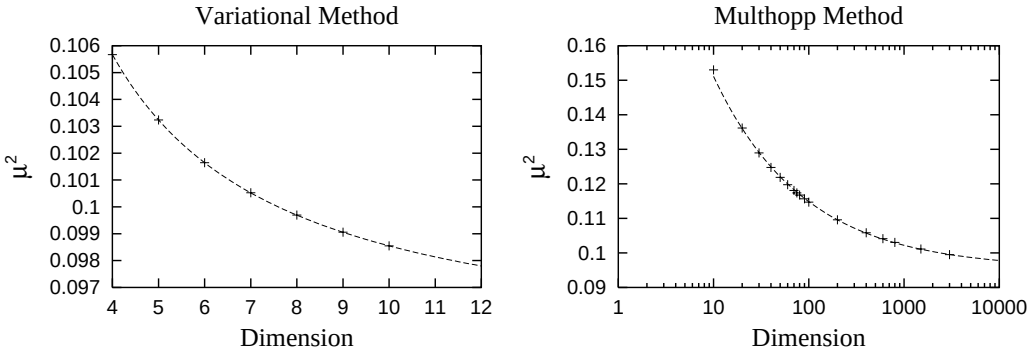

Figure B.1: Extrapolation of the numerical data for the variational method and Multhopp's method. In this example, $G = G_5 = 1$ and $\beta = 0.1$ and $\mu^2 = 0.095 \pm 0.002$.

Appendix C

Perturbation theory in the mass differences for the spectrum

Here, we shall briefly outline how to perform perturbation in the relative constituent mass difference, Δ, for the methods to obtain the spectrum as explained in section 5.3. The standard perturbation methods can not be applied here. One major reason is that the boundary conditions (5.19) depend on the masses of the constituents so that they need to be perturbed also. There are additional complications for both the methods used in section 5.3, as we shall describe below.

In both cases, we perturb in the relative mass difference Δ and obtain an expansion for the meson mass in terms of Δ, for the cases $(M_1^2, M_2^2) = (M_a^2, M_a^2), (M_b^2, M_b^2), (M_a^2, M_b^2)$.

$$\mu^2 \equiv \mu_0^2 + \Delta\mu_1^2 + \Delta^2\mu_2^2 + \mathcal{O}(\Delta^3). \tag{C.1}$$

In the first two cases, the first order terms exist and are of the same size but of opposite sign and in the last case the first order term is absent. Therefore, the leading order term in the mass difference $\delta\mu_{ab}$ will be of order Δ^2, as it should be.

Variational method

In the variational method, we need to consider a generalized eigenvalue problem with the normalization matrix not being the identity matrix. In theory, we can just orthonormalize the basis vectors, but in practice, this is not numerically equivalent since the normalization matrices can become almost singular even though we have tried to normalize the matrix elements to be of

order one. Furthermore, since the boundary conditions also are perturbed, the normalization matrices will also be have a non–trivial expansion in Δ.

Let us expand the matrices as

$$H \equiv H_0 + \Delta H_1 + \Delta^2 H_2 + \mathcal{O}(\Delta^3), \qquad N \equiv N_0 + \Delta N_1 + \Delta^2 N_2 + \mathcal{O}(\Delta^3). \quad \text{(C.2)}$$

Assume that we have the complete eigen system for the 0–th order problem:

$$H_0 w_{0n} = \mu_{0n}^2 N_0 w_{0n}, \qquad (w_{0m}, N_0 w_{0n}) = \delta_{mn}. \quad \text{(C.3)}$$

Then, we obtain the expansion for mass squared of the meson state labeled by n

$$\begin{aligned} \mu_{1n}^2 &= \left(w_{0n}, \left(H_1 - \mu_{0n}^2 N_1\right) w_{0n}\right) \\ \mu_{2n}^2 &= \left(w_{0n}, \left(H_2 - \mu_{0n}^2 N_2\right) w_{0n}\right) - \left(w_{0n}, N_1 w_{0n}\right) \left(w_{0n}, \left(H_1 - \mu_{0n}^2 N_1\right) w_{0n}\right) \\ &\quad + \sum_m \frac{1}{\mu_{0n}^2 - \mu_{0m}^2} \left|\left(w_{0n}, \left(H_1 - \mu_{0n}^2 N_1\right) w_{0m}\right)\right|^2. \end{aligned} \quad \text{(C.4)}$$

We need the expansions of the matrices H, N in terms of Δ for the three cases, $(M_1^2, M_2^2) = (M_a^2, M_a^2), (M_b^2, M_b^2), (M_a^2, M_b^2)$, to obtain the final results. Since this expansion is logically straightforward, it will be not be explicitly presented here to save space.

Multhopp's method

In Multhopp's method, the matrices are not Hermitian so that we need to perform the perturbation theory with some care. Furthermore, due to the perturbation in the boundary conditions, the matrix P will also be perturbed. To perform the expansion, we will reduce the equation to a mathematically equivalent problem,

$$\left(\mu^2 - P^{-1} M\right) v = 0. \quad \text{(C.5)}$$

Ideally, it is better not to invert matrices numerically, but it is a substantially more complicated numerical task to solve a generalized non–symmetric eigenvalue problem and also, in this case, the matrix P turns out to be quite robust against inversion even for moderately large basis spaces with dimensions of order 10^3.

We expand the matrices as

$$\begin{aligned} P &= P_0 + \Delta P_1 + \Delta^2 P_2, \qquad M = M_0 + \Delta M_1 + \Delta^2 M_2 \\ \left(P^{-1} M\right) &= \left(P^{-1} M\right)_0 + \Delta \left(P^{-1} M\right)_1 + \Delta^2 \left(P^{-1} M\right)_2 + \mathcal{O}(\Delta^3), \end{aligned} \quad \text{(C.6)}$$

where

$$\begin{aligned}\left(P^{-1}M\right)_0 &= P_0^{-1}M_0, \qquad \left(P^{-1}M\right)_1 = P_0^{-1}\left(M_1 - P_1P_0^{-1}M_0\right)\\ \left(P^{-1}M\right)_2 &= P_0^{-1}\left(M_2 - P_2P_0^{-1}M_0 - P_1P_0^{-1}M_1 + P_1P_0^{-1}P_1P_0^{-1}M_0\right).\end{aligned} \tag{C.7}$$

We need to first solve the 0–th order problem for the left and right eigenvectors, $\{u_n\}$ and $\{v_n\}$[1]

$$u_{0m}\left(P^{-1}M\right)_0 = \mu_{0m}^2 u_{0m}, \qquad \left(P^{-1}M\right)_0 v_{0n} = \mu_{0n}^2 v_{0n}, \qquad (u_{0m}, v_{0n}) = \delta_{mn}. \tag{C.8}$$

Then, we may obtain the expansion for the meson mass squared of the meson state labeled by n as

$$\mu_{1n}^2 = \left(u_{0n}, \left(P^{-1}M\right)_1 v_{0n}\right) \tag{C.9}$$

$$\mu_{2n}^2 = \left(u_{0n}, \left(P^{-1}M\right)_2 v_{0n}\right) + \sum_{k\neq n} \frac{\left(u_{0n}, \left(P^{-1}M\right)_1 v_{0k}\right)\left(u_{0k}, \left(P^{-1}M\right)_1 v_{0n}\right)}{\mu_{0n}^2 - \mu_{0k}^2}.$$

The rest proceeds as in the variational method case. As before, the explicit expressions for the matrices are not shown here to conserve space.

[1]From a mathematical point of view, additional complications can arise in general; namely the eigenvalues may be degenerate so that the matrix is not diagonalizable, or the eigenvalues may be complex. However, we need to keep in mind that we do not have to solve the problem for general dimensions of the basis space, but only for a sequence of spaces that will allow us to obtain the susceptibility. In practice, these complications do not hinder our computations.

Appendix D

Wess-Bagger notation and Supersymmetry

Throughout this thesis, we use Wess-Bagger notation [105], except that we use the Greek indices $(\mu, \nu, \dots,)$ as spacetime indices: $\mu, \nu, \dots = 0, 1, 2, 3$, instead of the Latin indices $(m, n, \dots,)$. We use the Latin indices as spatial indices: $m, n, \ldots$=1,2,3.

We summarize the notation and briefly review the supersymmetric theories.

Index The Greek indices $(\alpha, \beta, \dots, \dot{\alpha}, \dot{\beta}, \ldots)$ denote two-component Weyl spinors: $\alpha, \beta, \dots, \dot{\alpha}, \dot{\beta}, \ldots = 1, 2$. The capital Latin indices $(A, B, \ldots)$ denote extended supersymmetry indices: $A, B = 1, \ldots \mathcal{N}$.

Metric

$$\eta_{\mu\nu} = \mathrm{diag}(-1, 1, 1, 1). \tag{D.1}$$

Antisymmetric $\epsilon^{\mu\nu\rho\sigma}$ tensor

$$\epsilon^{0123} = -\epsilon_{0123} = 1. \tag{D.2}$$

Two-component spinor

$$\psi^{\alpha} = \epsilon^{\alpha\beta}\psi_{\beta}, \qquad \psi_{\alpha} = \epsilon_{\alpha\beta}\psi^{\beta}, \tag{D.3}$$

$$\epsilon_{21} = \epsilon^{12} = 1, \qquad \epsilon_{12} = \epsilon^{21} = -1, \tag{D.4}$$

$$\epsilon_{\alpha\beta}\epsilon^{\beta\gamma} = \delta_{\alpha}^{\gamma}, \tag{D.5}$$

$$\begin{aligned}
\psi\chi &= \psi^\alpha\chi_\alpha = -\psi_\alpha\chi^\alpha = \chi^\alpha\psi_\alpha = \chi\psi, \\
\bar\psi\bar\chi &= \bar\psi_{\dot\alpha}\bar\chi^{\dot\alpha} = -\bar\psi^{\dot\alpha}\bar\chi_{\dot\alpha} = \bar\chi_{\dot\alpha}\bar\psi^{\dot\alpha} = \bar\chi\bar\psi, \\
(\chi\psi)^\dagger &= (\chi^\alpha\psi_\alpha)^\dagger = \bar\psi_{\dot\alpha}\bar\chi^{\dot\alpha} = \bar\psi\bar\chi = \bar\chi\bar\psi.
\end{aligned} \tag{D.6}$$

$\sigma_{\alpha\dot\alpha}$ matrices

$$\begin{aligned}
\sigma^0 &= \begin{pmatrix} -1 & 0 \\ 0 & -1 \end{pmatrix}, \quad \sigma^1 = \begin{pmatrix} 0 & 1 \\ 1 & 0 \end{pmatrix}, \\
\sigma^2 &= \begin{pmatrix} 0 & -i \\ i & 0 \end{pmatrix}, \quad \sigma^3 = \begin{pmatrix} 1 & 0 \\ 0 & -1 \end{pmatrix},
\end{aligned} \tag{D.7}$$

$$\bar\sigma^{\mu\dot\alpha\alpha} = \epsilon^{\dot\alpha\dot\beta}\epsilon^{\alpha\beta}\sigma^\mu_{\beta\dot\beta}, \tag{D.8}$$

$$\begin{aligned}
\bar\sigma^0 &= \sigma^0, \\
\bar\sigma^{1,2,3} &= -\sigma^{1,2,3},
\end{aligned} \tag{D.9}$$

$$\begin{aligned}
P_{\alpha\dot\alpha} = P_\mu\sigma^\mu_{\alpha\dot\alpha} &= \begin{pmatrix} -P_0 + P_3 & P_1 - iP_2 \\ P_1 + iP_2 & -P_0 - P_3 \end{pmatrix}, \\
P^\mu &= -\tfrac{1}{2}\bar\sigma^{\mu\dot\alpha\alpha}P_{\alpha\dot\alpha},
\end{aligned} \tag{D.10}$$

$$\begin{aligned}
\sigma^{\nu\mu}{}_\alpha{}^\beta &= \frac{1}{4}(\sigma^\nu_{\alpha\dot\alpha}\bar\sigma^{\mu\dot\alpha\beta} - \sigma^\mu_{\alpha\dot\alpha}\bar\sigma^{\nu\dot\alpha\beta}), \\
\bar\sigma^{\nu\mu\dot\alpha}{}_{\dot\beta} &= \frac{1}{4}(\bar\sigma^{\nu\dot\alpha\alpha}\sigma^\mu_{\alpha\dot\beta} - \bar\sigma^{\mu\dot\alpha\alpha}\sigma^\nu_{\alpha\dot\beta}),
\end{aligned} \tag{D.11}$$

$$\begin{aligned}
\chi\sigma^\mu\bar\psi = -\bar\psi\bar\sigma^\mu\chi, &\qquad (\chi\sigma^\mu\bar\psi)^\dagger = \psi\sigma^\mu\bar\chi, \\
\chi\sigma^\mu\bar\sigma^\nu\psi = \psi\sigma^\nu\bar\sigma^\mu\chi, &\qquad (\chi\sigma^\mu\bar\sigma^\nu\psi)^\dagger = \bar\psi\bar\sigma^\nu\sigma^\mu\bar\chi.
\end{aligned} \tag{D.12}$$

Four-component spinor

$$\mathbf{\Phi}_{\rm D} = \begin{pmatrix} \chi_\alpha \\ \bar\psi^{\dot\alpha} \end{pmatrix}, \tag{D.13}$$

$$\Gamma^\mu = \begin{pmatrix} 0 & \sigma^\mu \\ \bar\sigma^\mu & 0 \end{pmatrix}. \tag{D.14}$$

Chiral superfield The chiral superfield Φ consists of a scalar field A, a spinor field ϕ, and an auxiliary field F:

$$\Phi(x,\theta) = A(y) + \sqrt{2}\theta\psi(y) + \theta\theta F(y), \tag{D.15}$$

where $y^\mu = x^\mu + i\theta\sigma^\mu\bar{\theta}$ and θ is Grassmann coordinate. The chiral superfield is characterized by the condition:

$$\bar{D}_{\dot{\alpha}}\Phi = 0, \tag{D.16}$$

where $\bar{D}_{\dot{\alpha}}$ is differential operator:

$$D_\alpha = \frac{\partial}{\partial\theta^\alpha} + i\sigma^\mu_{\alpha\dot{\alpha}}\bar{\theta}^{\dot{\alpha}}\partial_\mu, \qquad \bar{D}_{\dot{\alpha}} = -\frac{\partial}{\partial\bar{\theta}^{\dot{\alpha}}} - i\theta^\alpha\sigma^\mu_{\alpha\dot{\alpha}}\partial_\mu. \tag{D.17}$$

Their fields are transformed by supersymmetry transformation as:

$$\begin{aligned}
\delta_\xi A &= \sqrt{2}\xi\phi, \\
\delta_\xi\phi &= i\sqrt{2}\sigma^\mu\bar{\xi}\partial_\mu A + \sqrt{2}\xi F, \\
\delta_\xi F &= i\sqrt{2}\bar{\xi}\bar{\sigma}^\mu\partial_\mu\phi.
\end{aligned} \tag{D.18}$$

The Lagrangian of the simplest model involving only chiral superfields is given by

$$\begin{aligned}
\mathcal{L} = &\int d^2\theta d^2\bar{\theta}\Phi_i^\dagger\Phi_i \\
&+ \left[\int d^2\theta \left(\frac{1}{2}m_{ij}\Phi_i\Phi_j + \frac{1}{3}g_{ijk}\Phi_i\Phi_j\Phi_k + \lambda_i\Phi_i\right) + \text{h.c.}\right].
\end{aligned} \tag{D.19}$$

In terms of component fields, $\mathcal{L}$ becomes

$$\begin{aligned}
\mathcal{L} = &i\partial_\mu\bar{\psi}_i\bar{\sigma}^\mu\psi_i - \partial_\mu A_i^*\partial^\mu A_i + F_i^* F_i \\
&+ \left[m_{ij}\left(A_i F_j - \frac{1}{2}\psi_i\psi_j\right)\right. \\
&\left. + g_{ijk}(A_i A_j F_k - \psi_i\psi_j A_k) + \lambda_i F_i + \text{h.c.}\right].
\end{aligned} \tag{D.20}$$

The auxiliary fields F_i may be eliminated through their Euler equations. After the elimination, we can find that the potential $\mathcal{V}$ takes the form

$$\mathcal{V} = F_k^* F_k. \tag{D.21}$$

This potential is always greater than or equal to zero. Thus, a supersymmetric vacuum expectation value of F_k must vanish.

General Wess-Zumino model The Lagrangian of the most general non-gauge model, so-called (general) Wess-Zumino model, takes form

$$\mathcal{L} = \int d^2\theta d^2\bar{\theta}\, K(\Phi^i, \Phi^{\dagger j}) + \left[\int d^2\theta \mathcal{W}(\Phi^i) + \text{h.c.}\right], \tag{D.22}$$

where $K(\Phi^i, \Phi^{\dagger j})$ is called Kähler potential, and $\mathcal{W}(\Phi^i)$ is called superpotential. It is important that the superpotential $\mathcal{W}$ is holomorphic.

In terms of component fields, $\mathcal{L}$ becomes

$$\mathcal{L} = -K_{ij^*}\partial_\mu A^i \partial^\mu A^{*j} - K^{ij^*}\frac{\partial \mathcal{W}}{\partial A^i}\frac{\partial \mathcal{W}^*}{\partial A^{*j}} + (\chi \text{ terms}), \tag{D.23}$$

where K_{ij^*}, so-called Kähler metric, is

$$K_{ij^*} = \frac{\partial}{\partial A^i}\frac{\partial}{\partial A^{*j}}K, \qquad \text{and} \qquad K_{ij^*}K^{kj^*} = \delta_i^k. \tag{D.24}$$

The potential $\mathcal{V}$ is

$$\mathcal{V} = K^{ij^*}F_i F_j^*, \qquad F_i = \frac{\partial \mathcal{W}}{\partial A^i}. \tag{D.25}$$

Vector superfield The vector superfield V consists of a gauge potential field v_μ, a spinor field λ, and an auxiliary field D in Wess-Zumino gauge:

$$V = -\theta\sigma^\mu\bar{\theta}v_\mu(x) + i\theta\theta\bar{\theta}\bar{\lambda}(x) - i\bar{\theta}\bar{\theta}\theta\lambda(x) + \frac{1}{2}\theta\theta\bar{\theta}\bar{\theta}D(x). \tag{D.26}$$

The vector superfields satisfy the condition

$$V = V^\dagger. \tag{D.27}$$

The supersymmetric field strength W_α is

$$W_\alpha = -\frac{1}{4}\bar{D}\bar{D}D_\alpha V, \qquad \bar{W}_{\dot{\alpha}} = -\frac{1}{4}DD\bar{D}_{\dot{\alpha}}V. \tag{D.28}$$

The supersymmetric field strength W_α is a chiral superfield, and

$$\int d^2\theta W^\alpha W_\alpha = -2i\lambda\sigma^\mu\partial_\mu\bar{\lambda} - \frac{1}{2}v^{\mu\nu}v_{\mu\nu} + D^2 + \frac{i}{4}v^{\mu\nu}v^{\rho\sigma}\epsilon_{\mu\nu\rho\sigma}, \tag{D.29}$$

where $v_{\mu\nu} = \partial_\mu v_\nu - \partial_\nu v_\mu$. The Lagrangian of supersymmetric pure $U(1)$ gauge model is

$$\mathcal{L} = \frac{1}{4}\int d\theta^2 WW + \text{h.c.} \tag{D.30}$$

$$= \frac{1}{2}D^2 - \frac{1}{4}v^{\mu\nu}v_{\mu\nu} - i\lambda\sigma^\mu\partial_\mu\bar{\lambda}. \tag{D.31}$$

$U(1)$ **gauge theories** The gauge transformation is

$$\begin{aligned} \Phi_i &\to \Phi_i' = e^{-ie_i\Lambda}\Phi_i, \\ V &\to V' = V + i(\Lambda - \Lambda^\dagger), \end{aligned} \tag{D.32}$$

where e_i are the $U(1)$ charges of the Φ_i.

The Lagrangian of the $U(1)$ gauge theories is

$$\begin{aligned} \mathcal{L} = &\int d^2\theta d^2\bar{\theta}\, {\Phi_i}^\dagger e^{e_i V}\Phi_i \\ &+ \left[\int d^2\theta \left(\mathcal{W}(\Phi) + \frac{1}{4}WW\right) + \text{h.c.}\right] \\ &+ 2\kappa \int d^2\theta d^2\bar{\theta} V, \end{aligned} \tag{D.33}$$

The κ term is called Fayet-Iliopoulos term. The potential $\mathcal{V}$ is

$$\mathcal{V} = \frac{1}{2}D^2 + F_k^* F_k, \tag{D.34}$$

where

$$D = -\kappa - \frac{e_i}{2}A_i^* A_i. \tag{D.35}$$

The gauge covariant derivatives are

$$\mathcal{D}_\mu A_i = \partial_\mu A_i + \frac{ie_i}{2}v_\mu A_i. \tag{D.36}$$

Non-Abelian gauge theories The gauge transformation is

$$\begin{aligned} \Phi &\to \Phi' = e^{-i\Lambda}\Phi, \qquad \Lambda_{ij} = T^a_{ij}\Lambda_a, \\ e^V &\to e^{V'} = e^{-i\Lambda^\dagger}e^V e^{i\Lambda}, \qquad V_{ij} = T^a_{ij}V_a, \end{aligned} \tag{D.37}$$

where T^a_{ij} are the hermitian generators of of the gauge group in the representation defined by the chiral field Φ. In the adjoint representation, we normalized our generators as follows:

$$\text{tr}(T^a T^b) = k\delta^{ab}, \qquad k > 0. \tag{D.38}$$

With this convention, the structure constants t^{abc}

$$[T^a, T^b] = it^{abc}T^c \tag{D.39}$$

are completely antisymmetric.

The supersymmetric field strength W_α is generalized to the non-Abelian case:

$$W_\alpha = -\frac{1}{4}\bar{D}\bar{D}e^{-V}D_\alpha e^V, \tag{D.40}$$

and transforms as follows:

$$W_\alpha \to W'_\alpha = e^{-i\Lambda}W_\alpha e^{i\Lambda}. \tag{D.41}$$

The Lagrangian of the non-Abelian gauge theories is

$$\begin{aligned}\mathcal{L} = &\int d^2\theta d^2\bar{\theta}\Phi_i{}^\dagger e^{2gV}\Phi_i \\ &+ \left[\int d^2\theta\left(\mathcal{W}(\Phi) + \frac{1}{4k}\mathrm{tr}(WW)\right) + \mathrm{h.c.}\right],\end{aligned} \tag{D.42}$$

The potential $\mathcal{V}$ is

$$\mathcal{V} = \frac{1}{2}D^{(a)2} + F_k F_k^*. \tag{D.43}$$

From Euler equations, we can find that

$$D^{(a)} = -g\, A^{i\dagger}T^{(a)}A^i. \tag{D.44}$$

The supersymmetric transformation for A, ψ, F, $v_m^{(a)}$, $\lambda^{(a)}$ and $D^{(a)}$ in Wess-Zumino gauge is

$$\begin{aligned}\delta_\xi A &= \sqrt{2}\xi\psi, \\ \delta_\xi\psi &= i\sqrt{2}\sigma^\mu\bar{\xi}\mathcal{D}_\mu A + \sqrt{2}\xi F, \\ \delta_\xi F &= i\sqrt{2}\bar{\xi}\bar{\sigma}\mathcal{D}_\mu\psi + i2gT^{(a)}A\bar{\xi}\bar{\lambda}^{(a)}, \\ \delta_\xi v_m^{(a)} &= -i\bar{\lambda}^{(a)}\bar{\sigma}^\mu\xi + i\bar{\xi}\bar{\sigma}^\mu\lambda^{(a)}, \\ \delta_\xi\lambda^{(a)} &= \sigma^{\mu\nu}\xi v_{\mu\nu}^{(a)} + i\xi D^{(a)}, \\ \delta_\xi D^{(a)} &= -\xi\sigma^\mu\mathcal{D}_\mu\bar{\lambda}^{(a)} - \mathcal{D}_\mu\lambda^{(a)}\sigma^\mu\bar{\xi},\end{aligned} \tag{D.45}$$

where $\mathcal{D}_\mu$ are the gauge covariant derivatives:

$$\begin{aligned}\mathcal{D}_\mu A &= \partial_\mu A + igv_\mu^{(a)}T^{(a)}A, \\ \mathcal{D}_\mu\psi &= \partial_\mu\psi + igv_\mu^{(a)}T^{(a)}\psi, \\ \mathcal{D}_\mu\lambda^{(a)} &= \partial_\mu\lambda^{(a)} - gt^{abc}v_\mu^{(b)}\lambda^{(c)}, \\ v_{\mu\nu}^{(a)} &= \partial_\mu v_\nu^{(a)} - \partial_\nu v_\mu^{(a)} - gt^{abc}v_\mu^{(b)}v_\nu^{(c)}.\end{aligned} \tag{D.46}$$

Appendix E

Fermionic contributions to central charges

We shall derive the central charges including fermionic contributions in the case of a general Wess-Zumino model with an arbitrary superpotential $\mathcal{W}$. For simplicity, Kähler metric is assumed to be minimal $K_{ij^*} = \delta_{ij^*}$.

$$\begin{aligned}\mathcal{L} &= -\partial_\mu A^{*j}\partial^\mu A^j + F^{*j}F^j + \frac{i}{2}\partial_\mu\bar{\psi}^j\bar{\sigma}^\mu\psi^j - \frac{i}{2}\bar{\psi}^j\bar{\sigma}^\mu\partial_\mu\psi^j \\ &+ F^j\frac{\partial\mathcal{W}}{\partial A^j} - \frac{1}{2}\psi^i\psi^j\frac{\partial\mathcal{W}}{\partial A^i\partial A^j} + F^{*j}\frac{\partial\mathcal{W}^*}{\partial A^{*j}} - \frac{1}{2}\bar{\psi}^i\bar{\psi}^j\frac{\partial\mathcal{W}^*}{\partial A^{*i}\partial A^{*j}}. \quad \text{(E.1)}\end{aligned}$$

We have added a surface term to eq.(9.10) to make the variational principle meaningful. This is the starting Lagrangian to derive central charges and we will not neglect any total divergences from now on. The canonical supercurrent is found to be

$$\begin{aligned}J^\mu_\alpha &= \sqrt{2}\left(\sigma^\nu\bar{\sigma}^\mu\psi^i\right)_\alpha\partial_\nu A^{i*} + i\sqrt{2}\left(\sigma^\mu\bar{\psi}^i\right)_\alpha F^i \\ &= \sqrt{2}\left(\sigma^\nu\bar{\sigma}^\mu\psi^i\right)_\alpha\partial_\nu A^{i*} - i\sqrt{2}\left(\sigma^\mu\bar{\psi}^i\right)_\alpha\frac{\partial\mathcal{W}^*}{\partial A^{*i}} \quad \text{(E.2)} \\ \bar{J}^{\mu\dot{\alpha}} &= \sqrt{2}\left(\bar{\sigma}^\nu\sigma^\mu\bar{\psi}^i\right)^{\dot{\alpha}}\partial_\nu A^i + i\sqrt{2}\left(\bar{\sigma}^\mu\psi^i\right)^{\dot{\alpha}}F^{i*} \\ &= \sqrt{2}\left(\bar{\sigma}^\nu\sigma^\mu\bar{\psi}^i\right)^{\dot{\alpha}}\partial_\nu A^i - i\sqrt{2}\left(\bar{\sigma}^\mu\psi^i\right)^{\dot{\alpha}}\frac{\partial\mathcal{W}}{\partial A^i} \quad \text{(E.3)}\end{aligned}$$

The canonical energy momentum tensor is given by

$$\begin{aligned}T^{\mu\nu} &= \partial^\mu A^j\partial^\nu A^{*j} + \partial^\mu A^{*j}\partial^\nu A^j + \frac{i}{2}\bar{\psi}^j\bar{\sigma}^\mu\partial^\nu\psi^j + \frac{i}{2}\psi^j\sigma^\mu\partial^\nu\bar{\psi}^j \\ &+ g^{\mu\nu}\left[-\partial_\lambda A^{*j}\partial^\lambda A^j - \left|\frac{\partial\mathcal{W}}{\partial A^j}\right|^2 + \frac{i}{2}\partial_\lambda\bar{\psi}^j\bar{\sigma}^\lambda\psi^j - \frac{i}{2}\bar{\psi}^j\bar{\sigma}^\lambda\partial_\lambda\psi^j\right]\end{aligned}$$

$$-g^{\mu\nu}\left[\frac{1}{2}\psi^i\psi^j\frac{\partial\mathcal{W}}{\partial A^i\partial A^j}+\frac{1}{2}\bar{\psi}^i\bar{\psi}^j\frac{\partial\mathcal{W}^*}{\partial A^{*i}\partial A^{*j}}\right]. \tag{E.4}$$

Canonical quantization gives (anti-) commutation relations

$$\begin{aligned}\left[A^i(x),\partial_0 A^{*j}(y)\right]_{x^0=y^0} &= i\delta^3(x-y)\delta^{ij}\\ \left\{\psi^i_\alpha(x),\bar{\psi}^j_{\dot{\beta}}(y)\right\}_{x^0=y^0} &= -\delta^3(x-y)\delta^{ij}\sigma^0_{\alpha\dot{\beta}}.\end{aligned} \tag{E.5}$$

The anticommutator between supercharges of the same chirality gives the supersymmetry algebra (9.8) with the central charge Z_k in eq.(9.11)

$$Z_k = 2\int d^3x\,\partial_k\mathcal{W}^*(A^*) \tag{E.6}$$

which turns out to have only bosonic contributions. The anticommutator between supercharges of the opposite chirality gives the supersymmetry algebra (9.9) with the central charge Y_k

$$Y_k = i\epsilon^{knm}\int d^3x\,\partial_n\left(A^{*j}\partial_m A^j-\frac{1}{2}\bar{\psi}^j\bar{\sigma}_m\psi^j\right),\qquad \epsilon^{123}=1, \tag{E.7}$$

which has both bosonic and fermionic contributions.

Appendix F

Gamma matrices and fermion mode equations

In order to separate variables (x^1, x^2) and (x^0, x^3) for spinors, it is most convenient to use a gamma matrix representation where the direct product structure of 2×2 matrices in (x^1, x^2) and (x^0, x^3) becomes manifest. One such representation is

$$\gamma^0 = \rho^1, \quad \gamma^3 = i\rho^2, \quad \gamma^1 = i\sigma^1\rho^3, \quad \gamma^2 = i\sigma^2\rho^3, \tag{F.1}$$

where σ^a are Pauli matrices acting on 2×2 matrices and ρ^a acting on indices of blocks of these 2×2 matrices. The four component spinor can be decomposed into a pair of two component spinors ξ and χ in $0+2$ dimensions

$$\psi = \begin{bmatrix} \xi \\ i\chi \end{bmatrix}, \tag{F.2}$$

The B matrix for $1+3$ dimensions can be defined as a product of B matrices $B^{(1)}$ for $1+1$ dimensions and $B^{(2)}$ for $0+2$ dimensions

$$B = B^{(1)}B^{(2)}, \qquad B^{(1)} = \rho^3, \qquad B^{(2)} = -i\sigma^1. \tag{F.3}$$

The Majorana condition for the $1+3$ dimensional spinor and the pseudo-Majorana condition for the $0+2$ dimensional spinor are given by

$$\psi = B\psi^*, \qquad \xi = B^{(2)}\xi^*, \quad \chi = B^{(2)}\chi^*, \tag{F.4}$$

which implies $\xi_1 = -i\xi_2^*$ for components of the two component spinor $\xi = (\xi_1, \xi_2)^T$, and similarly for χ.

The Dirac equation for four component fermions in the general Wess-Zumino model reads

$$-i\gamma^\mu\partial_\mu\psi^i - \left(\frac{\partial^2\mathcal{W}}{\partial A^i\partial A^j}\frac{1+i\gamma^5}{2} + \frac{\partial^2\mathcal{W}^*}{\partial A^{*i}\partial A^{*j}}\frac{1-i\gamma^5}{2}\right)\psi^j = 0. \tag{F.5}$$

The mode equation in x^1, x^2 space is defined in terms of two component spinors ξ_n^j and χ_n^j

$$\begin{aligned}\left[\delta^{ij}\left(\sigma^1\partial_1+\sigma^2\partial_2\right)-\frac{\partial^2\mathcal{W}}{\partial A^i\partial A^j}\frac{1-\sigma^3}{2}-\frac{\partial^2\mathcal{W}^*}{\partial A^{*i}\partial A^{*j}}\frac{1+\sigma^3}{2}\right]\xi_n^j &= -m_n^{(1)}\chi_n^i,\\ \left[-\delta^{ij}\left(\sigma^1\partial_1+\sigma^2\partial_2\right)-\frac{\partial^2\mathcal{W}}{\partial A^i\partial A^j}\frac{1+\sigma^3}{2}-\frac{\partial^2\mathcal{W}^*}{\partial A^{*i}\partial A^{*j}}\frac{1-\sigma^3}{2}\right]\chi_n^j &= -m_n^{(2)}\xi_n^i.\end{aligned} \tag{F.6}$$

The two component spinors ξ_n^i, χ_n^i satisfy the pseudo-Majorana condition (F.4). Then we find that mass eigenvalues are real

$$m_n^{(1)} = \left(m_n^{(1)}\right)^*, \qquad m_n^{(2)} = \left(m_n^{(2)}\right)^*. \tag{F.7}$$

We can make a separation of variables for the Dirac equation (F.5) by means of real fermionic fields c_n and b_n

$$\psi^i = \sum_n \begin{bmatrix} c_n(x^0,x^3)\xi_n^i(x^1,x^2) \\ ib_n(x^0,x^3)\chi_n^i(x^1,x^2) \end{bmatrix}. \tag{F.8}$$

Using these mode functions we find that the fermion fields $(c_n, ib_n)^T$ satisfy the Dirac equation in $1+1$ dimensions in eq.(11.25).

This representation can be related to the usual Weyl representation in ref. [105] by the following unitary matrix U

$$U = \frac{1-\sigma^3}{2}\rho^3 + \frac{1+\sigma^3}{2}\rho^2, \quad \gamma^\mu_{\rm Weyl} = U^\dagger\gamma^\mu U, \quad B_{\rm Weyl} = U^\dagger B U^* = \sigma^2\rho^2. \tag{F.9}$$

The two component spinor in the Weyl representation is related to the components of the four component spinor (F.2) in the representation (F.1) in this appendix as

$$\begin{bmatrix} \psi_\alpha \\ \bar\psi^{\dot\alpha} \end{bmatrix}_{\rm Weyl} = \begin{bmatrix} \chi_1 \\ \xi_2 \\ i\xi_1 \\ -i\chi_2 \end{bmatrix}. \tag{F.10}$$

Thus we obtain the mode equations (11.20)– (11.23) in the Weyl representation.

Bibliography

[1] S. Weinberg, *Phys. Rev. Lett.* **19** (1967) 1264.

[2] A. Salam, *Elementary Particle Theory*, N. Svartholm ed. (Almqvist and Wiksell, Stockholm 1968).

[3] D. J. Gross and F. Wilczek, *Phys. Rev.* **D8** (1973) 3633.

[4] H. D. Politzer, *Phys. Rev. Lett.* **30** (1973) 1346.

[5] K. G. Wilson, *Phys. Rev.* **D10** (1974) 2445.

[6] M. Creutz, L. Jacobs, and C. Rebbi, *Phys. Rep.* **95**, 201 (1983).

[7] M. Creutz, *Quarks, Gluons, and Lattices*, (Cambridge University Press, Cambridge,1983).

[8] I. Montvay, Rev. Mod. Phys. **59**, 263 (1987).

[9] M. B. Green, J. H. Schwarz and E. Witten, *Superstring theory 1,2*, Cambridge Univ. Press (1987).

[10] J. Polchinski, *String Theory*, Cambridge Univ. Press (1998).

[11] A. Giveon and D. Kutasov, Rev. Mod. Phys. **71** (1999) 983, hep-th/9802067.

[12] E. Witten, *Nucl. Phys.* **B500** (1997) 3-42.

[13] J. M. Maldacena, Adv. Theor. Math. Phys. **2** (1998) 231, hep-th/9711200.

[14] E. Witten, Adv. Theor. Math. Phys. **2** (1998) 253, hep-th/9802150.

[15] E. Witten, Adv. Theor. Math. Phys. **2** (1998) 505, hep-th/9803131.

[16] O. Aharony, S. Gubser, J. Maldacena, H. Ooguri and Y. Oz, *Phys. Rep.* **323** (2000) 183, hep-th/9905111.

[17] P. Di Vecchia, hep-th/9908148.

[18] M. J. Duff, hep-th/9912164.

[19] G. 't Hooft, *Nucl. Phys.* **B72** (1974) 461.

[20] G. 't Hooft, *Nucl. Phys.* **B75** (1974) 461.

[21] C. G. Callan, N. Coote and D. J. Gross, Phys. Rev. D13. (1976) 1649.

[22] D. J. Gross and A. Neveu, *Phys. Rev.* **D10** (1974) 3235.

[23] S. Coleman and E. Weinberg, *Phys. Rev.* **D7** (1973) 1888.

[24] S. Coleman, Commun. Math. Phys. 31. (1973) 259.

[25] E. Witten, *Nucl. Phys.* **B146** (1978) 110.

[26] S. Coleman, *"Aspects of symmetry"*, Cambridge University Press (1985).

[27] B. Rosenstein, B. J. Warr and S. H. Park, *Phys. Rep.* **C205** (1991) 59.

[28] N. Andrei and J. H. Lowenstein, *Phys. Rev. Lett.* **43** (1979) 1698; *Phys. Lett.* **B90** (1980) 106.

[29] M. Burkardt, *Phys. Rev.* **D56** (1997) 7105.

[30] K. Itakura, Ph. D. thesis, Tokyo University (1996).

[31] K. Aoki and T. Ichihara, *Phys. Rev.* **D52** (1995) 6435.

[32] K. Aoki and K. Ito, *Phys. Rev.* **D60** (1999) 096004.

[33] W. A. Bardeen, R. B. Pearson and E. Rabinovici, *Phys. Rev.* **D21** (1980) 1037.

[34] A. J. Hanson, R. D. Peccei and M. K. Prasad, *Nucl. Phys.* **B121** (1977) 477.

[35] R. C. Brower, W. L. Spence and J. H. Weis, *Phys. Rev.* **D19** (1979) 3024.

[36] S. Huang, J. W. Negele and J. Polonyi, *Nucl. Phys.* **B307** (1988) 669.

[37] R. L. Jaffe and P. F. Mende, *Nucl. Phys.* **B369** (1992) 182.

[38] R. F. Lebed and N. G. Uraltsev, "Precision Studies of Duality in the 't Hooft Model", hep-ph/0006346.

[39] Y. Nambu and G. Jona-Lasinio *Phys. Rev.* **122** (1961) 345.

[40] J. L. Rosner, hep-ph/9812537.

[41] R. S. Chivukula, hep-ph/9903500.

[42] Y. Nambu, in *New Theories in Physics*, Z. Ajduk, S. Pokorski, A. Trautman (eds), World Scientific, Singapore (1989).

[43] M. Bando, T. Muta and K. Yamawaki (eds), in *New Trends in Strong Coupling Gauge Theories*, World Scientific, Singapore (1989).

[44] V. A. Miransky, M. Tanabashi and K. Yamawaki, *Mod. Phys. Lett.* **A4** (1989) 1043.

[45] V. A. Miransky, M. Tanabashi and K. Yamawaki, *Phys. Lett.* **B221** (1989) 177.

[46] W. A. Bardeen, C. T. HIll and M. Lindner, *Phys. Rev.* **D41** (1990) 1647.

[47] L. Jacobs, *Phys. Rev.* **D10** 3956 (1974).

[48] B. J. Harrington and A. Yildiz, *Phys. Rev.* **D11** 779 (1975).

[49] R. F. Dashen, S. Ma and R. Rajaraman, *Phys. Rev.* **D11** 1499 (1975).

[50] W. Dittrich and B. G. Englert, *Nucl. Phys.* **B179** 85 (1981).

[51] B. J. Harrington and A. Yildiz, *Phys. Rev.* **D11** 1705 (1975).

[52] A. Chodos and H. Minakata, *Nucl. Phys.* **A191** (1994) 39–45.

[53] H. Minakata and A. Chodos, hep-th/9709179.

[54] A. Chodos and H. Minakata, hep-th/9709197.

[55] I. L. Buchbinder and E. N. Kirillova, Int. J. Mod. Phys. **A4** (1989) 143–149.

[56] H. Itoyama, Prog. Theor. Phys. **64** 1886 (1980).

[57] I. Sachs and A. Wipf, *Phys. Lett.* **B 326** (1994) 105–110.

[58] S. Kanemura and H. Sato, Mod. Phys. Lett. **A10** (1995) 1777–1785.

[59] S. Kanemura and H. Sato, Mod. Phys. Lett. **A11** (1996) 785–793.

[60] B. J. Harrington, S. Y. Park and A. Yildiz, *Phys. Rev.* **D11** 1472 (1975).

[61] D. Weingarten, *Phys. Lett.* **51**, 1830 (1983).

[62] C. Vafa and E. Witten, *Nucl. Phys.* **B234**, 173 (1984).

[63] C. Vafa and E. Witten, *Phys. Rev. Lett.* **53**, 535 (1984).

[64] C. Vafa and E. Witten, *Comm. Math. Phys.* **95**, 257 (1984).

[65] E. Witten, *Phys. Rev. Lett.* **51**, 2351 (1983).

[66] S. Nussinov, *Phys. Rev. Lett.* **51**, 2081 (1983).

[67] I. J. Muzinich and V. P. Nair, *Phys. Lett.* **B178**, 105 (1986).

[68] D. Espriu, M. Gross, and J. F. Wheater, *Phys. Lett.* **B146**, 67 (1984).

[69] O. Aharony, J. Sonnenschein, M. E. Peskin and S. Yankielowicz, *Phys. Rev.* **D52**, 6157 (1995), hep-th/9507013.

[70] H. Nishino, hep-th/9804162.

[71] S. Nussinov, M. A. Lampert, hep-ph/9911532.

[72] J. Goldstone, Nuovo Cimento **19**, 154 (1961).

[73] S. Weinberg, *Phys. Rev.* **19**, 1277 (1979).

[74] L. Susskind, *Phys. Rev.* **20**, 2619 (1979).

[75] R. S. Chivukula, hep-ph/9803219.

[76] D. E. Groom *et al.*, Eur. Phys. J. **C15**, 1 (2000).

[77] R. S. Chivukula, hep-ph/0011264.

[78] G. 't Hooft, in *Recent Developments in Gauge Theories, Proceedings of the Charge Summer Institute 1979*, ed. G. 't Hooft *et al.* (Plenum Press, New York, 1980).

[79] K. Aoki and K. Ito, "Mass Inequalities in two dimensional gauged four–Fermi models, in preparation.

[80] Particle Data Group, C. Caso *et al*, The European Physical Journal **C3**, 1 (1998).

[81] G. 't Hooft, *Phys. Rep.* **142**, 357 (1986).

[82] E. Witten, *Nucl. Phys.* **B156**, 269 (1979).

[83] G. Veneziano, *Phys. Lett.* **B95**, 90 (1980).

[84] M. Gell–Mann and Y. Ne'eman, *The Eightfold Way*, (Benjamin, New York, 1963).

[85] F. Gilman and R. Kauffman, *Phys. Rev.* **D36**, 2761 (1987).

[86] M. A. Shifman and A. I. Veinstein, *Nucl. Phys.* **B277** (1986) 456.

[87] M. A. Shifman and A. I. Veinstein, *Nucl. Phys.* **B359** (1991) 571.

[88] D. Amati, K. Konishi, Y. Meurice, G. C. Rossi and G. Veneziano, *Phys. Rep.* **162** (1998) 169.

[89] N. Seiberg, *Phys. Lett.* **B318** (1993) 469.

[90] N. Seiberg, *Phys. Rev.* **D49** (1994) 6857.

[91] K. Intriligator, R. Leigh and N. Seiberg, *Phys. Rev.* **D50** (1994) 1092.

[92] V. Kaplunovsky and J. Louis, *Nucl. Phys.* **B 422** (1994) 57–124.

[93] N. Seiberg, *Phys. Lett.* **B206** (1988) 75.

[94] E. Witten, *Phys. Lett.* **B86** (1979) 283.

[95] Y. Artstein, V. Kaplunovsky and J. Sonnenschein, "Domain Walls in the Large N Limit", hep-th/0010241.

[96] G. 't Hooft, *Nucl. Phys.* **B138**, 1 (1978).

[97] S. Mandelstam, *Phys. Rev.* **D19**, 2391 (1979).

[98] Y. Aharonov, A. Casher and S. Yankielowicz, *Nucl. Phys.* **B146**, 256 (1978).

[99] V. Kaplunovsky, J. Sonnenschein, and S. Yankielowicz, *Nucl. Phys.* **B552** (1999) 209, hep-th/9811195.

[100] E. Bogomol'nyi, *Sov. J. Nucl. Phys.* **24** (1976) 449.

[101] M. K. Prasad and C. H. Sommerfield, *Phys. Rev. Lett.* **35** (1975) 760.

[102] E. Witten and D. Olive, *Phys. Lett.* **B78** (1978) 97.

[103] E. R. C. Abraham and P. K. Townsend, *Nucl. Phys.* **B351** (1991) 313.

[104] J. A. de Azcaárraga, J. P. Gauntlet, J. M. Izquierdo, and P. K. Townsend, *Phys. Rev. Lett.* **63** (1989) 2443.

[105] J. Wess and J. Bagger, "Supersymmetry and Supergravity", 1991, Princeton University Press.

[106] K. Intriligator and N. Seiberg, *Nucl. Phys. Proc. Suppl.* **BC45** (1996) 1, hep-th/9509066.

[107] N. Seiberg and E. Witten, *Nucl. Phys.* **B426** (1994) 19.

[108] N. Seiberg and E. Witten, *Nucl. Phys.* **B431** (1994) 484.

[109] K. Intriligator and N. Seiberg, *Nucl. Phys.* **B431** (1994) 551.

[110] G. Gabadadze and M. Shifman, "D-Walls and Junctions in Supersymmetric Gluodynamics in the Large N Limit Suggest the Existence of Heavy Hadrons", hep-th/9910050.

[111] D. Binosi, "Domain Walls Junctions from a Distance", hep-th/9910057.

[112] J. Edelstein, C. Núñez and F. Schaposhnik, *Phys. Lett.* **B329** (1994) 39.

[113] A. A. Penin, V. A. Rubakov, P. G. Tinyakov and S. V. Troitsky, *Phys. Lett.* **B389** (1996) 13.

[114] S. C. Davis, A. Davis and M. Trodden, *Phys. Lett.* **B405** (1997) 257.

[115] A. A. Penin, *Nucl. Phys.* **B532** (1998) 83.

[116] N. Arkani-Hamed, S. Dimopoulos, and G. Dvali, *Phys. Lett.* **B429** (1998) 263, hep-ph/9803315.

[117] I. Antoniadis, N. Arkani-Hamed, S. Dimopoulos, and G. Dvali, *Phys. Lett.* **B436** (1998) 257, hep-ph/9804398.

[118] L. Randall and R. Sundrum, *Phys. Rev. Lett.* **83** (1999) 3370, hep-ph/9905221.

[119] L. Randall and R. Sundrum, *Phys. Rev. Lett.* **83** (1999) 4690, hep-th/9906064.

[120] N. Arkani-Hamed, S. Dimopoulos, G. Dvali, and N. Kaloper, *Phys. Rev. Lett.* **84** (2000) 586, hep-th/9907209.

[121] C. Csaki and Y. Shirman, *Phys. Rev.* **D61** (2000) 024008, hep-th/9908186.

[122] A. E. Nelson, "A new angle on intersecting branes in infinite extra dimensions", hep-th/9909001.

[123] K. Behrndt and M. Cvetič, "Supersymmetric domain wall world from $D = 5$ simple gauged supergravity", hep-th/9909058.

[124] K. Skenderis and P. Townsend, *Phys. Lett.* **B468** (1999) 46, hep-th/9909070.

[125] A. Chamblin and G. W. Gibbons, "Supergravity on the Brane ", hep-th/9909130.

[126] O. DeWolfe, D. Z. Freedman, S. S. Gubser, and A. Karch, "Modeling the fifth dimension with scalars and gravity", hep-th/9909134.

[127] G. Dvali and M. Shifman, *Phys. Lett.* **B396** (1997) 64, hep-th/9612128.

[128] G. Dvali and M. Shifman, *Nucl. Phys.* **B504** (1997) 127, hep-th/9611213.

[129] A. Kovner, M. Shifman, and A. Smilga, *Phys. Rev.* **D56** (1997) 7978, hep-th/9706089.

[130] A. Smilga and A. Veselov, *Phys. Rev. Lett.* **79** (1997) 4529, hep-th/9706217.

[131] B. de Carlos and J. M. Moreno, *Phys. Rev. Lett.* **83** (1999) 2120, hep-th/9905165.

[132] G. Dvali and Z. Kakushadze, *Nucl. Phys.* **B537** (1999) 297.

[133] G. Dvali, G. Gabadadze, and Z. Kakushadze, *Nucl. Phys.* **B562** (1999) 158, hep-th/9901032.

[134] B. Chibisov and M. Shifman, *Phys. Rev.* **D56** (1997) 7990; Erratum–ibid. **D58** 109901 (1998), hep-th/9706141.

[135] V. A. Rubakov and M. E. Shaposhnikov, *Phys. Lett.* **B125** (1983) 136.

[136] G. Gibbons and P. K. Townsend, *Phys. Rev. Lett.* **83** (1999) 1727, hep-th/9905196.

[137] S. M. Carroll, S. Hellerman and M. Trodden, *Phys. Rev.* **D61** (2000) 065001, hep-th/9905217.

[138] A. Gorsky and M. Shifman, *Phys. Rev.* **D61** (2000) 085001, hep-th/9909015.

[139] P. M. Saffin, *Phys. Rev. Lett.* **83** (1999) 4249, hep-th/9907066.

[140] D. Bazeia and F. A. Brito, *Phys. Rev. Lett.* **84** (2000) 1094, hep-th/9908090.

[141] H. Oda, K. Ito, M. Naganuma and N. Sakai, *Phys. Lett.* **B471** (1999) 148, hep-th/9910095.

[142] P. Townsend, *PASCOS/Hopkins* (1995) 0271, hep-th/9507048.

[143] P. Townsend, *Class. Quant. Qrav.* **17** (2000) 1267, hep-th/9911154.

[144] D. Binosi and T. tel Veldhuis, *Phys. Lett.* **B476** (2000) 124, hep-th/9912081.

[145] D. Bazeia and F. A. Brito, "Bags, junctions, and networks of BPS and non-BPS defects", hep-th/9912015.

[146] M. Shifman and T. tel Veldhuis, "Calculating the tension of domain wall junctions and vortices in generalized Wess-Zumino models", hep-th/9912162.

[147] S. M. Carroll, S. Hellerman, and M. Trodden, "BPS domain wall junctions in large extra dimensions", hep-th/9911083.

[148] N. Arkani-Hamed, S. Dimopoulos, G. Dvali, and N. Kaloper, "Many-fold universe", hep-ph/9911386.

[149] S. Nam, *JHEP.* **0003** (2000) 005, hep-th/9911104.

[150] I. Bakas, A. Brandhuber, and K. Sfetsos, "Domain walls of gauged supergravity, M-branes and algebraic curves", hep-th/9912132.

[151] M. Cvetič, H. Lü, and C. N. Pope, "Domain walls and massive gauged supergravity potentials", hep-th/0001002.

[152] C. Csaki, J. Erlich, T. J. Hollowood, and Y. Shirman, "Universal aspects of gravity localized on thick branes", hep-th/0001033.

[153] R. Kallosh and A. Linde, *JHEP.* **0002** (2000) 005, hep-th/0001071.

[154] S. Nam and K. Olsen, "Domain wall junctions in supersymmetric field theories in $D = 4$", hep-th/0002176.

[155] R. Altendorfer, J. Bagger, and D. Nemeschansky, "Supersymmetric Randall-Sundrum scenario", hep-th/0003117.

[156] N. Alonso-Alberca, P. Meessen, and T. Ortin, "Supersymmetric braneworlds", hep-th/0003248.

[157] J. P. Gauntlett, G. W. Gibbons and P. K. Townsend, "Intersecting domain walls in MQCD", hep-th/0004136.

[158] J. P. Gauntlett, D. Tong and P. K. Townsend, "Supersymmetric Intersecting Domain Walls in Massive Hyper–Kähler Sigma Models", hep-th/0007124.

[159] K. Ito, M. Naganuma, H. Oda and N. Sakai, *Nucl. Phys.* **B586**: 231-260, 2000, hep-th/0004188.

[160] K. Ito, M. Naganuma, H. Oda and N. Sakai, hep-th/0012182 (Talk presented by N. Sakai at the SUSY 30 workshop in Minnesota, October 16-27, 2000. To appear in Nuclear Physics B (Proceedings Supplement)).